Preconcentration for Improved Long-term Monitoring of Contaminants in Groundwater

Final Report
ER-1604

Brandy J. White and Brian J. Melde

Center for Bio/Molecular Science and Engineering
Naval Research Laboratory
Washington, DC 20375

April 10, 2014

Revision #1

Approved for Public Release, Distribution is Unlimited

REPORT DOCUMENTATION PAGE

Form Approved
OMB No. 0704-0188

The public reporting burden for this collection of information is estimated to average 1 hour per response, including the time for reviewing instructions, searching existing data sources, gathering and maintaining the data needed, and completing and reviewing the collection of information. Send comments regarding this burden estimate or any other aspect of this collection of information, including suggestions for reducing the burden, to the Department of Defense, Executive Services and Communications Directorate (0704-0188). Respondents should be aware that notwithstanding any other provision of law, no person shall be subject to any penalty for failing to comply with a collection of information if it does not display a currently valid OMB control number.

PLEASE DO NOT RETURN YOUR FORM TO THE ABOVE ORGANIZATION.

1. REPORT DATE *(DD-MM-YYYY)*	2. REPORT TYPE	3. DATES COVERED *(From - To)*
08/31/2013	Final Technical Report	01/25/2008 - 06/15/2013

4. TITLE AND SUBTITLE

Preconcentration for Improved Long-term Monitoring of Contaminants in Groundwater

5a. CONTRACT NUMBER

MIPR# W74RDV20729380

5b. GRANT NUMBER

5c. PROGRAM ELEMENT NUMBER

6. AUTHOR(S)

White, Brandy J.
Melde, Brian J.

5d. PROJECT NUMBER

ER-1604

5e. TASK NUMBER

5f. WORK UNIT NUMBER

69-9629-0-2-5

7. PERFORMING ORGANIZATION NAME(S) AND ADDRESS(ES)

Center for Bio/Molecular Science and Engineering
Naval Research Laboratory; Code 6900
Washington, DC 20375

8. PERFORMING ORGANIZATION REPORT NUMBER

9. SPONSORING/MONITORING AGENCY NAME(S) AND ADDRESS(ES)

Department of Defense
Strategic Environmental Research & Development Program
901 N Stuart St., Suite 303
Arlington VA 22203

10. SPONSOR/MONITOR'S ACRONYM(S)

SERDP

11. SPONSOR/MONITOR'S REPORT NUMBER(S)

12. DISTRIBUTION/AVAILABILITY STATEMENT

Approved for public release; distribution is unlimited

13. SUPPLEMENTARY NOTES

The original document contains color images and hyperlinks.

14. ABSTRACT

Materials for the concentration of nitroenergetic and perchlorate targets from groundwater were developed for monitoring applications. Novel molecular imprinting and structure direction techniques were used to obtain the necessary materials. The potential for concentration of targets from ground and surface waters as well as from soil extracts was demonstrated. The functional characteristics of the materials were evaluated in order to determine the constraints on there use in inline preconcentration of targets ahead of IMS and electrochemical sensing techniques. The systems were subsequently developed at the bench level and function was evaluated using commercially available portable sensors. An initial portable prototype was also developed and evaluated under a field scenario.

15. SUBJECT TERMS

mesoporous, sorbent, nitroenergetic, extraction, electrochemical detection, ion mobility spectrometry, perchlorate, preconcentration, solid-phase extraction

16. SECURITY CLASSIFICATION OF:			17. LIMITATION OF ABSTRACT	18. NUMBER OF PAGES	19a. NAME OF RESPONSIBLE PERSON
a. REPORT	b. ABSTRACT	c. THIS PAGE			Brandy J. White
U	U	U	SAR	130	19b. TELEPHONE NUMBER *(Include area code)* 202 404 6100

Reset

Standard Form 298 (Rev. 8/98)
Prescribed by ANSI Std. Z39.18

Table of Contents

Acronyms

2,4-DNT	2,4-dinitrotoluene
2-ADNT	2-amino-4,6-dinitrotoluene
2-NT	2-nitrotoluene
3-NT	3-nitrotoluene
4-ADNT	4-amino-2,6-dinitrotoluene
4-NT	4-nitrotoluene
APS	3-aminopropyltrimethoxysilane
BET	Brunauer-Emmett-Teller
BJH	Barrett-Joyner-Halenda
BS	benzene-bridged PMO material
BTE	1,2-bis(trimethoxysilyl)ethane
CMS	corrective measures study
DEB	1,2-bis(trimethoxysilylethyl)benzene
DMB	1,2-bis(trimethoxysilylmethyl)benzene
DNA	2,4-dinitroaniline
DNB	dinitrobenzene
DOC	dissolved organic carbon
GC	Gas chromatography
HMX	1,3,5,7-tetranitro-1,3,5,7-tetrazocane
HPLC	high performance liquid chromatography
IMS	ion mobility spectrometry
LC	Liquid chromatography
MIP	molecularly imprinted polymer
MS	mass spectrometry
NB	nitrobenzene
P123	Pluronic P123
pCR	p-cresol
PMO	periodic mesoporous organosilica
pNP	p-nitrophenol
PTFE	polytetrafluoroethylene
PTS	phenyltrimethoxysilane
RAM	restricted access materials
RDX	1,3,5-Trinitroperhydro-1,3,5-triazine
REMUS	Remote Environmental Monitoring Units
SEM	scanning electron microscope
SPE	solid phase extraction
SPME	solid phase microextraction
TEM	Transmission electron microscopy
TGA	Thermogravimetric analysis
TMB	mesitylene; 1,3,5-Trimethylbenzene
TNB	trinitrobenzene
TNT	2,4,6-trinitrotoluene
USERDC	US Army Corps of Engineers, Engineer Research and Development Center
UUA	Unmanned Undersea Vehicle
XRD	X-ray diffraction

Figures

Tables

Acknowledgements

The research described in this final report was supported by the U.S. Department of Defense, through the Strategic Environmental Research and Development Program (SERDP; Work Unit #69-8764, FY08 and #69-9629, FY10-FY13) and through the Office of Naval Research via Naval Research Laboratory funding. Dr. Andrea Leeson, Sarah Hunt, Deanne Rider, Katie O'Toole, Brittany Wills, Cara Patton, and other SERDP staff are gratefully acknowledged for their assistance and support. The comments and insights of Dr. Paul Hatzinger (Shaw Environmental) and Mr. William Corl (Laboratory Quality and Accreditation, NAVSEA) are gratefully acknowledged.

Many people contributed to this effort; their support was critical and appreciated. Mr. Paul Charles (NRL) provided GC, electrochemical, and IMS analysis as well as participating in vapor system development and maintaining relationships with non-NRL collaborators. Dr. Brian Melde was responsible for development of materials and synthetic techniques as well as morphological characterization of the products. Mrs. Iwona Leska (Nova Research, Inc) provided technical support for characterization of sorbent-target interactions as well as HPLC and IC analysis. Ms. Jenna Taft (Nova Research, Inc) provided technical support for materials synthesis and characterization. Mr. Martin Moore (NRL) provided technical support for characterization of sorbent-target interactions. Dr. Mansoor Nasir (formerly NRL; currently Lawrence Technological University, MI) developed the initial prototypes for both the liquid/liquid and liquid/vapor systems as well as completing initial evaluations of those instruments and completing initial evaluations on thermal desorption conditions. Mr. Michael Dinderman (formerly NRL; currently NIST) provided TEM and SEM support for the project. Dr. Ronald Siefert (U.S. Naval Academy, at NRL through GLISP) provided technical support for characterization of sorbent-target interactions as well as IC analysis. Dr. Jeffrey Deschamps (NRL) and Dr. Syed Qadri (NRL) provided assistance with X-ray diffraction measurements. Dr. Anthony Malanoski (NRL) provided theoretical support to the effort. Dr. Scott Trammell (NRL) evaluated elution conditions and conducted electrochemical measurements for the offline system. Mr. Scott Vietch (formerly SubChem Systems) and colleagues were responsible for design and assembly of the portable prototype instrument.

The NSF/ONR funded HBCU summer research experience at NRL supported several students who contributed to this effort. Mr. Norris Dyson worked to determine conditions for thermal desorption (Summer 2010). Mr. Alejandro Medina participated in the bench scale liquid/liquid system evaluations (Summer 2011). Ms. Damaris Concepción work to optimize sorbent synthesis and characterized a number of sorbent variations (Summer 2008).

Testing sites and samples from representative sites were critical to this effort. Soil and groundwater samples were provided to us by Mr. Alan Hewitt of the US Army Corps of Engineers, Engineer Research and Development Center. Ms. Kim Granzow and Mr. Michael Dale from the New Mexico Environment Department, Department of Energy Oversight Bureau provided groundwater samples from sites local to their efforts. Mr. Matthew Malanoski provided groundwater samples from northern Maryland. Mr. William Johnson of the US Army Corps of Engineers, Tulsa District (recently retired) provided sites in northeastern Oklahoma for field trials as well as technical and logistical support and local transportation.

Executive Summary

Objectives: There are more than 12,000 sites in the United States that are contaminated with one or more compounds related to weapons technologies. These sites include former and current testing and training facilities where waste from weapons manufacture, storage, and reclamation processes has leached into the soil and groundwater. Key contaminants include energetic compounds such as TNT, RDX, and HMX; perchlorate propellants; and degradation products of these contaminants. Many of these compounds are known carcinogens or suspected cancer causing agents. One issue has been the potential health hazard posed to military personnel and their families resident on these installations, but the migration and leaching of these contaminants to the surrounding population, agricultural regions, and neighboring wildlife is also a concern. Long-term monitoring of sites undergoing remediation as well as sites that may eventually require cleanup is critical. This effort sought to develop materials, systems, and methods necessary to monitoring contaminants in surface and ground water through the use of target preconcentration prior to analysis by commercially available sensors.

Technical Approach: **P**eriodic mesoporous organosilicates (PMOs) are organic-inorganic polymers with highly ordered pore networks and large internal surface areas. They are synthesized using a surfactant template approach in combination with a phase separation technique to provide organization on both the macro- and meso-scales. This approach facilitates diffusion of targets throughout the entire available surface area. Using a template-directed molecular imprinting approach, a PMO surface can be engineered to have both a large adsorption capacity and selectivity for the target. The binding affinity and capacity of these materials make it possible to concentrate trace levels of targets from a large sample volume while eliminating other contaminants. The targets can be subsequently eluted from the sorbent in a small volume of solvent such as methanol or acetonitrile. This adsorption/elution approach is directly applicable to the development of methods and systems for use with electrochemical detection. Methods for utilization of these types of materials in the preparation of samples for IMS-based detection were less well developed. This application involves sampling from a water source and desorbing the concentrated target into a carrier gas.

Results and Benefits: This effort sought both to advance the state of the sorbent materials and to provide the methods and systems necessary for their use in in-line preconcentration of targets. Several advances in sorbent design were made including improvements in morphological character and in the template used. Production of the materials at larger scale was also demonstrated. The PMO materials were shown to enhance the sensitivity of currently available sensor systems by concentrating trace amounts of nitroenergetic targets from large sample volumes. Materials for the preconcentration of perchlorates were also developed. A breadboard level prototype was developed and used in a full range of laboratory demonstrations with electrochemical sensing. A brassboard level prototype was developed and used for one round of field trials with electrochemical sensing. A breadboard level prototype was also developed for use with a commercial ion mobility spectroscopy (IMS) detection system.

The novel porous materials and associated methods developed here provide a regenerable mechanism for the preconcentration and long-term monitoring of energetic materials. Though development of the systems described here is not ongoing, the materials developed under this effort are being utilized by another group in the design of an electrochemical sensor for use with the REMUS (Remote Environmental Monitoring Units) UUA. In addition to these types of active monitoring applications, the material developed during the course of this program has the potential for deployment for short- and long-term passive monitoring similar to the polyethylene passive sampling materials.

Objective

This work sought to develop and demonstrate the potential of porous nanostructures as a cost effective, regenerable mechanism for the pre-concentration and long-term monitoring of energetic materials contained in groundwater plumes from testing and training facilities. If successful, integration of the proposed materials into existing field deployable systems would enhance the sensitivity of those systems by orders of magnitude. The results presented here detail the outcomes of a one year SEED effort funded in FY08 as well as a three year follow-on effort (FY10-FY12). The goal of the SEED effort was to complete the development of methods for the synthesis of periodic mesoporous organosilicas (PMOs) in order to provide semi-selective sorbents for the pre-concentration of key contaminants in groundwater. At the onset of this program, preliminary work toward establishing these methods had been completed, but only a minimum demonstration of the materials function had been achieved. This work was intended to demonstrate the potential of the materials in bench-top experiments using laboratory generated and real-world samples. The follow-on effort sought to develop the systems and methods necessary for incorporation of the novel pre-concentration materials into *in situ* monitoring systems. The design of breadboard level prototypes for use with electrochemical and ion mobility spectrometer based detection platforms was undertaken as well as demonstrations of the function of the resulting systems.

Background

In the U.S. there exist over 12,000 sites that are contaminated with one or more compounds related to weapons technologies. These sites are former and current testing and training facilities where waste from weapons manufacture, storage, and reclamation processes has leached into the soil and groundwater.[1] Key contaminants include energetic compounds such as TNT, RDX, and HMX; chlorinated hydrocarbons such as tetrachloroethene and trichloroethene; and degradation products of these contaminants. These compounds pose a threat to the environment and many are known carcinogens or suspected cancer causing agents.[2,3] One issue has been the potential health hazard posed to military personnel and their families residing on these installations, but the migration and leaching of these carcinogens to the surrounding population, agricultural regions, and neighboring wildlife is also a serious concern.[4,5] Long-term monitoring of sites is necessary for tracking the movement of contaminants as well as the progress of decontamination efforts.

Several ongoing efforts are aimed at the development of systems for these applications. Often, the sensitivity of these systems is not useful for detection of targets at trace levels. Lower levels of detection provide a longer window for responding to progressing or emerging threats. An early indicator can make the difference between a minimal preventive measure and a major clean-up. Current monitoring is accomplished using laboratory based equipment. The costs associated with sampling and disposal of contaminated material as well as the time required for bench top analysis is prohibitive. *In situ* monitoring offers several advantages particularly when systems can be deployed over long periods of time without maintenance.

One technology that has shown promise for long-term monitoring applications is electrochemical detection. These types of instruments have the potential to provide low-cost, low-power solutions for *in situ* applications. Remote monitoring systems based on electrochemical measurements have been described.[6] The sensitivity of this technique as well as the potential for interference have limited interest and applications. Handheld instruments are commercially available (for example, Palm Instruments BV; CH Instruments, Inc). A previous

SERDP-funded effort (ER-1220) was directed at the development of electrochemical sensors for in situ monitoring of explosives in groundwater. The effort attained detection limits of 50 – 100 ppb for TNT (and similar compounds) and limits of 1 – 2 ppm for HMX and RDX.

Another promising technology for application as miniaturized sensors is ion mobility spectroscopy. An ion mobility spectrometer (IMS) pulls a gaseous sample into an ionization region. Ionized analyte is accelerated by a uniform electric field. Detection is accomplished via the current generated at a Faraday plate placed at the end of the drift region. Discrimination of analytes is accomplished based on their time-of-flight along the drift region. Unlike liquid chromatography techniques where separations occur on time scales stretching across several minutes, IMS separations occur over tens of milliseconds. Several hand-held instruments based on IMS are available.[7] The technology has also been applied to monitoring concentrations of contaminants in soils.[8] Current applications of the technology are limited to compounds of higher vapor pressures or to samples that are pre-heated due to the need for samples to be gaseous. An ongoing SERDP-funded effort (ER-1603) is focused on the development of a micro IMS system for monitoring groundwater. The program faces two major challenges: reduction of interference by non-target analytes and conversion of a liquid sample to vapor phase targets.

Several technologies exist which can be applied enhancing the ability to monitor key contaminants. Difficulties, however, often arise when detection of trace levels in complex matrices is necessary. A number of methods have been explored for concentration of target analytes from groundwater and other real-world samples: liquid-liquid extraction, salting-out techniques, and solid-phase extraction (SPE).[9,10] Major drawbacks have included the enormous amount of solvent used in extraction processes, time-consuming steps, and necessary conditioning processes. Solid-phase microextraction (SPME) fibers provide a method of pre-concentrating contaminants prior to analysis by high performance liquid chromatography (HPLC), ion mobility spectrometry (IMS), or gas-chromatography mass spectrometry (GC-MS)[11] and yield detection levels typically in the low nanogram per milliliter (ng/ml) range. Unfortunately, SPME fibers require long incubation times and degrade over repeated use. Restricted access materials (RAM) are porous graphite or bifunctional sorbents that have been combined with liquid chromatography-mass spectrometry (LC-MS) to provide enhanced sensitivity (low ng/L).[12] However, the increased pressure and biofouling associated with the RAM has resulted in higher variability in sample analysis. Resins packed as columns also have demonstrated some promise for the pre-concentration of trace contaminant levels resulting in enhanced HPLC sensitivities of up to three orders of magnitude.[13] The sorbents developed at NRL under previous efforts have been shown to enhance detection methods as well. The following sections provide a description of the materials and a summary of previous work.

Periodic Mesoporous Organosilicas (PMOs)

Periodic mesoporous organosilicas (PMOs) are organic-inorganic polymers with highly ordered pore networks and large internal surface areas (typically >1,000 m^2/g). First reported in 1999,[14-16] PMOs are synthesized using a surfactant template approach [17-19] and have narrow pore size distributions with few blocked pores or obstructions facilitating molecular diffusion throughout the pore networks. The alternating siloxane and organic moieties give PMOs properties associated with both organic and inorganic materials.[20,21] The siloxane groups provide the structural rigidity required to employ a template method while allowing for incorporation of a unique method for engineering porosity. If one were to prepare a composite with a conventional organic polymer using surfactant templates, the removal of the surfactant

templates would result in structural collapse of the polymer due to its flexibility on the molecular scale. In addition to structural rigidity, the silica component of the PMOs provides a degree of hydrophilic character useful for applications in aqueous systems. Organic functional groups within the PMO matrix offer those interactions with targets typically associated with organic polymers. Precursors containing different organic bridging groups have been used to produce a variety of PMOs with unique chemical properties. Experimental parameters, such as the selection of different precursors, surfactants, and functional silanes, allow the design of porous materials with structural and chemical properties optimized for a given application.

Figure 1 shows a typical protocol for the synthesis of one of the PMO materials. The surfactant and imprinting template (also a surfactant) are mixed in acidified ethanol at concentrations exceeding the critical micelle concentration. Various packing conformations for the micelles are possible depending on the choice of surfactant, acid, temperature, and concentration. When the micelles are established, the siloxane precursors are added in a drop wise manner to the solution. Condensation of the precursors results in a structure in which regions of surfactant and silicate alternate. Extraction of the surfactant, typically through refluxing, results in a porous structure. The organization of the pores is a result of the organization of the original micelles.

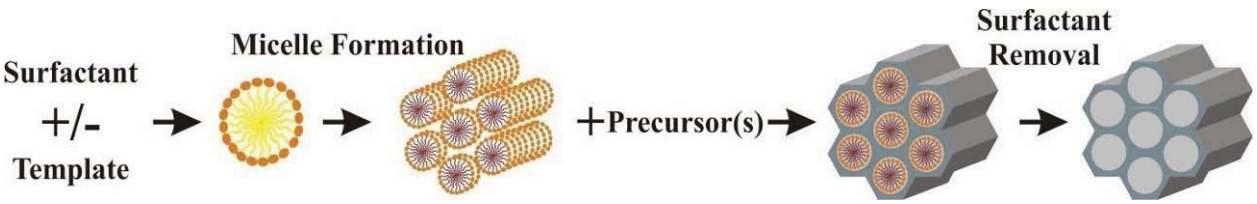

Figure 1. *Synthesis of periodic mesoporous organosilicas (PMOs).*

The tunable nature of these materials results from the potential for selecting various surfactants, imprint templates, and precursors. Figure 2 shows some of the precursors that have been applied by this group to the synthesis of these materials. 1,4-bis(trimethoxysilylmethyl)benzene (DMB) provides affinity for TNT, but materials synthesized with 1,4-bis(trimethoxysilylethyl)benzene (DEB) were found to provide higher affinity. Materials synthesized using 1,4-bis(trimethoxysilyl)benzene tend to be more organized (increased pore organization and surface area) than those synthesized using DEB and provide a strongly hydrophobic surface that is useful for the adsorption of solvents like hexane.[22] (3-Aminopropyl)trimethoxysilane (APS) provides primary amine groups which facilitate post synthesis modification. These groups have been used to provide sites at which catalysts can be attached. Further options can be obtained through combining two or more precursors in a co-condensation approach. For example, high binding capacities for phosgene have been obtained through co-condensation of APS and 1,2-bis(trimethoxysilyl)ethane. The material can be modified post-synthesis with a copper metalloporphyrin resulting in a highly porous, well organized material (surface area 1002 m^2/g; pore volume 1.19 cm^3/g; pore diameter 77 Å) with a high concentration of functional sites.[23,24]

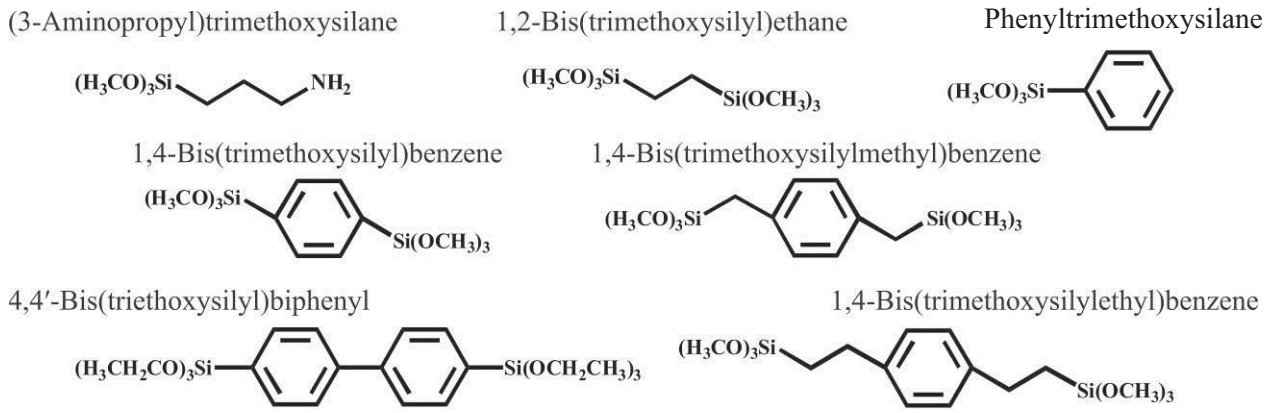

Figure 2. *Siloxane precursors.*

The organization of the PMO materials is directed by the surfactant micelles though it can be disrupted by poor choices of precursors and/or precursor concentrations. The surfactant most commonly employed in the syntheses outlined in Figure 1 is Brij®76 (polyoxyethylene (10) stearyl ether, $C_{18}H_{37}(OCH_2CH_2)_nOH$, n~10). This is an alkylene oxide surfactant. In general, pore sizes of about 30 Å are possible using Brij®76 under these conditions. Various pore organizations are possible including hexagonal, cubic, lamellar, and worm-like. Pore organization is dependent on the conditions of the synthesis including temperature and acid concentration. Variations in the concentrations of hydrophobic compounds, such as hydrophobic precursors, may alter the micelle conformation and, therefore the pore organization.

The surface of the pore results from the interactions between the head groups of the micelles and the siloxane precursors during condensation. The primary mechanism for adsorption of aromatic compounds by the PMO material is the π-π interactions existing between an aromatic target and the bridging groups of the PMO. We have found it possible to enhance the favorable interactions between these materials and targets of interest through "imprinting" the surface of the pores against a target analog. This target-like surfactant becomes part of the surfactant micelles around which the precursor materials form the porous structures of the PMO materials. The idea is similar to that used with molecularly imprinted polymers (MIPs). In the case of MIPS, polymerization is accomplished in the presence of a target (or target analog) which is then extracted from the pore. This process leaves a cavity that is structurally and electronically complimentary to the target in the material. The result with the PMOs is not quite as exact, but we have demonstrated that the surface interactions with targets are enhanced. This process provides enhanced selectivity in complex mixtures as well as enhanced capacity and affinity in some cases. The specificity obtained through careful selection of precursors as well as imprinting of the PMO surfaces gives the PMOs an advantage over options such as C8, C18, or other silicas. Silica phases function primarily through simple hydrophobic interactions and to some extent size exclusion.

Prior to the beginning of this program, we had demonstrated that, in batch studies, an arylene-bridged PMO preferentially adsorbed aromatic hydrocarbons.[25] Greater than 96% of p-nitrophenol, p-chlorophenol, and p-cresol were absorbed from aqueous solutions within the first minute of PMO contact with greater than 99% adsorbed within 15 minutes. Further studies using a DEB-bridged PMO demonstrated that a degree of selectivity could be achieved for TNT

over structurally similar compounds. In a competitive adsorption environment containing p-nitrophenol, p-cresol, and TNT, greater than 85% of TNT adsorption was completed within the first minute of contact (Figure 3).

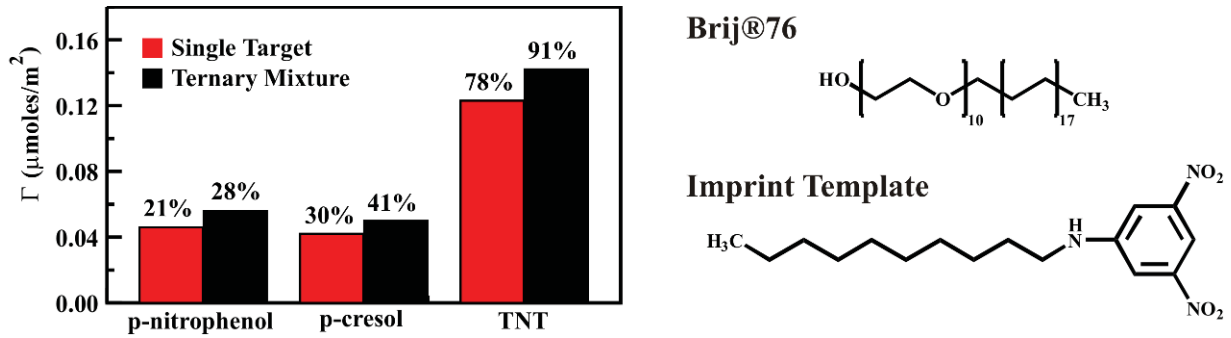

Figure 3. *Adsorption of analytes by a molecularly-imprinted PMO from single target and ternary target solutions. Γ is the amount of target bound per unit surface area. Percentages are of the total target concentration in the sample. Also shown are the structure of Brij®76 and the imprint template molecule used.*

The target binding capacity of the arylene-bridged PMO material was compared to that of activated carbon by monitoring target breakthrough using 1 mM p-nitrophenol. No breakthrough (the entire target in the applied solution was bound) was observed for the first 20 applied bed volumes (Figure 4). The same weight of activated carbon adsorbed 60 applied bed volumes before breakthrough was observed. While this indicates a PMO target capacity somewhat lower than that of commercially available activated carbon, the activated carbon materials cannot be applied to pre-concentration since targets cannot be easily eluted from them. In the case of the organosilica materials, desorption of the p-nitrophenol can be accomplished by a simple alcohol wash. After 10 adsorption-desorption cycles, no loss of adsorption capacity or performance was observed (Figure 4). Similar treatment of the activated carbon failed to remove any detectable amount of nitrophenol.

Figure 5 illustrates the increase in TNT adsorption for the PMO materials upon imprinting with a target analog. Binding of p-nitrophenol almost doubled from 47 nmoles/m^2 to 89 nmoles/m^2 while TNT binding increased from 128 nmoles/m^2 to 155 nmoles/m^2 in single target samples (similar increases are also shown in multiple target samples as illustrated). Equally important is the fact that little increase was observed for p-cresol. In fact, an increase of less than 10% was seen emphasizing the preferential binding of nitro-substituted compounds by the imprinted PMO. As illustrated in Figure 5, the imprinted material also preferentially binds TNT from multi-target mixtures where TNT binding was nearly double that of the other compounds present. Figure 6 illustrates the adsorption of TNT and RDX from soil extract. Soil extracts were obtained by mixing 2 g of soil collected at Umatilla Army Depot Activity (Umatilla, OR) with 10 mL acetone. Particles were allowed to settle for 15 min before the supernatant was filtered using a 0.22 μm syringe filter. In this case, the binding of TNT was increased by more than 7-fold as a result of the imprinting process. Although this PMO was originally targeted for TNT, a 4-fold increase in RDX binding was also realized. This further indicates preferential binding of nitro-moieties in the target mixture by the PMO even in the presence of a high dissolved organic carbon (DOC) concentration.

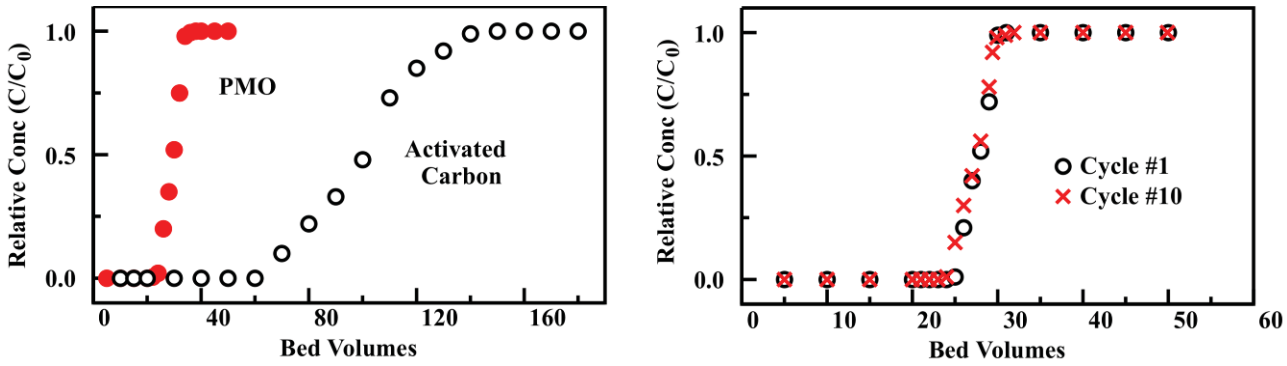

Figure 4. **A.** *Break through curves comparing the PMO to activated carbon are presented as the ratio of the eluent concentration to the initial sample concentration.* **B.** *Effect of ethanol washes on PMO adsorption performance over 10 cycles is presented as a ratio of the target concentration in the eluent versus that of the initial sample.*

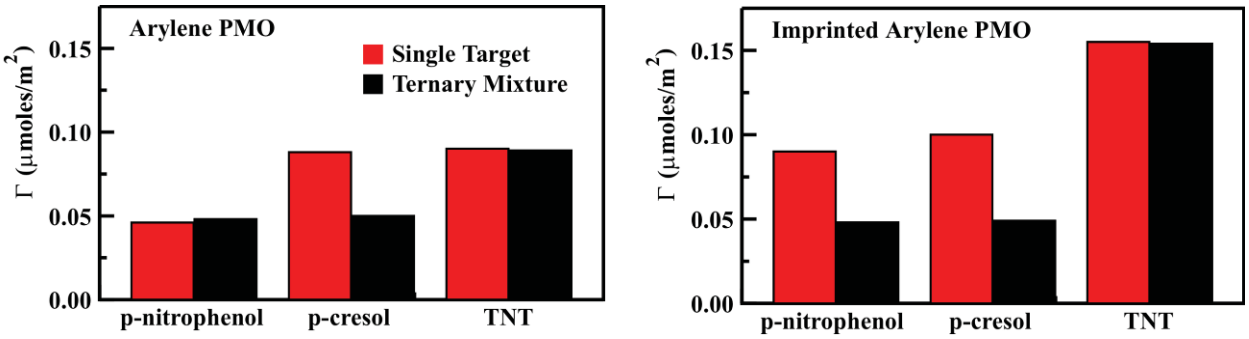

Figure 5. *Adsorption study using non-imprinted (Panel A) and imprinted (Panel B) arylene-bridged PMO from single target and ternary target solutions. Γ is the amount of target bound per unit surface area.*

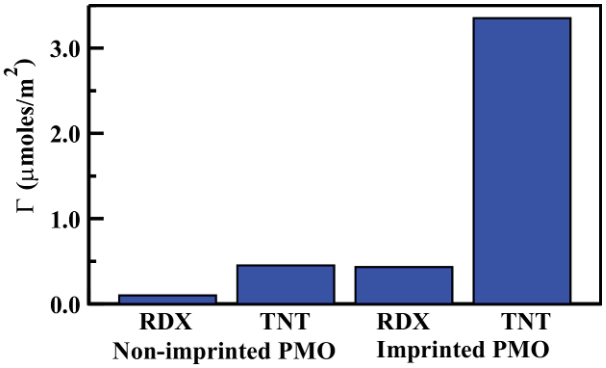

Figure 6. *Competitive binding of TNT and RDX from contaminated soil extract by arylene-PMO.*

PMOs and Electrochemical Detection

Preliminary studies have been conducted using PMO materials for the rapid pre-concentration and extraction of TNT for enhancement of electrochemical analysis. Electrochemical methods have shown promise for the detection of TNT.[6,26] The PMOs used as pre-concentration materials were imprinted against TNT and employed a benzene (BS) hybrid organic-inorganic polymer. Samples ranging from 0.5 mL to 10 mL containing 5 to 1000 ppb TNT in phosphate buffer were concentrated in-line before electrochemical detection using a micro-column containing 10 mg of the PMO. TNT was rapidly eluted from the column using

40% acetonitrile in 10 mM PBS. Square wave voltammetry was used to monitor the reduction of TNT in an electrochemical flow cell using a carbon working electrode and an Ag/AgCl reference electrode (Figure 7). Using the benzene-bridged PMO material, TNT detection levels of 10 ng/mL (ppb) were obtained when TNT was concentrated from a 2 mL original sample volume (Figure 8). It was also noted that nearly 100% recovery of TNT from the columns was achieved. This can be observed by noting that the areas under the peaks in Figure 7 are identical in all three cases. The benzene-bridged PMO provided the greatest enhancement in sensitivity owing to the rapid elution of TNT from that material as compared to the diethylbenzene-bridged material.

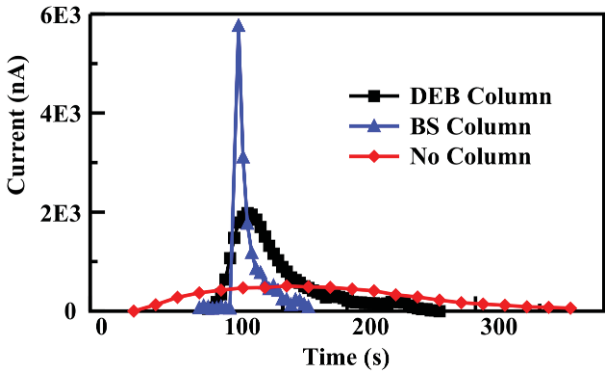

***Figure** 7. Electrochemical detection of TNT at 1000 ppb using square-wave voltammetry (SWV) by means of an electrochemical flow cell. SWV parameters: Potential range, 0.3 to - 0.8 V vs. Ag/AgCl at a frequency of 100 Hz and an amplitude of 25 mV. Flow rate 200 µL/min.*

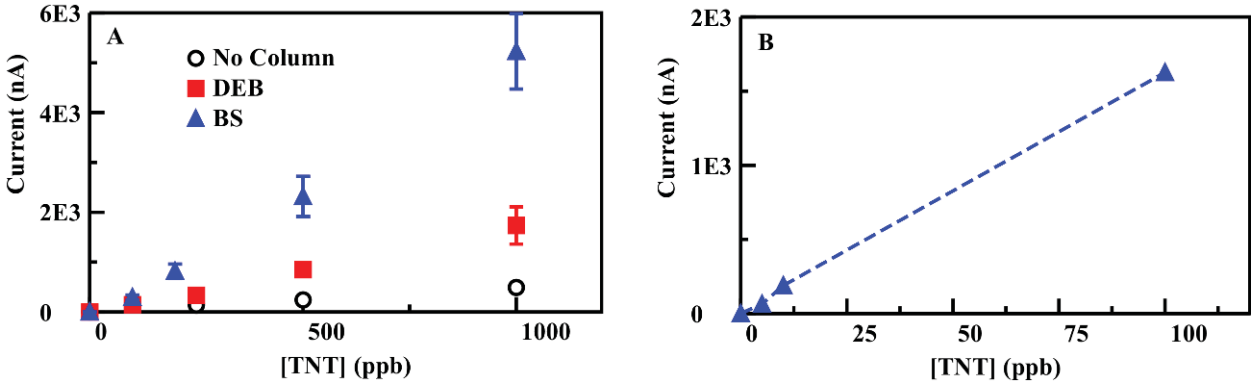

***Figure 8**. Peak current versus TNT concentration for the electrochemical detection of TNT using square-wave voltammetry. Presented data compares results obtained without pre-concentration to results obtained using benzene-bridged PMO and diethylbenzene-bridged PMO materials in-line with the detector. (Panel A) 0.5 mL original sample eluted in 0.5 mL from BS and DEB column. (Panel B) 2 mL original sample eluted in 0.5 mL from BS column.*

Materials and Methods

Sodium perchlorate, sodium perrhenate, ammonium nitrate, ammonium thiocyanate, ammonium sulfate, ammonium phosphate, p-cresol (pCr), and p-nitrophenol (pNP) were purchased from Sigma-Aldrich (St. Louis, MO). 2,4,6-Trinitrotoluene (TNT), hexahydro-1,3,5-trinitro-1,3,5-triazine (RDX), nitroglycerin (NG), octahydro-1,3,5,7-tetranitro-1,3,5,7-tetrazocane (HMX), and 2,4-dinitrotoluene (DNT) were purchased from Cerilliant (Round Rock, TX). Chemicals were used as received. Chemicals used for synthesis of materials are detailed in

Table 1. Purolite® A530E and A532E, strong base anion exchange resins, were gifts from Purolite (Bala Cynwyd, PA). Water was deionized to 18.2 MΩ cm using a Millipore Milli Q UV-Plus water purification system. Artificial sea water was prepared using sea salts as directed by the supplier (Sigma-Aldrich). Pond water samples were collected from a park in Alexandria, Virginia. Groundwater was collected from wells in Hanover, New Hampshire, and Fulton, Maryland (depth of 213 m). Soil samples were collected from munitions testing sites on Holloman Air Force Base, Alamogordo, New Mexico, and analyzed using Environmental Protection Agency (EPA) Method 8330B by the Cold Regions Research and Engineering Laboratory, Engineer Research and Development Center, U.S. Army Corps of Engineers, Hanover, New Hampshire.

Material Synthesis

Two major variations on material synthesis were utilized for nitroenergetic targets during the course of these studies. Here, we describe in general terms the approaches used. For detailed synthetic processes, please refer to the Tasks, associated tables, and cited papers.

PMO Synthesis

Figure 1 presents the basic steps in synthesis of a PMO material.[27,28] In general, the Brij®76 surfactant was dissolved in an aqueous solution of HCl with or without the appropriate imprint template. The precursor or precursor mixture was added to the solution dropwise, and the mixture was heated overnight. Product was collected by vacuum filtration, and the surfactant was extracted by refluxing aqueous HCl.

The target analog used for imprinting the PMOs (Figure 9) was generated through esterification of Brij®76 with 3,5-dinitrobenzoyl chloride [29-31]. Briefly, Brij®76 (2 g; 2.81 mmol) and 3,5-dinitrobenzoyl chloride (1.3 g; 6 mmol) were dissolved in 60 mL of dichloromethane. Magnesium turnings were added and the mixture was refluxed for 2 h. The liquid was shaken with 60 mL 2% $NaHCO_3$ in a separatory funnel. The organic phase was then extracted and evaporated under vacuum. The resulting dinitrobenzene (DNB)-modified Brij®76 was orange in color.[32-36]

Hierarchical Sorbent Synthesis

Synthesis of the hierarchical materials was accomplished using a variation of the technique described above.[32,37] Pluronic P123 surfactant was dissolved with mesitylene and with or without the appropriate template in aqueous nitric acid. The precursor or precursor mixture was added dropwise to the solution, forming a white gel. Following curing, the product was refluxed in acidified ethanol to remove the surfactant, and product was collected by vacuum filtration.

The target analog for imprinting the hierarchical materials (Figure 9) was prepared by esterification of Pluronic P123 with 3,5-dinitrobenzoyl chloride. This was accomplished as follows: 8 g P123, 1.27 g 3,5-dinitrobenzoyl chloride, and magnesium turnings were added to 60 mL dichloromethane and refluxed for 2 h. The solution was shaken with 60 mL 2% aqueous $NaHCO_3$. The organic phase was collected and evaporated to yield the yellow, modified surfactant.[38-40]

Table 1 *— Synthesis Reagents*

Compound	Abbrev	Supplier	Function	Notes
Nitroenergetic Target Directed Materials				
Bis(trimethoxysilylethyl)benzene	DEB	Gelest	Precursor	
Phenyltrimethoxysilane	PTS	Gelest	Precursor	
1,2-Bis(trimethoxysilyl)ethane	BTE	Gelest	Precursor	
3-aminopropyltriethoxysilane	APS	Gelest	Precursor	
Hydrochloric acid	HCl	Sigma-Aldrich	Solvent System	
Polyoxyethylene (10) stearyl ether, $C_{18}H_{37}(OCH_2CH_2)_nOH$, n~10	Brij®76	Sigma-Aldrich	Surfactant	
3,5-Dinitrobenzoyl chloride		Sigma-Aldrich	Target Analog	98%
Dichloromethane		Sigma-Aldrich	Template Synthesis	Solvent >99.5%
Sodium bicarbonate	$NaHCO_3$	Sigma-Aldrich	Template Synthesis	Purification
Magnesium turnings		Sigma-Aldrich	Phase Separation	98%
Ionic Target Directed Materials				
N-trimethoxysilylpropyl-N, N, N-trimethylammonium chloride	TSPMC, M	Gelest	Grafted Group	50% in methanol
N-trimethoxysilylpropyl-N, N, N-tri-n-butylammonium chloride	TSPBC, B	Gelest	Grafted Group	50% methanol
Tetramethyl orthosilicate	TMOS	Sigma-Aldrich	Precursor	98%
Toluene		Sigma-Aldrich	Grafting	Solvent
Used in Materials for Both Targets				
1,3,5-trimethylbenzene	TMB	Sigma-Aldrich	Spinodal Decomposition	Mesitylene
Poly(ethylene glycol)-*block*-poly(propylene glycol)-*block*-poly(ethylene glycol) average M_n~5800	P123	BASF	Surfactant	Pluronic P123
Nitric acid	HNO_3	Sigma-Aldrich	Solvent System	
Ethanol		Warner-Graham	Solvent System	200 proof

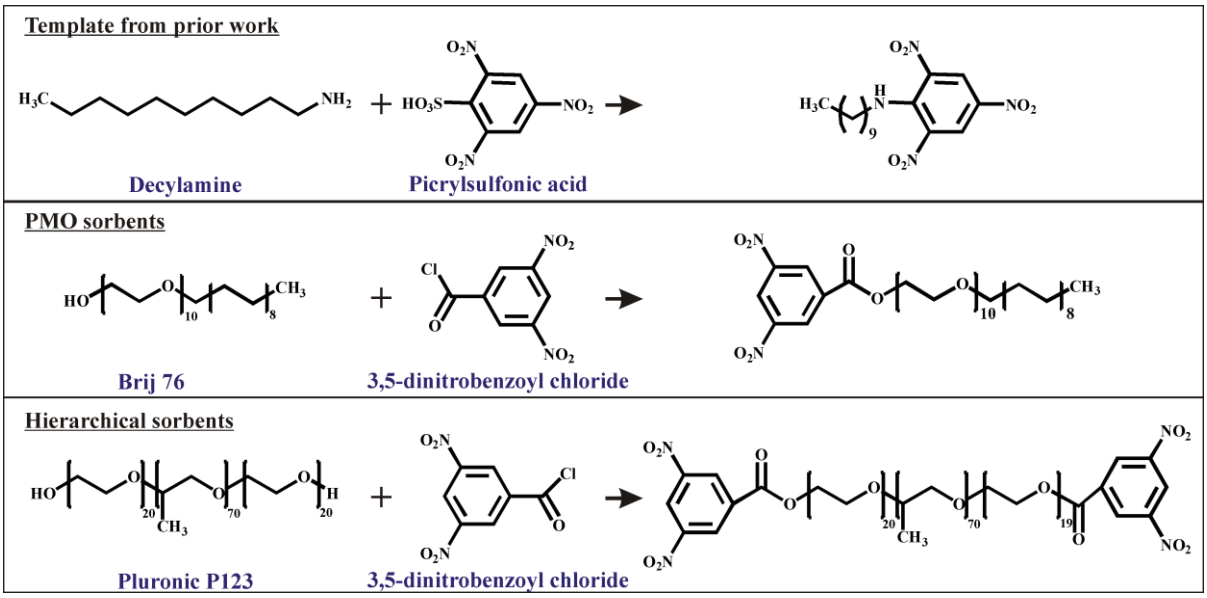

Figure 9. *Target analogs (or imprint templates) used for prior work with organosilicate sorbents (top), the PMO materials described here (center), and the hierarchical sorbents described here (bottom).*

Perchlorate Sorbent Synthesis

For materials directed at capture of perchlorates, a similar approach was taken to synthesis of a scaffold. The materials were synthesized based on a previously published approach.[41,42] Pluronic P123 and mesitylene were dissolved in HNO_3 with magnetic stirring and heating. The stirring mixture was allowed to cool to room temperature and TMOS was added dropwise. The mixture was stirred until homogeneous, transferred to a culture tube or a Teflon jar container, sealed tightly, and heated overnight. The white monolith was dried in the unsealed container for approximately 5 d. Surfactant was removed by calcination under ambient atmosphere. Materials were dried at 110 °C prior to grafting with alkylammonium silanes. Grafting of alkylammonium groups was accomplished using materials thoroughly dried at 110 °C. Sorbent material was added to toluene followed by addition of a designated amount of TSPMC and/or TSPBC. The mixture was refluxed for 24 h. Grafted product was collected by vacuum filtration, washed with toluene and ethanol, and dried at 110 °C. The nomenclature of functionalized materials reflects the amounts of TSPMC and/or TSPBC used in the grafting procedure. For example, material designated HX1M3B was prepared by refluxing 1 g of HX with 1 mmol of TSPMC (M) and 3 mmol of TSPBC (B).

Material Characterization

A Micromeritics accelerated surface area and porosimetry analyzer (ASAP 2010) was used for N_2 sorption experiments performed at 77 K. Prior to analysis, samples were degassed to 1 μm Hg at 100 ºC. Standard methods were applied to the calculation of characteristics. Surface area was determined by use of the Brunauer-Emmett-Teller (BET) method; pore size was calculated by the Barrett-Joyner-Halenda (BJH) method from the adsorption branch of the isotherm; total pore volume was calculated by the single point method at relative pressure (P/P_0) 0.97. Thermogravimetric analysis was performed using a TA Instruments Hi-Res 2950

Thermogravimetric Analyzer under a N_2 atmosphere; temperature was ramped 5 ºC/min to 800 ºC. Powder X-ray diffraction (XRD) patterns were obtained with one of two systems: (1) a Rigaku high-resolution powder diffractometer with 18 kW CuKα radiation derived from a high-power Rigaku rotating anode X-ray generator or (2) CuKα radiation from a Brüker MICROSTAR-H X-ray generator operated at 40 kV and 30 mA equipped with a 3 mRadian collimator, and a Brüker Platinum-135 CCD area detector (room temperature). A custom fabricated beamstop was mounted on the detector to allow data collection to approximately 0.4° 2θ (approximately 210 Å) with a sample-to-detector distance of 30 cm. After unwarping the images, the XRD^2 plug-in was used to integrate the diffraction patterns from 0.6° to 8° 2θ.

Conducting carbon tape was used to mount samples on stubs for imaging by scanning electron microscopy (SEM). Sputter coating with gold under argon was accomplished using a Cressington 108 auto sputter coater (duration 60 sec). Scanning electron micrographs of the samples were collected using a LEO 1455 SEM (Carl Zeiss SMT, Inc., Peabody, MA). For imaging via transmission electron microscopy (TEM), samples were deposited onto a holey carbon grid (200 mesh copper, SPI, West Chester, PA) and viewed under an energy filtering transmission electron microscope (LIBRA 120 EFTEM, Carl Zeiss SMT, Peabody, MA) operated at 120 kV. Zero loss, brightfield, energy filtered (EF) TEM images were captured on a bottom-mounted digital camera (KeenView, Olympus SIS, Montvale, NJ).

Target Analysis

Analysis of samples containing nitroenergetic targets was carried out on a Shimadzu high performance liquid chromatography (HPLC) system with dual-plunger parallel flow solvent delivery modules (LC-20AD) and an auto-sampler (SIL-20AC) coupled to a photodiode array detector (SPD-M20A). A modification of EPA Method 8330 was employed. The stationary phase was a 250 × 4.6 mm Altech Alltima C18 (5 μm) analytical column; an isocratic 50:50 methanol:water mobile phase was employed. A 100 μL sample injection was used with a flow rate of 1.3 mL/min. UV/vis detection of targets was accomplished at 254 nm with the exception of nitroglycerin which was detected at 214 nm. This method gives reliable detection at 8 ppb for the targets considered. Eight-point target calibration curves were used with all experiments to verify method performance, and stock target concentrations were measured as a reference for each experiment. The variation in the calibration curves was ±5%.

Ion chromatography (IC) was used for analysis of perchlorate and other ionic targets. Analysis was carried out on a Dionex ICS 1000 system using suppressed conductivity. An anion self-regeneration suppressor (ASRS 300 4 mm) was used with 50 mM KOH as the eluent at 1 mL/min. For analysis of sulfate, the KOH eluent concentration was reduced to 25 mM. The stationary phase was an Ion Pac AS23 Analytical 4 × 250 mm column. An applied current of 200 mA was used with an injection volume of 250 μL and a cell temperature of 35 °C. Six-point target calibration curves were used, and stock target concentrations were measured as a reference for each experiment.

Several types of experiments were used to characterize the binding capacity and affinity of the materials synthesized. Batch experiments were conducted in 20 mL scintillation vials (EPA Level 3; clear borosilicate glass; PTFE/silicone-lined cap). A fixed mass of sorbent was weighed directly into the vial using an analytical balance. Target solutions were added to the sorbents in the vials with a portion of the sample retained for use as a control during HPLC or IC analysis. A series dilution of the retained sample was prepared for generation of a standard curve allowing for analysis of target binding by the sorbents. The vials were incubated on rotisserie mixers.

Following incubation, samples were filtered using 25 μm Acrodisc 0.2 μm syringe filters with PTFE membranes. The filtered solutions were analyzed by HPLC or IC, and difference method analysis was applied to determine the target removed from solution.

Columns of the sorbent materials were prepared in BioRad disposable polypropylene columns, HPLC column housings, and Omnifit column housings. Depending on the material under consideration and the housing, both gravity flow and controlled flow experiments were conducted. Controlled flow was accomplished using a peristaltic pump. As with batch experiments, HPLC difference analysis was used to determine the target bound. Elution from the columns was accomplished using acetonitrile or methanol for nitroenergetic targets. Commercially available preconcentration sorbents LiChrolute EN (VWR International), Sep-Pak RDX (125–150 μm; Waters Corporation, Milford, MA), and Purolite® A530E and A532E were handled identically to the sorbents prepared in-house. Elution of perchlorate and other ionic targets from the columns was accomplished using aqueous HCl.

Results and Accomplishments

The initial SEED effort comprised Tasks 1 through 3 and was focused on synthesis and characterization of new sorbent materials. Beginning with lessons learned from previous studies (Background), materials were optimized to provide balance between structural and binding characteristics in order to provide stand-alone or in-line concentration of targets. Upon successful synthesis of material with the necessary characteristics, batch studies were conducted to characterize the binding affinities, capacities and kinetics. Finally, column formats were used to evaluate the adsorption and elution characteristics under varying conditions including the use of soil extracts and ground water samples.

Task 1. Materials Development

For Phase I of this project, the primary focus was on the synthesis and evaluation of the mesoporous materials and their capacity to concentrate energetic materials from groundwater. Materials optimization consisted of studies to optimize the desired properties, i.e. target capacity, binding affinity and selectivity, and elution characteristics. These optimizations included looking at variations on the imprint template as well as evaluating adjustments to the synthesis protocol including alternative precursors, alternate surfactant to precursor (bridging group) ratios, template imprint molecule variations, and hydrothermal treatments. The first step toward producing materials for these applications was synthesis of a new type of imprinting template. The template used previously (Figure 9) provided marginal results at best and could only be used in low concentrations in the surfactant mixture. To alleviate these issues, we employed esterification of the surfactant head groups to provide a template that would fully integrate with the surfactant. This allows incorporation of a higher concentration of the template as well as providing enhanced contact between the target analog and the pore surfaces during condensation.

Co-condensation Variants.

The exceptional binding characteristics of the DEB-bridged materials described previously lead to consideration of co-condensation approaches for the generation of materials with improved structural characteristics. The goal was to generate high surface area materials with uniform pores which demonstrated binding affinities approaching those observed in the 100%

DEB materials. In addition, it was expected that material structures with uniform pores would be more susceptible to the imprinting process and would, therefore, offer advantages in selectivity and tunability. With these points in mind, several materials, both imprinted and non-imprinted, were synthesized with varying ratios of DEB to BTE (Table 2). As expected, incorporation of the large organic bridging group (DEB) was found to disrupt the structure of the resulting materials. This is evidenced by the decrease in surface area, pore diameter, and pore volume as the DEB precursor was increased from 0 to 100% of the total precursor used (Table 2). At 40% DEB (M-60:40) a transition from mesoporous (pore diameters 20 to 500 Å according to the IUPAC definition) to microporous (pore diameters less than 20 Å) was noted. All materials attained equilibrium adsorption in less than 30 min. Materials with uniform mesopores, such as M-70:30, were found to reach equilibrium adsorption in less than 3 minutes.

The binding capacity and selectivity for each material were evaluated through a combination of experiments. First, materials were exposed to single analyte solutions (including TNT, pNP, and pCr) overnight on a rotisserie shaker in order to determine the total binding capacity for each analyte under identical conditions. HPLC difference method was used to determine the amount of target bound from each solution (Table 2). As expected, the binding capacity of M-100:0 (100% BTE) was low (0.34μg/m^2 for TNT). The binding capacity for all three analytes increased with increasing DEB incorporation with the capacity for TNT reaching a value of 16.3 μg/m^2 for the 100% DEB material (M-0:100). The binding capacity for pNP and pCr remained relatively low for materials with 50% or less DEB incorporated (Figure 10). The M-0:100 material, however, bound pCr equivalent to 62% and pNP equivalent to 21% of the TNT bound. Because TNT was the target of interest, these results would tend to indicate a significant degree of undesirable binding.

As TNT was the target of interest for these studies, competitive binding in a three component mixture (TNT, pNP, and pCr each at 22 μM) was used to evaluate the tendency for TNT binding over that of other compounds of similar structure. While the binding of TNT by M-100:0 and M-90:10 was not impacted by the presence of pCr and pNP in the sample, the other materials showed a reduction in TNT bound per surface area when the target was presented in the mixed sample (Table 2). The pCr bound from the mixture was less than that bound from single analyte solutions for the materials while the binding of pNP was only slightly impacted. The exception was M-0:100 for which the binding of pNP was reduced by 72% and that of pCr by 85% in the mixed sample. This result reflects the dramatically increased capacity for the binding of these analytes from single target solutions by M-0:100.

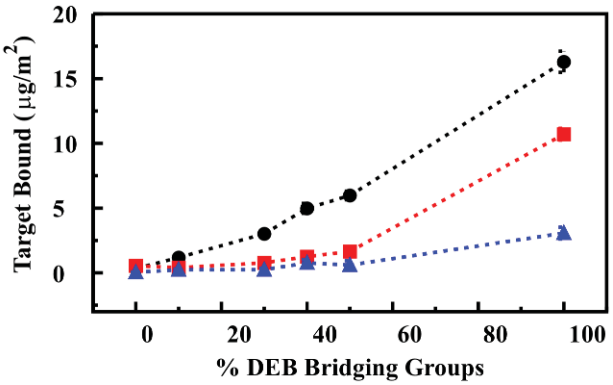

Figure 10. *Bridging group variations. The amount of target (TNT (●), pCr (■), pNP (▲)) bound by the materials increases as the percentage of DEB used during synthesis is increased. All target concentrations were 22 μM; data presented here is for adsorption from single target samples. The curves presented represent the average of three measurements.*

Imprinting the co-condensates through substitution of 12.5% DNB-Brij imprint molecule for Brij®76 was not found to significantly alter the materials characteristics (Table 2). The

effectiveness of imprinting in the co-condensates was evaluated by comparing the performance of the imprinted materials to that of the non-imprinted materials. Both single and multiple target experiments were employed. The adsorption of targets from mixtures must be considered with care due to the potential for solute-solute interactions. In addition, the relative affinity of each target for the available adsorption sites may vary resulting in more complicated adsorption behavior. Binding of the targets from single analyte solutions was similar for the imprinted and non-imprinted materials when less than 50% DEB bridging group was incorporated. An increase in TNT capacity was noted upon imprinting of M-0:100 (M-0:100 Imp; Table 2, based on single analyte solutions). The total pNP and pCr binding from single analyte solutions was not significantly impacted upon imprinting of the materials against the dinitrobenzene (DNB) analog (Table 2).

The effect of imprinting was more clearly observed when co-condensate materials were incubated with the mixture of TNT, pNP, and pCr. While M-100:0 and M-90:10 showed no difference in adsorption of TNT whether from the mixture or single analyte solution, M-100:0 Imp, M-90:10 Imp, and M-70:30 Imp showed a slight enhancement (~15%) in TNT absorption (Figure 11). This was in contrast to the decrease in TNT absorption seen with the non-imprinted materials upon incubation with the mixed sample. M-60:40 Imp, M-50:50 Imp, and M-0:100 Imp did not demonstrate enhanced TNT adsorption due to imprinting. In fact, these materials bound less TNT from the mixed sample as compared to single analyte samples (Figure 11). The involvement of non-specific binding sites may account for this behavior but the available data did not allow a conclusive determination. For all cases, the observed reduction in pCr and pNP binding from the mixed sample as compared to single analyte samples was greater for the imprinted materials than for the non-imprinted materials. This tended to indicate an enhancement in TNT selectivity upon imprinting. These results also indicated that the effectiveness of imprinting varied with percentage of incorporated DEB.

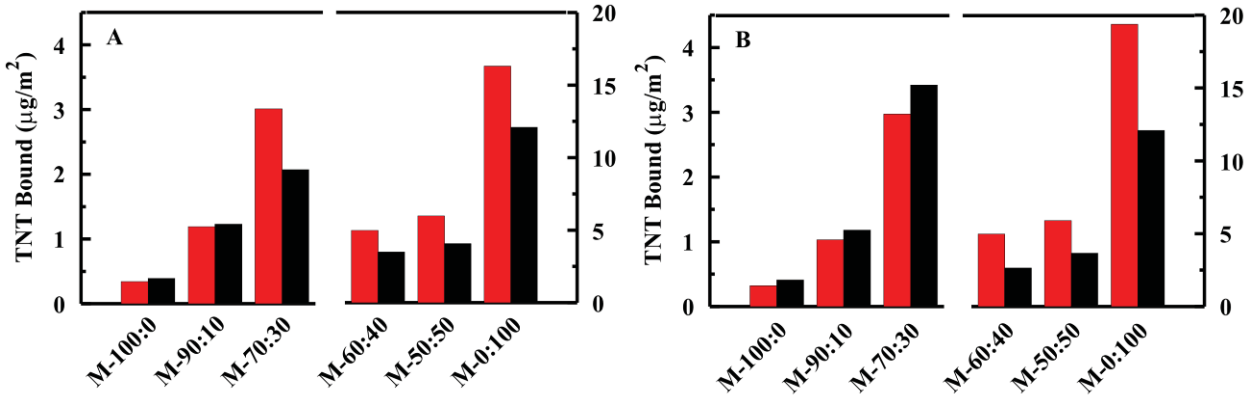

Figure 11. *Mixed samples. Here, the TNT bound from single (red) and mixed (black) target samples is compared for the nonimprinted (Panel A) and imprinted (Panel B) co-condensation variants. TNT, pNP, and pCr concentrations were 22 μM for all experiments. Note: The y-axes for the left and right sides of the graphs are different in order to provide scaling for low DEB content materials.*

Table 2. *Co-condensate materials characteristics and binding capacities.*

						Mixed Samples‡					
Material	% DEB†	% mod-Brij@	Surface Area (m^2/g)	Pore Volume (cm^3/g)	Pore Diameter (Å)	TNT*	TNT*	pNP*	pNP*	pCr*	pCr*
M-100:0	0	0	1180	1.07	38	0.34(0.02)	0.39(0.03)	0.04(0.03)	0.09(0.03)	0.55(0.03)	0.39(0.03)
M-100:0 Imp	0	12.5	1157	1.07	39	0.32(0.06)	0.41(0.07)	0.00(0.00)	0.03(0.01)	0.60(0.05)	0.29(0.02)
M-90:10	10	0	1071	0.75	28	1.19(0.04)	1.23(0.04)	0.24(0.04)	0.23(0.01)	0.40(0.02)	0.28(0.02)
M-90:10 Imp	10	12.5	1077	0.78	30	1.03(0.03)	1.18(0.03)	0.11(0.03)	0.00(0.00)	0.37(0.01)	0.19(0.02)
M-75:25	25	0	1056	0.63	22						
M-75:25 Imp	25	12.5	1075	0.64	23						
M-70:30	30	0	1004	0.56	21	3.01(0.05)	2.07(0.05)	0.24(0.02)	0.22(0.03)	0.77(0.01)	0.55(0.03)
M70:30 Imp	30	12.5	1095	0.60	22	2.97(0.02)	3.42(0.04)	0.35(0.03)	0.10(0.04)	0.74(0.05)	0.41(0.01)
M-60:40	40	0	922	0.52	<20	4.98(0.04)	3.49(0.05)	0.78(0.01)	0.73(0.04)	1.25(0.03)	0.90(0.07)
M-60:40 Imp	40	12.5	957	0.52	<20	4.97(0.05)	2.64(0.05)	0.75(0.01)	0.22(0.04)	1.32(0.03)	0.57(0.05)
M-50:50	50	0	813	0.46	<20	5.98(0.07)	4.07(0.04)	0.60(0.03)	0.73(0.03)	1.65(0.04)	1.14(0.02)
M-50:50 Imp	50	12.5	847	0.44	<20	5.90(0.05)	3.66(0.07)	1.59(0.05)	0.34(0.03)	1.69(0.02)	0.72(0.02)
M-0:100	100	0	356	0.20	<20	16.30(0.10)	12.09(0.10)	3.07(0.03)	0.86(0.05)	10.71(0.05)	1.65(0.03)
M-0:100 Imp	100	12.5	317	0.18	<20	19.36(0.08)	12.08(0.09)	3.03(0.02)	0.98(0.03)	12.93(0.06)	1.37(0.04)

** Amount of analyte bound in μg/ m^2. The number in parenthesis indicates the standard deviation of three measurements.*
@ Indicates the percentage of DNB-modified Brij®76 used to imprint the material.
† Indicates the percentage of DEB precursor used during synthesis.
‡ Gray shaded columns indicate the use of mixtures of targets.
All targets present at 22 μM.

Imprint Variations.

In order to determine the optimal imprint molecule concentration, M-70:30 materials were synthesized with 12.5%, 25%, 50%, and 100% of the Brij®76 surfactant replaced by DNB-Brij. This replacement was not found to strongly impact the surface area or total pore volume of the M-70:30 Imp, Imp 25, or Imp 50 materials (Table 3). The M-70:30 Imp 100 material showed significantly reduced surface area as compared to the other materials. The average pore diameter of the materials was found to increase with increasing imprint molecule incorporation from 21 Å (no imprint) to 31 Å (100% modified Brij®76). The changes in pore diameter appeared to be consistent with an alteration in the average length of the surfactant molecule employed.

Single analyte and mixed target solutions were again employed to determine binding capacities and to obtain estimates of the selectivity for TNT binding over that of similar molecules. Though a consistently increasing or decreasing trend was expected for this series of materials, this was not observed (Table 3). In fact, M-70:30 Imp 25 consistently bound less target than the other materials indicating some disruption of imprinting process. M-70:30 Imp 100 demonstrated marked improvement in TNT and DNT binding capacity as well as a slight enhancement in RDX binding capacity. With the exception of M-70:30 Imp 100, pNP, pCr, and RDX binding by the M-70:30 materials was minimal when compared to TNT binding. The addition of glycine (100 μM) to samples containing 22 μM TNT did not impact the adsorption of TNT by any of the M-70:30 materials (data not shown).

The imprint materials were incubated with several mixed sample solutions: TNT, pCr, and pNP (Solution A); TNT and DNT; TNT and RDX; and DNT and RDX (all analytes at 22 μM). Evaluation of target binding from Solution A indicated that the slight enhancement in TNT binding demonstrated by M-70:30 Imp (above) was also obtained for M-70:30 Imp 25 and M-70:30 Imp 50. It was not the case for M-70:30 Imp 100 where a significant decrease in TNT binding was observed when present in the mixture (Table 3). Although the M-70:30 Imp products did not exhibit meso-structures with long-range order that could be determined by XRD (contrast with M-100:0 products), most of them had uniform pore sizes as determined by nitrogen adsorption pore size distributions. These materials also yielded single low angle XRD reflections consistent with mesoporous materials that have uniform pore dimensions but disordered packing.[43,44] M-70:30 Imp 100 was notably different. It did not show a XRD reflection (Figure 12) and produced a broader, less sharply defined nitrogen adsorption pore size distribution compared to the other M-70:30 Imp variants (Figure 13). The nitrogen sorption isotherm (Figure 13) was distorted in shape with a wider hysteresis between the adsorption and desorption branches compared to the other variants which displayed type IV/type I isotherms common to mesoporous materials with uniform pore sizes ca. 20 Å. These distinct structural differences likely resulted in the unique behavior of M-70:30 Imp 100.

The DNT binding capacity of the M-70:30 materials was found to be comparable to that of the TNT. DNT was used as an alternative target in these studies because of the structural similarity to the imprint molecule and to TNT. The presence of DNT was found to compete for sites that bound TNT more strongly in M-70:30 Imp 100 than in the others with M-70:30 Imp showing the least impact (Table 4). Similarly, the presence of TNT had the least impact on DNT binding in M-70:30 Imp. The presence of RDX had little effect on either DNT or TNT binding in this material while strong competition between all three analytes was noted for M-70:30 Imp 100. M-70:30 Imp 25 showed the highest selectivity against RDX but the lowest total binding capacity for all targets.

Table 3. *Imprint variant materials characteristics and binding capacities.*

					Mixed Samples†							
Material	**% mod-Brij@**	**Surface Area (m^2/g)**	**Pore Volume (cm^3/g)**	**Pore Diameter (Å)**	**TNT***	**TNT***	**pNP***	**pNP***	**pCr***	**pCr***	**DNT***	**RDX***
M-70:30	0	1004	0.56	21	3.01(0.05)	2.00(0.05)	0.24(0.02)	0.22(0.03)	0.77(0.01)	0.54(0.03)	2.62(0.06)	0.87(0.03)
M-70:30 Imp	12.5	1095	0.60	22	2.97(0.02)	4.05(0.04)	0.35(0.03)	0.11(0.04)	0.74(0.05)	0.42(0.01)	3.05(006)	0.70(0.03)
M-70:30 Imp 25	25	977	0.59	23	2.13(0.04)	3.19(0.07)	0.33(0.03)	0.22(0.05)	0.63(0.03)	0.42(0.01)	2.55(0.05)	0.51(0.05)
M-70:30 Imp 50	50	1028	0.63	26	2.79(0.08)	3.80(0.05)	0.31(0.02)	0.13(0.02)	0.71(0.03)	0.33(0.02)	2.95(0.06)	0.64(0.04)
M-70:30 Imp 100	100	707	0.59	31	5.17(0.10)	2.44(0.10)	0.45(0.02)	0.23(0.02)	1.38(0.02)	0.51(0.04)	5.25(0.07)	1.17(0.05)

**Amount of analyte bound in μg/m^2. The number in parenthesis indicates the standard deviation of three measurements; @ Indicates the percentage of DNB-modified Brij®76 used to imprint the material; †Mixed samples are indicated by gray shading; All targets present at 22 μM.*

Table 4. *Targets bound from multi-target samples.*

Material	TNT*			DNT*			RDX*		
	TNT	TD†	TR‡	DNT	TD†	DR&	RDX	TR‡	DR&
M-70:30	3.01(0.05)	2.60(0.10)	2.95(0.09)	2.62(0.06)	2.06(0.09)	2.79(0.06)	0.87(0.03)	0.73(0.02)	0.47(0.03)
M-70:30 Imp	2.97(0.02)	2.81(0.10)	2.61(0.07)	3.05(0.06)	3.01(0.07)	2.95(0.08)	0.76(0.03)	0.57(0.05)	0.76(0.04)
M-70:30 Imp 25	2.13(0.04)	1.84(0.13)	1.97(0.10)	2.55(0.05)	2.05(0.08)	1.99(0.07)	0.51(0.05)	0.34(0.03)	0.04(0.03)
M-70:30 Imp 50	2.79(0.08)	2.32(0.11)	2.54(0.09)	2.95(0.06)	2.52(0.08)	2.77(0.07)	0.64(0.04)	0.50(0.03)	0.43(0.01)
M-70:30 Imp 100	5.17(0.10)	4.07(0.09)	4.38(0.11)	5.25(0.07)	4.43(0.06)	4.85(.010)	1.17(0.05)	0.85(0.02)	0.91(0.03)

** Amount of analyte bound in μg/m^2. The number in parenthesis indicates the standard deviation of three measurements. Single target samples contained 22 μM of the indicated compound; † Sample contained 22 μM TNT and DNT; ‡ Sample contained 22 μM TNT and RDX; &Sample contained 22 μM DNT and RDX.*

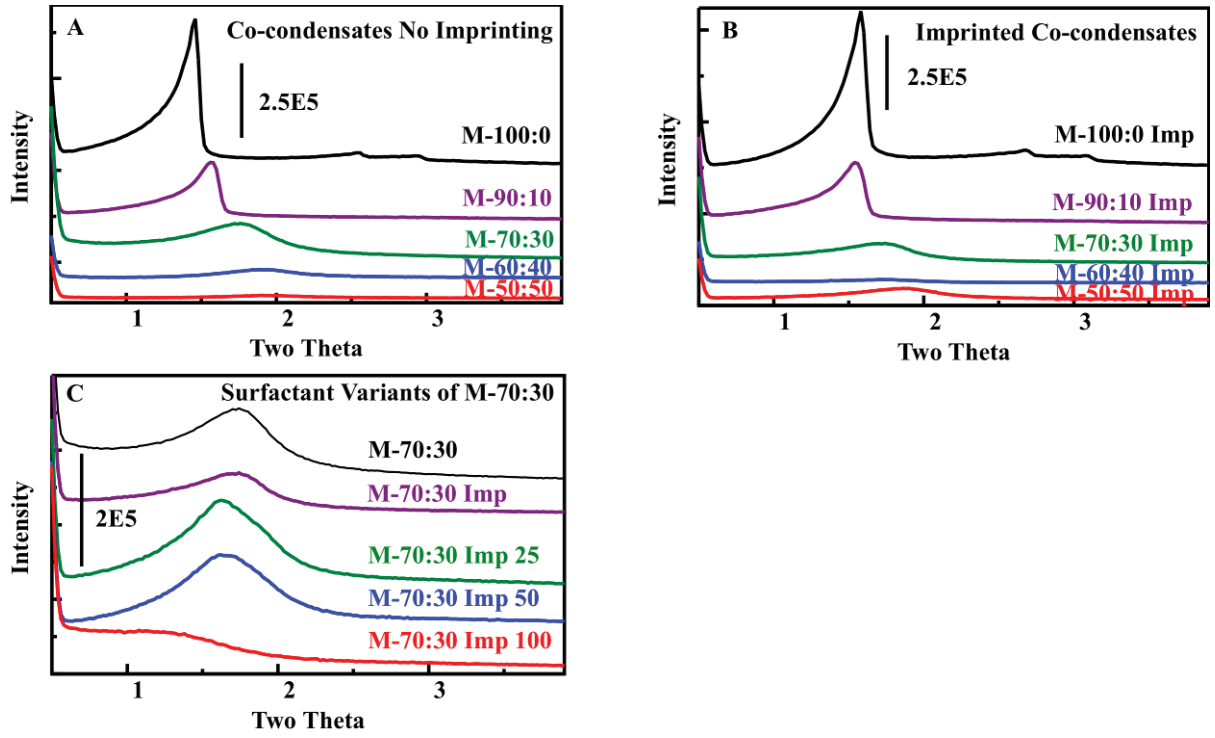

Figure 12. *XRD spectra for the materials synthesized: co-condensates with varying DEB concentrations (Panel A); co-condensates with varying DEB concentrations imprinted using 12.5% DNB-modified Brij®76 (Panel B); 70% BTE: 30% DEB co-condensates imprinted using varying ratios of Brij®76 to modified Brij®76 (Panel C). XRD spectra for 100% DEB materials are not presented due to the lack of features.*

In order to obtain a number indicative of affinity, linear fits for the double reciprocal form of the isotherms presented in Figure 14 were generated (Figure 15; units converted to μg/m^2 vs. μg). The fitting parameters obtained were used to determine the parameters of the Langmuir-Freundlich model isotherms of the form:

$$q = \frac{q_s k[L]^n}{1 + k[L]^n} \qquad \textit{(Equation 1)}$$

which allowed for calculation of q_s as the inverse of the y-intercept and k as the ratio of the y-intercept to the slope when n was held at a constant value of 1 (Table 5). Here, q_s is the saturation capacity; [L] is the concentration of unbound target, q is the bound target; and n is the heterogeneity index. The Langmuir-Freundlich model is a generalization of the Langmuir model used to account for surface heterogeneity (non-identical sites).[45,46] The Langmuir model, representing a general binding isotherm for identical, independent binding sites possessing an association constant of k for the specified ligand, is recovered for the case when the heterogeneity index is unity. Good fitting parameters for q_s and k were obtained when the heterogeneity index was fixed at unity. Accurate values of n could not be determined due to the limited range of concentrations available from the adsorption experiments. The range was limited due to two factors: First, TNT stocks are received as 1 mg/ml solutions in acetonitrile. In order to prevent alterations in target adsorption owing to adsorbent wetting conditions and target

solubility, the final acetonitrile concentration in samples was kept to a minimum and held constant. The other factor was the restraints implicit in the use of HPLC for determination of concentration. The range of concentrations tested in these studies was achieved by varying the amount of adsorbent while holding the TNT concentration constant. Based on this isotherm units of inverse µg for k and µg/m^2 for q_s were obtained These units did not allow for comparison to association constants in solution, for example, but they did provide a metric for comparison of the various materials to each other.

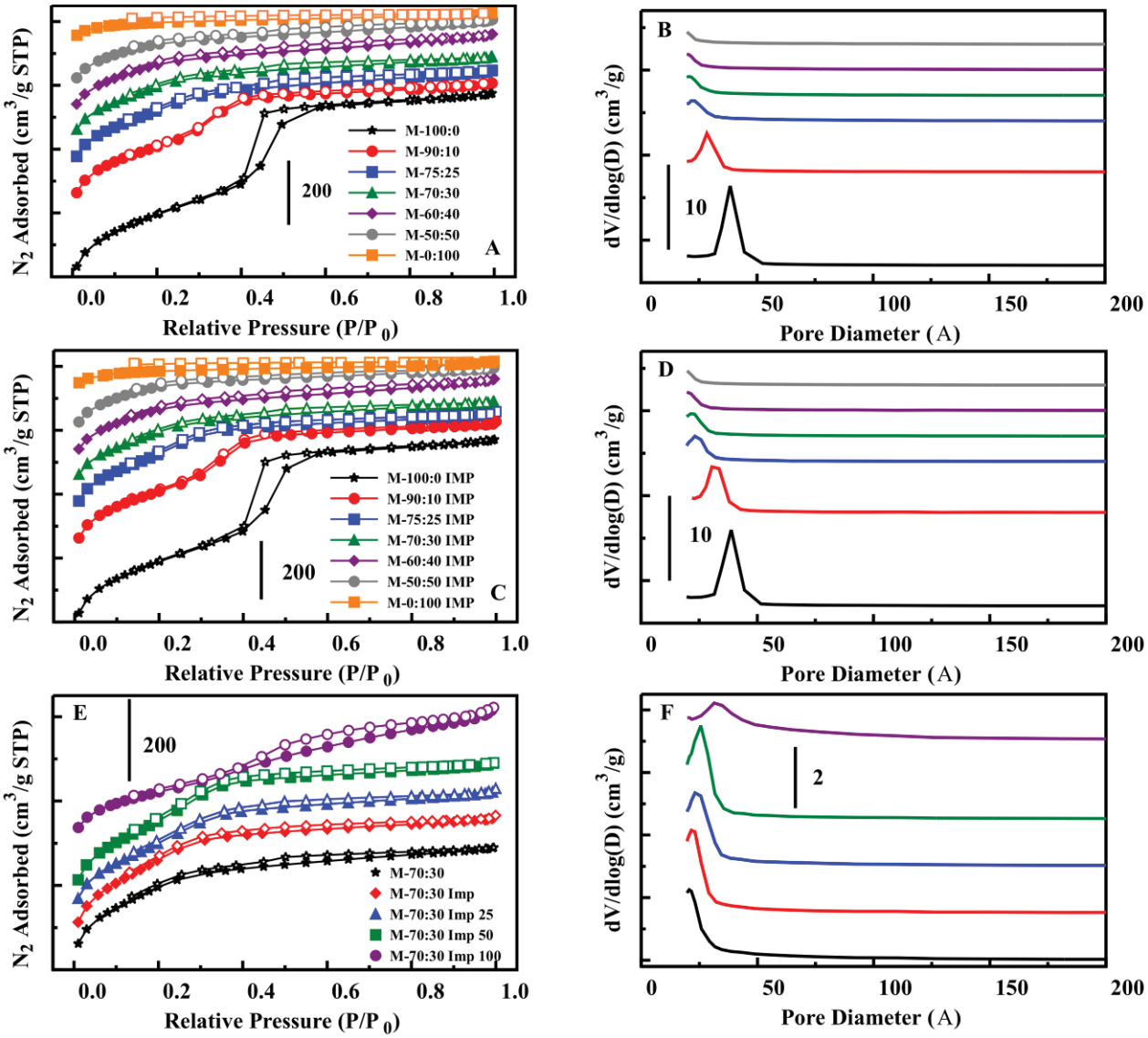

Figure 13. *Nitrogen sorption isotherms and pore diameter distributions for each of the materials synthesized: co-condensates with varying DEB concentrations (Panels A and B); co-condensates with varying DEB concentrations imprinted using 12.5% DNB-modified Brij®76 and 87.5% Brij®76 (Panel C and D); 70% BTE: 30% DEB co-condensates imprinted using varying ratios of Brij®76 to modified Brij®76 (Panel E and F).*

The method of Ockrent [47] and Weber [48] for prediction of the adsorption of two targets provides another method for determining the heterogeneity of binding sites. This technique is based on an extension of the Langmuir model and is analogous to the relationship proposed for mixed-gas adsorption. The following relationship is reported:

$$\frac{n_1^{mix}}{n_1^{\sin gle}} = 1 - \frac{n_2^{mix}}{n_2^{\sin gle}} \qquad \textit{(Equation 2)}$$

where n_1^{mix} is the concentration of target 1 absorbed from the mixture of target 1 and target 2 and n_1^{single} is the concentration of target 1 adsorbed from the single analyte solution when the total initial target and adsorbent concentrations are fixed at the same value for all solutions. Similarly for n_2, "mix" indicates the two target solution and "single" indicates the single analyte solution. Deviation from this relationship indicates heterogeneity; the greater the deviation the larger the diversity of sites. When this relationship was applied to the data obtained using the imprint variants, M-70:30 Imp 25 was found to display the strongest deviation from the expression (Equation 2). The other four materials performed similarly to one another with deviations of less than 0.15 from the linear function (Tables 6 and 7).

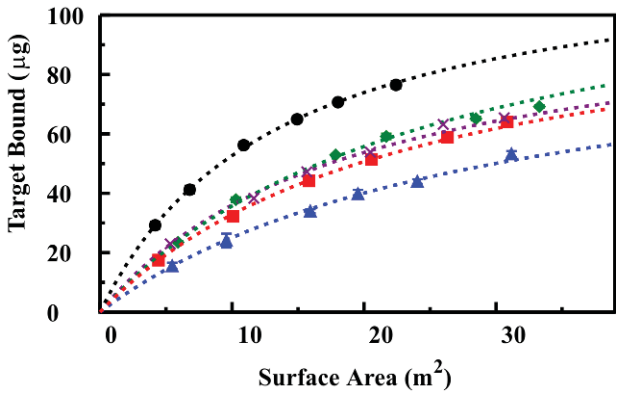

Figure 14*. Binding isotherms. TNT binding isotherms and the corresponding curve fits are presented for each of the surfactant variants: M-70:30 (**x**), M-70:30 Imp (♦), M-70:30 Imp 25 (▲), M-70:30 Imp 50 (■), M-70:30 Imp 100 (●). The TNT concentration was 22 µM for all experiments. Curve fit parameters are provided in Table 5.*

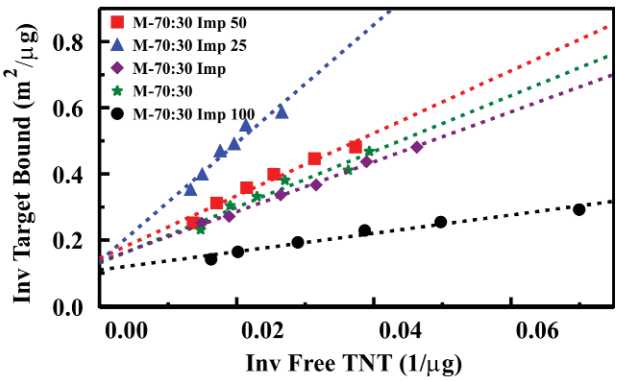

Figure 15. *Double reciprocal form of the TNT binding isotherms presented in Figure 14, used to generate fitting parameters for each of the materials (Table 5). These parameters were used to calculate association constants for the materials to facilitate comparisons between these and other materials.*

Table 5. *Fit parameters and calculated constants from TNT binding isotherms.*

	slope (m^2)	***y*-intercept ($m^2/\mu g$)**	**q_s ($\mu g/m^2$)**	**k (μg^{-1})**
M-70:30	8.44	0.1305	7.66	0.0155
M-70:30 Imp	7.54	0.135	7.41	0.0179
M-70:30 Imp 25	17.86	0.1362	7.34	0.0076
M-70:30 Imp 50	9.45	0.1451	6.89	0.0154
M-70:30 Imp 100	2.77	0.1097	9.12	0.0396

The calculated association constants further illuminated an unexpected trend in the materials (Table 5). While M-70:30 Imp 100 was superior to the other materials in terms of saturation capacity and association constant, the saturation capacity of the materials decreased with increasing imprint molecule concentration from 0 to 50%. M-70:30 Imp 25 demonstrated the weakest association constant. M-70:30 was found to have the second strongest association constant followed by nearly identical capacities for M-70:30 Imp and M-70:30 Imp 50. These trends may have resulted from surfactant partitioning during the synthesis of the materials. If the DNB-Brij and Brij®76 tended to separate within the micelles, transitions from Brij®76 regions to DNB-Brij regions would result. These transitions could cause disruption of the pore wall structure upon condensation, thereby reducing the functional surface area of the materials. The greatest impact of this effect would be observed for micelles with the highest number of transitions; there would be none for M-70:30 Imp 100 or M-70:30. M-70:30 Imp used a very low concentration of DNB-Brij, so formation of separate Brij®76/DNB-Brij regions would be unlikely. The high concentration of DNB-Brij in M-70:30 Imp 50 should result in formation of large regions of DNB-Brij within the micelles and, therefore, the number of transitions would be reduced as compared to M-70:30 Imp 25.

Table 6. *Targets bound from mixed samples.*

Material	**TNT***			**DNT***			**RDX***		
	TNT	TD†	TR‡	DNT	TD†	DR&	RDX	TR‡	DR&
M-70:30	3.01	1.64	1.77	2.62	1.40	1.55	0.87	0.31	0.30
M-70:30 Imp	2.97	1.65	1.73	3.05	1.39	1.54	0.70	0.29	0.29
M-70:30 Imp 25	2.13	1.12	1.12	2.55	0.99	1.06	0.51	0.00	0.12
M-70:30 Imp 50	2.79	1.58	1.71	2.95	1.34	1.50	0.64	0.27	0.26
M-70:30 Imp 100	5.17	2.73	2.96	5.25	2.33	2.61	1.17	0.47	0.47

** Amount of analyte bound in $\mu g/m^2$; all samples contained 22 µM target; † Sample contained 11 µM TNT and DNT; ‡ Sample contained 11 µM TNT and RDX; & Sample contained 11 µM DNT and RDX.*

Table 7. *Heterogeneity as indicated by ratios of target adsorption from single and multi-target solutions.*

Material	**TNT and DNT**		**TNT and RDX**		**DNT and RDX**	
	TNT(TD)/TNT(1)*	DNT(TD)/DNT(1)	TNT(TR)/TNT(1)	RDX(TR)/RDX(1)	DNT(DR)/DNT(1)	RDX(DR)/RDX(1)
M-70:30	0.54	0.46	0.59	0.35	0.59	0.35
M-70:30 Imp	0.56	0.54	0.58	0.41	0.51	0.42
M-70:30 Imp 25	0.52	0.61	0.52	0.00	0.41	0.23
M-70:30 Imp 50	0.57	0.55	0.61	0.42	0.51	0.41
M-70:30 Imp 100	0.53	0.56	0.57	0.40	0.50	0.40

** Ratio of target adsorbed from multi-target solution to that adsorbed from single target solution from Table 5.*
(1) indicates single target solution; TD, TR, and DR are two-target solutions as defined in Table 5.

Hierarchical Materials.

While PMO sorbents provide the desired binding characteristics for TNT, the mesoporous nature of the materials presents disadvantages for their application in in-line preconcentration formats. Small particle sizes result in dense packing. When combined with poor interconnectivity and small pore sizes (~30 Å), flow in a column format experiences high backpressure levels. Mixing with sand or other such materials can resolve this issue, but these approaches also lead to reduced active site concentration within the column. Materials may also slowly compact at the end of the column, resulting in increasing backpressure over time. We applied the lessons learned with the PMO sorbents to the development of a new type of material with a view toward addressing this issue.[38] This material uses a larger surfactant (Pluronic P123) with a swelling agent to effect a process called spinodal decomposition during synthesis. The result is a hierarchical sorbent with mesopores organized within macropores to provide improved access and reduced pressure.

The development of the hierarchical macroporous-mesoporous DEB-bridged organosilicates involved consideration of many of the variables described for the PMO materials. As indicated above, DEB offers enhanced functionality over benzene and ethane bridging groups. This utility in the adsorption of nitroenergetic targets from aqueous solution makes the development of materials of this type in column applicable formats desirable. The materials developed include hierarchical co-condensed BTE-DEB materials, hierarchical DEB materials, and mesoporous DEB materials into which additional functionality has been incorporated through the inclusion of pendant functional groups.

Ethane-diethylbenzene-bridged silicas (ED)

Based on previous success in the application of bis(trimethoxysilylethyl)benzene (DEB) bridged mesoporous materials, a hierarchical material of similar composition was desired. This material was expected to offer the binding characteristics of the mesoporous material with improved performance in a column format. The procedure of Nakanishi et al. for synthesizing macroporous-mesoporous monoliths of ethane-bridged silica [37] was adapted to accommodate the incorporation of 50-75 mol% DEB. The amount of 0.1 M aqueous nitric acid was fixed at 6.07 g, and materials were synthesized using 0.3, 0.35, and 0.4 g TMB. A temperature of 80 ºC was effective for evaporation drying. After refluxing in ethanol to remove surfactant, nitrogen sorption isotherms of the products designated ED1-ED3 were type IV in shape with H2 hysteresis between the adsorption and desorption branches (Figure 16). The desorption branches closed with the adsorption isotherms ca. relative pressure 0.4. This is the lower limit of stability for a meniscus of capillary condensed nitrogen and, therefore, does not necessarily reflect the presence of pore obstructions or irregularities.[49] Pore size distributions for the materials were relatively narrow and indicative of uniform mesopores (Figure 17).

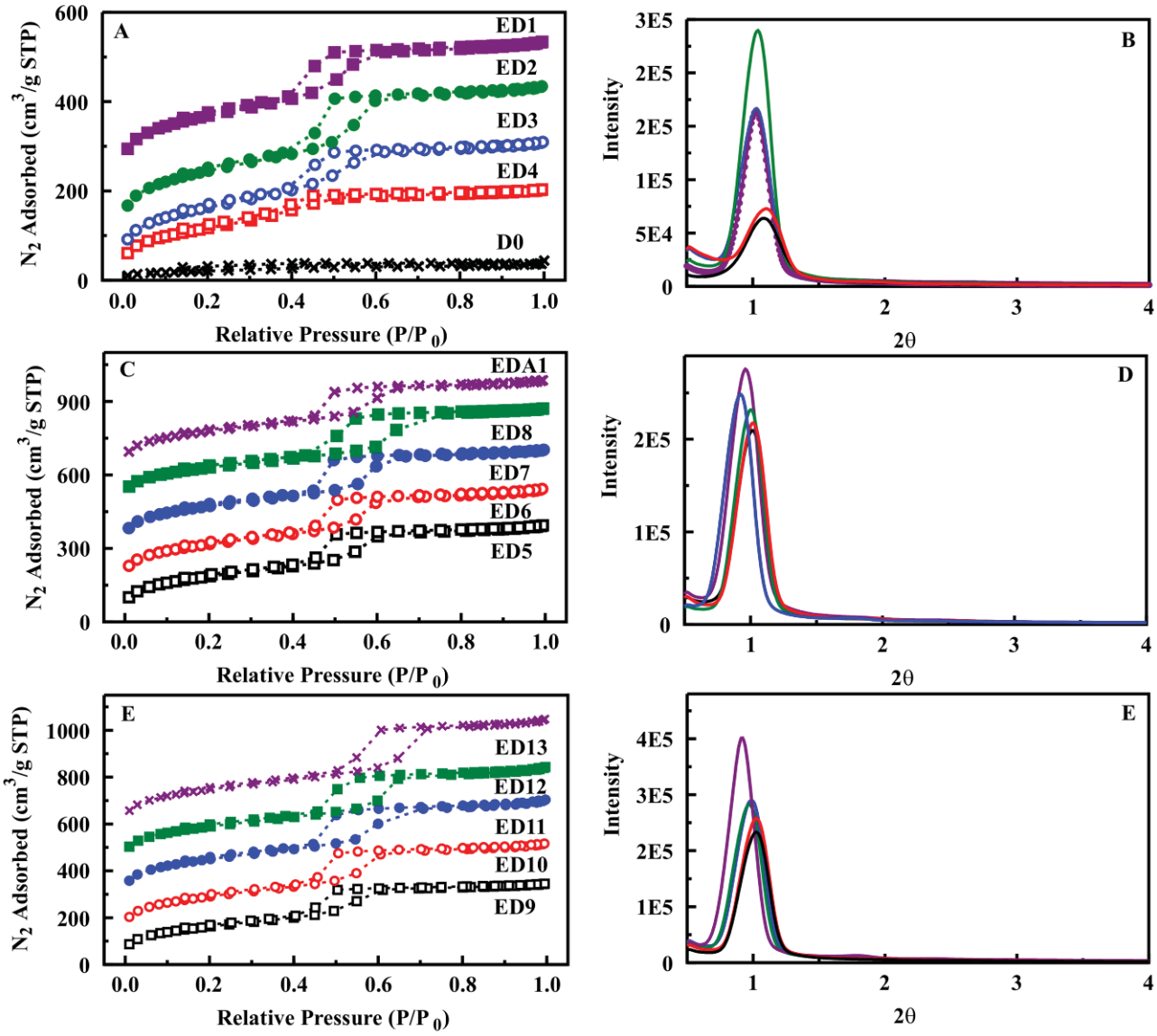

Figure 16. *Nitrogen sorption isotherms (A, C, E) and XRD patterns (B, D, E) for ethane-diethylbenzene silica materials (Panel A) ED1 shifted by 200, ED2 shifted by 75, ED3, ED4, and D0. (Panel B) ED5, ED6 shifted by 125, ED7 shifted by 275, ED8 shifted by 450, and EDA1 shifted by 600. (Panel C) ED9, ED10 shifted by 100, ED11 shifted by 250, ED12 shifted by 400, and ED13 shifted by 550.*

Porosity data for the ED products are listed in Table 8. Increasing the amount of TMB in the syntheses did not significantly alter the measured surface areas (ca. 600 m^2/g) or pore volumes (0.47-0.55 cm^3/g) for the resulting materials. Although TMB is normally an effective micelle swelling agent applied to obtain larger mesopores, the data did not demonstrate a direct relationship between TMB concentration and pore size (Table 8). It is possible that π-π interactions between phenylene bridges in DEB might counter the activity of TMB under some conditions. This could lead to penetration of the micelles with resultant lower pore sizes. More

evidence of this possibility will be presented below. Overall, porosity values were lower than those of similarly synthesized materials consisting of 100% BTE. BTE materials were found to have surface areas of 700-800 m^2/g, pore volumes greater than 1 cm^3/g, and mesopore sizes ca. 75 Å (not shown). Powder X-ray diffraction patterns of ED1-ED3 (Figure 16) displayed a peak in the low angle region near 1° 2θ which could be attributed to the (100) reflection common for mesoporous materials with hexagonal order. However, a weak increase in intensity was observed in the general region where resolved (110) and (200) reflections would be expected. This indicated that order did not encompass long ranges. The low angle XRD peak, produced by these materials, was notably absent in a non-porous 50 BTE: 50 DEB material synthesized without TMB additive.

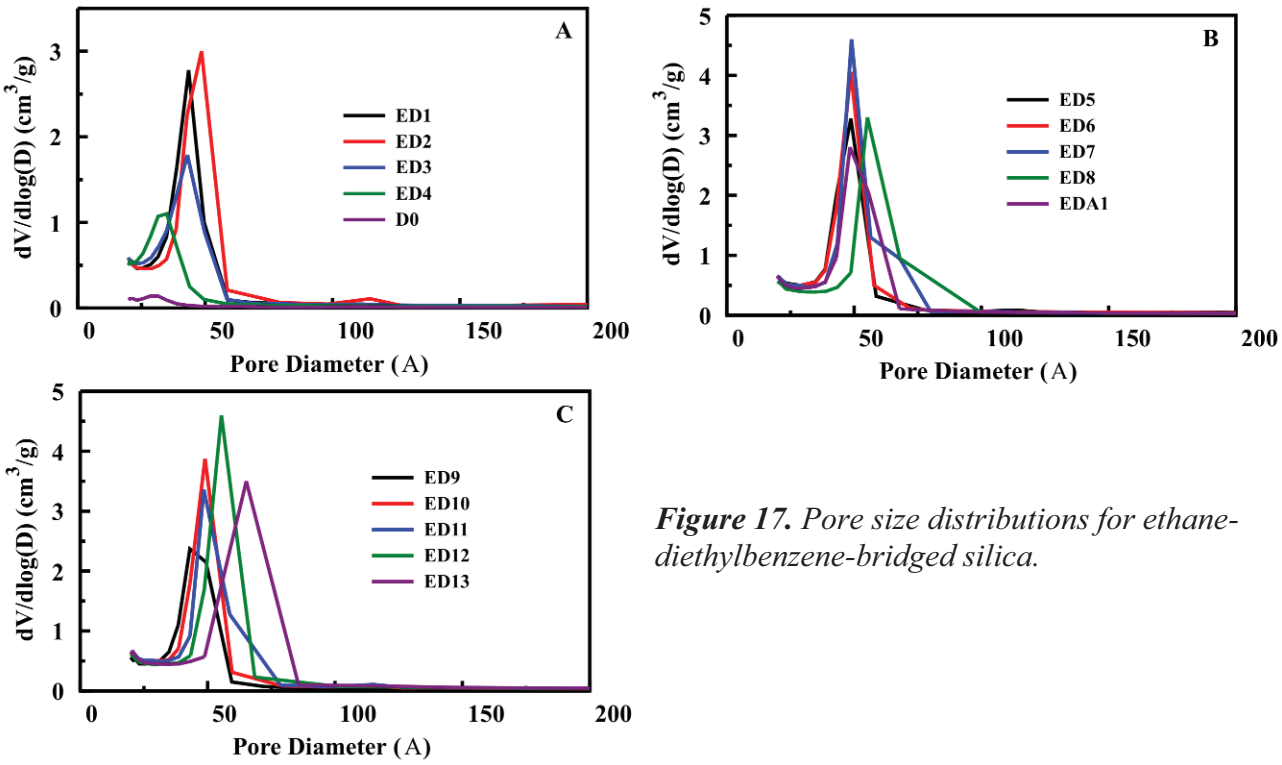

Figure 17. *Pore size distributions for ethane-diethylbenzene-bridged silica.*

Incorporating greater amounts of DEB in the materials was, as expected, detrimental to mesoporosity. ED4 was synthesized with 75% DEB and had a reduced mesopore size of 35 Å. The isotherm and XRD characteristics for ED4 were similar to those of ED1 – ED3. A 29 Å pore size was measured for a product synthesized using 100% DEB (D0), but it yielded a very low pore volume of 0.0549 cm^3/g and an isotherm that had more Type I character than those of the ED products. Thermogravimetric analysis (TGA) showed that surfactant accounted for only approximately 5% of the weight of D0 indicating that the low porosity was due to a lack of mesostructure and not to entrapped surfactant. XRD patterns of ED4 and D0 with more incorporated DEB and smaller pore sizes showed reflections ca. 1.1° 2θ that were less intense than those observed for the ED1, ED2, and ED3 products.

Table 8. *Nitrogen adsorption data for ethane-diethylbenzene-bridged silica materials.*

Material	Ratio BTE:DEB	Mass TMB (g)	Mass 0.1 M HNO_3	BET Surface Area (m^2/g)	Pore Volume (cm^3/g)	BJH pore size (Å)
ED1	50:50	0.3	6.07	606	0.509	44
ED2	50:50	0.35	6.07	614	0.548	49
ED3	50:50	0.4	6.07	587	0.471	43
ED4	25:75	0.4	6.07	427	0.310	35
D0	0:100	0.4	6.07	75	0.0549	29
ED5	50:50	0.3	6.5	675	0.599	49
ED6	50:50	0.3	7.0	696	0.633	49
ED7	50:50	0.3	7.5	715	0.653	49
ED8	50:50	0.3	8.5	648	0.644	55
ED9	50:50	0.35	7.5	589	0.527	46
ED10	50:50	0.4	7.5	691	0.632	49
ED11	50:50	0.5	7.5	722	0.632	49
ED12	50:50	0.55	7.5	683	0.667	55
EDA1	*50:50	0.55	7.5	648	0.587	48
ED13	50:50	0.6	7.5	712	0.749	65

** 0.05 g APS included in synthesis.*

SEM images of the ED1 – ED3 materials showed significant differences in morphology with variations in TMB concentration (Figure 18). ED1 (0.3 g TMB) exhibited spherical cavities with some, though not extensive, interconnectivity. Such distinct pores were not present in ED2 and ED3 synthesized with increased amounts of TMB (0.35 and 0.4 g, respectively). These materials were roughly textured and appeared to be agglomerations of small irregularly shaped particles. When the amount of DEB was increased to 75% to produce ED4, a macroporous morphology similar to that of ED1 was obtained (Figure 18).

Based on the results presented above, the amount of TMB in a synthesis was fixed at 0.3 g and the amount of aqueous nitric acid was varied (6.5 to 8.5 g) for 50% DEB materials. Macropores of indistinct shape with some torturous connectivity resulted (ED5 - ED8; Figure 18). None of these materials had the highly open co-continuous macropore morphologies that have been reported for 100% ethane-bridged silicates. ED5 – ED8 were found to have improved mesoporosity characteristics as compared to ED1 – ED3 with surface areas greater than 600 m^2/g, pore volumes greater than 0.6 cm^3/g, and larger pore sizes (up to 55 Å for ED8). XRD reflections (Figure 16) appeared at slightly lower 2θ values for these materials. Nitrogen sorption isotherms (Figure 16) indicated that capillary condensation occurred at higher relative pressure (P/P_0), ca. 0.55 in the adsorption branches. The nitrogen desorption branches tended to close with the adsorption branches at $P/P_0 > 0.4$, with ED8 having a type H1 hysteresis shape in which the branches were parallel to each other.

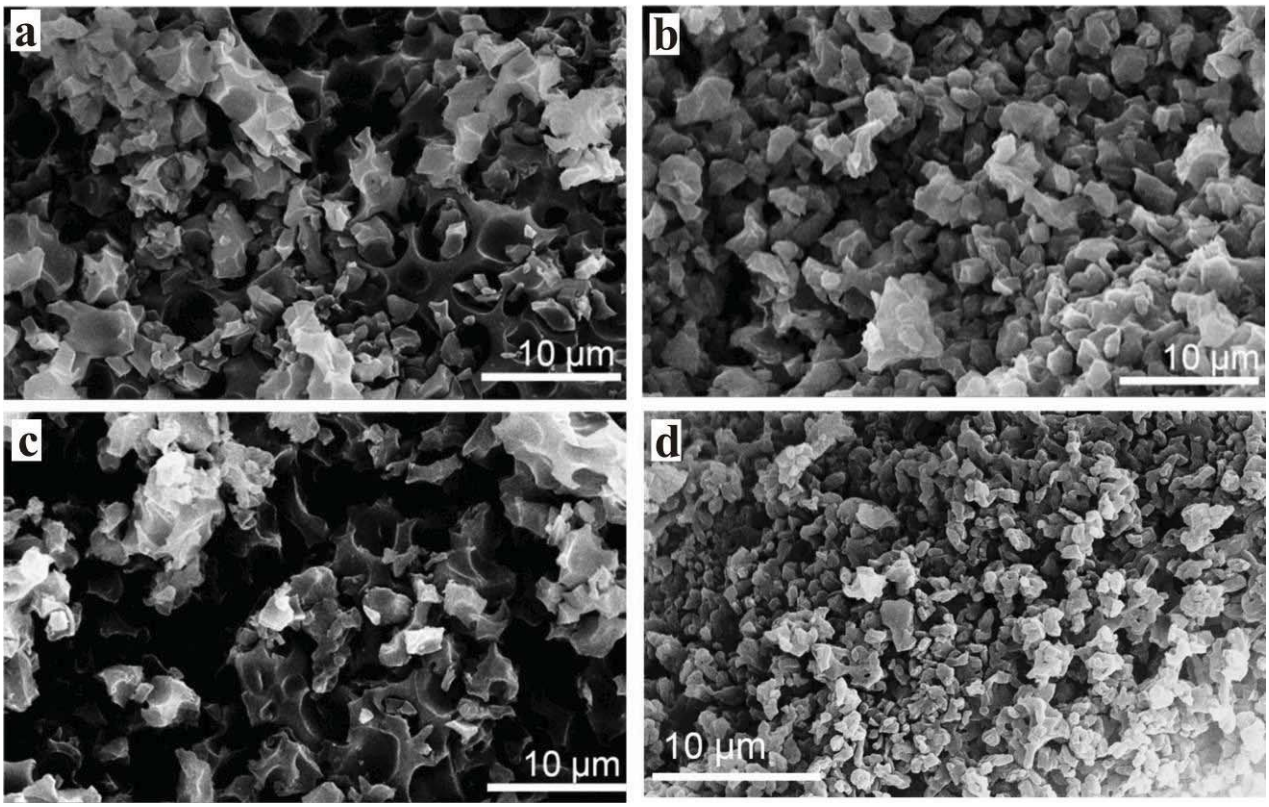

Figure 18. *Scanning electron micrographs of a) ED1 b) ED2 c) ED4 and d) ED6*

To further investigate optimization of the materials, the nitric acid amount was fixed at 7.5 g and the amount of TMB was varied. The resulting materials had higher mesoporosity values (Table 8) and enhanced macroporous structures. SEM images of ED10 with 0.4 g of TMB showed evidence of micron-scale spherical cavities not seen in ED3 synthesized with less acid (Figure 19). Inclusion of 0.5 - 0.6 g of TMB (ED11-ED13) resulted in larger mesopore sizes (≥ 49 Å) and nitrogen sorption isotherms with type H1 hystereses (Figure 16). The SEM of ED11 displayed aggregates of cylindrical and curved particles with less evidence of distinct spherical voids (Figure 19). A slightly greater amount of TMB (0.55 g) resulted in connectivity that formed a strut-like framework with extensive macroporosity (ED12; Figure 19). This structure strongly resembled the co-continuous morphology that was reported for P123-templated ethane-bridged[37] and benzene-bridged silicas.[50,51] Inclusion of 0.6 g TMB (ED13) coarsened the struts and somewhat disrupted the continuity of the macropores (Figure 19); however, ED13 had the highest mesoporosity characteristics of the materials synthesized for this study with a surface area of 712 m^2/g, total pore volume of 0.749 cm^3/g, and a mesopore size of 65 Å.

Transmission electron micrographs of ED12 and ED13 are shown in Figure 19. Hexagonally ordered mesostructures are clearly observable in these images and those of various other ED materials. Secondary XRD peaks that are the fingerprint of well-ordered mesoporous silicates such as MCM-41 and SBA-15 were not observed. ED13 diffracted X-rays more intensely than other materials according to its powder pattern, but (110) and (200) reflections were not resolved (Figure 16). This can be interpreted as an effect of these ED products having more irregularities

in their mesostructures compared to previously reported mesoporous materials and may contribute to the lack of DEB PMOs reported despite the commercial availability of the silane precursor.

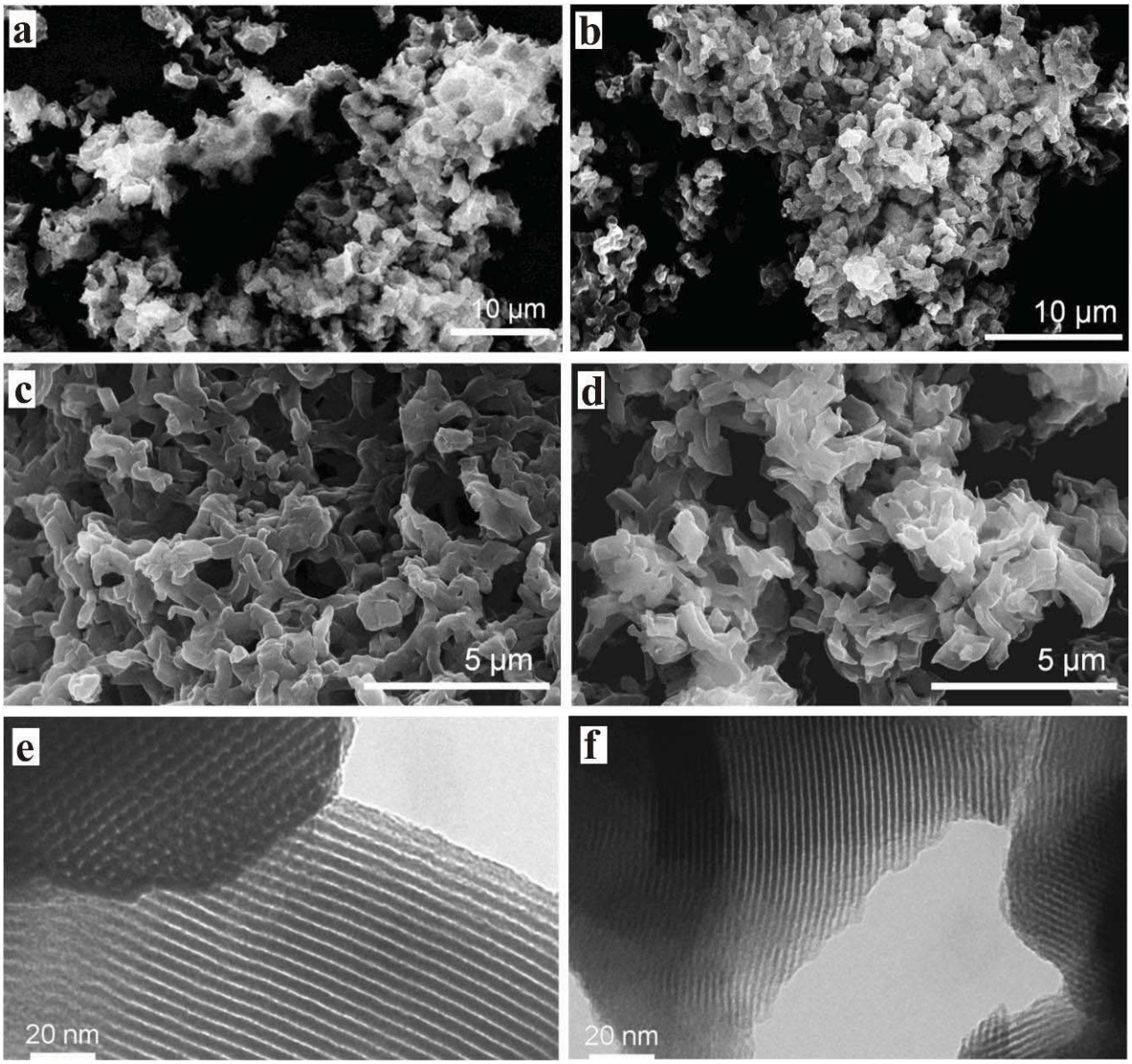

Figure 19. *Scanning electron micrographs of a) ED10 b) ED11 c) ED12 and d) ED13. Transmission electron micrographs of e) ED12 and f) ED13.*

TGA of materials with high DEB compositions was used to evaluate the efficiency of surfactant removal from the silicate frameworks. It was determined that measurable amounts of P123 remained after three reflux extractions in ethanol. An example is presented in Figure 20 of a 50% DEB product (ED12) after three ethanol extractions and after a fourth extraction with acidic ethanol. A small mass loss occurring before 100 ºC of < 5% is common due to adsorbed solvent and/or moisture. P123 decomposes by 400 ºC and accounted for a loss of 21 wt%. This

tends to indicate that some triblock copolymer chains were entangled in the pore walls, although nitrogen sorption data proved that there was significant mesoporosity with a surface area of 456 m^2/g despite incomplete removal of surfactant. The measured surface area increased to 683 m^2/g after a subsequent extraction with 1 M hydrochloric acid in ethanol, and TGA weight loss due to P123 was reduced to 7%. Calcination of the materials for surfactant removal was not possible because, as indicated by TGA, bridging groups start to decompose before 300 °C. Multiple refluxes resulted in fine particle sizes, as is apparent in the SEM images.

Characterization by solid-state NMR spectroscopy would confirm the incorporation of DEB bridging groups in the final products, however, this technique was unavailable. Mesoporous powders previously reported by Li et al. in which DEB was co-condensed with other silanes or used as a sole precursor were characterized using ^{13}C cross-polarization magic-angle spinning and ^{29}Si magic-angle spinning NMR spectroscopy.[52] It was determined that diethylbenzene bridging groups were incorporated in the pore walls for those materials without observable Si-C bond cleavage. We have previously reported significant enhancement in binding capacities for nitroenergetic targets upon increasing the ratio of DEB to BTE in mesoporous precipitates prepared by co-condensation.[32] The materials described here were synthesized as gels under relatively gentle conditions, so intact DEB bridging groups were expected in the pore walls. Figure 20 provides TGA evidence of surfactant-extracted D0 (100 % DEB) and a 100 % BTE analog of composition P19E-40 reported by Nakanishi et al. [37] Based on the difference in masses of ethane and diethylbenzene bridging groups, a 100 % BTE material is expected to undergo a weight loss that is approximately 38 % of that observed for a 100 % DEB material. Direct comparison is complicated by adsorbed solvent and surfactant residue as noted above along with incomplete combustion under a nitrogen atmosphere, however, a difference in the materials was apparent (Figure 20). TGA of the 100 % BTE product showed a mass loss in the temperature range 200-600 ºC that was approximately 39 % of that measured for the 100 % DEB material.

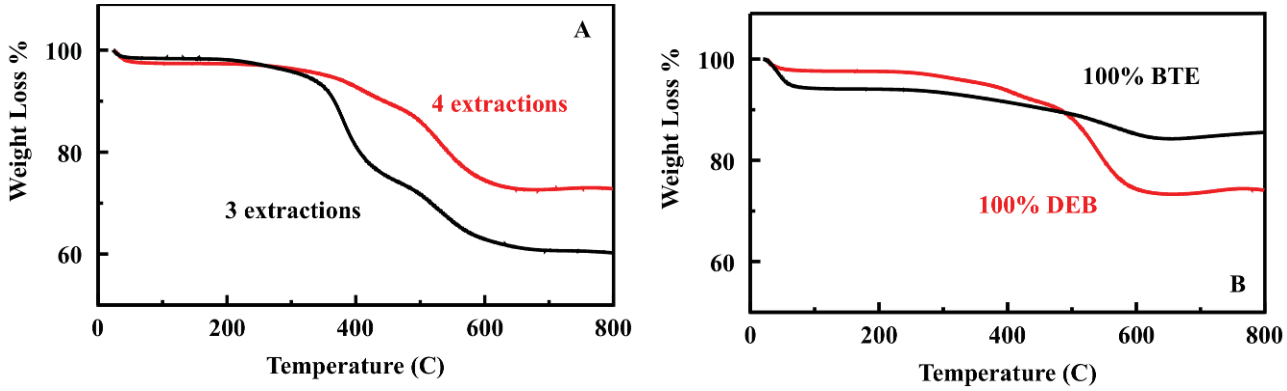

Figure 20. *Thermogravimetric analysis of (Panel A) 50 BTE:50 DEB material (ED12) after three reflux extractions with ethanol and a fourth reflux extraction with 1 M HCl in ethanol; (Panel B) 100% BTE (P19E-40) and 100% DEB (D0) materials after extraction.*

Macroporous-mesoporous silica monoliths have potential as columns for chromatographic separations.[53] All of the materials described here were originally obtained as cylindrical monoliths as a result of using culture tubes for reaction chambers. Refluxing in alcohol crumbled the monoliths into fine particles, but was convenient for removing P123 without damaging the

organic bridging groups in the pore walls. Monolithic morphology could be retained by performing a Soxhlet extraction (Figure 21). The process is time-consuming and less efficient than refluxing; however, enough surfactant could be removed to take advantage of the mesostructure of the material. A monolith (composition ED12) that was Soxhlet extracted with 1 M HCl in ethanol for five days had a measured surface area of 246 m^2/g and pore volume equal to 0.421 cm^3/g. Extraction with supercritical carbon dioxide using an alcohol co-solvent may offer a more efficient alternative for removing surfactant if monolithic morphology in the material is desired.[54]

Figure 21. *Photograph of a 50% DEB monolith as-synthesized (left) and following Soxhlet extraction with 1 M HCl in ethanol for 5 days (right).*

Ethane-diethylbenzene-bridged amine and phenyl silicas (EDA, EDP, and EDPA)

Hierarchical pore structures are expected to enhance the utility of diethylbenzene-bridged silicas for adsorbing compounds of interest. PMOs with both DEB and amine functionalities can simultaneously adsorb phenyl compounds and metal ions.[25] Surface amine groups can also be used to anchor molecules for sensing or catalytic applications. A product (EDA1) was prepared similarly to macroporous-mesoporous ED12 with the addition of 0.05 g of 3-aminopropyltrimethoxysilane (APS) in the reaction sol. The slightly reduced porosity values of EDA1 were expected due to the disrupting effect of the APS precursor (Table 8). The material was mesoporous with a surface area of 648 m^2/g and a narrow pore size distribution at 48 Å. The direct addition of APS to the synthesis appeared to coarsen and disrupt the co-continuous macropore structure seen for ED12. TEM confirmed that the material maintained a mesostructure with hexagonal order. Post-synthesis grafting would be an alternative for functionalizing the surfaces of an ED material while maintaining its co-continuous macropore morphology.

Motivation to design porous adsorbents targeting particular toxic and nitroenergetic compounds led to further modification of the sorbent structure through incorporation of pendant phenyl groups. Materials were synthesized for which 10 mol% of the silicon in an ED (subtracted from the DEB component) was replaced with phenyltrimethoxysilane (PTS). EDP materials prepared with Si molar ratio 50 BTE: 40 DEB: 10 PTS were mesoporous as indicated by their type IV nitrogen sorption isotherms with H2 hystereses (Figure 22). They featured reduced surface areas, pore volumes, and pore sizes (Table 9) compared to their ED counterparts. Again, this was not unexpected for materials having pendant phenyl groups on the mesopore surfaces and/or encapsulated in the mesopore walls. The corresponding XRD peaks in Figure 22 appeared at higher 2θ values (lower *d*-spacings) indicating, along with the smaller pore sizes,

that PTS did not contribute as much to mesopore wall thickness as DEB did. EDP materials were further modified through inclusion of APS in the reaction sols. Addition of 0.05 g of APS required 2 g more aqueous nitric acid to obtain a homogeneous mixture and prevent immediate precipitation or gelation. The resultant EDPA materials yielded type IV nitrogen sorption isotherms and narrow pore size distributions with greatly reduced surface areas and pore volumes (Figure 22, Figure 23, Table 9) as well as XRD peaks of lower intensity (Figure 22). Increasing the amount of structure enhancing BTE at the expense of DEB to a ratio 75 BTE: 15 DEB: 10 PTS resulted in a surface area of 224 m^2/g for EDPA4. Each EDPA material had a measured BJH adsorption pore size of 46 Å, regardless of the BTE: DEB ratio (Figure 23). Phase separation or segregation of multiple bridging groups incorporated in the pore walls of PMOs has been investigated by Yang et al.[55] There may exist domains that are relatively rich in BTE and DEB in these multifunctional PMOs for which templated mesoporosity is more prevalent in the ethane-silicate partitions.

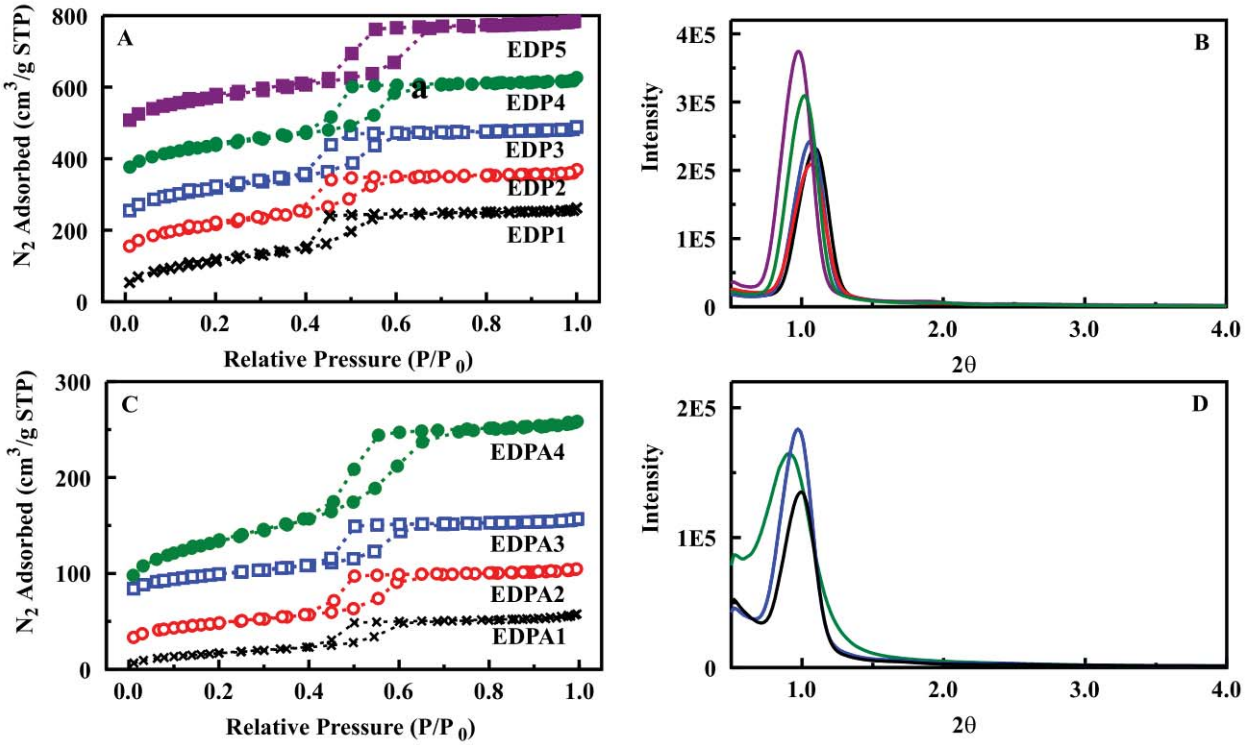

Figure 22. *Nitrogen sorption isotherms (A, C) and XRD patterns (B, D) for phenyl-functionalized ethane-diethylbenzene-bridged silica materials (Panel A) EDP1, EDP2 shifted by 100, EDP3 shifted by 200, EDP4 shifted by 325, and EDP5 shifted by 450; phenyl and amine-functionalized ethane-diethylbenzene-bridged silica materials (Panel B) EDPA1, EDPA2 shifted by 25, and EDPA3 and EDPA4 shifted by 75 cm^3/g.*

SEM images showed that the EDP materials and EDPA1 consisted of aggregates of irregularly shaped micrometer-scale particles. A co-continuous morphology was not observed, and any macropores in the materials resulted from voids formed by the aggregated micro-particles. There was a notable contrast between EDP3 and ED12 products synthesized with 0.55 g TMB and 7.5 g aqueous nitric acid. Replacement of 10 mol% Si from DEB with PTS in EDP3 prevented the formation of interconnected macroporosity observed for ED12. Gelation occurred

quickly in these syntheses and likely solidified the product before the development of a micro-phase separation. Only bulk morphology was seen for EDPA2-EDPA4.

Table 9. *Nitrogen adsorption data for phenyl-functionalized ethane-diethylbenzene-bridged silica materials with and without amine modification.*

Material	Ratio BTE:DEB:PTS	Mass TMB (g)	Mass 0.1 M HNO_3	Mass APS (g)	BET Surface Area (m^2/g)	Pore Volume (cm^3/g)	BJH pore size (Å)
EDP1	50:40:10	0.4	7.5	0	422	0.392	43
EDP2	50:40:10	0.5	7.5	0	430	0.399	43
EDP3	50:40:10	0.55	7.5	0	440	0.434	43
EDP4	50:40:10	0.6	7.5	0	420	0.450	48
EDP5	50:40:10	0.7	7.5	0	456	0.511	57
EDPA1	50:40:10	0.55	9.5	0.05	64	0.0848	46
EDPA2	60:30:10	0.55	9.5	0.05	90	0.121	46
EDPA3	70:20:10	0.55	9.5	0.05	93	0.124	46
EDPA4	75:15:10	0.55	9.5	0.05	224	0.279	46

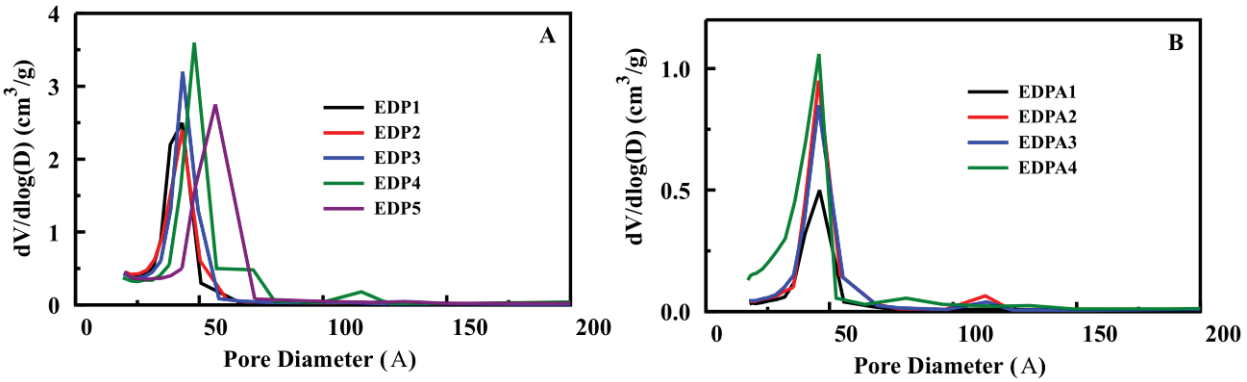

Figure 23*. Nitrogen adsorption pore size distributions for phenyl-functionalized ethane-diethylbenzene-bridged silica materials a) EDP1-EDP5 and phenyl- and amine-functionalized ethane-diethylbenzene-bridged silica materials b) EDPA1-EDPA4.*

Diethylbenzene-bridged silicas (D)

Previous reports have indicated increased binding capacity for materials with greater concentrations of DEB.[25,32] It has been shown that this increased DEB concentration comes at the expense of mesoscale order within the materials and often results in reduced selectivity in binding. Mesoporous materials were obtained using 100% DEB (0.00784 mol) with 7.5 g of aqueous nitric acid and 0.3 - 1.0 g of TMB as evidenced by their distinct type IV nitrogen sorption isotherms in Figure 24. It is notable that some isotherms have hystereses that do not close at low relative pressure. This has been observed with other surfactant-templated DEB silicates.[32,52,56] Nitrogen sorption analysis was repeated twice on the same sample of D2 to insure that the technique itself did not cause restructuring. No variation was observed upon repetition of the measurement, so the cause of this hysteresis remains unclear. There was a significant change in porosity characteristics as well as XRD peak intensities between samples

prepared using 0.4 and 0.5 g TMB (Table 10, Figure 24 and 25). It seems that a crucial amount of swelling additive was required to obtain pore sizes comparable to those of 50% DEB materials. Products D3 and D4 prepared with 0.5 and 0.6 g of TMB respectively had predictably lower measured porosity characteristics than their counterparts with 50 BTE: 50 DEB ratios (ED11 and ED13). Despite the absence of structure enhancing BTE, the materials had surface areas greater than 400 m^2/g, total pore volumes near 0.4 cm^3/g, and a mesopore size of 45 Å. To our knowledge, these values are the highest yet reported for surfactant-templated mesostructured diethylbenzene-bridged silicas. Li et al. employed KCl with TMB to aid the interaction of P123 surfactant with silicate in acidic solution.[56] It should be noted that the cited material was a precipitate while the syntheses described here used more concentrated surfactant solutions (20 wt% in water) and a higher molar ratio of surfactant to DEB to form monoliths. This approach made the use of a salt unnecessary in mesostructure assembly. Mesitylene was required for these syntheses, but relatively high amounts of TMB did not improve surface area or pore volume. D8 prepared with 1 g TMB was less mesoporous than D3 and D4. This result provided additional evidence related to how interactions between mesitylene and DEB can counter the swelling effect. Those interactions may have also prevented the morphological evolution of cylindrical to spheroid micelles in templating a mesostructured cellular foam [57,58] in this study. This is in contrast to what has been obtained with other macro-mesoporous silicas and organosilicas.[37,42] Regardless of the amount of TMB added, isolated spherical macropores were observed in the materials by SEM (Figure 24).

Table 10. *Nitrogen adsorption data for diethylbenzene-bridged silica materials.*

Material	Mass TMB (g)	Mass 0.1 M HNO_3	BET Surface Area (m^2/g)	Pore Volume (cm^3/g)	BJH pore size (Å)
D1	0.3	7.5	375	0.256	32
D2	0.4	7.5	368	0.254	32
D3	0.5	7.5	455	0.414	45
D4	0.6	7.5	419	0.391	45
D5	0.7	7.5	426	0.411	44
D6	0.8	7.5	386	0.345	44
D7	0.9	7.5	414	0.419	49
D8	1.0	7.5	365	0.305	35

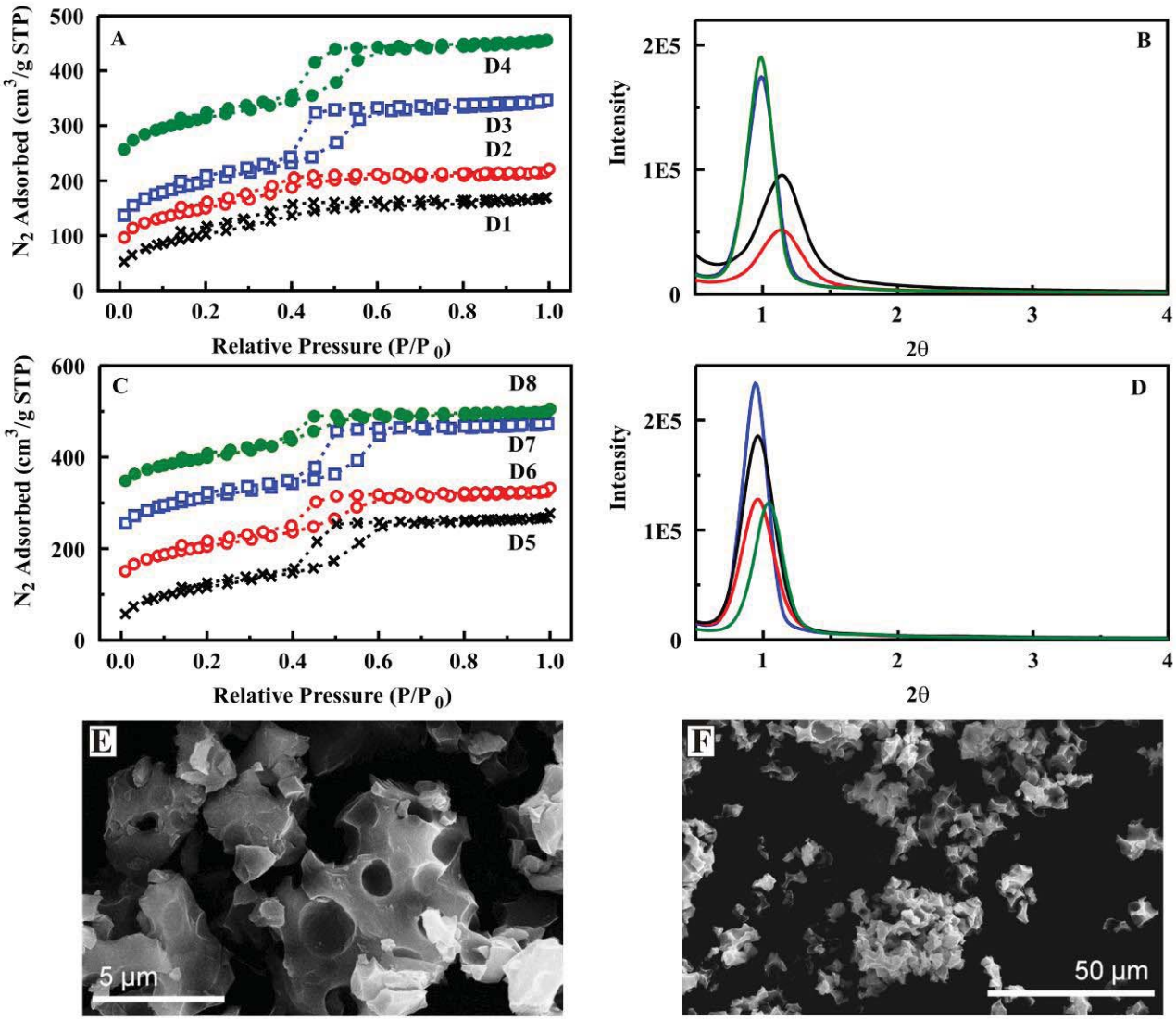

Figure 24. *Nitrogen sorption isotherms (A, C) and XRD patterns (B, D) for diethylbenzene-bridged silica materials (Panel A) D1, D2 shifted by 50, D3 shifted by 75, and D4 shifted by 200; (Panel B) D5, D6 shifted by 100, D7 shifted by 200, and D8 shifted by 300 cm^3/g STP. Scanning electron micrographs of (Panel E) D4 and (Panel F) D7.*

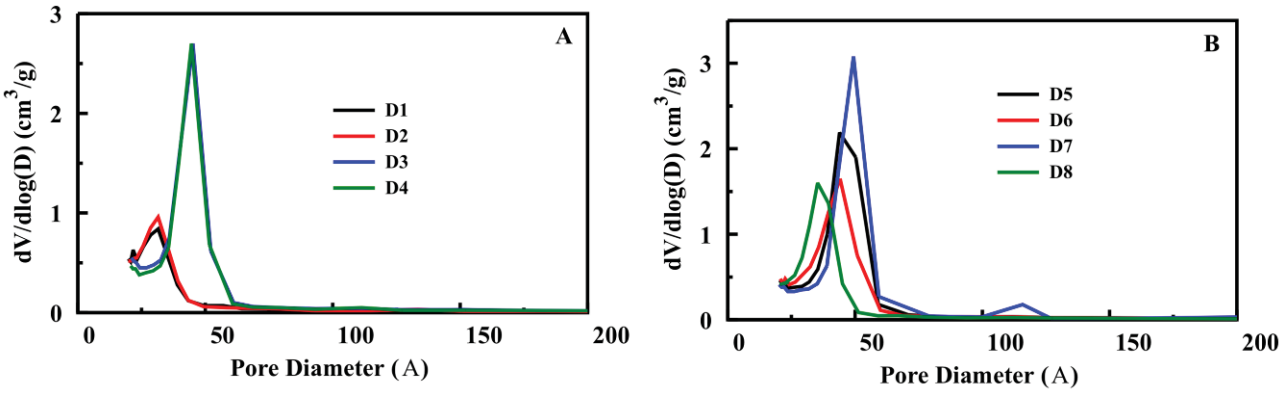

Figure 25. *Nitrogen adsorption pore size distributions for diethylbenzene-bridged silica materials a) D1-D4 and b) D5-D8.materials b) EDPA1-EDPA4.*

Task 2. Kinetic and Binding Analysis: Selected Sorbents

Two hierarchical sorbent materials were selected for complete evaluation: MM1 and P10. Figure 26 presents SEM and TEM images of the MM1 hierarchical material. This material utilizes a 50:50 BTE:DEB ratio with 12.6% imprint template. The SEM image clearly shows pores of approximately 1 µm. Bands of lighter and darker regions in the TEM image are indicative of ordered pore structure. XRD further confirms the presence of ordered mesopores (Figure 26). The sharp profile of the primary reflection, as well as the presence of additional reflections in the spectrum, indicate increased mesoscale order over PMO sorbents. This increase in order on the mesoscale typically provides improved access to the pore volume in a material. The increase in order is unexpected considering the concentration of DEB in MM1. For the PMO sorbents, using 50% DEB with 50% BTE resulted in poor material characteristics and a greater degree of disorder (Figure 26). Nitrogen sorption analysis of MM1 yielded a type IV isotherm with uniform pore sizes (Figure 26). The surface area of MM1 (366 m^2/g) is reduced in comparison to the mesoporous material prepared with the same precursor mixture (813 m^2/g) as expected with losses due to the macroscale structure. Mesopore volume is also reduced (from 0.46 cm^3/g to 0.26 cm^3/g for MM1), while the average pore size diameter is increased (from microporous to 35 Å for MM1).

An alternative material, P10, incorporates terminal phenyl groups (PTS) into the hierarchical material. The terminal phenyl groups provide potential binding sites that extend further outside of the electric double layer of the sorbent surface. This material has reasonable materials characteristics, but is missing the macroporous characteristics observed for MM1. An SEM image of P10 is presented in Figure 26. TEM imaging did not reveal ordered pores on the mesoscale. Nitrogen sorption analysis of P10 yielded a type IV/type I isotherm with surface area 276 m^2/g, pore volume 0.226 cm^3/g, and average pore diameter 43 Å (Figure 26). The XRD spectrum for P10 is also presented.

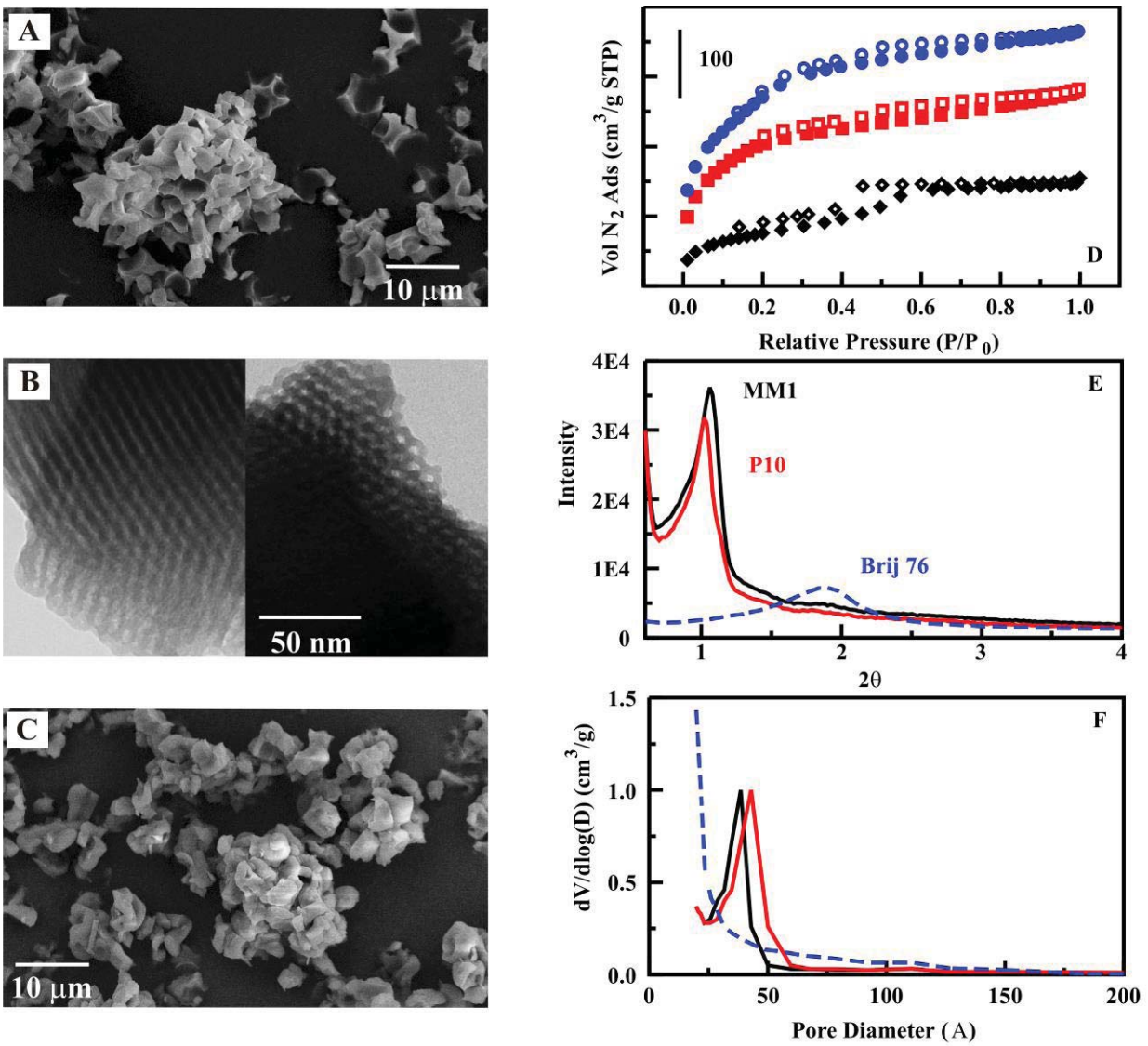

Figure 26. *Hierarchical material characteristics. Shown here are SEM (panel A) and TEM (panel B) images of MM1 and an SEM image of P10 (panel C). Also presented are the nitrogen sorption isotherms (panel D) for MM1 (black), P10 (red), and the 50:50 BTE:DEB material synthesized using Brij®76 (blue). Open symbols are for desorption, and filled symbols are for sorption. The pore diameter distributions (panel E) and XRD spectra (panel F) are presented as well.*

Adsorption Experiments

Binding isotherms for RDX and TNT by P10 and MM1, respectively, are presented in Figure 27. Binding kinetics for these materials were slower than those of the PMO sorbents. A period of 20 min was necessary to achieve 95% of maximal target binding. The reasons for the difference in rate are unclear. Analysis of binding site homogeneity was conducted based on the method described above (Equation 2). TNT and RDX binding (for MM1 and P10, respectively)

in the presence of p-cresol were evaluated (Figure 28). When the evaluated targets bind to the same sites, this plot is typically linear. When targets are bound by differing sites, there is divergence from the line. On the basis of this data, it appears unlikely that compounds with structures similar to p-cresol will compete with targets (TNT or RDX) for binding sites. This semi-selectivity of MM1 was expected based on the results obtained for the PMO sorbents.

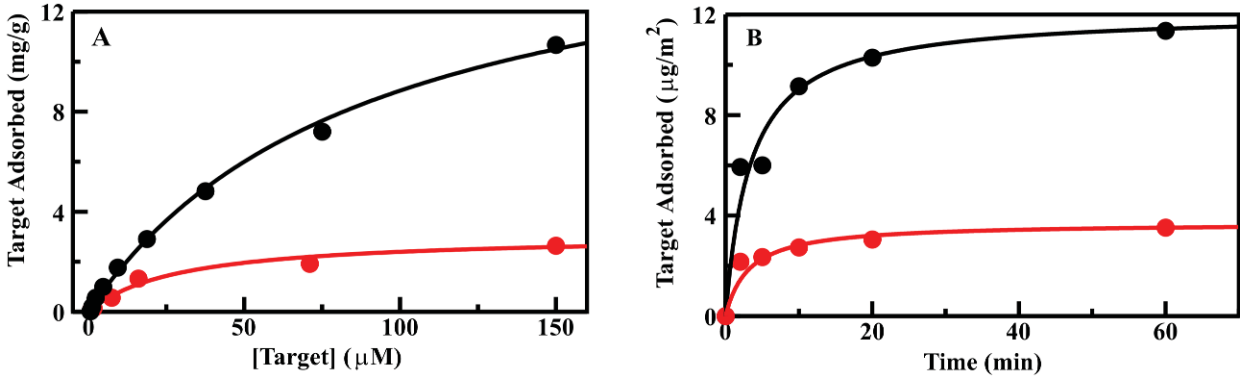

Figure 27. *Target binding. (Panel A) Standard binding isotherms for TNT by MM1 (black) and RDX by P10 (red). (Panel B) Kinetics for binding of TNT and RDX by MM1 (black) and P10 (red), respectively.*

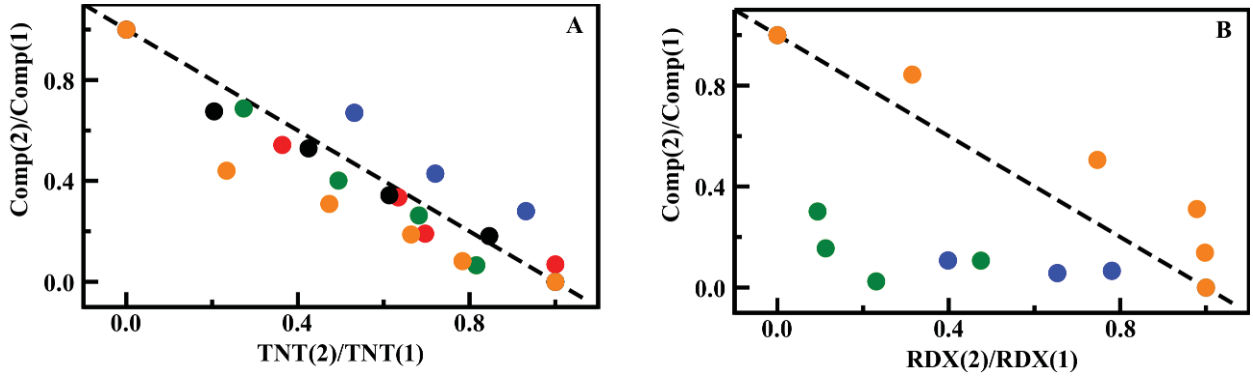

Figure 28. *Competitive binding. From Eq. (2), these graphs show competitive binding of targets by MM1 in mixtures with TNT (panel A) and P10 in mixtures with RDX (panel B). Here, "comp" indicates the competitive target: pCr (blue), NG (red), pNP (green), DNT (black). Orange points indicate competition between TNT and RDX.*

TNT, DNT, RDX, and nitroglycerin are commonly found as co-contaminants. Additional competitive binding experiments were performed using mixtures of these targets (Figure 28). The concentrations used for these experiments are well below the binding capacity of the material for all of the evaluated targets. Results indicate that TNT and RDX are bound by differing sites within the materials. TNT, DNT, p-nitrophenol, and nitroglycerin, on the other hand, all interact with the same sites. Competition between TNT and DNT is expected due to their very similar structures. RDX is much more rigid than the nitroglycerin structure, which may result in reduced affinity for the compound at the sites of high affinity for TNT. These results are valid under the conditions evaluated; however, competition for sites of lower TNT affinity would be likely at higher target loading levels.

Numbers indicative of affinity for these materials were generated based on fitting by the Langmuir-Freundlich model isotherm (Equation 1). In the case of MM1, the heterogeneity index was 0.83 (unlike the PMO sorbents, for which a value of 1 was obtained). This tends to indicate that TNT is bound by sites of varying affinity. In the case of RDX binding by P10, a heterogeneity coefficient of 0.87 yields a good fit. The TNT saturation capacity of MM1 was significantly higher than that of the PMO sorbents (70 μg/m^2 compared to 3.3 μg/m^2). RDX capacity was much lower, likely due to the lack of interaction with the π-bonds of the DEB bridging group. Further evidence of these differences was provided by the competitive binding data (Figure 28) and the difference in binding affinity (MM1, 0.003 μg^{-1}; P10, 0.046 μg^{-1}).

Batch experiments were performed in artificial sea water and in pond water collected locally (Alexandria, Virginia) to obtain an idea of the potential for application of these materials to targets in complex matrices. Water samples were spiked with TNT or RDX. While the binding of TNT by MM1 was slightly reduced by the pond water matrix, the binding of RDX by P10 was completely abrogated in both of the matrices. As a result, P10 will not be useful for application outside of a laboratory situation. MM1 is expected to perform under a range of different sample conditions. Binding of TNT by MM1 was not impacted by varying pH (Figure 29). Increasing temperature, however, reduced the amount of target bound. This is likely due to the decreased residence time of the target on the sorbent surface.

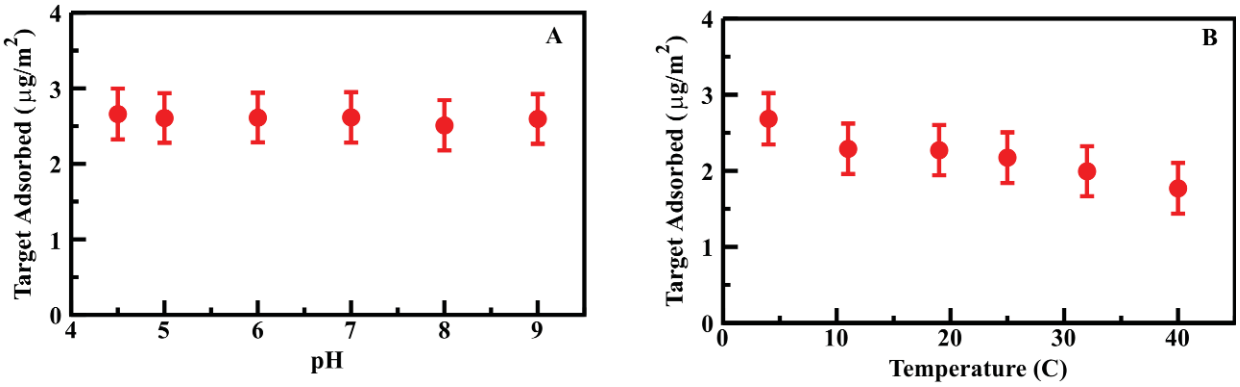

Figure 29. *Effects of pH and temperature on target binding. (Panel A) Altering the pH of samples through addition of phosphate buffer had little impact on the binding of TNT by MM1. (Panel B) As sample temperature increased, TNT binding by MM1 decreased.*

Column Adsorption

Hierarchical sorbents were packed as 200 mg columns to evaluate their potential for application to preconcentration. Columns were characterized by measuring breakthrough capacity and elution characteristics in comparison to activated charcoal (Figure 30). MM1 and P10 performed similarly in the column format. The total TNT binding capacities for the 200 mg columns were found to be approximately 530 μg (2.6 mg/g). The total RDX binding capacity was found to much less (46 μg for MM1 and 67 μg for P10). Initial TNT breakthrough for P10 was noted at 400 μg and for MM1 at 450 μg. Initial RDX breakthrough for P10 was noted at 25 μg and for MM1 at 50 μg. Partial breakthrough for both targets was noted from the first application on the activated charcoal column, but total capacity was not reached for the carbon for either target (>700 μg). Based on the calculations described above, TNT breakthrough on MM1 was expected at 5 mg; MM1 bound significantly less TNT than expected under the conditions used for the column experiments.

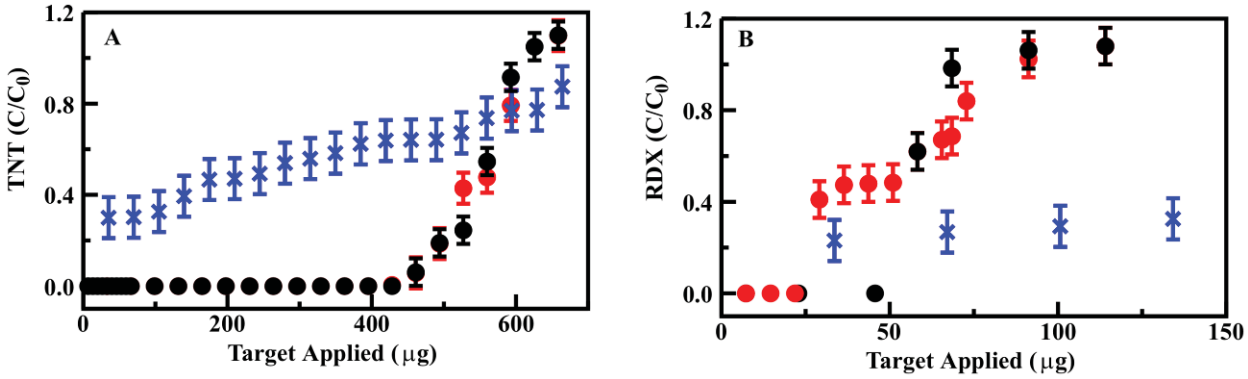

Figure 30. *Column breakthrough. (Panel A) TNT breakthrough for MM1 (black), P10 (red), and activated charcoal (blue). (Panel B) RDX breakthrough for the same sorbents.*

MM1 was also compared to two commercially available preconcentration sorbents, LiChrolut EN and Sep-Pak. Samples of TNT solution in deionized water were applied to 200 mg columns of each of the sorbents. No breakthrough was observed for any of the materials. Elution was accomplished using 1 mL of actetonitrile (based on directions provided for LiChrolut and Sep-Pak). The concentration of TNT recovered upon elution from MM1 was greater than that obtained from either of the commercial sorbents for all applied volumes. Elution of targets from MM1 was also possible using methanol with similar recovery. The recovery of TNT using MM1 for greater than 120 capture/elution cycles showed no degradation in performance for the sorbent.

Task 3: Groundwater Testing

Having made significant improvements in the sorbent characteristics and demonstrated their performance in laboratory samples, it was of interest to evaluate performance in real-world matrices [40]. These evaluations were completed in parallel with evaluation of LiChrolut EN and Sep-Pak RDX as representatives of state-of-the-art preconcentration materials. Because nitroenergetic targets in general are of interest for this application, the target list was expanded to include TNT, RDX, HMX, DNT, and NG. These targets have relevance for water quality at munitions testing and training sites as well as sites of storage and manufacture. A baseline for performance was established using samples spiked into deionized water. HPLC analysis was utilized, and spiked target concentrations were selected to cover those within and below the range of the analytical method (0.9 to 200 ppb). In all cases, 20 mL of the target solution was applied to the column, it was rinsed with deionized water (6 mL), and target was eluted in 4 mL acetonitrile. The column was rinsed with acetonitrile (4 mL) and water (6 mL) prior to application of the next sample. All of the volumes (effluent, eluent, and rinses) were analyzed by HPLC. Figure 31 provides a comparison of the performance of MM1 to the commercial sorbents. Overall, MM1 (blue) provided effective capture and elution of TNT, RDX, DNT, and NG. Results were comparable to the LiChrolut sorbent (red) and exceeded those of the Sep-Pak sorbent (black). None of the materials performed well for HMX. Table 11 provides detailed results for all spiked deionized water samples. Commercial sorbents performed poorly against NG. Sep-Pak showed target breakthrough and bleeding into washes for nearly all compounds.

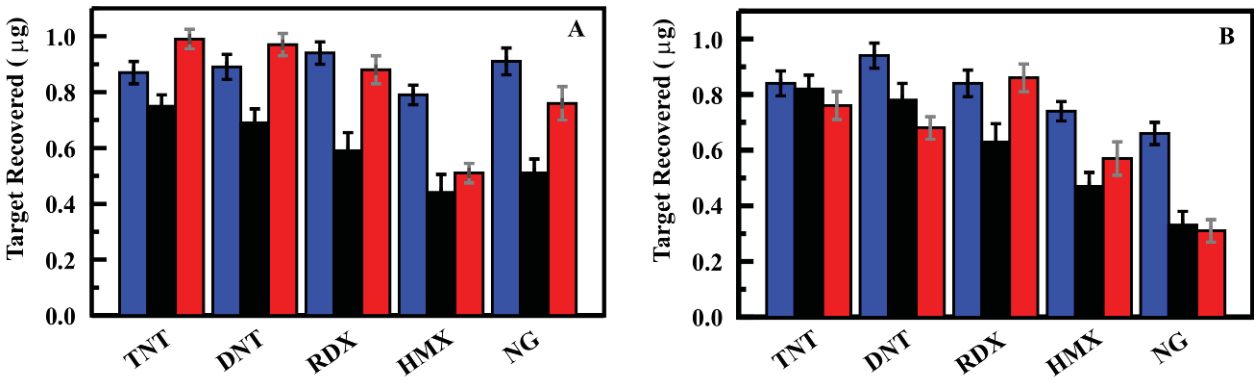

Figure 31. *Target preconcentration. (Panel A) Target recovered in the eluent for each of the three sorbents from targets in deionized water. (Panel B) Target recovered in the eluent for each of the three sorbents from targets in artificial sea water. MM1 (blue), Sep-Pak (black), LiChrolut (red). Applied target at 50 ppb.*

Samples prepared in artificial sea water and in natural water samples (ground and surface) were also evaluated. Figure 31 presents representative results for samples in artificial sea water; Table 12, Table 13, and Table 14 provide results for samples in sea water, groundwater, and surface water, respectively. For MM1, recovery of targets from artificial sea water was similar to that observed for deionized water samples, indicating that target binding is not dependent on ionic strength. Recovery of TNT and DNT by LiChrolut was reduced in this matrix while recovery of RDX and HMX was not. Recovery of RDX, HMX, TNT, and DNT by Sep-Pak was slightly increased in artificial sea water. NG recovery was negatively impacted for all sorbents. Surface water (pond; Table 14) and groundwater (well; Table 13) samples were filtered prior to spiking. For MM1, recovery of DNT, TNT, and RDX from these matrices was similar to that from deionized water. HMX and NG recovery were reduced. TNT, DNT, and NG recovery by LiChrolut was negatively impacted with little change in RDX and HMX recovery. Sep-Pak performance was poor for both matrices. Because of the potential for varied pH in water samples, recovery of targets at pH 3.0 and 9.0 was also evaluated (Table 15). For MM1, recovery of TNT, HMX, and NG were reduced at low pH, with only slight effects observed at high pH. Low pH had a stronger impact on LiChrolut performance and little impact on Sep-Pak performance.

Table 11. *Recovery of Targets from Deionized Water*

Target	[Applied] (ppb)		MM1	Sep-Pak	LiChrolute EN
TNT	200	Eluant	85	71	85
		Total	87	99	98
	50	Eluant	88	75	99
		Total	88	86	99
	5	Eluant	97	88	101
		Total	97	88	101
	0.9	Eluant	ND	ND	ND
		Total	ND	ND	ND
RDX	200	Eluant	92	59	99
		Total	92	96	100
	50	Eluant	94	59	88
		Total	94	128	88
	5	Eluant	96	ND	ND
		Total	96	ND	ND
	0.9	Eluant	ND	ND	ND
		Total	ND	ND	ND
HMX	200	Eluant	78	52	53
		Total	78	81	64
	50	Eluant	79	44	51
		Total	79	89	65
	5	Eluant	ND	ND	56
		Total	ND	ND	56
	0.9	Eluant	ND	ND	ND
		Total	ND	ND	ND
DNT	200	Eluant	91	73	95
		Total	91	107	107
	50	Eluant	89	69	97
		Total	89	92	110
	5	Eluant	90	65	87
		Total	90	65	87
	0.9	Eluant	ND	ND	ND
		Total	ND	ND	ND
NG	200	Eluant	87	57	74
		Total	87	69	74
	50	Eluant	91	51	76
		Total	91	51	76
	5	Eluant	ND	ND	ND
		Total	ND	ND	ND
	0.9	Eluant	ND	ND	ND
		Total	ND	ND	ND

Values provided in percent recovered. ND indicates not detected.

Table 12. *Recovery of Targets from Artificial Sea Water*

Target	[Applied] (ppb)		MM1	Sep-Pak	LiChrolute EN
TNT	200	Eluant	90	81	78
		Total	90	93	78
	50	Eluant	84	82	76
		Total	82	82	76
	5	Eluant	72	68	93
		Total	72	68	93
	0.9	Eluant	ND	ND	ND
		Total	ND	ND	ND
RDX	200	Eluant	82	73	86
		Total	93	81	95
	50	Eluant	84	63	86
		Total	84	74	86
	5	Eluant	ND	ND	ND
		Total	ND	ND	ND
	0.9	Eluant	ND	ND	ND
		Total	ND	ND	ND
HMX	200	Eluant	78	51	56
		Total	92	51	61
	50	Eluant	74	47	57
		Total	74	47	56
	5	Eluant	67	ND	52
		Total	67	ND	58
	0.9	Eluant	ND	ND	ND
		Total	ND	ND	ND
DNT	200	Eluant	94	79	81
		Total	94	113	91
	50	Eluant	94	78	68
		Total	94	130	68
	5	Eluant	81	ND	ND
		Total	81	ND	ND
	0.9	Eluant	ND	ND	ND
		Total	ND	ND	ND
NG	200	Eluant	63	41	37
		Total	72	41	37
	50	Eluant	66	33	31
		Total	66	33	31
	5	Eluant	ND	ND	ND
		Total	ND	ND	ND
	0.9	Eluant	ND	ND	ND
		Total	ND	ND	ND

Values provided in percent recovered. ND indicates not detected.

Table 13. *Recovery of Targets from Groundwater*

Target	[Applied] (ppb)		MM1	Sep-Pak	LiChrolute EN
TNT	200	Eluant	87	48	57
		Total	87	71	59
	50	Eluant	92	46	60
		Total	92	83	60
RDX	200	Eluant	92	64	81
		Total	92	75	84
	50	Eluant	90	50	71
		Total	90	50	75
DNT	200	Eluant	91	59	71
		Total	91	84	77
	50	Eluant	88	63	73
		Total	88	73	80
HMX	200	Eluant	3	51	41
		Total	70	75	50
	50	Eluant	ND	37	44
		Total	ND	44	54
NG	200	Eluant	86	41	51
		Total	86	41	51
	50	Eluant	74	50	59
		Total	74	50	59

Values provided in percent recovered. ND indicates not detected.

Table 14*. Recovery of Targets from Surface Water*

Target	[Applied] (ppb)		MM1	Sep-Pak	LiChrolute EN
TNT	200	Eluant	89	46	52
		Total	89	66	55
	50	Eluant	87	63	83
		Total	87	85	91
RDX	200	Eluant	89	82	82
		Total	90	66	87
	50	Eluant	84	63	90
		Total	84	70	90
DNT	200	Eluant	89	72	87
		Total	90	111	92
	50	Eluant	87	71	89
		Total	87	84	98
HMX	200	Eluant	55	49	61
		Total	55	82	73
	50	Eluant	50	30	51
		Total	50	30	73
NG	200	Eluant	81	59	60
		Total	81	59	60
	50	Eluant	85	53	54
		Total	85	53	54

Values provided in percent recovered.

Table 15. *Recovery of Targets from Samples of Varied pH*

Target	pH	[Applied] (ppb)		MM1	Sep-Pak	LiChrolute EN
TNT	3	200	Eluant	77	44	60
			Total	77	78	67
		50	Eluant	70	51	56
			Total	70	65	67
	9	200	Eluant	84	73	68
			Total	97	86	76
		50	Eluant	85	59	62
			Total	85	72	74
RDX	3	200	Eluant	86	58	74
			Total	86	76	78
		50	Eluant	86	55	63
			Total	86	63	66
	9	200	Eluant	97	64	80
			Total	97	71	82
		50	Eluant	96	59	84
			Total	96	64	86
HMX	3	200	Eluant	88	56	66
			Total	89	87	73
		50	Eluant	87	51	59
			Total	87	62	68
	9	200	Eluant	91	74	83
			Total	93	105	90
		50	Eluant	80	64	80
			Total	80	79	89
DNT	3	200	Eluant	67	51	65
			Total	70	92	75
		50	Eluant	61	46	42
			Total	61	82	53
	9	200	Eluant	69	42	57
			Total	72	70	66
		50	Eluant	68	41	59
			Total	68	68	69
NG	3	200	Eluant	63	39	39
			Total	63	97	39
		50	Eluant	55	44	47
			Total	55	44	47
	9	200	Eluant	63	54	56
			Total	63	54	56
		50	Eluant	65	50	62
			Total	65	50	62

Values provided in percent recovered.

Soil samples were provided by A.D. Hewitt from former munitions testing sites on Holloman Air Force Base, Alamogordo, NM (Table 16). The photos below show the sites from which the 2000 lb bomb crater samples were collected (Figure 32). This was an area where a 2000 lb bomb had low-ordered (bottom of crater with man on rim) scattering Tritonal over the surface, in mainly one direction, for several 100's of meters. As seen in the pictures, the TNT in the Tritonal had reacted to the sun, thus leading to the formation of TNB and DNA. Some TNT had also washed from the surface during the infrequent rain events in the area leading to the formation of 2 & 4-ADNT. 2,4-DNT is also found as an impurity in the manufacturing of TNT. The samples were collected, air dried and ground, subsampled and analyzed in accordance with Method 8330B. A. Hewitt also provided well water samples taken at his home in New Hampshire.

Figure 32. *Photos of soil sample collection sites on Holloman AFB. (top left) 2000 lb bomb crater with low-level scattering. (top right) Wider angle view of the collection site. (bottom left and bottom right) These images show Tritonal in which the TNT has reacted to the sun to produce TNB and DNA.*

The samples contained various contaminants at differing concentrations. Sample sites varied in the size of ordnance and the age of the site. The samples were handled and analyzed in accordance with EPA Method 8330B by the Engineer Research and Development Center, U.S. Army Corps of Engineers. Complete results of this analysis are provided in Table 17. The soils were extracted into water to prepare samples for analysis. If sample HO-004 is taken as an example, the EPA method indicated a high concentration of TNT and lower concentrations of RDX and DNT as well as trace amounts of 2-amino-4,6-dinitrotoluene (2-ADNT) and 4-amino-2,6-dinitrotoluene (4-ADNT). When preconcentration of this sample was attempted with the MM1 sorbent column, TNT in the sample saturated the sorbent, resulting in some TNT found in the column effluent. The concentration in the eluent was enhanced by nearly ten times (Table

18). Trinitrobenzene (TNB), 2-ADNT, and 4-ADNT were below the detectable limit in the as-extracted sample, but were detected in the eluent following preconcentration. The concentration of RDX was enhanced by seven times. Target concentration enhancements by MM1 were impacted by the affinity of the sorbent for the targets and by the relative concentrations in the mixed samples. Comparative data for the commercial sorbents on a single soil extract is provided in Table 19.

Table 16. *Soil Samples from Sites on Holloman Air Force Base*

Sample ID	Site	Grid
HO-001	Old 2,000-lb crater	
HO-004	Old 2,000-lb crater	
HO-006	Old 500-lb crater	
HO-018	Low-order bomb crater	Hot
HO-019	Low-order bomb crater	Hot
HO-020	Low-order bomb crater	Hot
HO-022	2,000-lb crater	Hot
HO-023	2,000-lb crater	Hot
HO-024	2,000-lb crater	Hot
HO-025	No visible low-order debris	Cold
HO-026	No visible low-order debris	Cold
HO-027	No visible low-order debris	Cold

Table 17. *Analysis of Soil Samples Using EPA Method 8330B*

Sample	HMX	RDX	TNB	DNB	TNT	2-ADNT	4-ADNT	2,4-DNT	DNA
HO-001	ND	ND	0.01	ND	0.14	0.03	0.04	0.01	ND
HO-004	ND	0.01	0.03	ND	0.05	0.02	0.02	ND	0.01
HO-006	ND	0.01	ND	ND	ND	0.10	ND	ND	ND
HO-018	ND	ND	0.01	ND	0.15	ND	0.04	ND	ND
HO-019	ND	ND	0.01	ND	0.54	0.04	0.01	ND	ND
HO-020	ND	ND	ND	ND	2.02	0.05	0.04	ND	ND
HO-022	ND	0.25	0.03	ND	12.50	0.11	0.11	ND	ND
HO-023	ND	0.04	0.03	ND	2.60	0.12	0.09	0.08	ND
HO-024	ND	0.01	0.01	ND	2.70	0.12	0.11	ND	ND
HO-025	ND	ND	0.08	ND	0.58	ND	ND	ND	ND
HO-026	0.01	ND	0.03	ND	0.19	0.06	ND	ND	0.01
HO-027	ND	0.02	0.02	ND	0.08	0.11	0.03	0.01	ND

Results provided by Cold Regions Research and Engineering Laboratory, Engineer Research and Development Center, U.S. Army Corps of Engineers; ND denotes levels below the detection limit for the analytical method; Concentrations are provided as parts per million (ppm) under the sample conditions applied in this study; DNA = dinitroaniline.

Table 18. *Analysis of Soil Samples Using MM1 Sorbent Column*

Target	Sample	HO-001	HO-004	HO-006	HO-018	HO-019	HO-020	HO-022	HO-023	HO-024	HO-025	HO-026	HO-027
2,4-DNT	Extracted	0.01	ND	ND	ND	ND	ND	ND	ND	ND	ND	ND	ND
	Effluent	ND	ND	ND	ND	ND	ND	ND	ND	ND	ND	ND	ND
	Eluate	0.33	ND	ND	ND	ND	0.06	ND	<0.01	ND	ND	ND	<0.01
2-ADNT	Extracted	0.01	ND	ND	ND	0.03	0.02	ND	ND	ND	ND	ND	ND
	Effluent	ND	ND	ND	ND	ND	ND	ND	ND	ND	ND	ND	ND
	Eluate	0.29	0.01	0.01	ND	0.43	0.50	0.09	0.08	0.07	0.02	0.01	0.01
4-ADNT	Extracted	0.02	ND	ND	<0.01	ND	ND	ND	ND	ND	ND	ND	ND
	Effluent	ND	ND	ND	ND	ND	ND	ND	ND	ND	ND	ND	ND
	Eluate	0.35	0.24	ND	0.92	0.50	0.63	0.09	0.01	0.03	ND	ND	ND
DNB	Extracted	ND	ND	ND	ND	ND	ND	ND	ND	ND	ND	ND	ND
	Effluent	ND	ND	ND	ND	ND	ND	ND	ND	ND	ND	ND	ND
	Eluate	ND	ND	ND	ND	ND	ND	ND	ND	ND	ND	ND	ND
HMX	Extracted	ND	ND	ND	ND	ND	ND	ND	ND	ND	ND	ND	ND
	Effluent	ND	ND	ND	ND	ND	ND	ND	ND	ND	ND	ND	ND
	Eluate	ND	ND	ND	ND	ND	ND	ND	ND	ND	ND	ND	ND
RDX	Extracted	1.32	<0.01	<0.01	ND	ND	ND	<0.01	ND	<0.01	ND	ND	<0.01
	Effluent	0.80	ND	ND	ND	ND	ND	ND	ND	ND	ND	ND	ND
	Eluate	5.23	0.07	0.07	ND	ND	ND	0.22	<0.01	<0.01	ND	ND	<0.01
TNB	Extracted	0.48	ND	ND	ND	ND	ND	ND	ND	ND	ND	ND	ND
	Effluent	0.21	ND	ND	ND	ND	ND	ND	ND	ND	ND	ND	ND
	Eluate	3.30	0.01	ND	<0.01	0.13	0.10	<0.01	<0.01	ND	ND	ND	ND
TNT	Extracted	6.59	0.29	ND	0.64	0.59	1.12	0.71	0.10	0.11	ND	ND	ND
	Effluent	1.73	<0.01	ND	0.04	ND	0.02	0.06	ND	ND	ND	ND	ND
	Eluate	54.59	2.87	ND	6.76	5.06	11.94	6.69	1.67	1.51	0.10	0.01	<0.01

Concentrations in parts per million (ppm). ND indicates not detected.

Table 19. *Comparison of MM1 and Commercial Sorbents on Soil Sample HO-022*

Target	Method 8330B	NRL Extract		MM1	LiChrolut	Sep-Pak
2,4-DNT	ND	ND	Eluant	ND	ND	ND
			Total	ND	ND	ND
2-ADNT	110	16	Eluant	84	72	39
			Total	84	72	50
4-ADNT	110	68	Eluant	679	689	398
			Total	679	689	489
DNB	ND	ND	Eluant	ND	ND	ND
			Total	ND	ND	ND
HMX	ND	ND	Eluant	ND	ND	ND
			Total	ND	ND	ND
RDX	250	27	Eluant	127	36	21
			Total	127	36	45
TNB	30	8	Eluant	17	ND	ND
			Total	17	ND	ND
TNT	1250	386	Eluant	2950	2371	1798
			Total	2969	2814	2301

Concentrations in parts per million (ppm). ND indicates not detected.

Task 4. Sorbents for Perchlorate

Binding of nitroenergetic targets by the NRL-developed sorbents is accomplished through hydrophobic/hydrophilic interactions, π–π stacking, and other target surface interactions. Capture of perchlorates requires interaction via a charged group. Commercial materials are typically strong base resins that provide no selectivity. Other materials using alkylammonium groups have been described with similar results.[41,42] Ideally, such a material should combine high surface area and dense population of binding sites with a texture that enables facile diffusion of solvent through the length of column. The syntheses used here combined surfactant templating of mesostructured materials and polymerization-induced phase separation to create macroscale textures.[42] An alternative approach might include the use of materials with very large mesopores to improve diffusion through the sorbent materials.[59,60]

The protocols for synthesis of HX and CF were adapted from the literature to provide macroporous silica supports offering significantly different mesostructures.[41,42] HX was synthesized with the intention of obtaining hexagonal packing of cylindrical pore channels. CF was intended to be a "mesostructured cellular foam" with a relatively disordered arrangement of spherical pores. These morphological considerations are evident in their nitrogen sorption isotherms (Figure 33). HX showed a steep increase in adsorption around $P/P_0 = 0.7$ and a parallel hysteresis between the adsorption and desorption branches. This is in contrast to the pronounced hysteresis observed for CF and the increase in adsorption extending over a wide relative pressure region ($P/P_0 = 0.5–1.0$). HX yielded a narrow pore size distribution peak at 77 Å (Figure 33). The pore size distribution of CF was less defined and peaked ca. 111 Å. CF did not provide reflections in a powder X-ray diffraction pattern (Figure 33). HX demonstrated a more crystalline pattern having a primary reflection at $2\theta = 1.0°$ and a secondary reflection ca. $2\theta = 1.8°$. Open, co-continuous macropores in a strut-like framework were observed for the HX material (Figure 33). CF, however, displayed an inconsistent morphology comprised largely of bulk particles with some regions of open macroporosity (Figure 33).

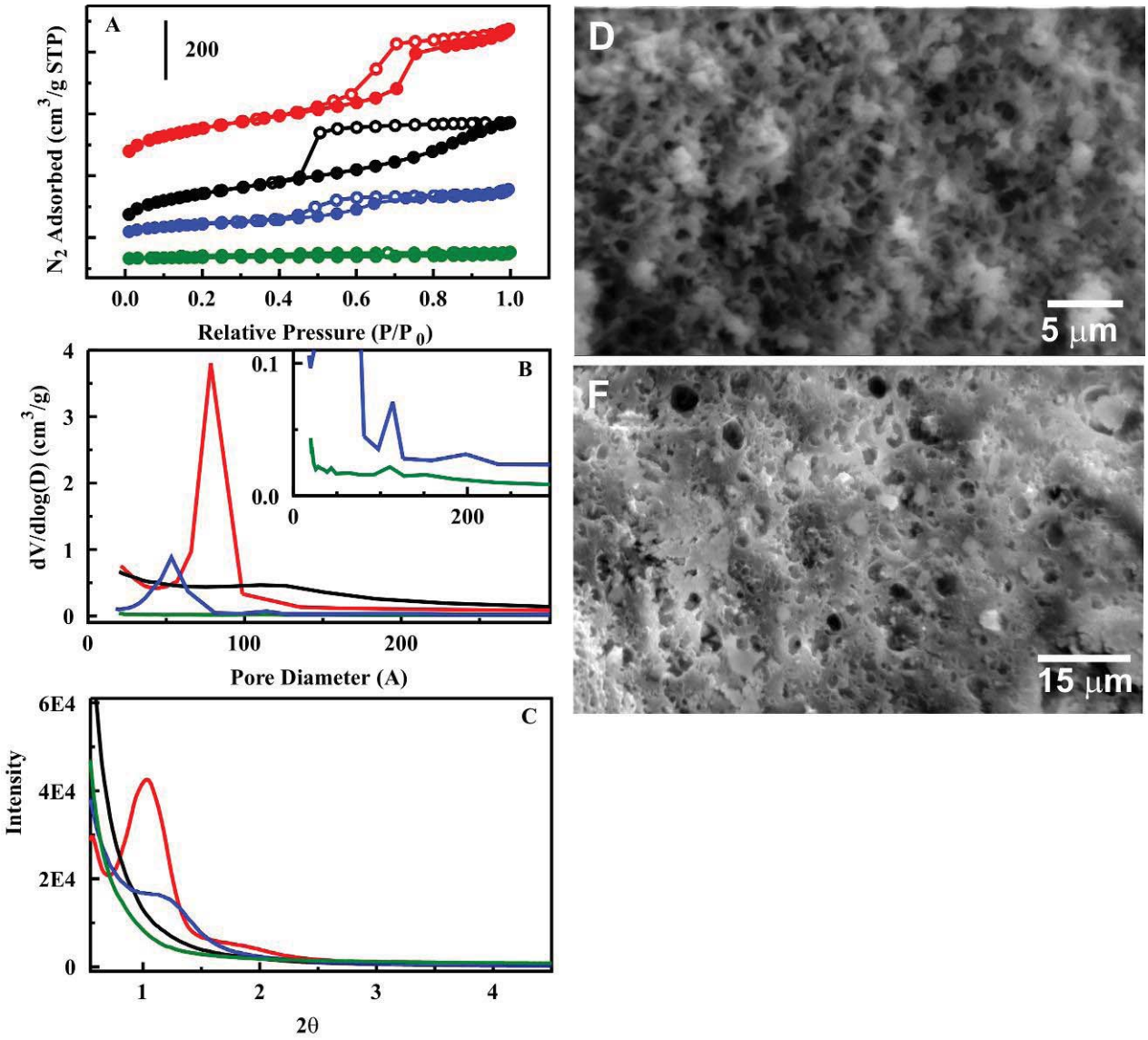

Figure 33. *(Panel A) Nitrogen sorption isotherms for sorbent with hexagonally packed pores (HX) (red, shifted +200), sorbent with disordered pore arrangement (CF) (black, shifted +110), HX1M3B (blue), and CF1M3B (green) sorbents; (Panel B) Pore size distributions for HX, CF, HX1M3B, and CF1M3B. The inset shows a zoom view of the HX1M3B and CF1M3B pore size distributions; (Panel C) X-ray diffraction patterns for HX (red), CF (black), CF2 (blue), and CF3 (green) sorbents. Scanning electron microscopy (SEM) images of HX (Panel D) and CF (Panel E) showing differing macroscale morphologies.*

Post-synthesis grafting of quaternary alkylammonium groups onto these sorbents was used to provide sites for perchlorate anion binding. The naming scheme used the scaffold abbreviation (HX or CF) followed by the quantity of functional compound utilized in the grafting step (mmol), so 1 g of CF functionalized with 4 mmol of TSPMC chloride was abbreviated CF4M while functionalization with 4 mmol of TSPBC would be abbreviated as CF4B. The selection of

the alkylammonium groups was based on the reported performance of an ordered mesoporous SBA-15 silica grafted with TSPMC and TSPBC.[61] SBA-15 typically consists of rope-like particles of about 1 mm in size.[62] The sorbents used here, HX and CF, offered both meso and macrostructures that differentiate them from the previously evaluated SBA-15 (Figure 33). Grafting of the TSPMC and TSPBC functional groups, results in changes in the nitrogen sorption characteristics of the sorbents (Table 20). Reacting 1 g of HX material with up to 4 mmol of ammonium silanes did not compromise its mesoporosity (Figure 33 and 34). Pore sizes > 60 Å and surface areas exceeding 100 m^2/g were measured. Loading of CF with such high amounts of ammonium silanes, however, resulted in low surface areas around 25 m^2/g (Figure 33 and 34). Previously evaluated SBA-15 materials utilized 4 mmol per gram loading of the functional groups through incipient wetness impregnation and reported losses in surface area and pore volume of 50% to 75%. Quantitative loading was assumed for the sorbents in that study.[61]

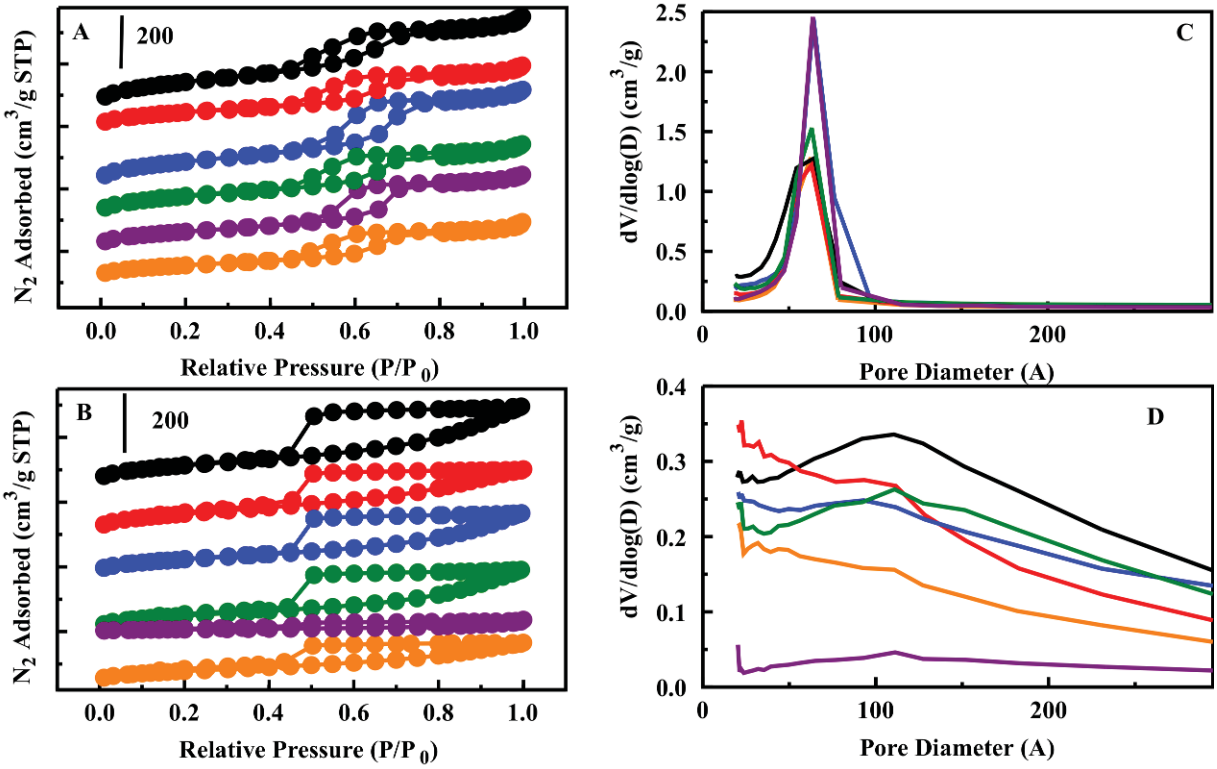

Figure 34. *Nitrogen sorption isotherms and pore size distributions for grafted HX (**A**,**C**) and CF (**B**,**D**) sorbents. Panel A—HX05M05B (black) shifted by +450, HX 1M1B (red) shifted by +390, HX2M (blue) shifted by +200, HXB4 (green) shifted by +110, HX4M (purple), HX2M2B (orange) shifted by −90; Panel B—CF05M05B (black) shifted by +450, CF 1M1B (red) shifted by +300, CF2M (blue) shifted by +170, CFB4 (green), CF4M (purple), CF2M2B (orange) shifted by −160; Panel C—colored as in Panel A. Panel D—colored as in Panel B.*

Table 20. *Morphological characteristics and target binding for base and alkylammonium functionalized sorbents with a disordered pore arrangement (CF) and with hexagonally packed pores (HX).*

Material	Surface Area (m^2/g)	Pore Volume (cm^3/g)	Pore Diameter (Å)	[Functional Group] (mmol)%	Perchlorate Bound (mg)*	Perchlorate Bound ($\mu g/m^2$)
HX Products						
HX	566	0.70	77	–	–	–
HX05M05B	342	0.43	64	1	–	–
HX2M	321	0.47	64	2	1.80	187
HX1M1B	206	0.29	63	2	1.25	202
HX4M	232	0.36	64	4	1.35	194
HX4B	342	0.34	63	4	1.33	130
HX2M2B	169	0.26	63	4	1.42	280
HX1M3B	163	0.22	53	4	1.66	339
HX2M4B	226	0.34	60	6	0.37	55
CF Products						
CF	523	0.57	111	–	–	–
CF05M05B	236	0.36	111	1	–	–
CF2M	197	0.29	93	2	1.30	220
CF1M1B	239	0.30	93	2	1.11	155
CF4M	25	0.04	111	4	1.73	2,310
CF4B	185	0.38	111	4	1.29	232
CF2M2B	143	0.18	93	4	1.51	352
CF1M3B	23	0.03	111	4	1.66	2,406
CF2	520	0.56	48	–	–	–
CF2-4M	108	0.12	38	6	1.27	392
CF3	562	0.52	64	–	–	–
CF3-4M	70	0.12	64	7	1.95	929

% Total functional groups (TSPMC + TSPBC) applied per gram of sorbent during grafting step;
** By 30 mg of sorbent from 5 mL of 500 ppm solution.*

Batch Binding Experiments

Generation of CF and HX sorbents with various combinations of surface functional groups initially provided twelve materials. In order to select those most likely to provide desirable binding characteristics, batch binding experiments using sorbent masses of 15 and 30 mg (5 mL, 500 ppm solution) were performed for perchlorate (Table 20). Based on the previous report [61], it was expected that combinations of the two functional groups would provide increased target binding. It was also expected that higher loading levels would be advantageous at least to the point at which transport of the targets through the sorbents was negatively impacted. Of the twelve sorbents initially evaluated, HX2M bound the most perchlorate from the batch experiment. Neither loading of the sorbent using 4 mmol of the TSPMC nor addition of 2 mmol TSPBC increased the total target bound. Both of these modifications decreased the surface area of the sorbent (27% and 48%, respectively) and likely restricted access to significant portions of the pore volume. When perchlorate binding by HX4M and HX4B was compared to that by HX1M3B and HX2M2B, increased binding was observed for the mixed functional groups. This point was interesting considering the surface area of the mixed functional group sorbents is 27% less than that of the HX4M sorbent. It is important to note that the surface area, as determined by nitrogen adsorption, may not reflect that accessible by the ionic targets under consideration here.

Mobility of surface functional groups and permeability through the organosilane layer may be different under aqueous conditions than under the conditions used for morphological analysis.

In the per gram comparison, HX sorbents largely outperformed the CF variants. HX sorbents with 2 mmol functional group bound perchlorate at levels similar to those of the 4 mmol CF variants. On closer inspection, it was interesting to note that the surface area of the 4 mmol CF variant was an order of magnitude less than that of the 4 mmol HX variant. The HX1M3B and CF1M3B sorbents bound equivalent amounts of perchlorate per gram while their respective surface areas would tend to indicate much greater site availability on the HX sorbent. When target bound was normalized to surface area, the results had a dramatically different appearance (Table 20). CF4M and CF1M3B bound nearly ten times more perchlorate per unit surface area than the other sorbents initially evaluated. There are several possible causes for these differences. It is possible that the HX sorbents have a lower degree of functionality, *i.e.*, a smaller fraction of the functional groups are bound during grafting of the sorbent. It is also possible that sites within the HX sorbent are subject to different restrictions and steric hindrance resulting in a lower activity and/or that regions of the HX sorbent that are penetrated by nitrogen (used for calculation of surface area) are not accessible to the ionic target. Determining the specific factors influencing the results was not possible with the available analyses.

Due to the possible differences between determined surface area and that accessible to the ionic targets, surface area normalization of the data was not appropriate to selection of a final candidate. This type of normalization, however, can provide insights useful in additional materials development. On the basis of those results, the CF sorbent was redesigned through modification of the synthetic protocol to provide two new variants CF2-4M and CF3-4M (Table 20; Figure 35) with increased nitrogen accessible surface area. CF2 had a narrow pore size distribution similar to the HX materials peaking at 48 Å. The CF3 sorbent had the wide H2-type hysteresis loop observed for CF. The CF3-4M sorbent bound 13% more perchlorate than the CF4M sorbent with only a slight increase in surface area. It is possible that the total target binding capacity could be further increased through improved accessibility to the pore volume. This was not, however, pursued as it is not the only consideration for this effort. In addition to providing binding capacity for perchlorate, this effort sought to provide preferential binding for perchlorate over other environmental targets such as perrhenate. With that in mind, similar batch binding experiments were conducted for nitrate, perrhenate, thiocyanate, sulfate, and phosphate using 10 mg of sorbent in 200 ppm target solutions (5 mL; Tables 21 and 22).

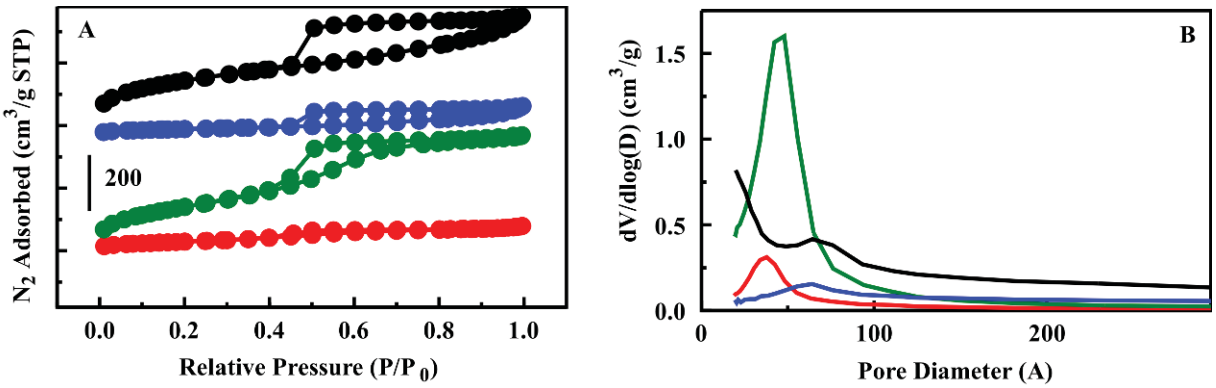

Figure 35. *Nitrogen sorption isotherms (Panel A) and pore size distributions (Panel B) for CF2 (green) and CF3 (black, shifted +390) and the grafted variants CF2-4M (red) and CF3-4M (blue, shifted +370).*

Table 21. *Summary of ions bound by materials variants using 10 mg of sorbent in a 200 ppm solution (5 mL).*

Material	Target Bound (µg)					
	Perchlorate	**Perrhenate**	**Nitrate**	**Thiocyanate**	**Sulfate**	**Phosphate**
HX Products						
HX2M	239	333	114	166	311	200
HX1M3B	216	547	116	84	146	178
HX2M4B	54	330	68	20	121	164
CF Products						
CF4M	188	359	101	112	191	199
CF1M1B	339	633	158	180	78	168
CF2-4M	168	137	60	134	197	163
CF3-4M	258	257	91	191	250	191
Purolite Products						
A530E	670	1000 *	610	750	–	270
A532E	680	1000 *	760	750	–	270

** 100% of target bound; when concentrations of targets were increased to 500 ppm, the Purolite resins also bound 100% of perrhenate (2510 µg), but only 1740 µg (A530E) and 650 µg (A532E) perchlorate.*

Overall, binding ratios varied widely for different ions on different sorbents (Table 22). In these materials, each of the binding sites consists of a single alkylammonium group. Though variations in selectivity between TSPMC and TSPBC might be expected, variations in binding by TSPMC in different structures would not be. The top binding HX sorbents (HX2M and HX1M3B) demonstrated greater binding of perrhenate over perchlorate, though more perchlorate than thiocyanate was bound. Similarly, the CF sorbents bound more perrhenate than perchlorate from identical conditions. The CF2-4M and CF3-4M sorbents, however, bound at least as much perchlorate as perrhenate and bound more perchlorate than most other ions. This data tended to indicate preference for perchlorate binding by functional groups for which perrhenate preference would be expected. When the Purolite resins (A530E and A532E) were evaluated for comparison (Tables 21 and 22), the resins bound significantly more perrhenate than perchlorate. It should be noted that perchlorate binding from batch experiments by these resins was several times greater than that of the organosilicate sorbents. While for larger targets, size exclusion can contribute to the binding properties of mesoporous sorbents, the large pore sizes (53 to 111 Å) and small targets (Table 23) considered here make this effect unlikely. Further, the total target bound from the batch experiments is only a few percent of the total TSPMC/TPSBC used during the grafting steps, and the volume of the target bound is less than 10% of the pore volume available even in the CF4M sorbent.

Table 22. *Ratio of perchlorate bound to ions bound by materials variants using 10 mg of sorbent in a 200 ppm solution (5 mL).*

Material	Target Ratio				
	ClO_4/ReO_4	ClO_4/NO_3	ClO_4/SCN	ClO_4/SO_4	ClO_4/PO_4
	HX Products				
HX2M	0.72	2.10	1.43	0.77	1.20
HX1M3B	0.39	1.86	2.57	1.48	1.21
HX2M4B	0.16	0.79	2.70	0.45	0.33
	CF Products				
CF4M	0.52	1.86	1.68	0.98	0.94
CF1M1B	0.54	2.14	1.88	4.35	2.02
CF2-4M	1.23	2.80	1.25	0.85	1.03
CF3-4M	1.00	2.84	1.35	1.03	1.35
	Purolite Products				
A530E	0.67*	1.10	0.89	–	2.48
A532E	0.68*	0.89	0.91	–	2.52

** Artificially limited by experimental conditions. When target concentrations were increased to 500 ppm for perchlorate and perrhenate, target bound for A530E was increased to 1.74 and 2.39 mg, respectively indicating a ratio of 0.73. For A532E under these conditions, binding of perchlorate was 0.68 mg and perrhenate was 2.37 mg giving a ratio of 0.28.*

Table 23. *Radii for ionic targets considered in these studies.*

Ion	Crystal	Radius (Å) Stokes	CSD [63]	Ionic [64]	References
Perchlorate	–	1.37	1.40(6)	1.81	[65]
Perrhenate	2.60	1.79	1.70(3) *	0.56	[66]
Phosphate	–	–	1.50(4)	0.38	–
Sulfate	–	–	1.47(3)	0.37	–
Nitrate	1.79	1.40	1.24(6)	0.13	[66]
Thiocyanate	2.13	1.58	1.39(5)§	–	–

** search screens refined to select for ionic form only; § reported value is half the S–N distance.*

Batch experiments were completed to provide more thorough characterization of selected materials. Binding isotherms were generated based on a system in which univalent ligands of varying affinity compete for immobilized sites.[67] The expression accounts for the concentration of sites and both ligands (perchlorate and chloride) as well as the affinity of each ligand for the sites. It is:

$$[Perchlorate]_{Bound} = \frac{\frac{K_P}{1 + K_C[Chloride]_{Free}}\,[Sites]_{Total}\,[Perchlorate]_{Free}}{1 + \frac{K_P}{1 + K_C[Chloride]_{Free}}[Perchlorate]_{Free}} \quad (3)$$

where K_P and K_C are the site affinity for perchlorate and chloride, respectively. Concentrations for bound and free perchlorate and free chloride were obtained from IC data. In our implementation, site concentration was a variable to be determined where the volume and mass of sorbent were known quantities. This allowed for calculation of the sites (mole) per gram of sorbent. Figure 36 presents both the experimental data and the calculated data (perchlorate bound) based on fitting of this expression for CF4M. Additional data for other materials is provided in Figure 37 and a summary of the association constants and site loading levels is provided in Table 24.

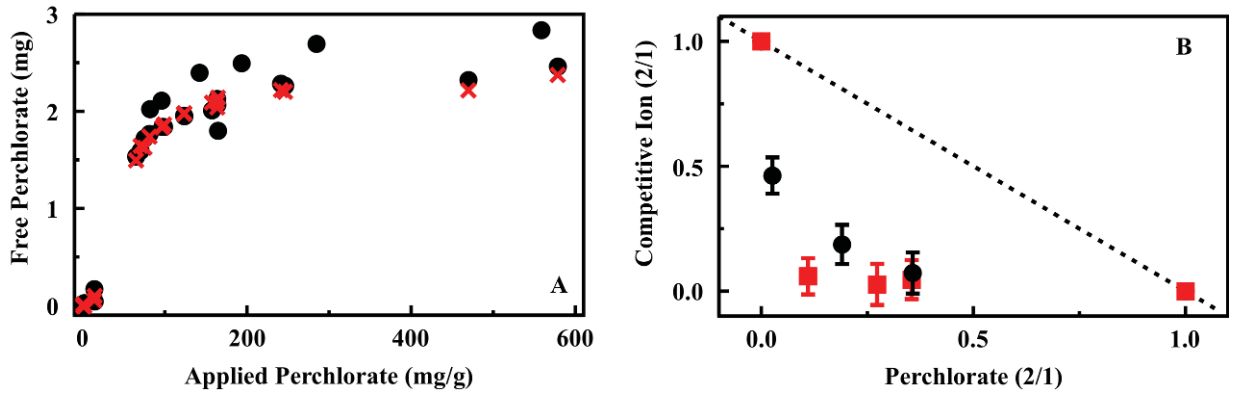

Figure 36. *(Panel A) Perchlorate binding by CF4M from batch experiments. Shown are experimental data (black circle) as well as the results of fitting that data (red ×); (Panel B) Competitive ion binding from mixed target solutions by CF3-4M. Data for each axis is plotted as the ratio of the target bound from the two target solution to that bound from the single target solution: binding from solutions of perchlorate and perrhenate (black circles) and binding from solutions of perchlorate and thiocyanate (red squares).*

Table 24. *Parameters from fits generated for perchlorate binding isotherms. Here, K_P and K_C are the site affinity for perchlorate and chloride, respectively. X is the effective site concentration per gram of sorbent.*

Material	K_P (M^{-1})	K_C (M^{-1})	X (mmol/g)
HX Products			
HX2M	662	494	1.86
HX1M1B	1428	985	1.92
HX4M	6380	881	0.45
HX2M2B	625	844	0.91
HX1M3B	1076	112	0.79
CF Products			
CF2M	1424	789	1.79
CF1M1B	2738	4359	1.85
CF4M	7550	741	0.28
CF4B	8984	265	0.56
CF2M2B	776	3102	1.46
CF1M3B	833	192	1.09
CF2-4M	2348	1104	0.81
CF3-4M	6719	3974	1.74

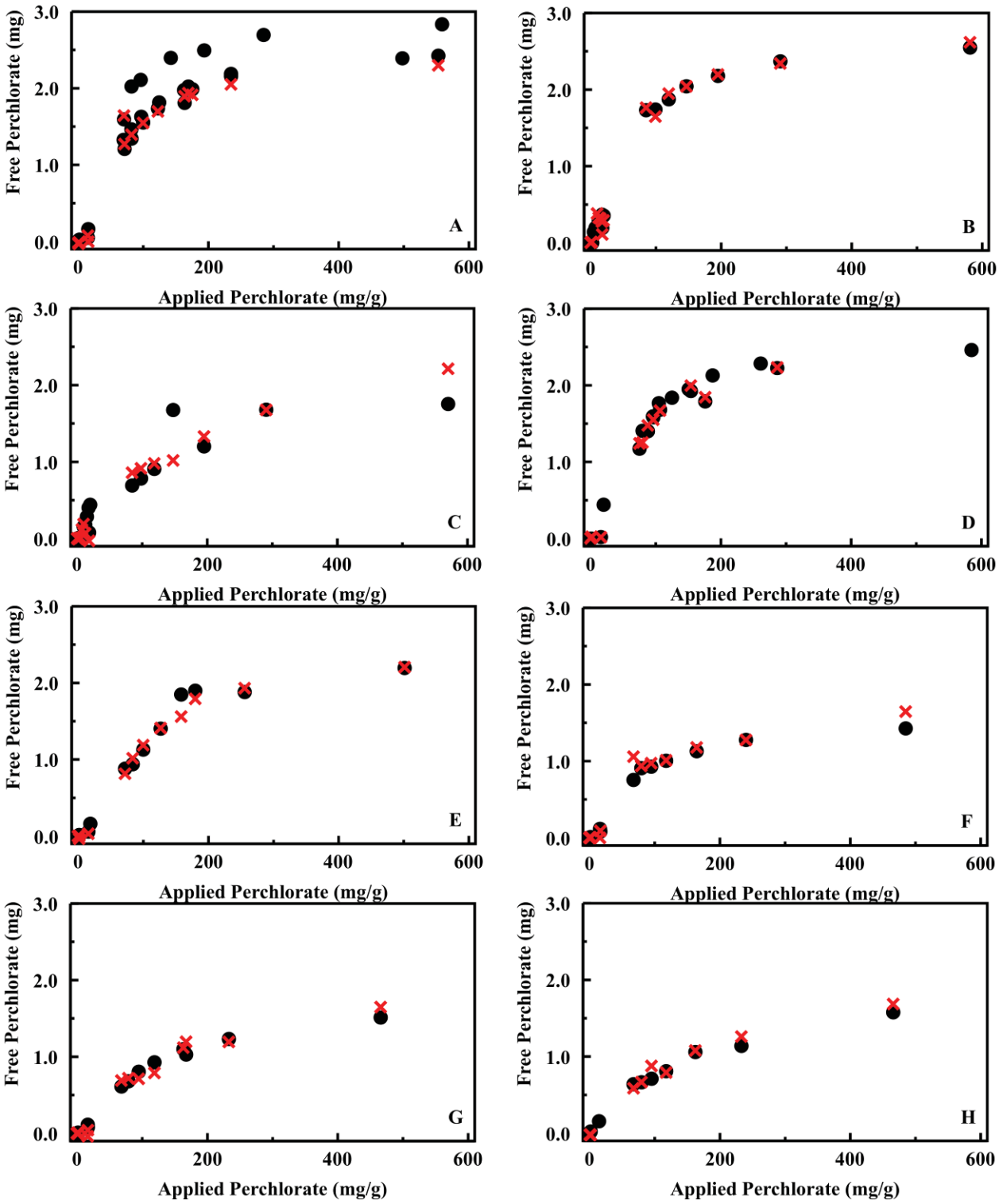

Figure 37. *Perchlorate binding from batch experiments by HX4M (**A**), CF2-4M (**B**), CF3-4M (**C**), CF4B (**D**), CF2M2B (**E**), CF1M1B(**F**), HX1M1B (**G**), CF2M (**H**), HX2M (**I**), HX2M2B (**J**), CF1M3B (**K**), HX1M3B (**L**). Shown are experimental data (black circles) as well as the results of fitting that data (red ×).*

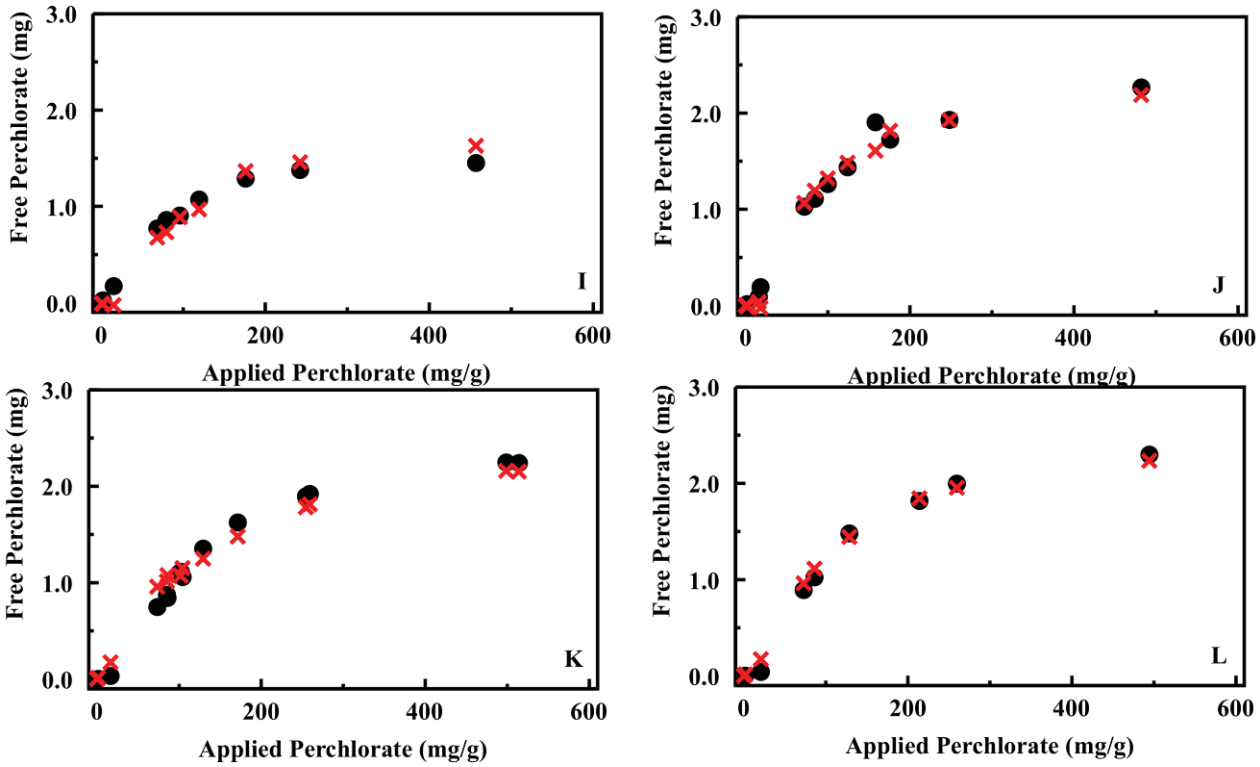

Figure 37. *continued*

From Table 24, the variation in affinity for a specific ligand immobilized in each of the sorbents becomes more apparent. It is also important to note that increasing the functional group loading levels does not necessarily result in additional sites in the sorbents. If site concentrations for HX2M and HX4M are compared in Table 24, HX2M has 1.86 mmol/g and HX4M has 0.45 mmol/g. This result would tend to indicate that loading of HX with 4 mmol of the alkylammonium group resulted in blockage of pores and inaccessible regions in the sorbent. The result is supported by the differences in surface area for the two materials (321 m^2/g for HX2M *versus* 232 m^2/g for HX4M). Another example is CF4M where site concentration is only 0.28 mmol/g and surface area has been reduced by 95% from the base material.

Additional batch binding studies from mixtures of compounds were completed for selected materials to obtain a better understanding of the relative binding of the different ionic targets (Equation 2). In this adapted approach [38,47,48], total target concentration is held constant while the ratios of the ionic compounds are varied. These types of studies tend to indicate whether non-target compounds will interfere with binding of targets. They can also provide an indication of whether two compounds bind to similar sites within a sorbent. This use of the analysis is traditional when the system under consideration involves monolayer binding on surfaces. While the sorbents considered here do not fit that model (based on isotherm analysis), the approach still provides insight into competitive binding by the sorbents. As shown in Figure 36, significant amounts of thiocyanate were not bound from mixtures including perchlorate at any of the concentration ratios (4:1, 1:1, 1:4) by the CF3-4M sorbent. Perrhenate was bound from mixtures, but that binding had only a small effect on the perchlorate bound.

Binding from mixed targets was highly variable across the other sorbents (Figure 38). CF3-4M, CF2-4M, and HX2M preferentially bound perchlorate over perrhenate or thiocyanate. CF4M, CF1M3B, and HX1M3B preferentially bound perrhenate over perchlorate, but bound similar amounts of perchlorate and thiocyanate. These differences capture the effects of varying the functionality of the surfaces through differing ratios of TSPMC and TSPBC. In light of the differences in results for CF4M, CF2-4M, and CF3-4M, however, those effects alone do not account for all of the factors influencing the performance of the materials. It seems likely that factors such as surface curvature and crowding at the alkylammonium group sites influence the performance of the sorbents as well.

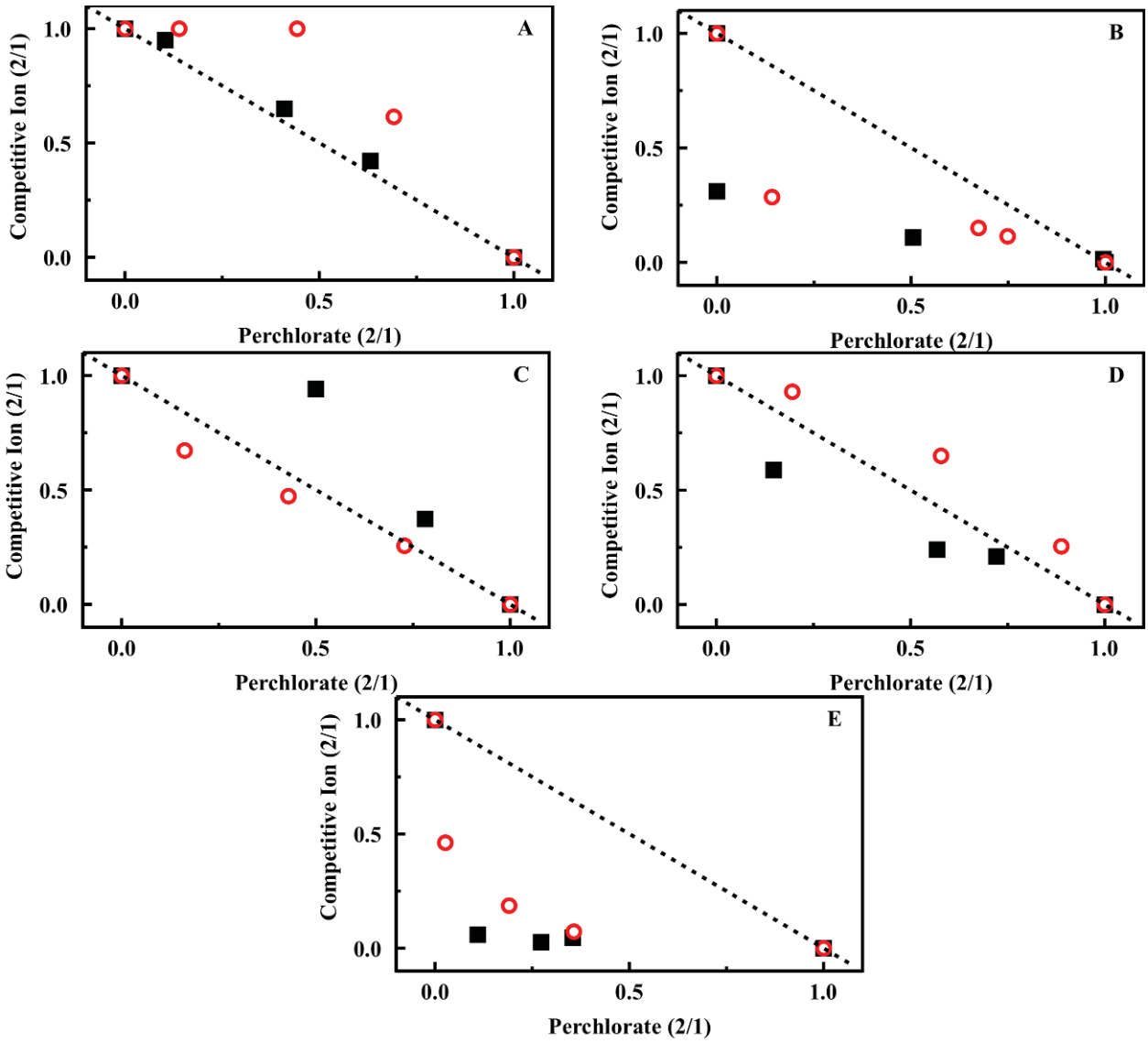

Figure 38. *Competitive ion binding from mixed target solutions. Data for each axis is plotted as the ratio of the target bound from the two target solution to that bound from the single target solution: binding from solutions of perchlorate and perrhenate (red circles) and binding from solutions of perchlorate and thiocyanate (black squares). Target ratios of 4:1, 1:1, and 1:4 were utilized. (**A**) CF4M; (**B**) CF2-4M; (**C**) CF1M3B; (**D**) HX1M3B; (**E**) HX2M.*

Column Binding Experiments

The intention is for these sorbents to be applied in column format for the capture of targets from natural water sources. Column breakthrough experiments were used to evaluate the potential of CF4M, CF2-4M, and CF3-4M (Figure 39) for this application (200 mg sorbent columns). Initial perchlorate breakthrough was observed at approximately 2 mg for CF4M (2.02) and CF3-4M (1.96). For CF2-4M, perchlorate was detected in all effluent volumes. The total capacity before complete perchlorate breakthrough for the columns was 11.40 mg for CF4M, 9.51 mg for CF2-4M, and 13.75 mg for CF3-4M. Binding of all applied target in the initial applications is important to allow quantification of target in the original sample based on that recovered in the eluant. As a result, CF2-4M is a poor candidate for application in this format. The greater capacity of CF3-4M should provide a wider range of applicability for that sorbent. When considered in light of the ion binding ratios described above, CF3-4M offers the combination of features desirable for capture of perchlorate from natural water. Perchlorate breakthrough was similarly evaluated for the commercial resin Purolite A530E (Figure 40). The perchlorate binding capacity of the A530E resin is much higher than that of the sorbents developed here. The column breakthrough studies indicate significant target breakthrough from the initial application. In addition, repeated application of the 0.2 M HCl eluent resulted in recovery of only 27% of the bound target.

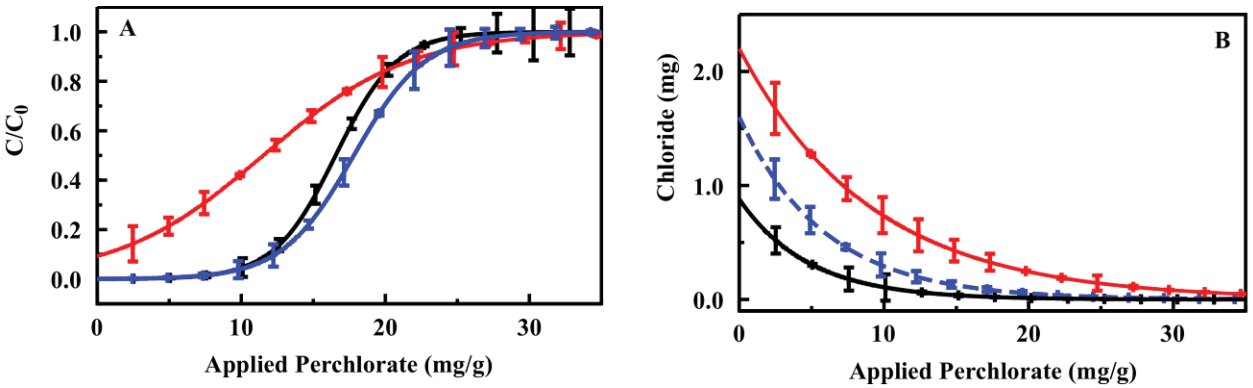

Figure 39. *(Panel A) Perchlorate breakthrough for 200 mg columns of CF4M (solid), CF2-4M (red), and CF3-4M (blue) using a 10 ppm solution at a flow rate of 1 mL/min; (Panel B) Chloride recovered in volumes collected during breakthrough experiments. Similar data for a column of Purolite A530E is provided in Figure 40.*

A single CF3-4M column was used for preconcentration of perchlorate from a series of 100 samples including single and two target spiked deionized water and groundwater samples. No degradation in column performance was observed over the series. Degradation in column performance (reduced target retention) was noted beyond 130 repeated uses (data not shown). Targets were applied as 50 mL samples and elution was accomplished using 2 mL 0.2 M HCl. Figure 41 shows the eluant concentrations for perchlorate applied in deionized water. The complete data set is provided in Table 25. Complete binding of target and full recovery in the eluant volume would have resulted in a concentration enhancement of 25 times. Here, the concentration was enhanced by only 14 times (on average) following preconcentration. A linear dependence between concentration applied and that in the eluant was, however, observed for perchlorate. For these experiments, all perchlorate was bound from samples at less than 2 ppm. Some target was detected in effluent and first wash volumes for target concentrations at 5 and 10

ppm. For the higher target concentrations, perchlorate was also detected in the final HCl purge volume. This residual perchlorate indicates that an increased concentration of HCl may result in greater concentrations in the eluant volume. Unfortunately, the IC method applied here could not be applied with increased HCl concentrations as broadening of the chloride peak interfered with analysis of perchlorate concentrations.

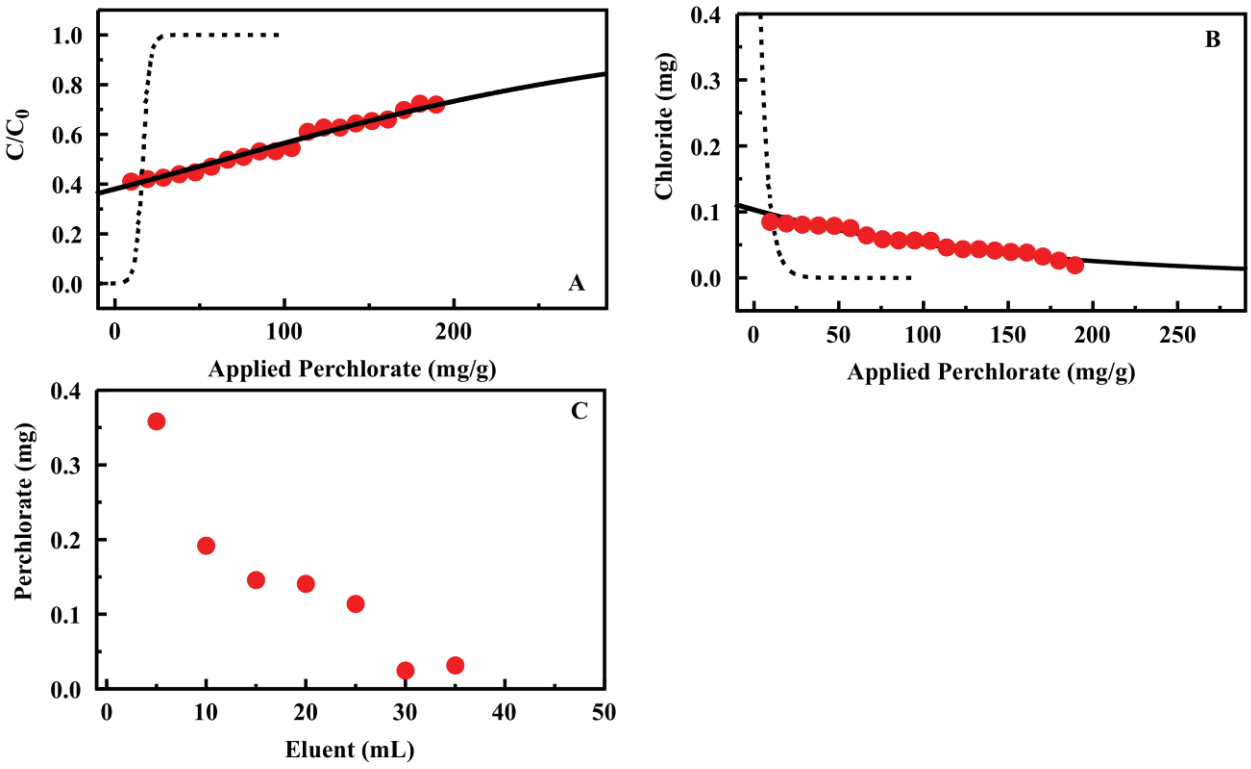

Figure 40. *(**A**) Perchlorate breakthrough for 50 mg column of Purolite A530E using a 10 ppm solution at a flow rate of 1 mL/min; (**B**) Chloride recovered in volumes collected during breakthrough experiment. Dashed lines are from data for CF4M (Figure 39). The capacity of the commercial sorbent is much greater than that of the CF sorbents developed for this study.*

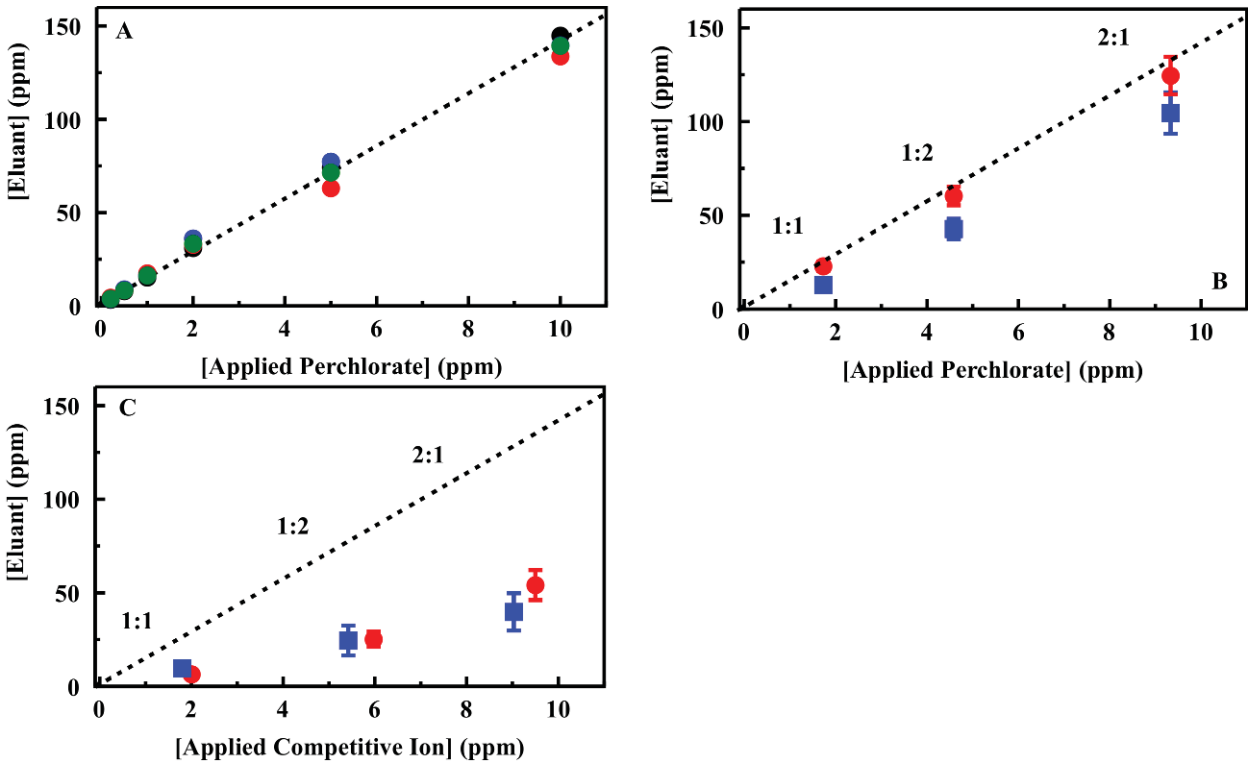

Figure 41. *(Panel A) Perchlorate recovery following preconcentration using a 200 mg column of CF3-4M. Target was applied to the column as a solution of the indicated concentration (50 mL). The column was then rinsed with deionized water (3 mL) before elution of the target in 0.2 M HCl (2 mL). Data points are the concentration of target recovered in the eluent volume for experiments completed in deionized water. The four data sets here were collected prior to (black, red) and following (blue, green) analysis of groundwater samples. A complete data set is provided in Table 25; (Panels B & C) Recovery of perchlorate (Panel B) and competitive ion (Panel C) from mixed solutions in deionized water following preconcentration using a 200 mg column of CF3-4M. Data points are the concentration of ion recovered in the eluent volume for experiments completed using the indicate ratio of perchlorate to perrhenate (red circles) or thiocyanate (blue squares). Dashed lines indicate the fit from Figure 36 for comparison. Complete data sets are provided in Table 26.*

A series of samples containing mixtures of perchlorate and perrhenate or thiocyanate at varying concentrations was prepared (Figure 41) to evaluate the impact of target mixtures on column performance. Total ion concentrations of 4 and 15 ppm were used for which ratios of 1:1, 2:1 and 1:2 perchlorate to competing ion were prepared. Under these conditions, the recovery of perchlorate in the presence of perrhenate (Figure 41) was not statistically different from perchlorate recovery from single target solutions (within 1.5 standard deviations from the mean). The presence of thiocyanate, however, did significantly reduce the recovery of perchlorate. In the eluant volumes for these samples, both perrhenate and thiocyanate concentrations were enhanced by less than the perchlorate concentration enhancement (Figure 41, complete data set provided Table 26).

Table 25. *Perchlorate preconcentration from deionized water. The target recovered in each volume for perchlorate application and recovery from a column of CF3-4M. Target was applied to the column as a solution in 50 mL of deionized water at 1 mL/min (effluent). The column was then rinsed with 3 mL of deionized water (rinse 1) before elution of the target in 2 mL of 0.2 M HCl (eluent). The column was purged with 10 mL of 0.2 M HCl (purge) and rinsed with 3 mL deionized water (rinse 2) before application of the next target sample.*

Target	unit	Applied	Effluent	Rinse 1	Eluent	Purge	Rinse 2	Total
0.2 ppm	µg	10.7	0	0.14	6.60	2.81	0	9.55
	ppm	0.2	0	0.05	**3.30**	0.28	0	–
	%	–	0	1	62	26	0	89
0.5 ppm	µg	26	2.14	0.25	15.85	8.03	0	26.26
	ppm	0.5	0.04	0.08	**7.92**	0.80	0	–
	%	–	8	1	62	31	0	102
1 ppm	µg	50	4.70	0.51	30.46	11.96	0	47.63
	ppm	1.0	0.09	0.17	**15.23**	1.20	0	–
	%	–	9	1	61	24	0	95
2 ppm	µg	99	13.43	1.08	62.08	24.13	0	100.72
	ppm	2.0	0.27	0.36	**31.04**	2.41	0	–
	%	–	14	1	63	24	0	102
5 ppm	µg	250	52.95	3.66	148.59	46.35	0	252
	ppm	5.0	1.06	1.22	**74.30**	4.64	0	–
	%	–	21	1	59	19	0	101
10 ppm	µg	500	115.30	0.39	289.62	9.61	0	501
	ppm	10	2.31	0.13	**144.81**	96.08	0	–
	%	–	23	0	58	19	0	100

Table 26. *Perchlorate preconcentration from mixed target solutions. The target recovered in each volume for perchlorate plus competing ion application and recovery from a column of CF3-4M. Target was applied to the column as a solution in 50 mL of water at 1 mL/min (effluent). The column was then rinsed with 3 mL of deionized water (rinse 1) before elution of the target in 2 mL of 0.2 M HCl (eluent). The column was purged with 10 mL of 0.2 M HCl (purge) and rinsed with 3 mL deionized water (rinse 2) before application of the next target sample.*

Target mixture	unit	Applied	Effluent	Rinse 1	Eluent	Purge	Rinse 2	Total
2 ppm perchlorate + 2 ppm perrhenate	µg	84.64	33.05	1.89	38.74	5.17	0	78.86
	ppm	1.69	0.66	0.63	19.37	0.52	0	–
	%	–	39	2	46	6	0	93
	µg	85.54	89.81	0	21.84	0	0	61.64
	ppm	1.71	0.80	0	10.92	0	0	–
	%	–	47	0	26	0	0	72
10 ppm perchlorate + 5 ppm perrhenate	µg	462.34	207.02	14.81	239.35	15.42	0	476.59
	ppm	9.25	4.14	4.94	119.67	1.54	0	–
	%	–	45	3	52	3	0	103
	µg	284.73	107.72	7.43	97.52	4.60	1.68	218.64
	ppm	5.69	2.15	2.48	48.76	0.46	0.46	–
	%	–	38	3	34	2	0	77
5 ppm perchlorate + 10 ppm perrhenate	µg	238.38	9.68	6.46	115.76	6.87	0	228.77
	ppm	4.77	1.99	2.15	57.88	0.69	0	–
	%	–	42	3	49	3	0	95.97
	µg	508.72	293.62	19.31	205.03	6.56	1.38	525.88
	ppm	10.17	5.87	6.44	102.51	0.65	0.46	–
	%	–	58	4	40	1	0	103
2 ppm perchlorate + 2 ppm thiocyanate	µg	84.57	33.88	2.02	38.93	0	0	74.83
	ppm	1.69	0.68	0.67	19.47	0	0	–
	%	–	40	2	46	0	0	88
	µg	91.70	43.42	3.30	37.64	5.57	0	89.93
	ppm	1.83	0.87	1.10	18.82	0.56	0	–
	%	–	47	4	41	6	0	98
10 ppm perchlorate + 5 ppm thiocyanate	µg	426.25	214.34	10.66	222.18	10.60	0	457.78
	ppm	8.53	4.26	3.55	111.09	1.06	0	–
	%	–	50	3	52	2	0	107
	µg	218.90	119.92	5.74	91.31	8.89	0	225.86
	ppm	4.38	2.40	1.91	46.65	0.89	0	–
	%	–	55	3	42	4	0	103
5 ppm perchlorate + 10 ppm thiocyanate	µg	246.12	113.86	21.62	79.05	0	0	214.53
	ppm	4.92	2.28	7.21	39.53	0	0	–
	%	–	46	9	32	0	0	87
	µg	474.76	234.37	45.60	149.43	9.63	0	439.02
	ppm	9.50	4.69	15.20	74.71	0.96	0	–
	%	–	49	10	31	2	0	92

Groundwater Samples

When spiked groundwater samples were analyzed, little or no target was retained by the CF3-4M sorbent column. Analysis of perchlorate in other matrices (pond water, tap water, barrel collected rain water and soil extracts) showed similar results with little or no retained target. Column degradation was initially suspected, but additional analysis of samples in deionized water returned the expected results (Figure 41). Analysis of the water samples by IC indicated

varying concentrations of sulfates, phosphates, and chloride, but not at levels that would be expected to fully prevent perchlorate binding. It was possible to achieve some perchlorate binding through dilution of the water samples (in deionized water) indicating the presence of other competing compounds. It was not clear whether this competition was the result of other small ionic targets not included in the IC analysis or to proteins and other organic compounds which may adsorb to the charged surface of the sorbents. The commercial sorbents retained perchlorate at levels similar to those observed for deionized water samples (Table 27).

Table 27. *Perchlorate preconcentration from groundwater using Purolite resins. The target recovered in each volume for perchlorate application and recovery. Target was applied to the column as a solution in 50 mL of water at 1 mL/min (effluent). The column was then rinsed with 3 mL of deionized water (rinse 1) before elution of the target in 20 mL of 0.2 M HCl (eluent). The column was rinsed with 5 mL deionized water (rinse 2) before application of the next target sample. Groundwater was collected from a household wells in Fulton, MD, USA (depth of 213 m) and filtered using a 0.7 µm filter flask before spiking with the indicated target concentration.*

Material	Target	Unit	Applied	Effluent	Rinse 1	Eluent	Rinse 2	Total
Purolite A530E	10 ppm	µg	500	34.12	0	90.71	0.53	125.35
		ppm	10	0.68	0	4.53	0.11	–
		%	–	7	0	18	0	26
Purolite A530E	50 ppm	µg	2500	108.01	0.16	105.06	0.71	213.94
		ppm	50	2.16	0.05	5.25	0.14	–
		%	–	5	0	4	0	9
Purolite A532E	10 ppm	µg	500	10.25	0	8.48	0	18.73
		ppm	10	0.21	0	0.42	0	–
		%	–	2	0	2	0	4
Purolite A532E	50 ppm	µg	2500	44.04	0	10.01	0	54.05
		ppm	50	0.88	0	0.50	0	–
		%	–	2	0	0	0	2

In order to address the difficulty presented by complex matrices, an activated charcoal (AC) preparatory step was utilized. The AC column was prepared identically to the CF3-4M column using 200 mg of the material. For the concentration range evaluated (0.2 to 100 ppm), 85% of the perchlorate passed through the AC column (Table 28). When effluent recovered from the AC column was applied to the CF3-4M column, perchlorate was retained. Elution using HCl as described above resulted in enhanced perchlorate concentrations; however, the enhancements were not as significant as those observed for samples in deionized water (Figure 42; Table 29). Sampling from the groundwater matrix resulted in increased noise in the baseline of IC chromatographs leading to an increased limit of detection for perchlorate and greater difficulty in analysis of low concentrations. As a result, concentrations in effluent, wash, and purge steps were not detected for several of the samples evaluated. It is likely that reduced enhancement is due to decreased target retention in these samples even following the AC step. As an alternative to the AC preparatory step, samples were treated with hydrogen peroxide.[68] For this process, spiked groundwater samples were prepared as above at 100 ppm and 50 ppm. The samples were then diluted 1:3 using either 30% hydrogen peroxide or deionized water. A larger percentage of target was retained from samples treated with peroxide (10%). This result further supports the likely interaction of organic carbon in the samples with the sorbent surfaces.

Table 28. *Perchlorate recovered from activated charcoal preparatory step in parts per million (ppm).*

Applied	Effluent	Variation
0.28	0.23	0.02
1.38	1.14	0.03
6.71	5.59	0.15
10.55	8.19	1.01
46.30	40.53	1.03
88.30	81.49	4.71

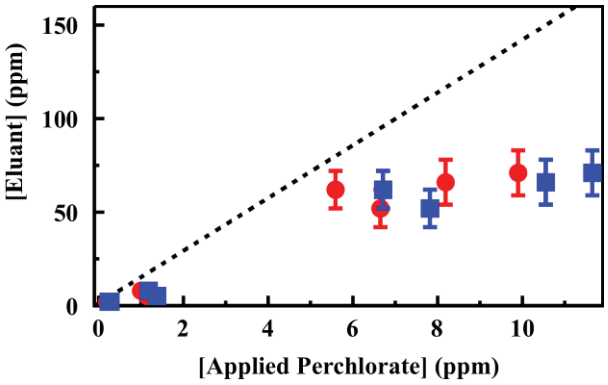

Figure 42. *Perchlorate recovery from groundwater using a 200 mg column of CF3-4M. Target was applied to the column following preparation using a 200 mg activated charcoal column (50 mL). The column was then rinsed with deionized water (3 mL) before elution of the the target in 0.2 M HCl (2 mL). Data points are the concentration of target recovered in the eluent volume versus the concentration recovered from the AC column (circles) and versus the initial target concentration (squares). Complete data sets are provided in Tables 28 and 29.*

Table 29. *Perchlorate preconcentration from groundwater. The target in each volume for perchlorate application and recovery from a column of CF3-4M. Target was applied to the column as a 50 mL solution recovered following the AC preparatory column (Table 28; 1 mL/min; effluent). The column was then rinsed with 3 mL of deionized water (rinse 1) before elution of the target in 2 mL of 0.2 M HCl (eluent). The column was purged with 10 mL of 0.2 M HCl (purge) and rinsed with 3 mL deionized water (rinse 2) before application of the next target sample.*

Target	unit	Applied	Effluent	Rinse 1	Eluent	Purge	Rinse 2	Total
0.2 ppm	µg	11.5	0	0	4.1	0	0	4.1
	ppm	0.2	0	0	**2.1**	0	0	–
	%	–	0	0	36	0	0	36
1 ppm	µg	57	0	0	10	0	0	10
	ppm	1.1	0	0	**5.2**	0	0	–
	%	–	0	0	18	0	0	18
5 ppm	µg	333	0	0	104	0	0	104
	ppm	6.65	0	0	**52**	0	0	–
	%	–	0	0	31	0	0	31
10 ppm	µg	411	96	0	132	0	0	228
	ppm	8.2	1.9	0	**66**	0	0	–
	%	–	23	0	32	0	0	55

Task 5. Liquid/Liquid Approach

Having developed materials that would address the needs of preconcentration, it was necessary to address development of systems for the application of these sorbents with a view toward their combination with electrochemical and ion mobility spectrometry based detection. During this process, the necessity for alterations to the morphological characteristics of the SPE sorbents was identified for application with the systems under development. The initial effort focused on diethylbenzene bridged organosilicate sorbents and determining precursor ratios providing a balance between morphological and binding characteristics and on development of semi-selective binding characteristics within the sorbents.[8,38,39] Proof of concept data demonstrating the function of those materials in relevant matrices was provided.[38,40,69] Several of the subsequently developed materials were evaluated to determine what, if any, advantages they offer over the originally developed MM1 sorbent. MM1 was synthesized using a 1 to 1 ratio of diethylbenzene (DEB) bridging groups to ethane (BTME) bridging groups with 12.6% of the total surfactant consisting of a modified surfactant imprint template (Table 30).[38] The material offers macroscale texture with an ordered mesopore structure. The macroscale texture provided reduced the pressure needed to drive fluid flow when sorbents were applied in column formats for solid phase extraction. The subsequently developed ED13 was synthesized with increased concentrations of acid and swelling agent.[39] The result was a more defined macroscale texture (Figure 43) as well as increased surface area, pore volume, and pore diameter (Table 30). D7 was synthesized using 100% DEB bridging groups with further modified acid and swelling agent concentrations.[39] DEB groups were initially found to provide higher binding capacity for nitroenergetic targets at the expense of morphological characteristics and selectivity.[32] The synthetic protocol developed for D7 provided morphological characteristics similar to MM1.

Table 30. *Material composition and characteristics.*

Material	Composition	Mass TMB (g) [1]	Mass HNO_3 (g) [2]	Surface Area (m^2/g)	Pore Vol (cm^3/g)	Pore Dia (Å)	Sorbent Mass (mg) [3]	TNT Capacity (mg/g)	Initial TNT breakthrough (mg/g)
MM1 [38]	50:50 BTE:DEB	0.20	6.0	366	0.26	35	200	2.7	2.1
ED13 [39]	50:50 BTE:DEB	0.60	7.5	712	0.75	65	141	3.2	0.3 [4]
D7 [39]	100 DEB	0.90	7.5	414	0.42	49	82	3.1	0.4

[1] Mass of TMB included with 1.9 g total surfactant; [2] Mass of 0.1 M HNO_3 solution included in synthesis; [3] Sorbent mass utilized for column breakthrough experiment; [4] Reduction of flow rate to 1 mL/min increases the value to 0.74 mg/g

The performance of the newly developed materials was compared to that of MM1 (Figure 43) using column format, target breakthrough testing. While D7 provided a total TNT binding capacity similar to MM1 (Table 30), the breakthrough profile showed early initial target breakthrough with total capacity reached through slow partial target binding. MM1, on the other hand, initially bound all applied target reaching a sharp breakthrough much closer to the total binding capacity. ED13 provided an improved TNT binding capacity; however, the breakthrough characteristics of this sorbent were similar to those of D7. The increased binding capacity was likely due to the increased available surface area (Table 30) and improved accessibility of that surface area due to larger mesopore diameters. ED13 also offered less resistance to flow of solutions through the sorbent column than either the D7 or MM1 sorbents. This reduced

resistance contributed to the observed breakthrough characteristics as contact time with the sorbent was reduced under an equivalent driving pressure. When the flow rate through ED13 (initially 2.5 mL/min) was reduced to match that achieved with MM1 and D7 (1 mL/min), an extended region of complete target binding was obtained (Figure 43).

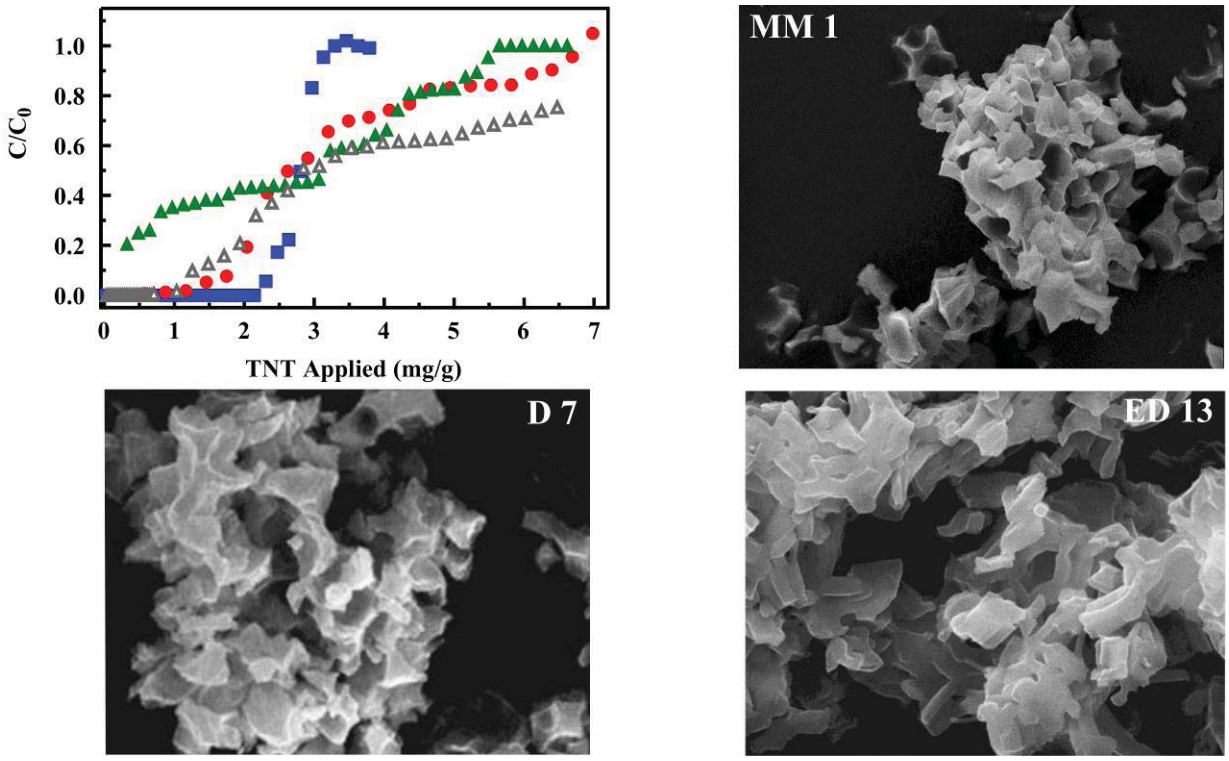

Figure 43. *Impact of sorbent variations. (top left) TNT breakthrough curves for MM1 (blue squares; 200 mg sorbent), D7 (red circles; 82 mg sorbent), and ED13 (green triangles; 141 mg sorbent). Data for ED13 at a lower flow rate (gray triangles) is also presented. SEM images of MM1, D7, and ED13 show variations in macro-morphology.*

Though the earlier initial breakthrough observed for ED13 would appear to make MM1 the favored material, there are other considerations in selection of the best sorbent for the applications of interest here. First, the issue of backpressure is a critical consideration when forcing liquids through the column. The goal, here, is to develop a portable system for target preconcentration, so power requirements are an important consideration. Greater pressure in the system requires a larger driving force and, therefore, greater energy consumption. This aspect and the advantages of the ED13 sorbent over MM1 are discussed in detail in the selection of system components in the section below. Initial breakthrough for the ED13 column occurred at 0.74 mg/g. At the drinking water equivalent level (DWEL) of 20 µg/L for TNT, a system using a 100 mg sorbent column could bind 100% of the target from 3.7 L of water before reaching the breakthrough loading level. This volume is well beyond the sample volume intended for the application under consideration. Sampling volumes of less than 0.1 L are expected. Given these considerations, ED13 offers a significant advantage over MM1 in the reduction of backpressure.

Liquid/Liquid Preconcentration

Having developed novel sorbents providing binding characteristics necessary for preconcentration, it was necessary to have the applicable associated systems. Figure 44 presents

a schematic of the system concept for use of the sorbents with aqueous samples and liquid target elution. The system was intended to provide sample collection, preconcentration, and elution prior to analysis by an electrochemical detector. Here, aqueous samples are pulled through a filter stack to eliminate particulate (size exclusion). A peristaltic pump is employed to pull the sample through filters and a 3-way solenoid valve and to push it through the column where target is captured by the sorbent. A peristaltic pump is desirable as the liquid does not come in contact with the pump machinery and, therefore, issues related to corrosion and clogging are minimized. The use of a single pump also provides the potential for a more compact final system. The post column solenoid valve ensures that the sample that has passed through the column is discarded. Once target is adsorbed to the sorbent, the pre-column valve is switched and eluent is pushed through the column by the peristaltic pump. The desorbed targets are then directed to the electrochemical detector by switching the post-column solenoid valve. In order to evaluate this approach to design of a system, a bench scale, bread-board level, prototype was assembled using a peristaltic pump with a 900:1 motor and 0.143" rollers (P625/900.143, Instech Laboratories, Plymouth Meeting, PA, USA). The pump was combined with 0.031" silicone tubing to provide flow rates up to 0.8 mL/min through the sorbent column using a 9 V battery. The operation voltage for the solenoid valves (5 V, Lee Products, Westbrook, CT, USA) is controlled using on/off switches. Sorbent columns (MM1) were prepared in stainless steel HPLC column housings (4.6 × 33 mm, Bischoff Chromatography, Leonburg, Germany) using a mass of 60 mg.

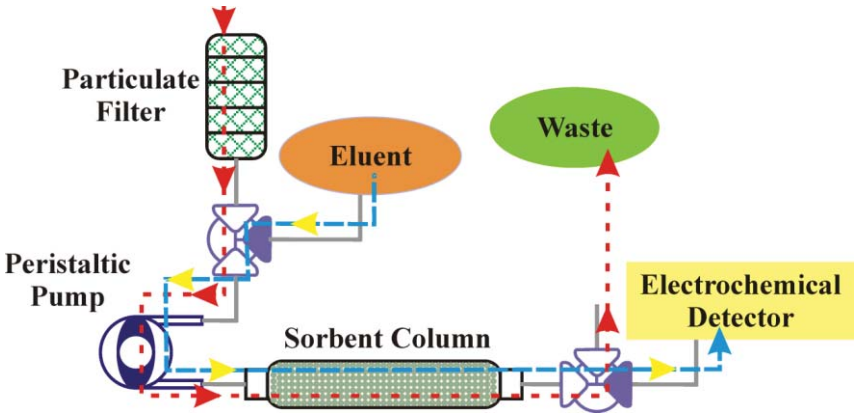

Figure 44. *Schematic of the liquid/liquid system. Here, the red line indicates the flow of the sample solution through the system, and the blue line indicates the flow of eluent through the system.*

A series of experiments using nitroenergetic targets in deionized water was completed using the prototype system. Sample solutions containing target concentrations of 200, 50, 5, and 0.9 ppb for TNT, RDX, DNT, NG, and HMX were evaluated in triplicate. For each sample, 20 mL of the sample solution was passed through the sorbent. A water wash of 3 mL was then passed through the column followed by 2 mL acetonitrile and an additional 3 mL water wash. Each of the volumes was analyzed by HPLC to determine target retention and the preconcentration potential of the system (Figure 45). These experiments yielded highly variable results. We found that, though the system performed for five to eight samples, column pressures increased with successive usage cycles. The result of increasing back pressure was a reduction in flow rate (0.8 mL/min to as little as 0.2 mL/min) and tailing of the eluted target into the final rinse volume. Alternatively, tunneling through the sorbent (passing of solutions through voids in the column rather than through pores in the sorbent) resulted, leading to poor target retention. Tunneling was observed as failure of the column to bind the targets and higher than expected flow rates (>0.8

mL/min). The frits provided with the column housings were also highly subject to clogging both by particluate in the samples and by sorbent material.

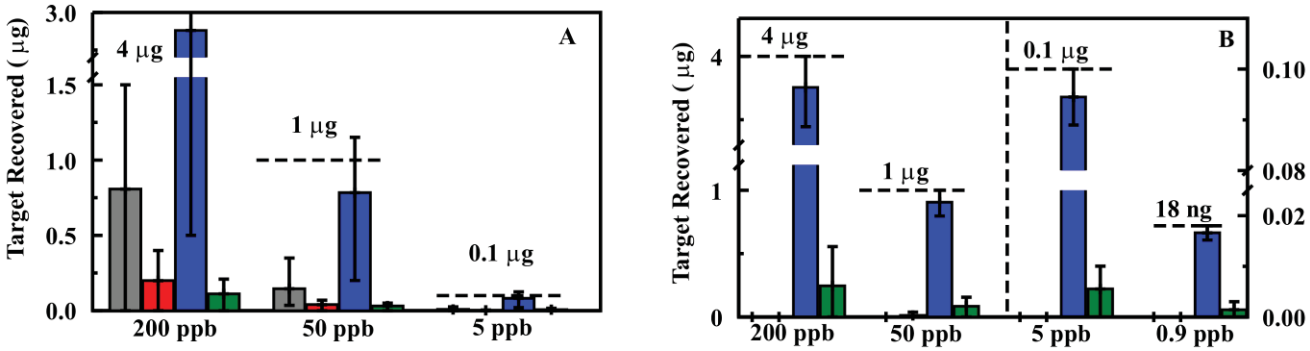

Figure 45. *Analysis of samples using the liquid/liquid system with an HPLC column housing (60 mg, MM1 sorbent). Flow rates varied between 1.0 and 0.3 mL/min. Adsorption of target (effluent; gray) was followed by a water rinse (3 mL; red), target elution (2 mL acetonitrile; blue), and an additional water rinse (3 mL; green). (A) TNT experiments for which there was tunneling through the sorbent column. (B) TNT experiments for which the flow rate was slowed to 0.3 mL/min by the excessive pressure in the system. All data points are the average of three target adsorption/elution cycles. Similar results were obtained for RDX, HMX, and DNT (not shown).*

The column housing was changed in an attempt to improve flow rates and reduce pressure while providing the desired target retention. An Omnifit borosilicate column housing (6.6 × 50 mm, Diba Industries, Mahopak, NY, USA) was selected, and a 75 mg sorbent column (MM1) was packed. The experiments described above were repeated using this sorbent column in the prototype system with somewhat improved results; however, the performance still fell short of what was expected based on previous experiments.[32,38,40] Both the increased pressure and tunneling effect observed for the HPLC column housing were observed for this housing as well. Based on the reduced pressures observed for the ED13 sorbent, this sorbent was substituted for MM1 in the experiment. This led to a significant improvement in the pressure in the system over repeated tests. Further improvement was achieved through replacement of the column housing with one of a larger diameter (10 mm) allowing for an increase in the sorbent mass utilized (200 mg; Figure 46). The results achived with the prototype system were comparable to those observed for the sorbents when used in an offline configuration.[32,38,40]

A sensing system of this type requires filters to protect the column from particulate. Combinations of standard filters were evaluated to determine which would provide the necessary level of particulate removal without nonspecific target capture. Given the pressure issues noted above, filters providing minimal increase in pressure were also desired. Whatman GF/F (0.7 µm pores) and GF/D (2.7 µm pores) glass fiber filters were selected. Nonspecific binding of targets to these types of filters is negligible. Combinations of these filters were evaluated, and a two filter series (GF/D followed by GF/F) was found to provide the necessary protection for the system components (Figure 47).

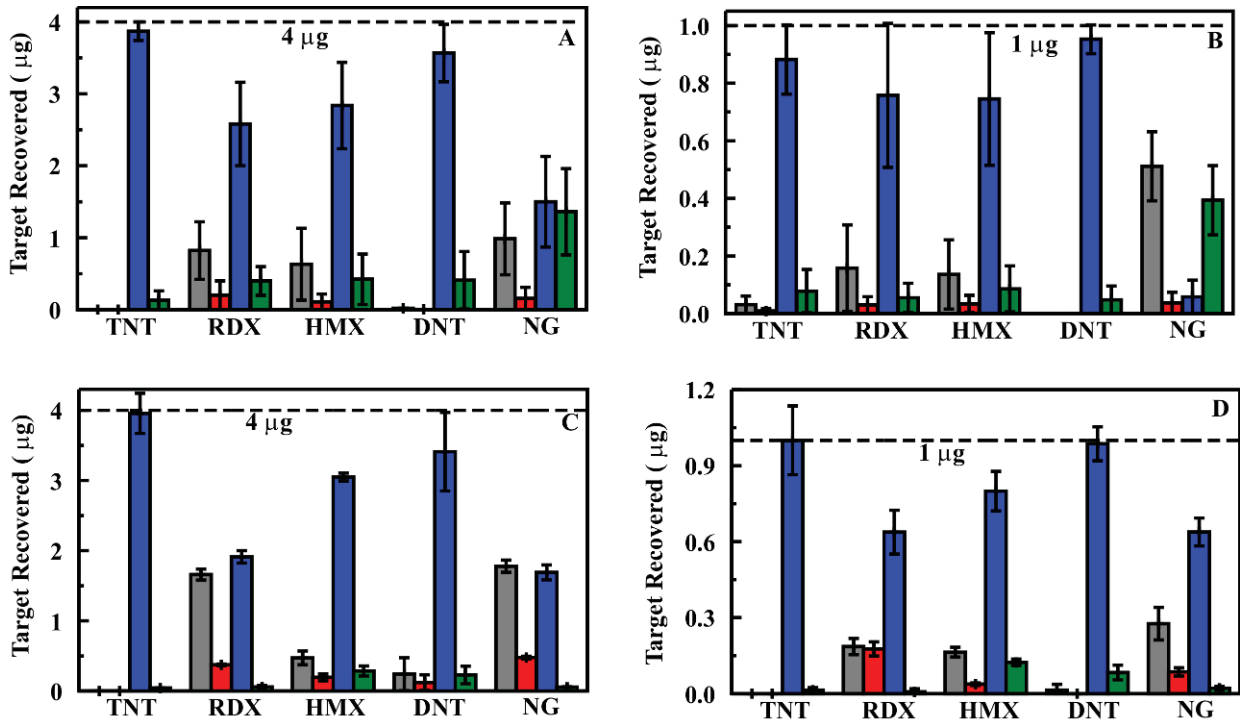

Figure 46. *Analysis of samples using the liquid/liquid system with a 10 mm Omnifit column housing and 200 mg ED13 sorbent. Targets were applied at 0.8 mL/min. Adsorption of target (effluent; gray) was followed by a water rinse (3 mL; red), target elution (2 mL acetonitrile; blue), and water rinse (3 mL; green). All data points are the average of three target adsorption/elution cycles. Samples were prepared in deionized (200 ppb (**A**) and 50 ppb (**B**)) and well water (213 m well; 200 ppb (**C**) and 50 ppb (**D**)).*

Having established a prototype system that would function as desired, a number of samples were evaluated to provide an indication of performance over an extended use period. A single sorbent column (the same used for samples in deionized water, 200 mg ED13; Figure 46) was utilized for evaluation of spiked ground water samples (Figure 48). Ground water samples were collected from household wells in Clarksville, MD (depth of 114 m) and Fulton, MD (depths of 122 and 213 m), USA to provide matrices of varying composition. The well at 213 m provides water that smells of sulfur while water from the other wells was free of odor. Water from the well at 213 m appeared slightly cloudy while water from the other wells was clear. In total, 175 samples were evaluated using the column with 75 of those in ground water (15 samples at 200 ppb, 15 samples at 50 ppb, and 45 samples at 5 ppb). Each sample consisted of application of the target solution (20 mL) followed by rinsing of the column with deionized water (3 mL). The target was then eluted in acetonitrile (2 mL) and the column was again rinsed with water (3 mL) to prepare it for the next sample. All four of these volumes were analyzed individually by HPLC to determine target content and concentration.

The total time for the solid phase extraction processing using the 200 mg ED13 column in the prototype system was 30 min. This time requirement is dependent on the flow rate of solutions through the system (1 mL/min in this case). In all cases, target was detected in the spiked ground water samples. The enhancement in target concentration in the eluent volume varied from target to target as expected based on previous results.[38,40] There was some variation between the matrices as well. The pH of all of the water samples was between 6 and 6.5. Since all samples were filtered prior to validation by HPLC or passage through the prototype, the particulate levels were the same. Ion chromatography (EPA Method 314) indicated varied levels of sulfate and nitrate in the samples, with the 213 m well showing the highest concentrations as well as smelling of sulfur. We have reported similar variations in enhancement for experiments in which samples were prepared in artificial sea water or for targets extracted from soil samples.[38,40] Though the factors influencing the differences have not been thoroughly identified, the variations are not unexpected in complex sample matrices.

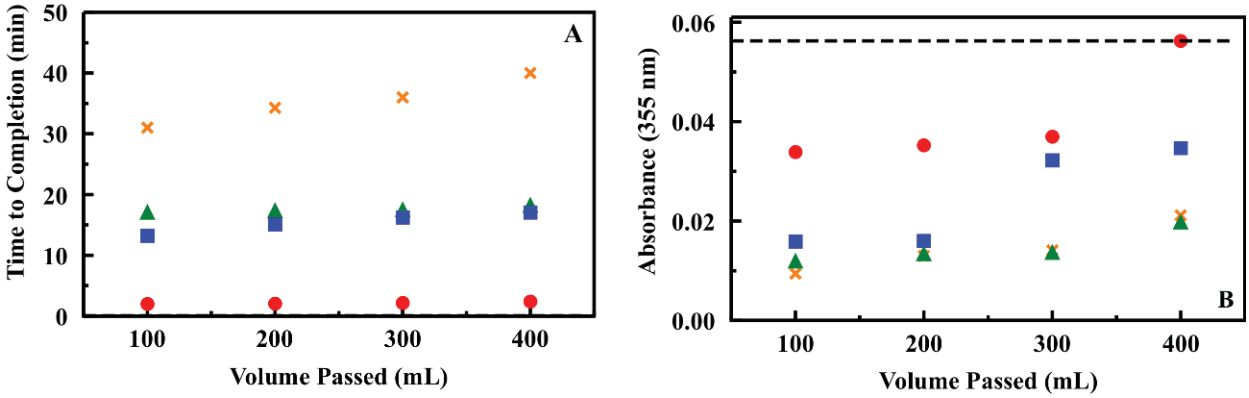

Figure 47. *Filtration of particulate using Whatman GF/F and GF/D filters. The pressure generated by the filter configurations was determined based on the time to complete passage of 100 mL with no additional applied pressure (Panel A). The filtration setup used a Chemglass beaker with glass frit (40 µm pore size). A Millipore dual opening funnel was clamped to the beaker. The filter configuration was placed between the funnel and the beaker frit. The solution to be filtered was prepared by addition of fine soil to deionized water (5 g/L). The effectiveness of filtration was determined from turbidity based on the absorbance intensity of the solution at 355 nm (Panel B). GF/D (red); GF/F (blue); stack of two GF/F filters (orange); stack of one GF/D and one GF/F filter (green); dashed line indicates turbidity of initial solution.*

During analysis of this sample series, it was necessary to replace the silicon tubing used in the peristaltic pump three times. Continued use of a single tubing set resulted in damage and eventual rupture of the tubing after 100 to 150 h of system use. Reduction in the pressure within the system is necessary to stabilize the pump and prevent this damage. The pressure in the prototype system is overwhelmingly due to the sorbent column. We found that a significant portion of the pressure generated by the column could be reduced through changing the frits used. The frits supplied with the Omnifit columns are PTFE with 10 µm pores. Use of 25 µm PTFE frits reduced the pressure in the system (as evidenced by greater flow rates under identical driving pressure). Alternative frits or pumps, such as miniature hydraulic or external gear pumps, may be necessary for extending the use time of such a system between maintenance.

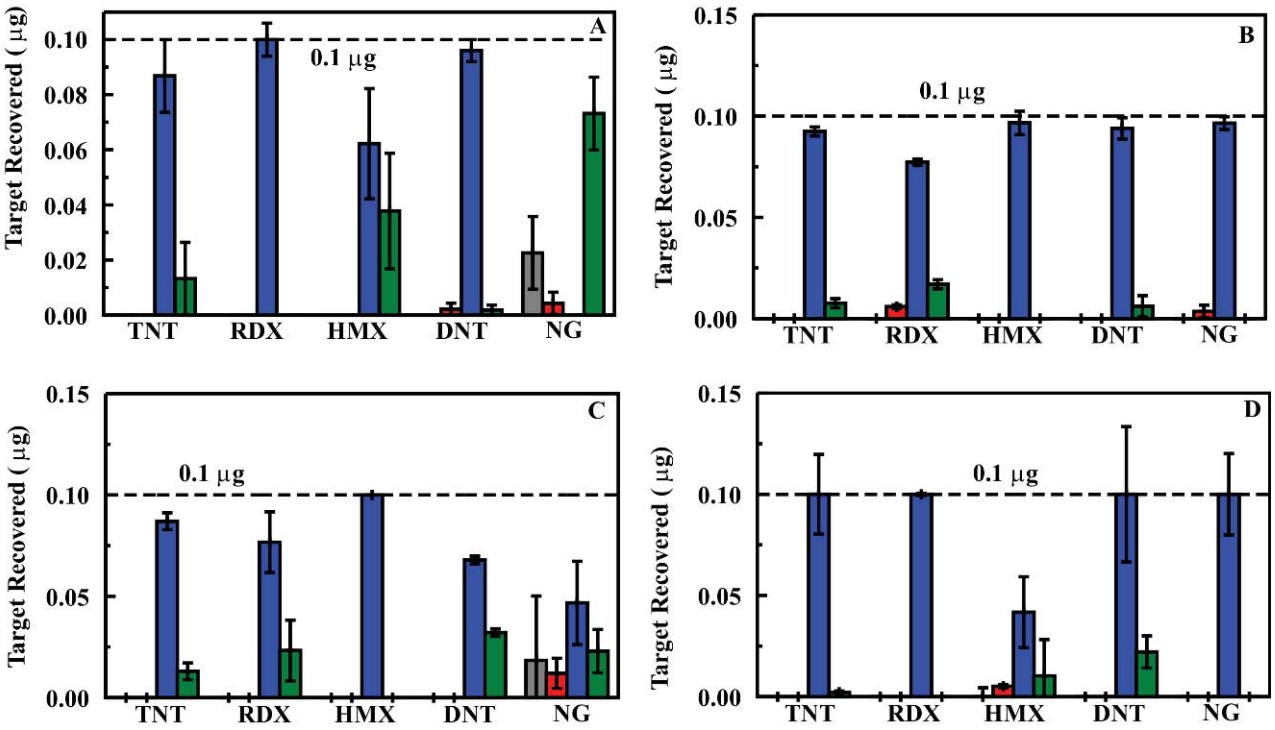

Figure 48. *Analysis of samples in varied matrices. Here, the liquid/liquid system was used with a 10 mm Omnifit column housing and 200 mg ED13 sorbent. Targets were applied at 0.8 mL/min. Adsorption of target (effluent; gray) was followed by a water rinse (3 mL; red), target elution (2 mL acetonitrile; blue), and an additional water rinse (3 mL; green). All data points are the average of three target adsorption/elution cycles. Samples (5 ppb) were prepared in deionized water (**A**), 114 m well water (**B**), 122 m well water (**C**), and 213 m well water (**D**).*

Electrochemical measurements

A major obstacle to application of electroanalytical techniques in a fielded platform is their limited sensitivity. Preconcentration of targets utilizes large volume samples to provide sufficient analyte mass for obtaining a detectable signal. Solid-phase extraction (SPE) techniques have been successfully applied to the preconcentration of aromatic explosives from aqueous samples; however, the numerous steps involved in SPE can be lengthy and time-consuming.[9,11,13,70] Commercially available resins such as divinylbenzene-vinyl-pyrrolidone (Porapak R), and divinylbenzene-ethylvinylbenzene (LiChrolute EN) have been evaluated for microscale SPE of nitroaromatics and show promise for enhancing LODs.[13] These types of materials offer only low selectivity and a limited number of reuse cycles. The materials developed under this effort offer significant advantages. It is necessary, however, to develop methods appropriate to their use in-line with electrochemical detection. We have evaluated the effect of differing buffer compositions on pre-concentration and release of TNT from these novel sorbents and optimized protocols for use of the sorbents with electrochemical detection

Pre-concentration and rapid release experiments were performed using a Shimadzu HPLC equipped with two pumps (model # LC-10AS) and a UV-vis spectrophotometric detector (model # SPD-10AV). Approximately 40 mg of DEB sorbent (D7 from Table 10 with and without imprint) was wet packed into a metal jacketed pre-column (with a diameter of 4 mm and a length of 10 mm) and placed in-line before the UV-vis spectrophotometric detector. An electrochemical flow cell from BASi (West Lafayette, IN) was attached after the UV-vis detector. The electrochemical flow cell contained a glassy carbon working electrode (3mm in diameter) and an Ag/AgCl reference electrode. The glassy carbon working electrode was polished with an alumina suspension as suggested by the manufacturer.

Sample volumes of 2 to 480 mL of TNT at concentrations between 0.5 and 500 ppb in various buffers were injected into the system under a constant flow rate of 500 µL/min. An injection loop was used to deliver 2 mL volumes. The second pump was used to deliver the larger volumes and the flow rate was increased to 2 mL/min to pre-concentrate volumes larger than 100 mL. During the pre-concentration step for samples > 200 ppb no breakthrough of TNT from the column was detected at 230 nm. Using the 2 mL injection loop, TNT was released from the column with various solvent mixtures at a flow rate of 500 µL/min. TNT was detected at 230 nm and then detected electrochemically using square wave voltammetry driven by a model 440 electrochemical workstation (CH Instruments, Austin, TX). A potential range of -0.3 to - 0.8 V vs. Ag/AgCl was scanned 134 times using square wave voltammetry parameters of frequency 100 Hz and amplitude 25 mV to detect the first electrochemical reduction of TNT.[71] To correct for the sloping background in the square wave voltammograms, a 5 factor polynomial was fit to each voltammogram on each side of the base of the TNT peak by a least-squares minimization routine using Solver in an Excel spreadsheet.

Liquid chromatography with electrochemical detection is a common technique for the analysis of compounds that are easily oxidized or reduced. For nitroenergetic compounds such as TNT, electrochemical detection is possible because of the ease of reduction. Amperometric detection can be less than optimal for compounds that are reduced due to the high background currents generated from dissolved oxygen. Square wave voltammetry is often used to detect TNT in field samples where the square wave voltammogram of the dissolved oxygen can easily be subtracted.[72] Square wave chromatovoltammographic detection provides additional signal improvement since a potential window can be interrogated rapidly and the waveform can discriminate against the non-faradic background current.[73]

We examined the square wave voltammetry of TNT in different solvent mixtures in order to optimize conditions for rapid elution from the column material without significant loss in electrochemical signal. Organic solvents are often used to rapidly release the TNT bound to DEB sorbents. For electrochemical detection, the solvent mixture used to release the TNT needs to contain an electrolyte. In Figure 49, we show square wave voltammograms of TNT at 10 ppm dissolved differing buffer/solvent mixtures: ½ PBS buffer, 2:1 acetonitrile/water containing 1/6 PBS buffer components (AN/PBS), and 99% MeOH in 1% water with 0.1 M sodium acetate as electrolyte. The voltammogram of TNT in the PBS buffer between -0.3 to -0.8 V vs. Ag/AgCl shows the first two reduction peaks of TNT as reported. There is a third reduction peak (not shown) which is at more negative potentials. In both the AN/PBS and MeOH buffer systems, the first reduction peak is significantly shifted to more negative values and the second reduction peak is no longer in the potential window. In addition, the current from the initial reduction peak of TNT is attenuated compared to the PBS buffer.

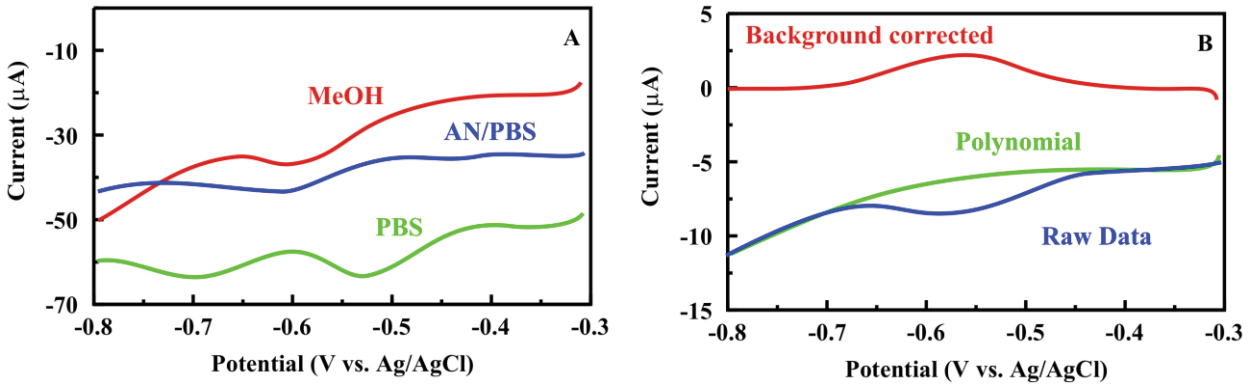

Figure 49. A. *Square wave voltammetry of 10 ppm TNT at a glassy carbon electrode in various solvent mixtures and electrolytes: 1/2 PBS (green), MeOH = 99% MeOH and 1% water (red); AN/PBS = 2:1 solvent mixture of acetonitrile/water containing 1/6 PBS buffer components (blue).* ***B.*** *A square wave voltammetry trace at peak maximum for a 2 mL sample of 500 ppb TNT in 1/2 PBS pre-concentrated at a column packed with imp-DEB and rapidly released using AN/PBS. green = polynomial fit to background; blue = raw data; red = corrected data plotted with the reduction current in the positive direction.*

The current due to the reduction of oxygen in all samples contributes to the sloping background in the square wave voltammograms. For the MeOH buffer, this slope is more significant. A five factor polynomial was used to correct for the sloping background in the square wave voltammograms (shown in Figure 49). For this work, the reduction current for TNT in the background-corrected square wave voltammograms is plotted with current in the positive direction on the y-axis for the chromatograms and in the positive direction on the z-axis for the square wave chromatovoltammograms.

In Figure 50, we show a series of background corrected square wave chromatovoltammograms in which 2 mL TNT samples of various concentrations in PBS were pre-concentrated on a column packed with imp-DEB and rapidly released using the AN/PBS buffer. Both peak current and peak area scale linearly with increasing TNT concentration giving a linear response between 20 and 500 ppb with an estimated LOD of 13 ppb at 3 times signal-to-noise. There is a small negative shift in the reduction peak potential with an increase in TNT concentration (Figure 50). In addition, the peak shape of the chromatograms generated from the square wave voltammetric detection at the maximum peak current overlay the chromatograms generated from the UV detection of TNT at 230 nm for identical runs as shown in Figure 50. This suggests that the electrochemical parameters used in generating the square wave chromatovoltammograms give an adequate sampling rate to describe the peak shape for the TNT signal as it is released from the column. We also show the chromatogram (UV detection) for a 2 mL sample of 1 ppm TNT in the AN/PBS buffer passing through the imp-DEB material with no pre-concentration. Integration of the chromatographic peaks for pre-concentrated samples and samples that were not pre-concentrated suggests that ~100% of the TNT bound to the column was recovered.

The square wave chromatovoltammograms displayed in Figure 51 show the increase in amplitude of the TNT peak current as a result of increasing the volume of a TNT solution (10 ppb) pre-concentrated at the imp-DEB material (released using the AN/PBS buffer). In fact, when only 2 mL of sample is pre-concentrated, the TNT signal is below the LOD. By increasing the volume of the pre-concentrated sample to 20 mL or 40 mL, the TNT signal is easily

detectable with signal-to-noise ratios of 17 and 30, respectively. The pre-concentration factor was estimated using the ratio of the volume of sample pre-concentrated to the volume of target released and was plotted vs. the area of the peak from the square wave chromatovoltammograms. As seen in Figure 51, the factor scales linearly.

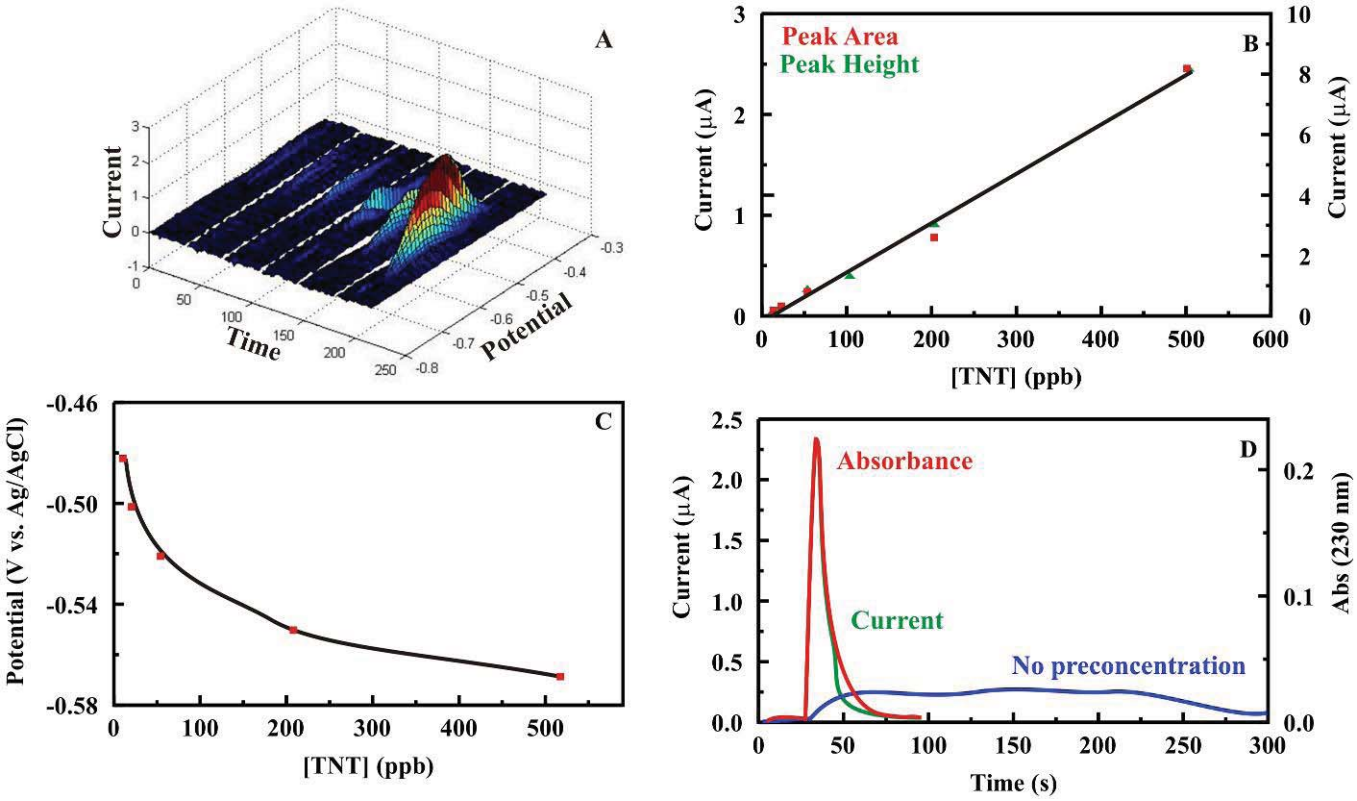

Figure 50. *(Panel A) Background corrected square wave chromatovoltammograms for 2 mL TNT samples in PBS pre-concentrated at a column packed with imp-DEB column and rapidly released using the AN/PBS buffer. (Panel B) Peak current and peak area vs. TNT concentration. (Panel C) Shift in peak potential of the first reduction peak of TNT as a function of TNT concentration taken from square wave chromatovoltammograms presented in Panel A. (Panel D) Background corrected chromatograms of 2 mL of 500 ppb TNT pre-concentrated in 1/2 PBS using an imp-DEB column and rapidly released using the AN/PBS buffer: monitored at 230 nm (red), (ii) monitored at the peak maximum from the square wave voltammetry (green), compared to 2 mL of 1 ppm of TNT in AN/PBS with no pre-concentration monitored at 230 nm (blue).*

Variation of solvent mixtures and column material

The MeOH buffer system was evaluated using sodium acetate as an electrolyte. Since sodium acetate is soluble in MeOH, we were able to match the concentration of buffer components in the water pre-concentrated with the MeOH used for rapid release. We chose to work at buffer component concentrations which, in water, give a pH of 6. In Figure 52, we compare the chromatograms of several systems. The MeOH buffer was able to rapidly release the TNT bound to imp-DEB; however, when compared to chromatograms of control samples prepared with and the same concentration of TNT in the MeOH buffer, we found that the integration of the peaks represented a signal of only 50% of the expected value. This suggests that using the sodium

acetate buffer to pre-concentrate the TNT at pH 6 was not ideal for the material. Under the same conditions, integration of the pre-concentrated/released TNT signal for the commercial product LiChrolute EN was near 100% as expected. The peak amplitude was significantly lower, however, with a broad base in the chromatograms which is not ideal for these types of measurements. When DEB and imp-DEB were compared (Figure 52), peak area vs. TNT concentration for 2 mL sample volumes showed a variation in performance for the two materials. At concentrations > 100 ppb, performance of the materials was similar; however, the efficiency of pre-concentration for DEB rapidly falls off at concentrations of TNT < 50 ppb. This result suggests that the imprinted material has a higher affinity for TNT.

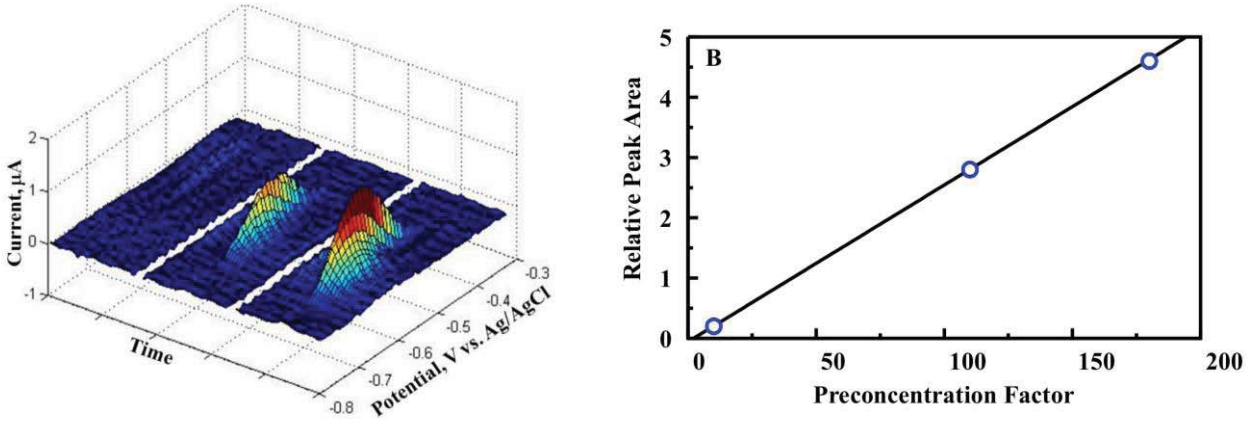

Figure 51. A. *Background corrected square wave chromatovoltammograms for (a) 2, (b) 20, and (c) 40 mL samples of 10 ppb TNT in ½ PBS pre-concentrated on an imp-DEB column and released using the AN/PBS buffer.* ***B.*** *Peak area vs. pre-concentration factor as defined in the text.*

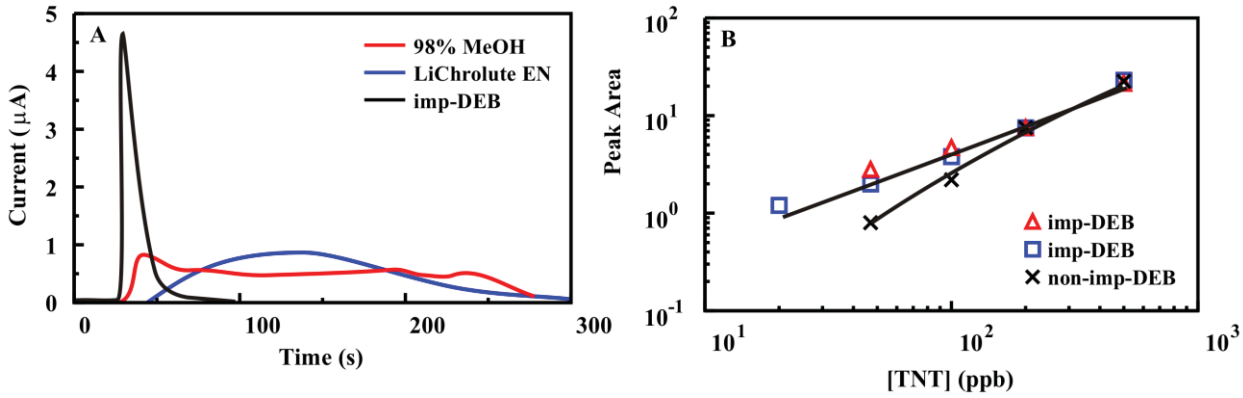

Figure 52. A. *Background corrected chromatograms for 2 mL samples of 500 ppb TNT monitored at the peak maximum from square wave voltammetry: (i) pre-concentrated with imp-DEB in 0.1 M sodium acetate (pH 6) and released with solvent mixture containing the same buffer components in 98% MeOH and 2% water (red), (ii) pre-concentrated with LiChrolute EN and released with the 98% MeOH buffer (blue), and (iii) no pre-concentration in 0.1 M sodium acetate at pH 6 (black).* ***B.*** *Peak area vs. TNT concentration from square wave chromatovoltammograms for 2 mL TNT samples in 0.1 M sodium acetate (pH 6): (i) released from imp-DEB using a 99% MeOH buffer (square), (ii) released from imp-DEB using the 98% MeOH buffer (triangle), and (iii) released from a DEB column with the 98% MeOH buffer (x).*

The AN/PBS solvent system was also compared to an AN/Tris solvent system in which the organic solvent percentage could be increased while retaining salts in solution to support electrochemical detection. An 80% acetonitrile solvent system with 25 mM Tris buffer components was found to release bound TNT from the imp-DEB in a 100 µL volume. By comparison, the AN/PBS system with 66 % acetonitrile released the TNT in a 200 µL volume. The more concentrated sample resulting from the 80% acetonitrile system provided increased peak amplitude in the chromatograms as measured by UV detection (Figure 53). For electrochemical detection, however, the peak current in the square wave voltammetry decreased in this system as compared to the AN/PBS buffer system suggesting that an increased percentage of acetonitrile significantly attenuates the redox chemistry of TNT at the carbon electrode surface (Figure 53). A balance between the percentage of organic solvent used in the electrolyte, necessary for rapid release, and the decline of the electrochemical TNT signal needs to be considered when designing pre-concentration protocols. For example with the AN/PBS buffer system, the detection of 0.5 ppb of TNT was achieved with a signal to noise ratio of 20 using this technique with a 480 mL sample volume in seawater (Figure 54).

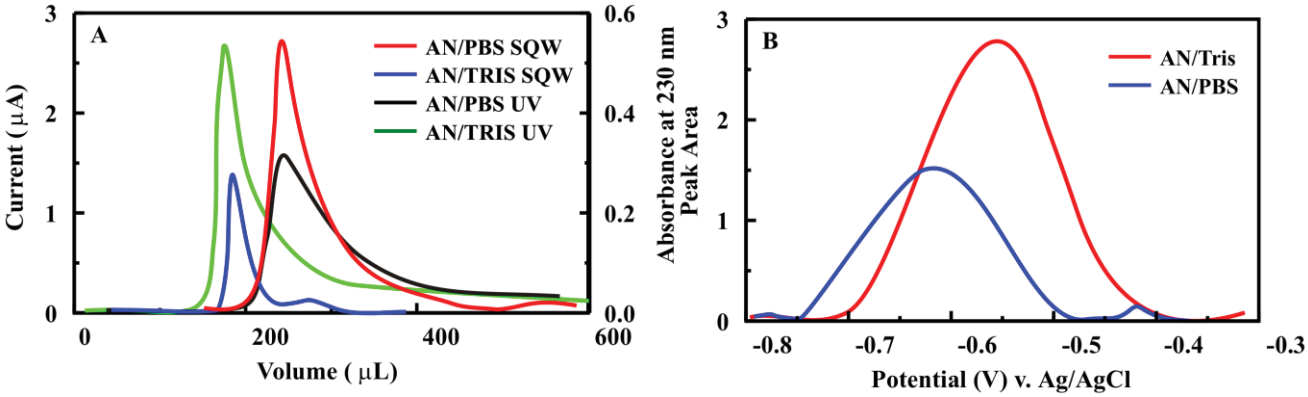

***Figure 53. A**. Background corrected chromatograms for 2 mL samples of 500 ppb TNT pre-concentrated using an imp-DEB column and rapidly released using either AN/PBS or AN/Tris collected using both UV (black and green, respectively) and square wave voltammetric (red and blue, respectively) detection. **B**. Background corrected square wave voltammetry traces at peak maximum comparing a 2:1 solvent mixture of acetonitrile/water containing 1/6 PBS buffer components (AN/PBS, red) to 25 mM Tris buffer pH 8 with 80% acetonitrile and 20% water (AN/Tris, blue).*

Task 6. Bench-Scale Demo: Liquid/Liquid

Figure 55 presents a schematic of the system concept using the sorbents to preconcentrate targets from aqueous solution ahead of detection by an electrochemical detector. Samples are pulled through the filter to eliminate particulate on the basis of size exclusion. The first peristaltic pump is employed both for pulling the sample through the filters and for pushing it through the column for target capture. A 3-way solenoid valve controls flowing solutions and directions. The use of a peristaltic pump prevents contact of the liquids with the pump machinery minimizing issues related to corrosion and clogging. When the pre-column valve is switched, eluent is pushed through the column by the pump. The pump utilized had a 66:1 motor and 0.143" rollers (P625/66.143, Instech Laboratories, Plymouth Meeting, PA). Silicone tubing (0.062") was used to provide flow rates up to 0.8 mL/min through the sorbent column using a 9

V battery. The operation voltage for the solenoid valves (5V, Lee Products, Westbrook, CT) is controlled using on/off switches. Desorbed targets are mixed with an electrolyte solution outside of the column, and a second peristaltic pump is used to direct the resulting solution to the electrochemical detector. This pump utilized a 900:1 gear ratio and 0.143" rollers (P625/900.143, Instech Laboratories, Plymouth Meeting, PA). The pump was combined with 0.015" silicone tubing to provide flow rates up to 0.08 mL/min using a 9V battery. Sorbent columns were (100 mg, +/- 2 mg) were packed in 10 x 50 mm borosilicate glass column assemblies (Omnifit; Danbury, CT) using 25 µm frits.

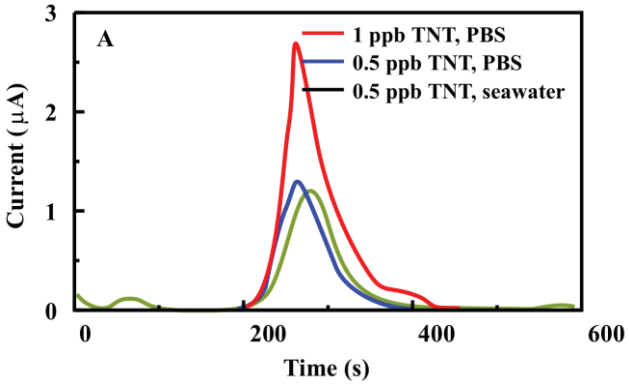

Figure 54*. Background corrected chromatograms using square wave voltammetric detection for 480 mL samples (PBS or filtered seawater) of TNT pre-concentrated on an imp-DEB column and rapidly released using the AN/PBS solvent mixture. Red = 1 ppb pre-concentrated from PBS, blue = 0.5 ppb pre-concentrated from PBS, and green = 0.5 ppb pre-concentrated for seawater.*

Electrochemical measurements

The desorbed targets were passed through a flow cell (FC2, BVT Technologies, Strážek, Czech Republic) and analyzed using a PalmSens handheld potentiostat (PalmSens, Utrecht, The Netherlands). Sensors were selected from among those specifically designed to work with the PalmSens system (AC1 Series, BVT Technologies, Strážek, Czech Republic). These sensors had graphite working (WE), platinum auxiliary (AUX), and silver/silver chloride reference electrodes (AC1.W4.R1). Comparison between platinum and graphite working electrodes showed that the latter provided in better signal-to-noise ratio and higher sensitivity to diminishing target concentrations. Also, platinum working electrodes yielded overlap between peaks from rising dissolved oxygen and TNT / DNT reduction [33,74] making determination of target concentrations difficult. A schematic of the flow cell is provided in Figure 55. The detection chamber had a volume of roughly 25 µL. The volume of desorbed solution was 2 ml to which 2 mL of 0.15 M potassium chloride (electrolyte solution in water) was added (1 mL of this mixture was utilized for HPLC analysis). The electrolyte and associated concentrations were selected on the basis of previous reports [71]. The slower flow rate of the pump (2) combined with the small chamber volume ensured that multiple measurements could be made of each solution for verification of signal reproducibility. Ideally, electrochemical measurements would have been made under constant flow conditions; however, system calibration showed that detection sensitivity was reduced under flow when all other conditions were maintained. The testing scheme, as a result, required flow of the sample through the detection chamber for 10 seconds, cessation of the flow, and measurement of the EC response. This method replenished the sample volume between replicate analyses and improved detection sensitivity.

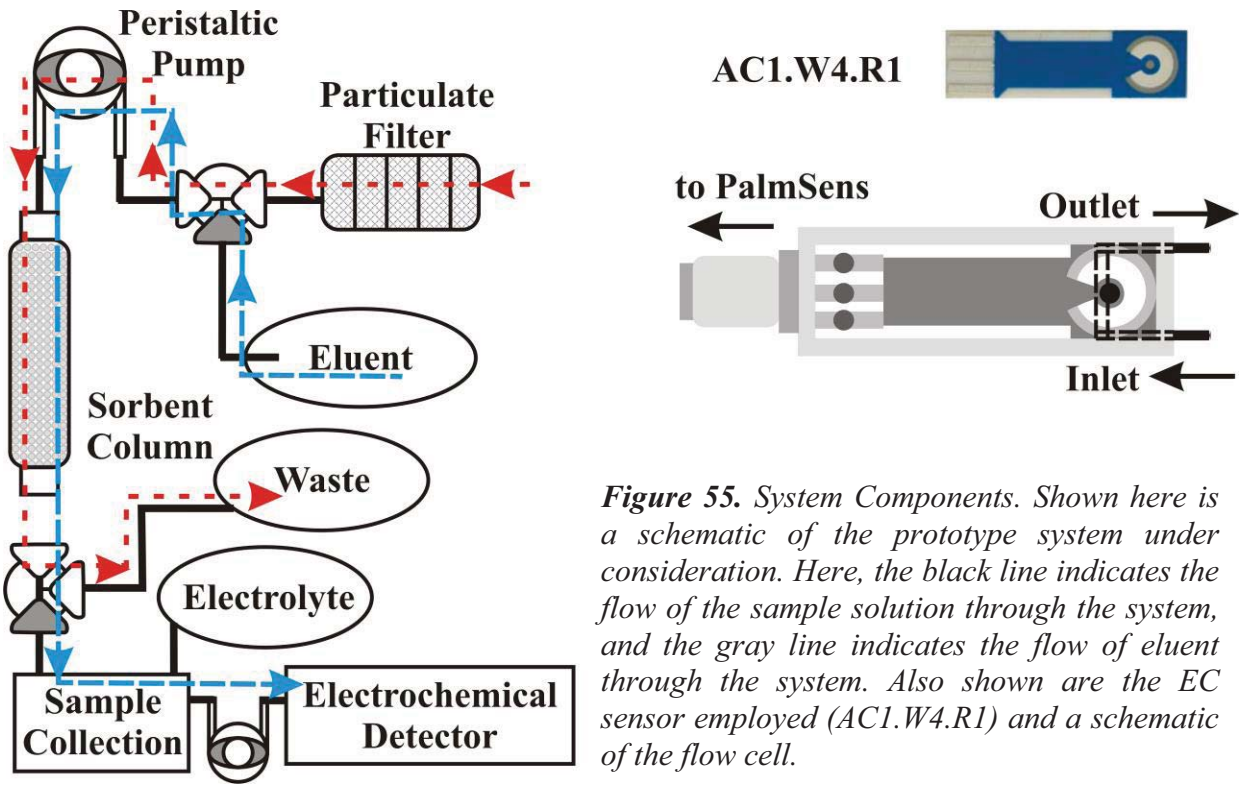

Figure 55. *System Components. Shown here is a schematic of the prototype system under consideration. Here, the black line indicates the flow of the sample solution through the system, and the gray line indicates the flow of eluent through the system. Also shown are the EC sensor employed (AC1.W4.R1) and a schematic of the flow cell.*

Square wave voltammetry (SWV) was used for detection of targets as it has been shown to produce the highest sensitivity in previous studies.[71] The potential was swept over a range of values (-0.1V to -0.9V) sufficient for detection of reduction peaks for both TNT and DNT (typically -0.45V and -0.6V, respectively). Other measurement parameters are as follows: 50 mV amplitude, 10 Hz frequency, 5 mV step. The sensors were typically reusable for many EC scans. For the sake of accuracy and to reduce the carryover effects, sensors were replaced after each series of target concentrations. Care was taken to ensure that the flow cell did not contain large air bubbles as their presence had detrimental effects on sensitivity. The data was recorded and analyzed using the PSTrace EC signal acquisition software (PalmSens, Utrecht, The Netherlands). In order to confidently measure target concentrations, SWV scans were first performed with blank samples. These provided the baseline signal that was subtracted from the SWV of target samples. At least five scans were completed for each evaluated sample or standard. The average values are presented here.

It was first necessary to evaluate the response of the PalmSens to the targets of interest. Overall, TNT, DNT, RDX, HMX, and NG have been of interest to this effort; however, the electrochemical sensors and methods utilized here are applicable only to detection of TNT and DNT. Electrolytes for use in electrochemical detection of TNT and DNT have been described previously.[71,74] Potassium chloride was selected based on the previously published studies and a concentration of 100 mM was utilized. While other electrolytes were evaluated early in these studies (sodium acetate & phosphate buffers, see Task 5),[74] we found that the performance of the sensors when used with potassium chloride was equal to or better than other electrolytes with respect to sensitivity and sensor lifetime. Reduction in concentration of the electrolyte (75 or 50 mM) resulted in a higher level of noise in EC analysis of samples. Variations in solvent content were also explored. Adsorption of the targets by the sorbents is

intended to provide enhancement in the concentration of the targets and elimination of potential interferents. The addition of water / electrolyte results in a dilution of the targets, so a minimal addition is preferred. We found that 75% methanol with 75 mM KCl could be utilized; however, the sensors degraded rapidly (one or two use cycles) and sensitivity was diminished (Figure 56 and Table 31).

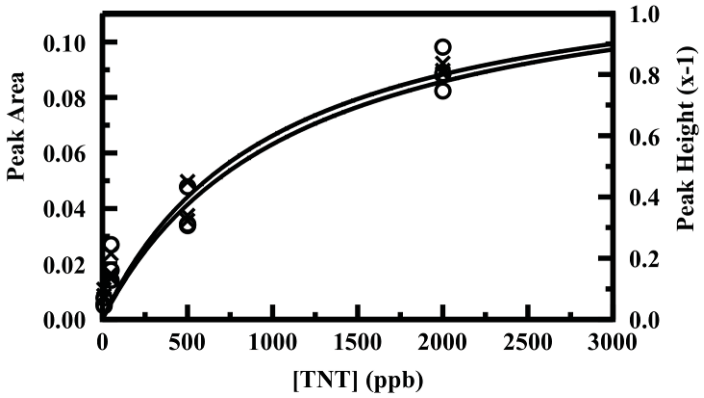

Figure 56. *Calibration of electrochemical sensor against TNT 75% methanol with 75 mM KCl.*

Table 31. *Complete data set for calibration of electrochemical sensor against TNT in 75% methanol with 75 mM KCl. TNT reduction peaks appeared between 0.57 and 0.61 V.*

[Prepared] (ppb)	Peak Height (µA)	Peak Area (µAV)
9	-0.08	5.75E-03
9	-0.07	5.00E-03
9	-0.10	7.85E-03
50	-0.22	2.70E-02
50	-0.15	1.78E-02
50	-0.13	1.42E-02
500	-0.45	4.78E-02
500	-0.32	3.39E-02
500	-0.34	3.44E-02
2000	-0.81	9.82E-02
2000	-0.80	8.86E-02
2000	-0.84	8.24E-02

Calibration curves for TNT and DNT were generated based on both peak height and peak area from the voltammograms (Figure 57). Each point in the figure represents the average of at least five SWV scans. Good agreement between peak height and area was obtained for TNT with similar reproducibility and sensitivity. The reliable limit of detection was found to be 200 ppb; at this concentration the signal was greater than three times the standard deviation in the measurements for both the peak height and area. In the case of DNT, peak height and area gave strongly differing results. Noise levels in the peak areas obtained were much higher than those of the peak height. Using a 3:1 signal to noise level as the threshold, the limit of detection based on peak area for DNT was 350 ppb. Peak height, on the other hand, achieved 3:1 signal to noise at only 250 ppb. In addition, when data for DNT peak area at high concentrations was included (1 ppm and greater), the data set was not monotonically increasing. The problem was likely a result

of baseline variations noted for EC measurements completed in the presence of solvent. Due to these issues, peak height analysis was utilized for all results presented below. The data sets (Figure 57) were used to generate functions of the form:

$$height = \frac{a[\text{target}]}{1 + b[\text{target}]} \qquad \text{(Equation 4)}$$

describing the dependence of the peak height on target concentration. For TNT, a = 1.4×10^{-4} and b = 9.4×10^{-4}; for DNT, a = 6.8×10^{-4} and b = 7.2×10^{-4}.

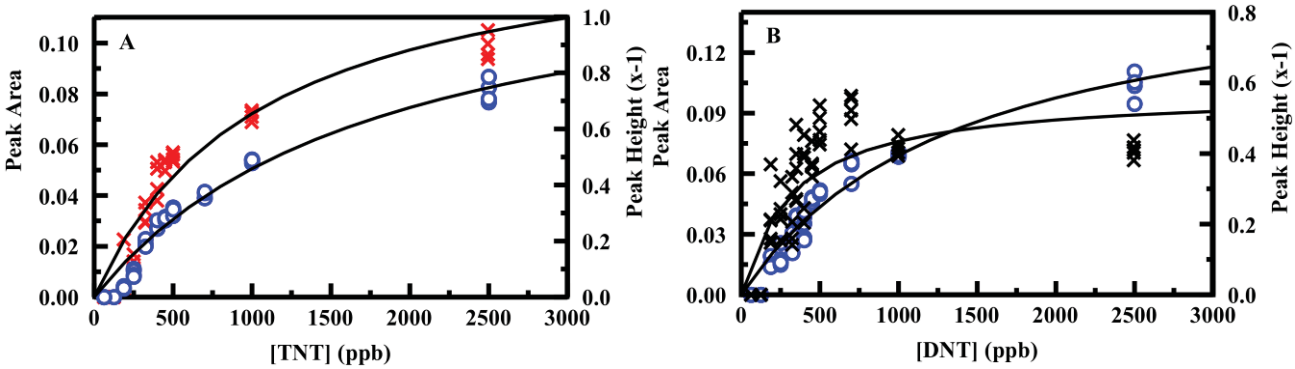

Figure 57. *Calibration of the electrochemical sensor in 100 mM KCl and 50% methanol (A) TNT (B) DNT: peak area (x) and peak height (circle). The complete data set is provided in Tables 32 and 33.*

Targets prepared in deionized water (30 mL) at concentrations between 20 and 250 ppb were applied to a 100 mg sorbent column at approximately 0.8 mL/min. The column was then rinsed with 3 mL of water prior to elution of the targets in 2 mL of methanol containing 0.05 M KCl. This eluant was diluted using 0.15 M KCl in water (1:1) to produce a final KCl concentration of 100 mM in 50% methanol. Analysis of the diluted eluent was accomplished using the EC flow cell as described above and averaging a minimum of five SWV scans. Each target was analyzed using a minimum of three independent cycles of this process. HPLC analysis was used to confirm target concentrations in samples, effluent, rinses, and eluants for all cycles. Target samples with concentrations below 10 ppb were also analyzed. In this case, 300 mL of the target solution was applied to the column; other analysis steps were as described above. The calibration functions (Figure 57; Equation 4) were applied to calculation of a concentration based on the peak height determined from EC analysis of the samples. Figure 58 compares this calculated value to the results of HPLC analysis. In the case of TNT, if samples at 250 ppb are excluded, the variability between HPLC determined values and EC determined values is 15% on average. If the points at 250 ppb are included this variation increases to 26%. The DNT data set has, on average, a 23% variation from the HPLC determined value.

Table 32. *Complete data set for calibration of electrochemical sensor against TNT in 50% methanol with 100 mM KCl.*

[Prepared] (ppb)	Potential (V)	Peak Height (µA)	Peak Area (µAV)
62.5	No Peak		
125	No Peak		
187.5	-0.63	-3.92E-02	2.27E-02
187.5	-0.64	-3.11E-02	3.01E-03
187.5	-0.62	-3.03E-02	3.04E-03
187.5	-0.625	-3.25E-02	3.17E-03
250	-0.615	-1.01E-01	1.68E-02
250	-0.62	-9.38E-02	1.41E-02
250	-0.62	-7.98E-02	1.15E-02
250	-0.605	-7.26E-02	1.07E-02
325	-0.625	-1.83E-01	2.97E-02
325	-0.615	-1.90E-01	3.43E-02
325	-0.62	-2.07E-01	3.72E-02
325	-0.625	-1.80E-01	2.93E-02
400	-0.625	-2.44E-01	3.80E-02
400	-0.625	-2.45E-01	4.25E-02
400	-0.62	-2.45E-01	5.06E-02
400	-0.625	-2.75E-01	5.31E-02
450	-0.625	-2.79E-01	4.97E-02
450	-0.62	-2.74E-01	5.38E-02
450	-0.625	-2.86E-01	5.32E-02
450	-0.625	-2.82E-01	5.40E-02
500	-0.63	-3.07E-01	5.34E-02
500	-0.63	-3.20E-01	5.70E-02
500	-0.625	-2.90E-01	5.43E-02
500	-0.63	-3.13E-01	5.61E-02
700	-0.615	-3.55E-01	-3.71E-02
700	-0.615	-3.53E-01	-4.37E-02
700	-0.615	-3.71E-01	-4.11E-02
700	-0.615	-3.76E-01	-4.18E-02
1000	-0.63	-4.78E-01	7.10E-02
1000	-0.63	-4.91E-01	7.35E-02
1000	-0.63	-4.88E-01	7.27E-02
1000	-0.635	-4.89E-01	6.89E-02
2500	-0.625	-7.48E-01	9.98E-02
2500	-0.625	-6.95E-01	9.37E-02
2500	-0.625	-7.08E-01	9.55E-02
2500	-0.625	-7.86E-01	1.05E-01

Table 33. *Complete data set for calibration of electrochemical sensor against DNT in 50% methanol with 100 mM KCl.*

[Prepared] (ppb)	Potential (V)	Peak Height (µA)	Peak Area (µAV)
62.5	No Peak		
125	No Peak		
187.5	-0.77	-8.63E-02	2.58E-02
187.5	-0.77	-1.10E-01	6.46E-02
187.5	-0.77	-8.70E-02	3.69E-02
187.5	-0.775	-8.18E-02	2.77E-02
187.5	-0.77	-7.91E-02	3.73E-02
250	-0.77	-8.54E-02	2.69E-02
250	-0.77	-9.36E-02	3.76E-02
250	-0.77	-1.01E-01	4.25E-02
250	-0.77	-9.10E-02	3.99E-02
250	-0.765	-1.47E-01	5.64E-02
325	-0.77	-1.71E-01	5.05E-02
325	-0.77	-1.41E-01	2.48E-02
325	-0.77	-1.36E-01	2.79E-02
325	-0.77	-1.18E-01	3.61E-02
325	-0.765	-1.76E-01	5.84E-02
350	-0.765	-2.13E-01	4.74E-02
350	-0.765	-2.25E-01	8.43E-02
350	-0.765	-2.08E-01	6.26E-02
350	-0.77	-2.22E-01	6.98E-02
350	-0.77	-1.66E-01	4.65E-02
400	-0.77	-1.62E-01	3.57E-02
400	-0.77	-1.54E-01	4.29E-02
400	-0.77	-2.01E-01	6.82E-02
400	-0.77	-2.20E-01	6.98E-02
400	-0.77	-2.37E-01	7.92E-02
450	-0.77	-2.73E-01	6.43E-02
450	-0.77	-2.76E-01	6.35E-02
450	-0.77	-2.73E-01	6.50E-02
450	-0.77	-2.62E-01	7.61E-02
450	-0.765	-2.72E-01	5.86E-02
500	-0.77	-2.86E-01	8.76E-02
500	-0.77	-2.94E-01	9.39E-02
500	-0.765	-2.96E-01	7.67E-02
500	-0.77	-2.93E-01	8.08E-02
500	-0.77	-2.92E-01	7.45E-02
700	-0.77	-3.80E-01	8.71E-02
700	-0.765	-3.71E-01	9.13E-02
700	-0.765	-3.70E-01	9.86E-02
700	-0.765	-3.74E-01	9.74E-02
700	-0.765	-3.14E-01	7.20E-02

[Prepared] (ppb)	Potential (V)	Peak Height (µA)	Peak Area (µAV)
1000	-0.765	-4.00E-01	6.88E-02
1000	-0.77	-4.05E-01	7.92E-02
1000	-0.765	-3.94E-01	7.05E-02
1000	-0.765	-3.91E-01	7.43E-02
1000	-0.765	-3.96E-01	7.26E-02
2500	-0.76	-5.40E-01	6.67E-02
2500	-0.755	-6.02E-01	7.31E-02
2500	-0.755	-6.32E-01	7.66E-02
2500	-0.755	-5.92E-01	7.04E-02
2500	-0.755	-6.02E-01	7.18E-02

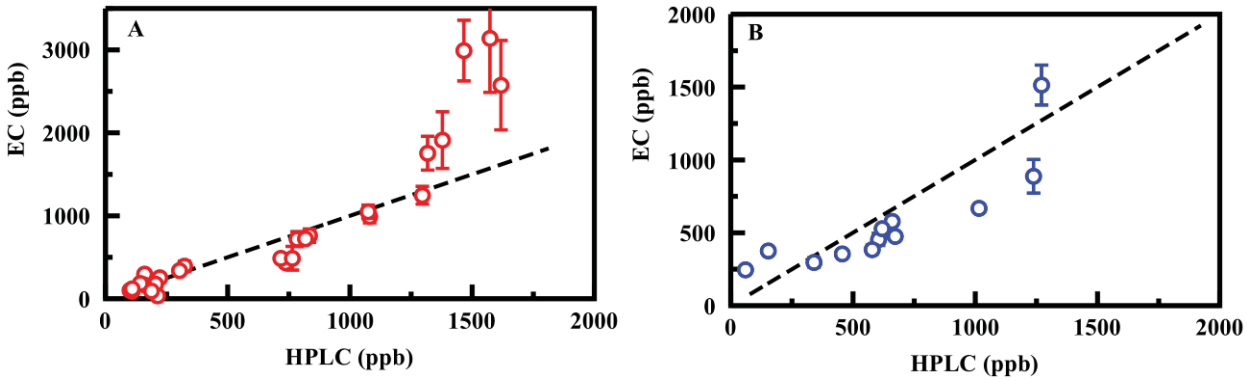

Figure 58. *Preconcentration from Milli-Q water. Points here represent the results for quantification of samples using the prototype system with analysis by HPLC (x-axis) and EC (y-axis): (A) TNT and (B) DNT. EC results presented use the peak height analysis. Error bars indicate the standard deviation. The line indicates the expected results based on HPLC analysis of the spiked samples. The complete data set is provided in Table 34.*

Because interferents are a significant concern for the application of electrochemical sensing to real-world samples, targets were spiked (3 to 250 ppb) into ground water samples obtained from an untreated well. We have previously demonstrated that ground water matrices have little impact on the performance of the sorbents.[40] Analysis was completed as described for the deionized water samples. For TNT, the variation between HPLC and EC analysis remained 26%. For DNT, however, the variation increased to 40%. This increased variation is a result of the difficulties inherent in DNT analysis by the method utilized here. The DNT peak occurs at a more negative potential than that of TNT (-0.77 V for DNT compared to -0.62 V for TNT). In this region of the voltammogram, the background current is often leveling off or beginning a downward trend. Dissolved oxygen may contribute to these voltammogram features.[75] The variability results in difficulties in establishing the background to be subtracted. The TNT peak occurs in a region of the voltammogram for which the background is linearly increasing leading to reduced complexity. The higher voltage may also cause changes to the electrode resulting in greater run to run variations.

It was also of interest to determine the impact that compounds of similar structure would have on the results obtained. Compounds such as RDX, HMX, and nitroglycerine are retained and concentrated by the sorbent column nearly as effectively as DNT and TNT.[40] The presence of multiple contaminants in a sample was also shown to impact the amount of each target captured and the resulting final concentration in the eluant. This effect can be seen in samples containing both TNT and another target (Table 35). While HPLC analysis of the eluant indicated the expected 7.5 times enhancement in TNT concentration, the other targets were found at consistently lower than expected concentrations. The affinity of the sorbents for TNT was shown to be greater than that for the other targets resulting in this observed performance. [38,40] When EC detected concentrations are compared to HPLC analysis of the eluent, a strong divergence is noted for both TNT and DNT (Figure 59). This difference is again related to difficulties in voltammogram analysis due to baseline variations caused by the other sample constituents. The variation would be expected to become greater as the complexity of the mixture increased and if other active compounds were introduced.

Table 34. *Analysis of samples in deionized water. All concentrations provided in ppb.*

Target	[Prepared][1]	[HPLC]	Height (µA)	[Height]	St. Dev. [Height]	Area (µAV)	[Area]	St. Dev [Area]
TNT[2]	1	63	Not Detected					
TNT[2]	1	67	Not Detected					
TNT[2]	3	213	-0.025	36	8	0.002	13	4
TNT[2]	3	188	-0.064	94	17	0.006	46	10
TNT[2]	5	160	-0.182	298	49	0.022	181	31
TNT[2]	5	222	-0.158	253	81	0.020	162	66
TNT	20	205	-0.115	177	43	0.018	146	64
TNT	20	156	-0.111	171	22	0.015	122	18
TNT	20	142	-0.119	185	25	0.017	138	10
TNT	20	108	-0.060	89	9	0.007	53	6
TNT	20	100	-0.069	103	42	0.008	60	28
TNT	20	109	-0.080	120	6	0.009	72	4
TNT	50	323	-0.230	394	121	0.031	279	136
TNT	50	303	-0.203	340	78	0.029	262	74
TNT	125	737	-0.250	437	48	0.035	325	86
TNT[2]	125	834	-0.381	762	159	0.083	1354	879
TNT[2]	125	784	-0.366	720	182	0.041	410	104
TNT	125	717	-0.273	488	69	0.039	379	55
TNT	125	764	-0.273	489	286	0.039	374	219
TNT	125	818	-0.368	724	47	0.051	554	41
TNT	200	1080	-0.456	992	152	0.054	598	134
TNT	200	1074	-0.472	1050	160	0.057	660	96
TNT	250	1466	-0.803	2992	731	0.106	2625	831
TNT	250	1618	-0.757	2575	1079	0.102	2311	1369
TNT	250	1573	-0.818	3140	1303	0.111	3165	2339
TNT	250	1296	-0.525	1248	213	0.075	1072	209
TNT	250	1318	-0.634	1755	407	0.090	1609	456
TNT	250	1378	-0.662	1913	683	0.094	1808	779
DNT[2]	1	97	Not Detected					
DNT[2]	1	75	Not Detected					
DNT[2]	5	153	-0.201	376	39	0.025	105	28
DNT[2]	5	60	-0.142	246	38	0.020	82	18
DNT[2]	5	240	Not Detected					
DNT	20	99	Not Detected					
DNT	20	99	Not Detected					
DNT	20	98	Not Detected					
DNT	50	340	-0.167	298	64	0.018	70	22
DNT	50	456	-0.192	355	41	0.027	117	19
DNT	50	206	Not Detected					
DNT	50	249	Not Detected					
DNT	50	240	Not Detected					
DNT	125	578	-0.205	385	61	0.021	88	24
DNT	125	619	-0.260	528	38	0.030	137	20
DNT	125	672	-0.241	476	23	0.025	105	5
DNT	200	604	-0.233	454	83	0.030	138	68
DNT	200	660	-0.278	578	35	0.035	176	19
DNT	250	1238	-0.368	887	232	0.051	336	148
DNT	250	1015	-0.307	668	53	0.044	251	39
DNT	250	1271	-0.493	1514	273	0.063	554	265

[1] Prepared sample concentration prior to preconcentration. Preconcentration involved passing 30 mL of the sample through the system with elution in 2 mL methanol. The eluant was then diluted into 2 mL of 0.15 M KCl in water; [2] Preconcentration of samples at less than 10 ppb involved passing 300 mL of the sample through the system with elution into 2 mL methanol. The eluant was then diluted into 2 mL of 0.15 M KCl in water.

Table 35. *Analysis of mixed target samples. All concentrations provided in parts per billion (ppb).*

Sample #	Target	[Prepared][1]	HPLC ID	[HPLC]	EC ID	[Height]	St. Dev. [Height]	[Area]	St. Dev [Area]
1	TNT RDX	21 85	TNT / RDX	185 / 270	TNT	199	8	222	19
				183 / 272		209	3	239	10
				184 / 279		211	8	247	6
2	DNT RDX	65 95	DNT / RDX	317 / 268	DNT	176	5	58	1
				369 / 297		203	26	70	14
				388 / 306		199	15	67	9
3	TNT DNT	79 77	TNT / DNT	557 / 464	TNT / DNT	177 / 157	18 / 3	145 / 48	12 / 3
				577 / 465		177 / 151	22 / 5	143 / 40	19 / 2
				591 / 485		159 / 152	13 / 5	121 / 40	11 / 2
4	DNT NG	74 103	DNT / NG	485 / 523	DNT	153	12	42	5
				469 / 525		196	26	60	11
				490 / 569		207	17	65	8
5	TNT NG	77 103	TNT / NG	526 / 630	TNT	244	15	223	15
				559 / 599		277	24	271	29
				578 / 626		325	15	366	15
6	TNT DNT	20 75	TNT / DNT	222 / 386	TNT / DNT	135 / 160	6 / 3	117 / 50	14 / 3
				197 / 412		113 / 178	15 / 15	93 / 58	32 / 8
				201 / 432		109 / 194	3 / 8	83 / 64	5 / 5
7	TNT	31	TNT	202	TNT	151	10	131	17
				185		174	12	171	26
				179		189	5	197	18

[1] *Prepared sample concentration prior to preconcentration as determined by HPLC. Preconcentration involved passing 30 mL of the sample through the system with elution in 2 mL methanol. The eluant was then diluted into 2 mL of 0.15 M KCl in water.*

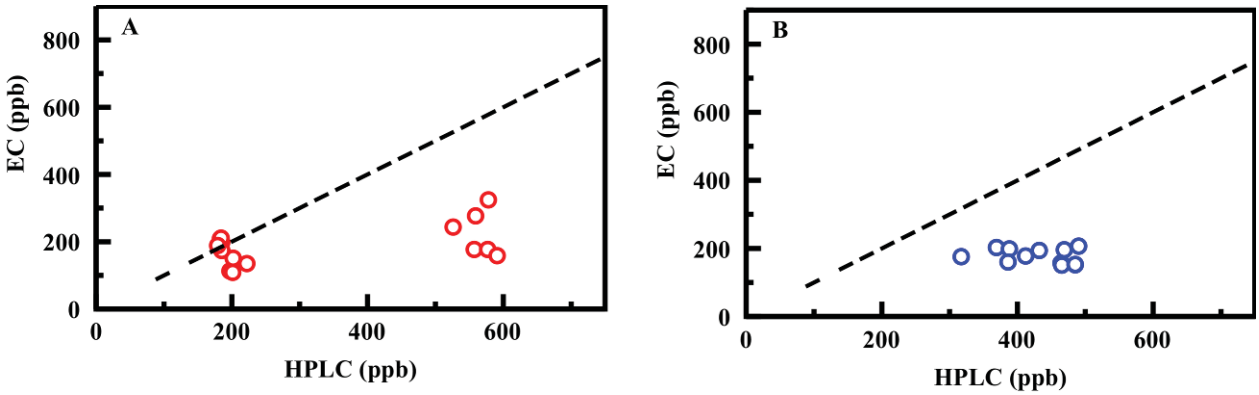

Figure 59. *Analysis of mixed target samples. Points here represent the results for quantification of samples using the prototype system with analysis by HPLC (x-axis) and EC (y-axis): (A) TNT and (B) DNT. EC results presented use the peak height analysis. The line indicates the expected results based on HPLC analysis of the spiked samples. The complete data set is provided in the Table 35.*

A series of samples was prepared to evaluate the potential for this system to identify the target present. This set was prepared so that the system operator had no knowledge of what targets were present or in what concentrations. The operator was not informed that some samples contained no target or that compounds other than TNT and DNT had been included in some of the samples. The fifteen blind samples were analyzed in triplicate as described above. Figure 60 summarizes the results (full results Table 37). TNT was identified for all samples in which it was present. One false positive resulted from a sample of nitroglycerine. DNT was identified in four of nine samples. False positives for DNT resulted in several of the TNT samples. As mentioned above, the baseline for the region of the voltammogram in which the DNT peak is located can vary. It is possible to misinterpret these variations leading to false positive indications. For samples in which the targets were properly identified, variations from the HPLC indicated concentrations were similar to those of the ground water samples.

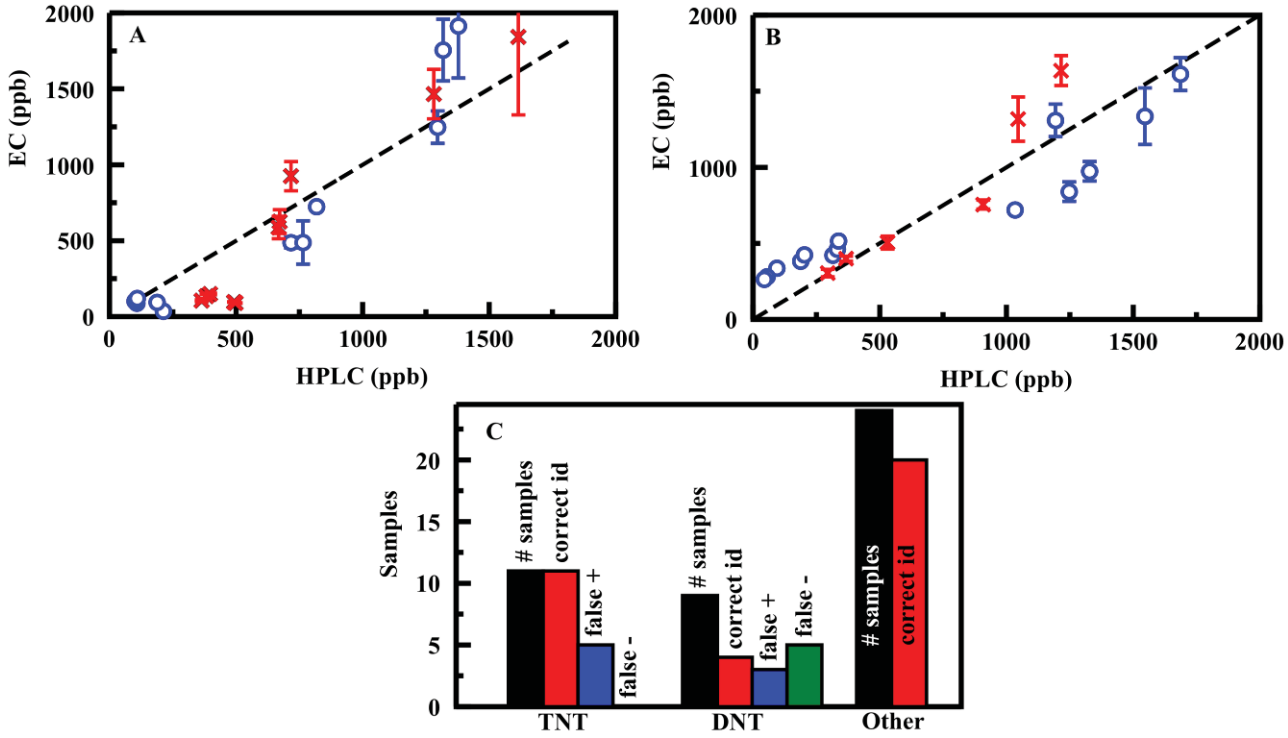

Figure 60. *(Panel A) Preconcentration from ground water and (Panel B) blind sample analysis: TNT (circle) and DNT (x). As in Figure 58, points here represent the results for quantification of samples using the prototype system with analysis by HPLC (x-axis) and EC (y-axis). The line indicates the expected results based on HPLC analysis of the spiked samples. Error bars indicate the standard deviation. The complete data sets are provided in Tables 36 and 37. (Panel C) From the blind sample analysis, the bars shown here indicate the total number of samples containing either TNT or DNT and the associated number of correct target identifications. Also shown are the numbers of false positive and negative responses. The third category of samples includes those with no target and those with targets not expected to be detected.*

Table 36. *Analysis of samples in ground water. All concentrations provided in parts per billion (ppb).*

Target	[Prepared][1]	[HPLC]	Height (µA)	[Height]	St. Dev. [Height]	Area (µAV)	[Area]	St. Dev [Area]
TNT[2]	3	213	-0.025	36	8	0.002	13	4
TNT[2]	3	188	-0.064	94	17	0.006	46	10
TNT	20	108	-0.060	89	9	0.007	53	6
TNT	20	100	-0.069	103	42	0.008	60	28
TNT	20	109	-0.080	120	6	0.009	72	4
TNT	125	717	-0.273	488	69	0.039	379	55
TNT	125	764	-0.273	489	286	0.039	374	219
TNT	125	818	-0.368	724	47	0.051	554	41
TNT	250	1296	-0.525	1248	213	0.075	1072	209
TNT	250	1318	-0.634	1755	407	0.090	1609	456
TNT	250	1378	-0.662	1913	683	0.094	1808	779
DNT[2]	7	492	-0.061	96	5	0.005	19	1
DNT[2]	7	498	-0.057	89	4	0.005	16	1
DNT	70	364	-0.066	105	13	0.006	21	3
DNT	70	383	-0.083	135	27	0.008	27	6
DNT	70	397	-0.091	149	11	0.008	29	3
DNT	125	668	-0.281	587	147	0.032	149	48
DNT	125	672	-0.293	626	156	0.032	154	47
DNT	125	717	-0.378	925	192	0.043	247	68
DNT	250	1281	-0.485	1466	326	0.057	425	106
DNT	250	1346	-0.599	2407	504	0.068	669	181
DNT	250	1615	-0.539	1843	1026	0.091	3191	3336

[1] Prepared sample concentration prior to preconcentration. Preconcentration involved passing 30 mL of the sample through the system with elution in 2 mL methanol. The eluant was then diluted into 2 mL of 0.15 M KCl in water; [2] Preconcentration of samples at less than 10 ppb involved passing 300 mL of the sample through the systemwith elution into 2 mL methanol. The eluant was then diluted into 2 mL of 0.15 M KCl in water.

Table 37. *Analysis of blind samples. All concentrations provided in parts per billion (ppb). Samples were analyzed in numerical order in triplicate.*

Sample #	Target	[Prepared][1]	HPLC ID	[HPLC]	EC ID	[Height]	St. Dev. [Height]	[Area]	St. Dev [Area]
1	None	--	--	--	--	--	--	--	--
					--	--	--	--	--
					--	--	--	--	--
2	TNT	250	TNT	1034	TNT	719	37	660	49
				1193	TNT	1308	214	1290	157
				1247	TNT	840	128	713	96
3	None	--	TNT	94	--	--	--	--	--
			TNT	55	--	--	--	--	--
			--	--	--	--	--	--	--
4	RDX	250	RDX	684	--	--	--	--	--
				711	--	--	--	--	--
				763	--	--	--	--	--
5	DNT	250	DNT	908	DNT	755	60	179	14
				1046	DNT	1317	291	345	101
				1216	DNT	1635	197	429	74
6	None	--	--	--	DNT	505	85	111	21
					--	--	--	--	--
					--	--	--	--	--
7	None	--	--	--	--	--	--	--	--
					--	--	--	--	--
					--	--	--	--	--
8	TNT	250	TNT	1328	TNT	974	128	707	93
				1546	TNT	1336	371	1006	278
					DNT	362	68	83	14
				1686	TNT	1613	216	1423	179
					DNT	362	50	80	11
9	NG	125	NG	997	TNT	351	14	323	17
				783	TNT	367	6	342	7
				731	TNT	361	5	331	6
10	None	--	--	--	--	--	--	--	--
					--	--	--	--	--
					--	--	--	--	--
11	TNT	30	TNT	147	TNT	383	20	405	17
			TNT	159	TNT	424	7	480	10
12	DNT	125	DNT	644	--	--	--	--	--
				706	--	--	--	--	--
				751	--	--	--	--	--
13	None	--	DNT	116	--	--	--	--	--
			--	--	--	--	--	--	--
			--	--	--	--	--	--	--
14	TNT	50	TNT	314	TNT	422	40	361	57
				333	TNT	462	21	412	31
				337	TNT	515	35	472	40
15	DNT	250	DNT	1282	DNT	352	32	81	11
				1446	--	--	--	--	--
				1503	--	--	--	--	--

[1] Prepared sample concentration prior to preconcentration. Preconcentration involved passing 30 mL of the sample through the system with elution in 2 mL methanol. The eluant was then diluted into 2 mL of 0.15 M KCl in water; [2] Preconcentration of samples at less than 10 ppb involved passing 300 mL of the sample through the system with elution into 2 mL methanol. The eluant was then diluted into 2 mL of 0.15 M KCl in water.

Task 7 & 8. Thermal Desorption and Vapor Approach

Application of polymers to the capture and preconcentration of targets prior to IMS analysis has been described in the literature. Often, those polymer materials are susceptible to swelling when exposed to increasing humidity levels restricting their use to air sampling only.[76,77] The sorbents utilized here are not subject to swelling or pore collapse upon change in humidity or exposure to liquids and, therefore, offer an alternative to polymer materials providing the potential for adsorption of targets from aqueous solution prior to thermal desorption. First, stability of the sorbent was evaluated by therogravimetric analysis (Figure 61). The results indicate that diethylbenzene bridging groups in these materials start to decompose before 300°C and account for significant mass loss above 500°C. An additional evaluation was conducted to characterize the impact of thermal cycling on sorbent performance. For this determination, a sorbent column in an HPLC housing, was utilized repeatedly for TNT adsorption followed by thermal cycling to 150ºC (45 min) and target elution. No performance degradation was observed for a sorbent column utilized over 20 cycles (Figure 61). Target stability was also considered. Experiments were conducted in which targets were adsorbed to the sorbents and then subjected to incubation at various temperatures for different durations. The targets considered were TNT, RDX, HMX, 2,4-DNT, and nitroglycerine. In Figure 62, we present a schematic of the protocol applied as well as representative data on TNT. As shown in the figure, TNT was stable for more than one hour of applied heat. Similar results were obtained for 2,4-DNT and RDX. HMX and nitroglycerine were evaluated only up to 150°C, but no degradation was observed at that temperature for more than one hour. Having determined that the sorbent and targets would be stable for the type of application considered, experiments were conducted to evaluate the potential for thermally desorbing the target materials. Thermogravimetric analysis of the sorbents was completed following adsorption of targets. Target desorption (TNT and RDX) was noted between 100 and 210ºC (Figure 63). This indicates the potential for desorption of the targets within a temperature range that can be tolerated by the sorbent materials.

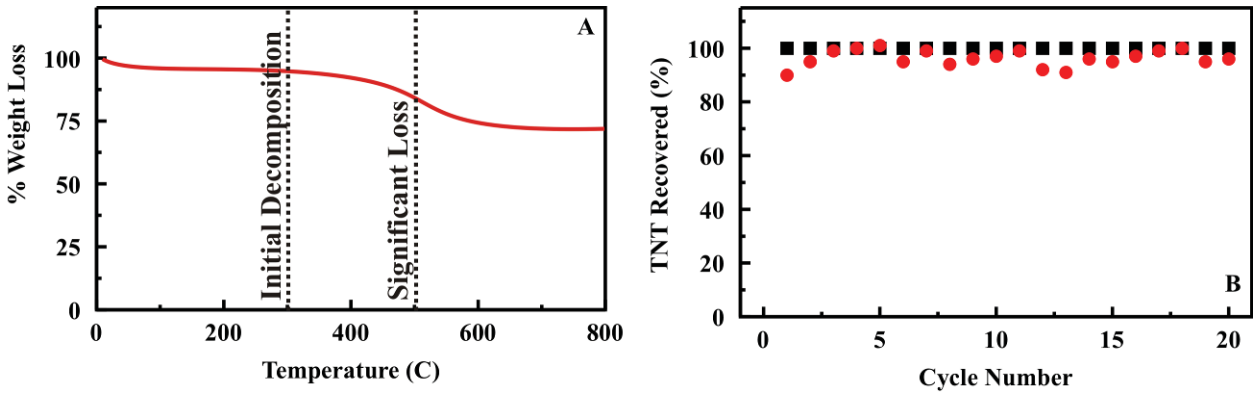

Figure 61. *(Panel A) The sorbent begins to degrade at 300ºC. (Panel B) The performance of the ED13 sorbent was not degraded over 20 heat/cool cycles. Each cycle was 45 mins at 150°C. The total percent target bound (from 10 mL of a 200 ppb TNT solution) and recovered (2 mL acetonitrile elution) is presented for each cycle.*

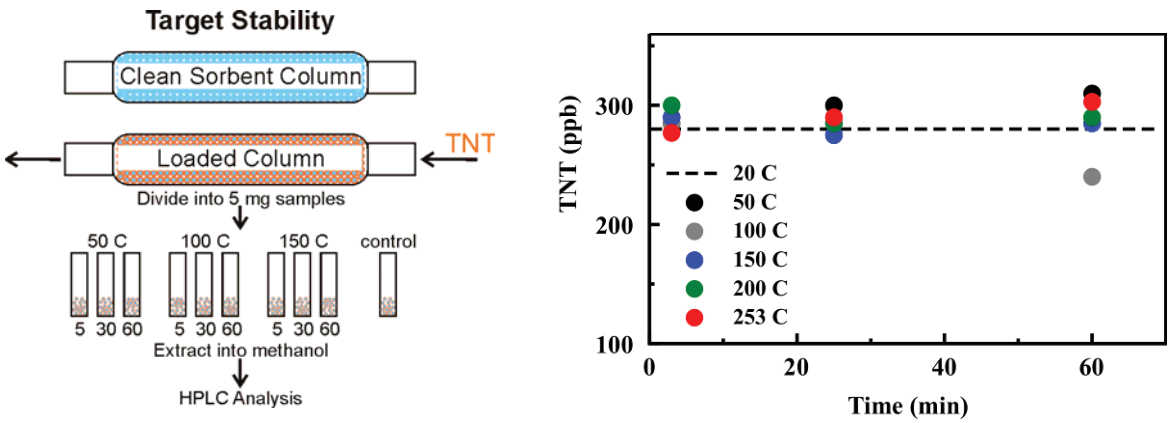

Figure 62. *Target Stability. Targets were loaded onto sorbent materials in a standard column flow format. The columns were then broken into controls and samples which were subjected to varied conditions.*

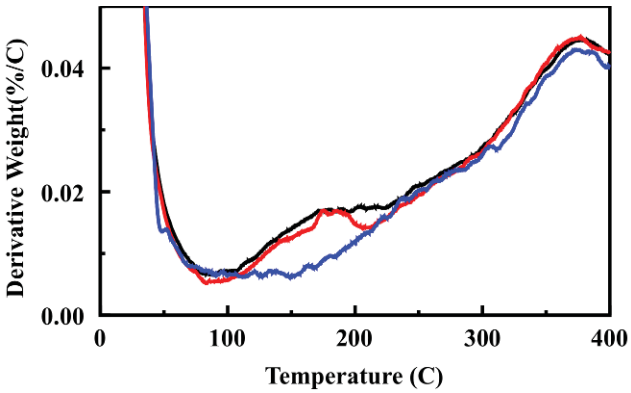

Figure 63. *Thermogravimetric analysis of ED13 sorbent (25 mg, blue) loaded in batch adsorption experiments with TNT (black) and RDX (red) (50 µg). Derivative weight is plotted versus temperature to provide better visualization of the differences between the data sets.*

Due to delays in receipt of the IMS instrument, thermal desorption was initially evaluated very similarly to those used to characterize the column for liquid extraction of samples. These experiments offer the potential for optimization of approaches applied to elution of targets. Dilute target in a sizable volume (generally 10 to 20 mL) was applied to a sorbent column containing approximately 60 mg of sorbent. We found that this sorbent mass provides sufficient material for capture of trace contaminants in a small size column that lends itself to a portable device. Air was then forced through the column to insure that the majority of the liquid had been expelled from the sorbent. The column was then heated by placing it into an oven where it was allowed to equilibrate for several minutes. Heated air was passed through the sorbent. The column was then cooled and solvent was passed through the sorbent to elute any target remaining. This experimental process is presented schematically in Figure 64. HPLC analysis was applied to the liquid effluent and the eluted target. Initially, desorbed target was captured using a charcoal bed. In later experiments, desorbed target was bubbled into water for analysis.

The first set of experiments completed in this way did not return desirable results. HPLC difference analysis indicated that 23% of target was desorbed at 50°C, 27% at 100°C, and 45% at 150°C. While the result at 150°C might produce samples detectable by the IMS, the residual target on the column is not acceptable. In addition, the loss of half the target to column retention would provide higher detection limits. After finding these results to be reproducible, we took a careful analysis of how the experiments were being conducted. We noted that the air passing

through the column was being moved slowly to provide time for the air to warm during transit from the ambient environment. This slow air flow provided ample time for target to condense into the tubing after the column resulting in its appearance in the eluted target sample. By altering the flow rate of air alone, we were able to significantly mediate this result. In addition by rinsing the exit lines separately from target elution, we found that significant desorption occurs from the column (Figure 65). Air moving at 5 mL/ min at 100°C provides excellent TNT and 2,4-DNT desorption. RDX desorption is more effective at slightly higher temperatures. We found that the rate of column heating is not critical to thermal desorption. It is the peak temperature reached that is the critical factor.

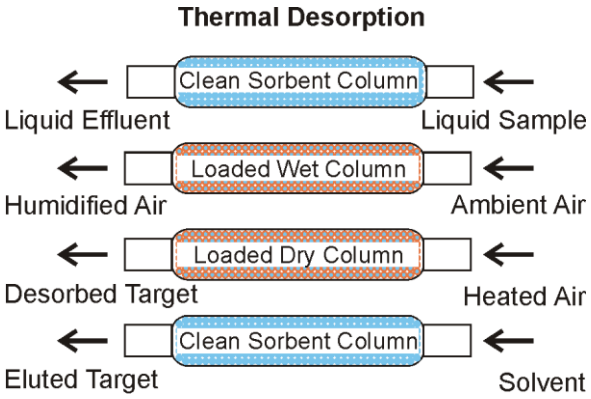

Figure 64. *Thermal Desorption. Target was applied to the column following standard protocols. Ambient air was used to expel remaining liquid. Heated air was applied to the column to desorb targets. A standard elution protocol was applied to collect remaining target on the column.*

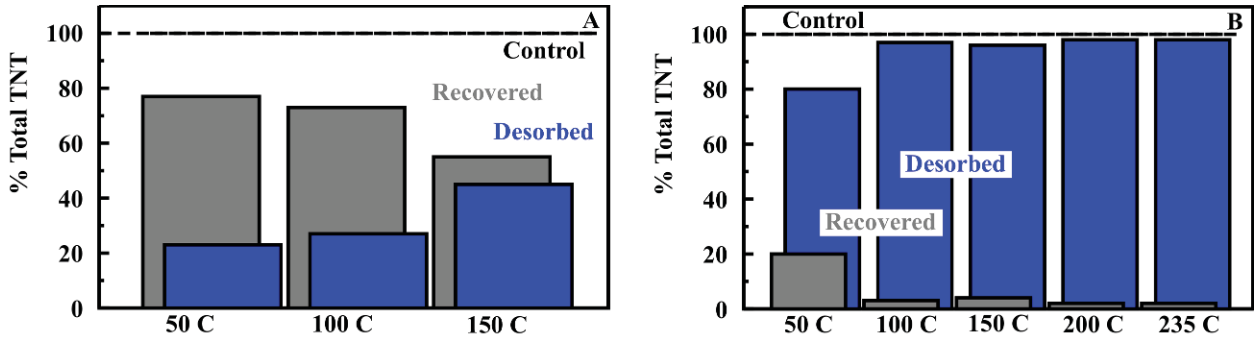

Figure 65. *Thermal Desorption. Graphs showing results for original (left) and optimized thermal desorption of TNT from the sorbent column.*

As described for the Liquid/Liquid System, column pressures in the stainless steel HPLC column housings increased with successive usage cycles. Alternatively, tunneling through the sorbent (passing of solutions through voids in the column rather than through pores in the sorbent) resulted after a few cycles, leading to poor target retention. In the case of the Liquid/Liquid System, the column housing was changed in an attempt to improve flow rates and reduce pressure while providing the desired target retention. Ultimately, an Omnifit borosilicate column housing (10 x 50 mm, Diba Industries, Mahopak, NY) was selected. In the case of systems utilizing thermal desorption these columns are not an option. It was necessary to find a column geometry that would provide the flow rates and column retention needed while still allowing for the column to be heated to the necessary temperatures. Several possibilities were considered: (1) use of a custom designed holder for the sorbent bed; (2) reduction in total sorbent mass in the column; (3) packing the sorbent with another material such as sand or glass

beads; (4) use of non-standard frits with commercial stainless steel housings. Detailed discussion of each approach is provided below.

The use of a custom designed holder would allow for a wider, shallower sorbent bed. This would reduce the pressure in the system while still allowing for the desired sorbent mass to be utilized. There are problems with this approach. The part is custom rather than off-the-shelf which will increase costs for future use. In addition, the sorbent must be heated. It is much more difficult to deliver heat evenly to the sorbent through the greater transverse distance. Finally, because the column will be used with small tubing, it is likely that the outer edges of the column will not see the same flow rates as the inner part of the sorbent. As a result, this option was discarded.

Reducing the sorbent mass in the column reduces the total number of binding sites. Affinity depends on both the concentration of the target and the concentration of the sites. When less sorbent is used, the capture of targets from the lowest concentration samples becomes less efficient. In addition, saturation of the column occurs at lower loading levels. Quantification of target in the original sample is not possible at or near column saturation. A compromise was determined for this point. Liquid/liquid evaluations used varying amounts of sorbent with varying success. It was determined that 60 mg of sorbent provided sufficient material for the types of applications planned.

Packing the sorbent as a mixture with glass beads (1 mm) has proven successful. Using this approach, the column diameter is narrow providing even heating and target exposure and the pressure is reduced to levels that can be managed by the portable pumps. Some sacrifice in total sorbent mass is made (see above), but the performance of the column in adsorption/desorption cycles is good.

The frits used with the HPLC columns are layered stainless steel and can be obtained in standard pore sizes of either 0.5 or 2 mm. In the case of the column housings we have utilized, the frits were 0.5 mm. When sorbent columns were packed in the earlier effort, the housings had glass fiber frits with a nominal pore size of 0.7 mm. From these columns, the fines were rinsed out of the housing during packing and prior to their use in experiments. The 0.5 mm stainless frits do not allow the fines to move out of the column. In fact, they are blocked by that component of the sorbent resulting in the observed high back pressures. By replacing the frits with steel mesh of a more appropriate size, it was possible to address this problem for the stainless column housings as well as extend the lifetime of the Omnifit housed columns described for the liquid/liquid system. The reduction in column pressure achieved when sorbents were mixed with glass beads not only made it possible to continuously use the sorbent column, it also provided more efficient desorption of target in a narrower profile (Figure 66). The temperature ramp rate was found to have no impact on the target desorption. The column temperature should be 125°C requiring a few minutes of equilibration time. Under these conditions with the geometry described, it is possible to utilize the system for preconcentration and detection of TNT and DNT repeatedly. We demonstrated that RDX and HMX can be thermally desorbed from the sorbent based on difference HPLC confirmation; however, flame ionization (the detector used by this GC) cannot be used to directly detect RDX or HMX.

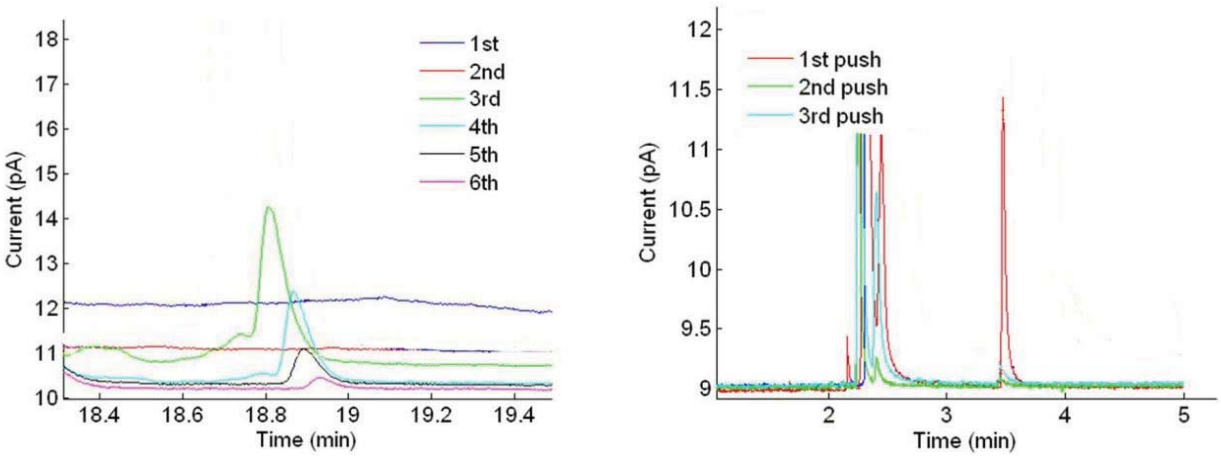

Figure 66. *Thermal Desorption of DNT (left) and TNT (right). The desorption profile is improved when the pressure in the column is reduced through incorporation of glass beads.*

Task 9. Integrated Approach

The performance of the portable IMS unit was initially evaluated in particulate mode to obtain an indication of sensitivity and accuracy of identification during routine laboratory use. For detection in this mode, samples are applied to manufacturer supplied swabs that are inserted into the instrument. A total of 120 samples including blank swabs as well as those loaded with target masses ranging from 0.1 µg to 200 µg were analyzed. For all of the studies presented here, factory optimized settings were utilized. Factory settings for the instrument do not include HMX detection. For the HMX samples (14) evaluated, the instrument reported positive responses for mixtures of other targets (typically including RDX). High mass samples (>50 µg) of any of the targets increased the prevalence of false responses in the subsequent samples even when the recommended two 'pass' responses were obtained before the next sample. They also caused an increase in the false positive rate. For 42 blind samples including TNT, DNT, RDX, NG, and HMX at 1, 20, 100, and 200 µg as well as blank samples, seven false positive responses and six improper identifications were obtained. A second set of 42 blind samples prepared using 0.5, 1, and 2 µg of the five targets as well as blank swabs, yielded five false positive results and thirteen improper identifications (Tables 38 and 39). HMX identification was not considered in totaling the number of improper identifications for these sets.

The intention of this effort was to improve the functionality of portable IMS sensing making it possible to apply the technology to samples traditionally below the limit of detection or in matrices that do not lend themselves to evaluation by IMS. In order to further establish functional parameters for the instrument. A series of seven samples was prepared in solution for each of the targets ranging from 78 ppb to 5 ppm. The samples were allowed to equilibrate with a 20 mL headspace (4 h, 26°C) from which the instrument sampled (vapor mode). The series was repeated twice. Under these conditions, none of the targets were detected. The vapor pressure of these compounds ranges from 10^{-2} to 10^{-7} Pa (26°C; exact values vary by source and target), so the maximum mass that could be expected in a 20 mL vapor sample would be 2 ng. The conditions utilized here would produce significantly less. Even when the instrument was used to sample the headspace above as received standards (Cerilliant; 1 mg/mL in acetonitrile), no detection of the targets resulted. When 5 ppm target samples were heated to 75°C (intended to increase headspace content), no positive responses were obtained from the instrument.

Table 38. *Blind sample set #1. These samples were measured and analyzed in randomized order by a technician with no knowledge of concentration range or target identification.*

Sample #	Evaluated Order	Target	Mass (µg)	Pass/Alarm	IMS ID	Indicator Level
1	4	TNT	1	Alarm	TNT	1
2	5	TNT	1	Alarm	TNT	1
3	2	RDX	200	Alarm	C4/RDX	3
4	6	RDX	20	Alarm	C4/RDX TNT	10 1
5	8	RDX	1	Alarm	C4/RDX TNT	6 1
6	12	TNT	20	Alarm	C4/RDX TNT	3 9
7	13	Blank	--	Alarm	C4/RDX TNT	2 8
8	1	RDX	200	Pass	RDX	--
9	9	RDX	1	Alarm	C4/RDX TNT	6 1
10	7	RDX	20	Alarm	C4/RDX TNT	10 1
11	3	TNT	200	Alarm	TNT	4
12	14	Blank	--	Alarm	C4/RDX TNT	2 6
13	10	TNT	200	Alarm	C4/RDX TNT	6 9
14	11	TNT	20	Alarm	C4/RDX TNT	3 9
15	39	DNT	20	Alarm	C4/RDX	6
16	28	RDX	200	Alarm	C4/RDX	5
17	41	Blank	--	Alarm	C4/RDX	3
18	36	HMX	1	Alarm	C4/RDX	6
19	34	HMX	20	Alarm	C4/RDX	7
20	37	DNT	1	Alarm	C4/RDX	4
21	31	HMX	200	Alarm	C4/RDX	5
22	30	HMX	200	Pass	--	--
23	29	RDX	200	Alarm	C4/RDX	7
24	40	DNT	20	Alarm	C4/RDX	4
25	35	HMX	1	Alarm	C4/RDX	5
26	32	Blank	--	Alarm	C4/RDX	4
27	33	HMX	20	Alarm	C4/RDX	4
28	38	DNT	1	Alarm	C4/RDX	5
29	27	RDX	200	Alarm	C4/RDX NG	10 7
30	24	NG	20	Alarm	NG	8
31	16	NG	200	Alarm	C4/RDX NG	1 8
32	25	NG	20	Alarm	NG	9
33	26	NG	1	Alarm	C4/RDX NG	4 8
34	18	TNT	50	Alarm	NG	10
35	21	HMX	50	Alarm	C4/RDX NG	1 10
36	22	Blank	--	Alarm	NG	10
37	42	NG	1	Pass	--	--
38	19	Blank	--	Alarm	C4/RDX NG	1 10
39	20	TNT	100	Alarm	C4/RDX NG	1 10
40	15	NG	200	Alarm	C4/RDX NG	1 8
41	17	NG	100	Alarm	C4/RDX NG	1 9
42	23	Blank	--	Alarm	NG	10

Table 39. *Blind sample set #2. These samples were measured and analyzed by a technician with no knowledge of concentration range or target identification.*

Sample #	Evaluated Order	Target	Mass (µg)	Pass/Alarm	IMS ID	Indicator Level
1	1	TNT	0.5	Alarm	NG	10
2	2	TNT	1	Alarm	NG	10
3	3	RDX	0.5	Alarm	C4/RDX NG	10 1
4	4	Blank	--	Pass	NG	--
5	5	NG	1	Alarm	NG	8
6	12	HMX	0.5	Alarm	NG	6
7	13	TNT	0.5	Alarm	NG	10
8	6	DNT	0.5	Alarm	C4/RDX NG Nitrate	10 2 1
9	7	HMX	0.5	Alarm	C4/RDX NG	10 2
10	8	NG	0.5	Alarm	NG	1
11	9	Blank	--	Pass	C4/RDX	--
12	10	RDX	0.5	Alarm	C4/RDX	10
13	11	RDX	1	Alarm	C4/RDX	10
14	14	NG	0.5	Alarm	NG	1
15	15	TNT	2	Alarm	C4/RDX NG Nitrate	10 6 2
16	16	NG	2	Alarm	C4/RDX NG Nitrate	10 4 2
17	17	HMX	1	Alarm	C4/RDX NG Nitrate	10 3 2
18	18	RDX	0.5	Pass	--	--
19	19	Blank	--	Alarm	C4/RDX TNT	10 1
20	20	NG	0.5	Alarm	C4/RDX TNT	10 1
21	21	RDX	2	Alarm	C4/RDX TNT	10 --
22	22	DNT	1	Alarm	C4/RDX TNT	10 1
23	23	HMX	2	Alarm	C4/RDX NG	7 1
24	24	TNT	0.5	Alarm	C4/RDX TNT	7 3
25	25	DNT	2	Alarm	C4/RDX TNT	7 3
26	26	Blank	--	Alarm	C4/RDX TNT	7 2
27	27	TNT	2	Alarm	C4/RDX TNT	6 4
28	28	Blank	--	Alarm	C4/RDX TNT	6 --
29	29	NG	1	Alarm	C4/RDX TNT	5 --
30	30	HMX	1	Alarm	C4/RDX TNT	5 --
31	31	Blank	--	Alarm	C4/RDX TNT	3 --
32	32	DNT	1	Alarm	C4/RDX TNT	3 --
33	33	TNT	1	Alarm	C4/RDX TNT	8 1
34	34	RDX	2	Alarm	C4/RDX TNT	10 --
35	35	NG	2	Alarm	C4/RDX TNT	9 --

36	36	RDX	1	Alarm	C4/RDX TNT	10 ---
37	37	DNT	2	Alarm	C4/RDX TNT	10 --
38	38	Blank	--	Alarm	C4/RDX TNT	9 --
39	39	HMX	1	Alarm	C4/RDX TNT	8 1
40	40	HMX	2	Alarm	C4/RDX TNT	6 1
41	41	DNT	1	Alarm	C4/RDX TNT	5 1
42	42	TNT	0.5	Alarm	C4/RDX TNT	5 1

A follow-on characterization was attempted for mapping expected IMS performance. Samples of the targets were generated using the particulate swabs. At the sampling point of clean swabs, target masses of 0.02, 0.1, 0.2, 0.5, 1, 2, and 4 µg were placed. The trend for analysis of TNT samples is presented in Figure 67. No detection was achieved for any samples below 0.1 µg. TNT was detected for 50% of 0.1 µg samples; no other targets were detected at this level. The electrochemical system design (Tasks 5 & 6) uses a typical sample volume of 20 mL. With 100% of the target thermally desorbed from the column, this indicates a limit of detection of 10 ppb for TNT in aqueous solution with limits for other targets falling below 50 ppb. Detection limits can be further reduced through increasing the sample volume utilized (see Task 6).

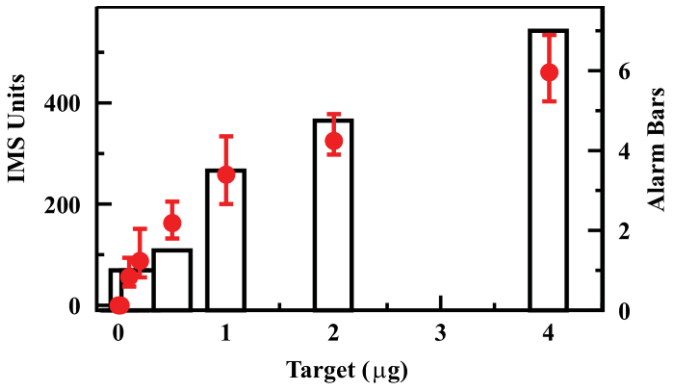

Figure 67. *TNT calibration. Shown here is the response of the IMS unit to a series of TNT masses. Analysis was completed four times for each sample. Symbols indicate IMS units from plasmographs. Bars indicate the alarm level indicator on the unit.*

The lack of response by the IMS to the headspace samples evaluated here made detection limits a concern. On the basis of the evaluations in Tasks 7 & 8 demonstrating desorption of target based on HPLC methods, it was determined that a sufficient concentration of target should be available in the desorption stream to obtain detection by the IMS instrument. Thermal desorption from a sorbent in a column format was evaluated based on IMS detection. Targets were loaded onto the sorbent column as 1 ppm solutions in water (3 mL). Air was then forced through the column, and it was heated to an external temperature of 135ºC. Having obtained a stable temperature, air was forced through the column (5 mL) while the instrument collected a sample. For TNT, positive responses were obtained for the first and second 5 mL air volumes. DNT, NG, and HMX (identified as DNT) yielded positive responses on the first volume only, and RDX yielded a positive response on the second volume only (Table 40). Representative plasmagraphs from the IMS are provided in Figure 68.

A large number of samples were evaluated using the prototype system for target capture prior to IMS analysis. TNT detection was consistent across the analyses. DNT samples often returned alarms, but the target identification varied significantly. Targets were identified as TNT/DNT or

NG/TNT mixtures. Ignoring inaccurate identification, reliable detection limits were in the 1 µg range for DNT. RDX is identified as C4/RDX by the instrument. Detection of this target was reliable with limits in the 0.2 µg range. NG was identified as NG/TNT by the instrument. While alarm levels for this target varied, reliable detection was possible in the 0.2 to 0.5 µg range.

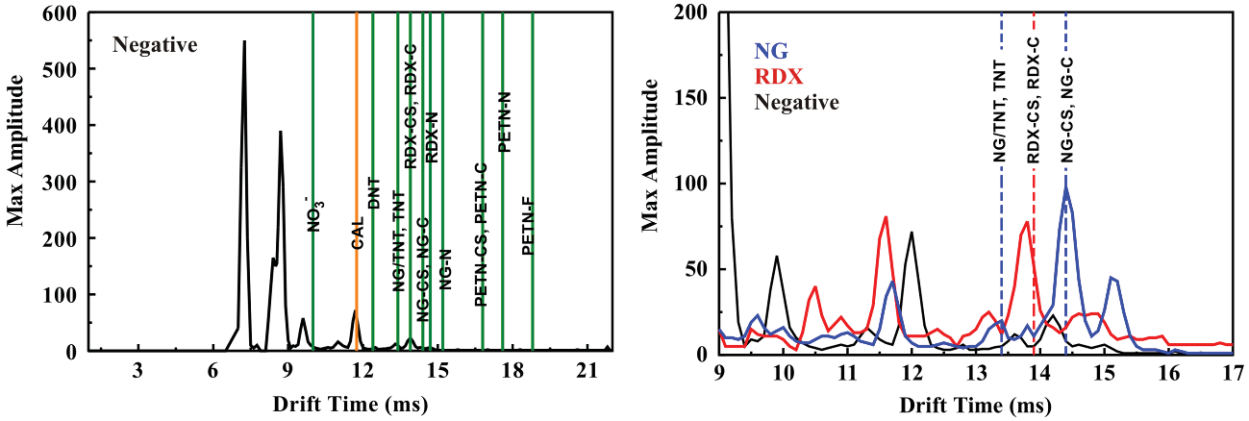

Figure 68. *Representative plasmographs from the SABRE 4000 IMS.*

Table 40. *Thermal desorption of targets loaded as 1 ppm solutions (3 mL) onto the sorbent column (20 mg). Detection based on sampling by IMS in vapor sampling mode during air push (5 mL). HPLC analysis of effluent and eluent volumes used for validation of experiment.*

Target	Applied Mass (µg)	HPLC Analysis (µg)	Air Push #	Pass/Alarm	IMS ID	Indicator Level
TNT	300	0.1	1 2 3	Alarm Alarm Pass	DNT/TNT DNT/TNT --	1 1 --
RDX	300	0.3	1 2	Pass Alarm	-- DNT/TNT	-- 1
DNT	300	0.1	1 2	Alarm Pass	DNT/TNT --	1 --
NG	300	0.6	1 2	Alarm Pass	NG --	1 --
HMX	300	0.5	1 2 3	Alarm Pass Pass	DNT/TNT -- --	1 -- --

Task 10. Bench-Scale Demo: Integrated

Figure 69 presents a schematic of the liquid/vapor system concept. The system would provide sample collection, preconcentration, and elution as a vapor prior to analysis by a commercial IMS detector. This system uses a similar approach to the liquid/liquid system described above. Aqueous samples are pulled through a filter stack, and a single pump is employed to move all volumes. Once target is adsorbed to the sorbent, the column is heated and the desorbed targets are directed to the IMS.

During the course of this effort, both of the engineers involved, Mansoor Nasir at NRL and Scott Veitch at SubChem, left their positions for other employment opportunities. These departures significantly hindered the ability of the other scientists involved to complete the proposed studies. The integrated system was not a completed prototype upon departure of the engineers, necessitating work on these aspects by chemists and technicians. While we were able to clearly demonstrate the potential of the proposed approaches, development of only breadboard

level components was completed. The system is not suitable to field demonstrations, and the remaining members of the team do not have the skills necessary to advancing the instrumentation.

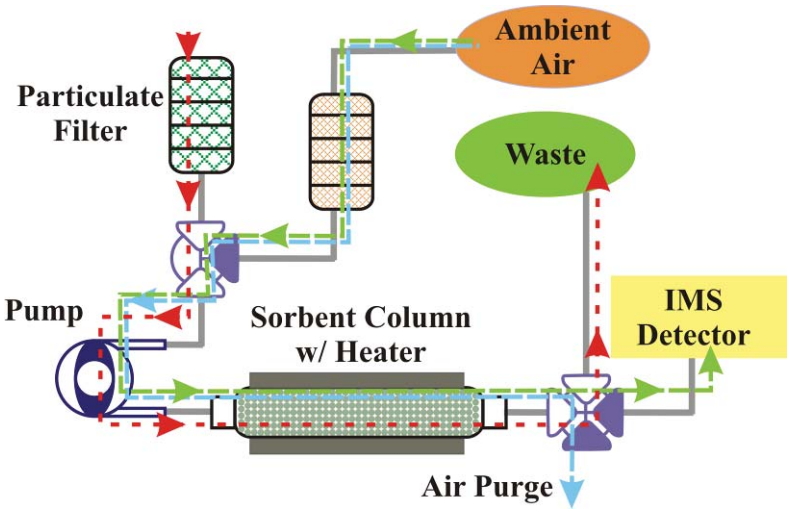

Figure 69. *Schematic of the liquid/vapor system.*

Heating a stainless steel column housing to an external temperature of 125 to 135ºC is necessary to achieve a suitable vapor. Flow of air through the heated housing at approximately 5 mL/min was determined to produce the necessary conditions for full target elution (Task 7). These are conditions that may be possible to achieve in the field, but they are high energy consumption tasks. The materials developed would potentially provide greater utility if used in combination with micro-IMS such as that developed under ER-1603.

Task 11. Field Trials

A prototype system for electrochemical detection of targets was prepared in collaboration with SubChem Systems based on the information collected during Tasks 3, 5, and 6. The design for a single-channel portable prototype included a weather-proof case, miniature electro-fluidic components (pumps, valves, and connections) and controller, reagent and waste reservoirs, and rechargeable battery. The report prepared by SubChem (Appendix B) indicates recommended components based both on the experience of the engineer and evaluations of equipment performed in conjunction with columns of the sorbent materials. The document also provides details of the graphical user interface designed using ChemView. This system was ultimately assembled and utilized for experiments conducted both in the laboratory and in the field.

Four sites were selected for evaluation of the instrument (Figure 70). Sites were over an area of 40 sq miles and included stagnant and running water sources in Cherokee County, Oklahoma. Site #1 was a pond located three miles east of Hulbert, OK. The pond is utilized for dogs and horses and has small wildlife as well as some algae. Site #2 was Ranger Creek located five miles east of Hulbert, OK. This site was a slow moving creek near residences and a through roadway. Site #3 was Double Spring Creek in Hulbert, OK. This creek is fast moving, shallow, and very clear. The sampling site was near a low water crossing. Site #4 was located on Hulbert Landing at the insertion point for 14 Mile Creek, 3 miles south of Hulbert, OK. This site was experiencing flood level waters due to recent heavy rains.

Figure 70. *Photographs of the prototype system (A) and sampling sites: #1 pond at residential site (B), #2 Ranger Creek (C), #3 Double Spring Creek (D, E), #4 Hulbert Landing (F).*

Samples were analyzed onsite using the prototype instrument and under laboratory conditions (EC and HPLC, respectively). All samples were evaluated as collected and after spiking with targets. Sample volumes used for analysis were 20 mL. HPLC analysis of the original sample, the post column effluent, and the post column eluent was completed. Table 41 summarizes the results of sample analysis.

Table 41. *Analysis of field samples. All concentrations provided in parts per billion (ppb). Samples were analyzed in triplicate.*

Site #	Spike	HPLC ID	[HPLC]	EC ID	[Height]	St. Dev. [Height]	[Area]	St. Dev [Area]
1	None	--	--	--	--	--	--	--
1	TNT, 50 ppb	TNT	303	TNT	349	122	280	137
1	DNT, 50 ppb	DNT	153	TNT/DNT	301	65	72	23
2	None	--	--		--	--	--	--
2	TNT, 50 ppb	TNT	323	TNT	409	131	294	150
2	DNT, 50 ppb	DNT	307	DNT	294	77	68	26
3	None	--	--	--	--	--	--	--
3	TNT, 50 ppb	TNT	315	TNT	371	121	258	133
3	DNT, 50 ppb	DNT	256	TNT/DNT	349	51	115	23
4	None	--	--	--	--	--	--	--
4	TNT, 50 ppb	TNT	304	TNT	339	99	265	77
4	DNT, 50 ppb	DNT	309	DNT	364	32	120	14
5	None	--	--	TNT	65	40	60	35
5	TNT, 50 ppb	TNT	311	TNT	340	65	259	83
5	DNT, 50 ppb	DNT	263	DNT	330	35	94	28

During the course of these trials several points were noted. The pumps supplied by SubChem in the prototype instrument could not push sample through the system at the specified rates. Processing through the solid phase extraction column required nearly 45 min per sample rather than the expected 15 to 20 min. Whether this reflects limitations of the components supplied only or limitations of those types of components in general is unclear. The PalmSens instrument is highly portable and offers the types of capabilities desired; however, during the course of its use, cables and flow cells had to be repeatedly replaced. The flow cell design (made of thin plastic) leaves it vulnerable to damage during chip mounting. In addition, the approach taken to alignment of the chip makes it easy to insert incorrectly resulting in leakage into the non-sample compartment. Once this component has been exposed to liquid, it must be allowed to dry completely before the flow cell can be put back into service. The USB and sensor cables were found to be fragile and subject to damage during the course of routine use. Their use in the field only exacerbated the issue.

Concluding Summary

In our early studies with nitroenergetics, we sought to optimize sorbent materials for improved binding capacity and affinity while also incorporating selectivity. The binding capacity of the BTE-DEB co-condensates was found to be strongly dependent upon the DEB content of the materials; however, as the DEB content of the material was increased, binding of non-target compounds also increased. A mixture of 70:30 DEB:BTE bridging groups offered a compromise in that it displayed a marked enhancement in TNT binding over that observed with the BTE only material while binding of compounds such as pNP and pCr was not strongly increased. In addition, imprinting of the material produced TNT binding that was apparently independent of the presence of pNP and pCr. While the TNT binding capacity of the sorbent could be further enhanced through the exclusive use of DNB-Brij as the surfactant, absorption was actually found to be less specific and was subject to reduction when pNP and pCr were present. In addition, the reduced degree of order and pore size homogeneity in this material resulted in the slowest adsorption kinetics observed.

The imprinting technique applied to the materials used in this study employed a new type of template molecule. Previously, the target analog employed for molecular imprinting was a ten carbon chain terminated with a di- or trinitrobenzene group.[35,36] Because it had low water solubility, it is likely that the majority of this molecule was contained within the hydrophobic cores of the Brij®76 micelles. In this case, there was little contact with the pore walls during condensation. This limited contact was reflected by the only marginal success obtained using this molecule for imprinting. The modified version of Brij®76 used here provided definitively successful imprinting. Inclusion of this template into the micelles was more favorable than for the previous template and the DNB groups were exposed to the pore walls. We have also been able to show that this technique is adaptable to the generation of templates against other targets of interest. We have imprinted a porous material using Pluronic P123 modified using diethyl chlorophosphate, an analog for paraoxon. The material shows selectivity for paraoxon and excludes p-nitrophenol (Figure 71).[78] The technique has also been used in the development of other sorbents as part of ongoing efforts.

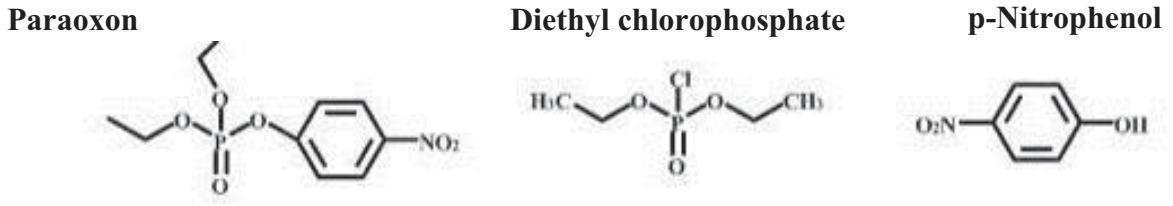

Figure 71. *Diethyl chlorophosphate is used as an imprint template in a material designed for selective binding of paraoxon. This material binds very little p-nitrophenol and the two compounds do not compete for binding sites.*

In order to address the back pressure issues typically encountered when employing mesoporous materials in column formats, we altered the synthesis of the materials to include a larger surfactant combined with a swelling agent. These changes result in materials with order on two length scales. The mesopores are slightly larger than those of the earlier materials, and they are on the pore walls of macropores of about 1 μm. This technique sacrifices some of the surface area of the mesoporous materials, but it improves interconnectivity. In fact, the saturation capacity of the hierarchical materials is greater than that of the earlier mesoporous materials while the affinity coefficient is only slightly reduced. In order to optimize the synthesis of this new type of material, variations in precursor ratios, template to surfactant ratios, and acid and swelling agent concentrations were evaluated. It was determined that a 50:50 DEB:BTE bridged material imprinted with modified Pluronic P123 (as described for templating above) provided the optimized sorbent that was sought. The sorbents developed here were compared to commercially available resins described for the concentration of nitroenergetics. The NRL material provided more concentrated target in the eluate than either of the commercial polymer resins. The material was used for pre-concentration of targets from soil and water samples from various locations and were shown to be applicable in repeated adsorption desorption cycles.

The lessons learned in the development of the nitroenergetics sorbents were applied to development of novel sorbents for the preconcentration of perchlorate. Though imprinting of those materials was not necessary, the advancements in sorbent structure and synthetic protocols were valuable. Though the materials developed provided significant improvements in selectivity

for perchlorate over typical competing analytes (other charged species), the interference of organic components in real-world samples may limit their ultimate utility. Activated charcoal and peroxide cleanup steps offer potential avenues for addressing this problem. The materials may be of value in isotopic analysis of materials sources.

Breadboard and brassboard level prototypes of the preconcentation system for use with electrochemical sensing were developed and testing was conducted in the laboratory for both. Limited field trials were conducted for the brassboard level prototype. The breadboard level prototype was used for component optimization and selection. The final NRL-developed system provided the necessary flow rates and controls for analysis of samples in 25 min cycles. The brassboard prototype was provided by SubChem Systems, Inc (Narragansett, RI). Though utilizing the analyses provided at the breadboard level, the system failed to produce the necessary pressure for analysis of samples at the 25 min rate. A breadboard level system for use with IMS based sensing was also developed. While this system provided clear evidence of the potential of the approach, a brassboard level prototype was not developed. Changing of personnel, including the departure of both engineers involved in the effort, and time constraints prevented the redesign of the system electrochemical system and advancement of the IMS system.

The materials developed under this effort are being utilized by another group within NRL (A. Kusterbeck) in the design of an electrochemical sensor for use with the REMUS (Remote Environmental Monitoring Units) UUA. The group is planning to use the materials developed during the course of this program to pre-concentrate nitroenergetic targets from sea water. Their current work is being funded through ONR. In addition to these types of active monitoring applications, the material developed during the course of this program has the potential for deployment for short- and long-term passive monitoring similar to the polyethylene passive sampling materials. The simple extraction method and exclusion of co-contaminants will specifically address the needs of that application.

References

1. Spalding, R.F.; Fulton, J.W., Groundwater munition residues and nitrate near grand island, nebraska, U.S.A. *Journal of Contaminant Hydrology* **1998**, *2*, 139-153.
2. Spain, J.C., Biodegradation of nitroaromatic compounds. *Annu. Rev. Microbiol.* **1995**, *49*, 523-555.
3. Spain, J.C.; Hughes, J.B.; Knackmuss, H.-J., *Nitroaromatic compounds and explosivies*. CRC Press: Boca Raton, 2000.
4. Valsaraj, K.T.; Qaisi, K.M.; Constant, W.D.; Thibodeaux, L.J.; Ro, K.S., Diffusive transport of 2,4,6-trinitrotoluene (tnt) from contaminated soil to overlying water. *J Hazard Mater* **1998**, *59*, 1-12.
5. Yinon, J., *Toxicity and metabolism of explosives*. CRC Press: Boca Raton, 1990.
6. Wang, J.; Bhada, R.K.; Lu, J.M.; MacDonald, D., Remote electrochemical sensor for monitoring tnt in natural waters. *Analytica Chimica Acta* **1998**, *361*, 85-91.
7. Cottingham, K., Ion mobility spectrometry rediscovered. *Analytical Chemistry* **2003**, *75*, 435A-439A.
8. Kanu, A.B.; Hill, H.H.; Gribb, M.M.; Walters, R.N., A small subsurface ion mobility spectrometer sensor for detecting environmental soil-gas contaminants. *Journal of Environmental Monitoring* **2007**, *9*, 51-60.
9. Jenkins, T.F.; Miyares, P.H.; Myers, K.F.; McCormick, E.F.; Strong, A.B., Comparison of solid-phase extraction with salting-out solvent-extraction for preconcentration of nitroaromatic and nitramine explosives from water. *Anal Chim Acta* **1994**, *289*, 69-78.
10. Leggett, D.C.; Jenkins, T.F.; Miyares, P.H., Salting-out solvent-extraction for preconcentration of neutral polar organic solutes from water. *Analytical Chemistry* **1990**, *62*, 1355-1356.
11. Monteil-Rivera, F.; Beaulieu, C.; Hawari, J., Use of solid-phase microextraction/gas chromatography-electron capture detection for the determination of energetic chemicals, in marine samples. *J. Chromatogr. A* **2005**, *1066*, 177-187.
12. Crescenzi, C.; Albinana, J.; Carlsson, H.; Holmgren, E.; Batlle, R., On-line strategies for determining trace levels of nitroaromatic explosives and related compounds in water. *J Chromatogr A* **2007**, *1153*, 186-193.
13. Smith, M.; Collins, G.E.; Wang, J., Microscale solid-phase extraction system for explosives. *J. Chromatogr. A* **2003**, *991*, 159-167.
14. Asefa, T.; MacLachlan, M.J.; Coombs, N.; Ozin, G.A., Periodic mesoporous organosilicas with organic groups inside the channel walls. *Nature* **1999**, *402*, 867-871.
15. Inagaki, S., Guan, S., Fukushima, Y., Ohsuna, T., Terasaki, O. , Novel mesoporous materials with a uniform distribution of organic groups and inorganic oxide in their frameworks. *J Am Chem Soc* **1999**, *121*, 9611-9614.
16. Melde, B.J.; Holland, B.T.; Blanford, C.F.; Stein, A., Mesoporous sieves with unified hybrid inorganic/organic frameworks. *Chem Mater* **1999**, *11*, 3302-3308.
17. Goto, Y.; Inagaki, S., Synthesis of large-pore phenylene-bridged mesoporous organosilica using triblock copolymer surfactant. *Chemical Communications* **2002**, 2410-2411.
18. Burleigh, M.C.; Markowitz, M.A.; Spector, M.S.; Gaber, B.P., Porous organosilicas: An acid-catalyzed approach. *Langmuir* **2001**, *17*, 7923-7928.

19. Kresge, C.T.; Leonowicz, M.E.; Roth, W.J.; Vartuli, J.C.; Beck, J.S., Ordered mesoporous molecular sieves synthesized by a liquid-crystal template mechanism. *Nature* **1992**, *359*, 710-712.
20. Corriu, R.J.P.; Leclercq, D., Recent developments of molecular chemistry for sol-gel processes. *Angewandte Chemie-International Edition in English* **1996**, *35*, 1420-1436.
21. Huo, Q.S.; Margolese, D.I.; Stucky, G.D., Surfactant control of phases in the synthesis of mesoporous silica-based materials. *Chem Mater* **1996**, *8*, 1147-1160.
22. Johnson, B.J.; Anderson, N.E.; Charles, P.T.; Malanoski, A.P.; Melde, B.J.; Nasir, M.; Deschamps, J.R., Porphyrin-embedded silicate materials for detection of hydrocarbon solvents. *Sensors* **2011**, *11*, 886-904.
23. Johnson, B.J.; Leska, I.A.; Melde, B.J.; Taft, J.R., Removal of phosgene by metalloporphyrin-functionalized porous organosilicates *Catal. Commun.* **2012**, *27*, 105-108.
24. Johnson, B.J.; Leska, I.A.; Melde, B.J.; Taft, J.R., Self-reporting materials: Dual use for porphyrin-embedded sorbents. *Sensor Actuat B-Chem* **2012**, *176*, 399-404.
25. Jayasundera, S.; Burleigh, M.C.; Zeinali, M.; Spector, M.S.; Miller, J.B.; Yan, W.F.; Dai, S.; Markowitz, M.A., Organosilica copolymers for the adsorption and separation of multiple pollutants. *J Phys Chem B* **2005**, *109*, 9198-9201.
26. Lewin, U.; Efer, J.; Engewald, W. "High-performance liquid chromatographic analysis with electrochemical detection for residues of explosives in water samples around a former ammunition plant," 19th International Symposium on Column Liquid Chromatography, Innsbruck, Austria, 1995;
27. Burleigh, M.C.; Markowitz, M.A.; Spector, M.S.; Gaber, B.P., Porous polysilisesquioxanes for the adsorption of phenols. *Environ Sci Technol* **2002**, *36*, 2515-2518.
28. Burleigh, M.C.; Jayasundera, S.; Thomas, C.W.; Spector, M.S.; Markowitz, M.A.; Gaber, B.P., A versatile synthetic approach to periodic mesoporous organosilicas. *Colloid Polym Sci* **2004**, *282*, 728-733.
29. Nozawa, A.; Ohnuma, T., Improved high-performance liquid-chromatographic analysis of ethylene-oxide condensates by their esterification with 3,5-dinitrobenzoyl chloride. *Journal of Chromatography* **1980**, *187*, 261-263.
30. Sun, C.; Baird, M.; Anderson, H.A.; Brydon, D.L., Separation and determination of oligomers and homologues of aliphatic alcohol ethoxylates in textile lubricants and lubricant emulsion by high-performance liquid chromatography. *J. Chromatogr. A* **1997**, *771*, 145-154.
31. Sun, C.; Baird, M.; Simpson, J., Determination of poly(ethylene glycol)s by both normal-phase and reversed-phase modes of high-performance liquid. *J. Chromatogr. A* **1998**, *800*, 231-238.
32. Johnson, B.J.; Melde, B.J.; Charles, P.T.; Cardona, D.C.; Dinderman, M.A.; Malanoski, A.P.; Qadri, S.B., Imprinted nanoporous organosilicas for selective adsorption of nitroenergetic targets. *Langmuir* **2008**, *24*, 9024-9029.
33. Trammell, S.A.; Zeinali, M.; Melde, B.J.; Charles, P.T.; Velez, F.L.; Dinderman, M.A.; Kusterbeck, A.; Markowitz, M.A., Nanoporous organosilicas as preconcentration materials for the electrochemical detection of trinitrotoluene. *Anal Chem* **2008**, *80*, 4627-4633.
34. Johnson, B.J.; Melde, B.J.; Charles, P.T.; Malanoski, A.P. "Porphyrin-embedded organosilicas for detection and decontamination," 2009 SPIE International Defense, Security and Sensing Symposium, Orlando, FL, 2009; SPIE

35. Johnson-White, B.; Zeinali, M.; Malanoski, A.P.; Dinderman, M., Sunlight catalyzed conversion of cyclic organics with novel mesoporous organosilicas. *Catalysis Comm* **2007**, *8*, 1052-1056.
36. Johnson-White, B.; Zeinali, M.; Shaffer, K.M.; C. H. Patterson, J.; Charles, P.T.; Markowitz, M.A., Detection of organics using porphyrin embedded nanoporous organosilicas. *Biosens Bioelectron* **2007**, *22*, 1154-1162.
37. Nakanishi, K.; Kobayashi, Y.; Amatani, T.; Hirao, K.; Kodaira, T., Spontaneous formation of hierarchical macro-mesoporous ethane-silica monolith. *Chem Mater* **2004**, *16*, 3652-3658.
38. Johnson, B.J.; Melde, B.J.; Charles, P.T.; Dinderman, M.A.; Malanoski, A.P.; Leska, I.A.; Qadri, S.A., Macroporous silica for concentration of nitroenergetic targets. *Talanta* **2010**, *81*, 1454-1460.
39. Melde, B.J.; Johnson, B.J.; Dinderman, M.A.; Deschamps, J.R., Macroporous periodic mesoporous organosilicas with diethylbenzene bridging groups. *Micropor Mesopor Mat* **2010**, *130*, 180-188.
40. Johnson, B.J.; Melde, B.J.; Leska, I.A.; Charles, P.T.; Hewitt, A.D., Solid-phase extraction using hierarchical organosilicates for enhanced detection of nitroenergetic targets. *J Environ Monitor* **2011**, *13*, 1404-1409.
41. Nakanishi, K.; Amatani, T.; Yano, S.; Kodaria, T., Multiscale templating of siloxane gels via polymerization-induced phase separation. *Chem Mater* **2008**, *20*, 1108-1115.
42. Amatani, T.; Nakanishi, K.; Hirao, K.; Kodaira, T., Monolithic periodic mesoporous silica with well-defined macropores. *Chem. Mater.* **2005**, *17*, 2114-2119.
43. Bagshaw, S.A.; Pinnavaia, T.J., Mesoporous alumina molecular sieves. *Angew. Chem. Int. Ed. Engl.* **1996**, *35*, 1102-1105.
44. Bagshaw, S.A.; Prouzet, E.; Pinnavaia, T.J., Templating of mesoporous molecular sieves by nonionic polyethylene oxide surfactants. *Science* **1995**, *269*, 1242-1244.
45. Kim, H.J.; Guiochon, G., Comparison of the thermodynamic properties of particulate and monolithic columns of molecularly imprinted copolymers. *Anal Chem* **2005**, *77*, 93-102.
46. Umpleby, R.J.; Baxter, S.C.; Bode, M.; Berch, J.K.; Shah, R.N.; Shimizu, K.D., Application of the freundlich adsorption isotherm in the characterization of molecularly imprinted polymers. *Anal Chim Acta* **2001**, *435*, 35-42.
47. Ockrent, C., Selective absorption by activated charcoal from solutions containing two organic acids. *J Chem Soc* **1932**, 613-630.
48. Weber, W.J., Competitive interactions in adsorption from dilute aqueous bi-solute solutions. *J Appl Chem-USSR+* **1964**, *14*, 565-572.
49. Kruk, M.; Jaroniec, M., Gas adsorption characterization of ordered organic-inorganic nanocomposite materials. *Chem. Mater.* **2001**, *13*, 3169-3183.
50. Brandhuber, D.; Peterlik, H.; Huesing, N., Facile self-assembly processes to phenylene-bridged silica monoliths with four levels of hierarchy. *Small* **2006**, *2*, 503-506.
51. Zhong, H.; Zhu, G.; Yang, J.; Wang, P.; Yang, Q., Periodic mesoporous hybrid monolith with hierarchical macro-mesopores. *Micropor Mesopor Mat* **2007**, *100*, 259-267.
52. Li, C.; Yang, J.; Shi, X.; Liu, J.; Yang, Q., Synthesis of sba-15 type mesoporous organosilicas with diethylenebenzene in the framework and post-synthetic framework modification. *Micropor Mesopor Mat* **2007**, *98*, 220-226.
53. Minakuchi, H.; Nakanishi, K.; Soga, N.; Ishizuka, N.; Tanaka, N., Effect of skeleton size on the performance of octadecylsilylated continuous porous silica columns in reversed-phase liquid chromatography. *J. Chromatography A* **1997**, *762*, 135-146.

54. Grieken, R.v.; Calleja, G.; Stucky, G.D.; Melero, J.A.; Garcia, R.A.; Iglesias, J., Supercritical fluid extraction of a nonionic surfactant template from sba-15 materials and consequences on the porous structure. *Langmuir* **2003**, *19*, 3966-3973.
55. Yang, Y.; Sayari, A., Mesoporous organosilicates from multiple precursors: Co-condensation or phase segregation/separation? *Chemistry of Materials* **2008**, *20*, 2980-2984.
56. Li, C.M.; Liu, J.; Shi, X.; Yang, J.; Yang, Q.H., Periodic mesoporous organosilicas with 1,4-diethylenebenzene in the mesoporous wall: Synthesis, characterization, and bioadsorption properties. *J Phys Chem C* **2007**, *111*, 10948-10954.
57. Schmidt-Winkel, P.; Glinka, C.J.; Stucky, G.D., Microemulsion templates for mesoporous silica. *Langmuir* **2000**, *16*, 356-361.
58. Schmidt-Winkel, P.; Lukens, W.W.; Yang, P.D.; Margolese, D.I.; Lettow, J.S.; Ying, J.Y.; Stucky, G.D., Microemulsion templating of siliceous mesostructured cellular foams with well-defined ultralarge mesopores. *Chemistry of Materials* **2000**, *12*, 686-696.
59. Mandal, M.; Kruk, M., Large-pore ethylene-bridged periodic mesoporous organosilicas with face-centered cubic structure. *J Phys Chem C 114*, 20091-20099.
60. Mandal, M.; Kruk, M., Versatile approach to synthesis of 2-d hexagonal ultra-large-pore periodic mesoporous organosilicas. *J Mater Chem 20*, 7506-7516.
61. Kim, T.H.; Jang, M.; Park, J.K., Bifunctionalized mesoporous molecular sieve for perchlorate removal. *Micropor Mesopor Mat* **2008**, *108*, 22-28.
62. Zhao, D.; Feng, J.; Huo, Q.; Melosh, N.; Fredrickson, G.H.; Chmelka, B.F.; Stucky, G.D., Triblock copolymer syntheses of mesoporous silica with periodic 50 to 300 angstrom pores. *Science* **1998**, *279*, 548-552.
63. Orpen, A.G., Applications of the cambridge stuctural database to molecular inorganic chemistry. *Acta Crystallogr. B* **2002**, *58*.
64. Barbalace, K., Periodic table of elements - sorted by ionic radius. In *Available online: http://EnvironmentalChemistry.com/yogi/periodic/ionicradius.html*.
65. Yoon, J.W.; Yoon, Y.; Amy, G.; Cho, J.; Foss, D.; Kim, T.-H., Use of surfactant modified ultrafiltration for perchlorate clo_4^- removal. *Water Res* **2003**, *37*.
66. Mbuna, J.T., T.; Oshima, M.; Motomizu, S., Evaluation of weak ion association between tetraalkylammonium ions and inorganic ions in aqueous solutions by capillary zone electrophoresis. *J. Chrom. A* **2004**, *1022*.
67. Winzor, D.J., Determination of binding constants by affinity chromatography. *J. Chromatogr. A* **2004**, *1037*, 351-367.
68. Mikutta, R.; Kleber, M.; Kaiser, K.; Jahn, R., Review: Organic matter removal from soils using hydrogen peroxide, sodium hypochloride, and disodium peroxodisulfate. *Soil Sci. Soc. Am. J.* **2005**, *69*, 120-135.
69. Johnson, B.J.; Malanoski, A.P.; Leska, I.A.; Melde, B.J.; Taft, J.R.; Dinderman, M.A.; Deschamps, J.R., Adsorption of organophosphates by porous organosilicates: Capillary phase-separation. *Micropor Mesopor Mat* **2013**, *submitted*.
70. Harvey, S.D.; Clauss, T.R.W., Rapid on-line chromatographic determination of trace-level munitions in aqueous samples. *J. Chromatogr. A* **1996**, *753*, 81-89.
71. Wang, J.; Lu, F.; MacDonald, D.; Lu, J.M.; Ozsoz, M.E.S.; Rogers, K.R., Screen-printed voltammetric sensor for tnt. *Talanta* **1998**, *46*, 1405-1412.
72. Wang, J.; Thongngamdee, S., On-line electrochemical monitoring of (tnt) 2,4,6-trinitrotoluene in natural waters. *Analytica Chimica Acta* **2003**, *485*, 139-144.

73. Kounaves, S.P.; Young, J.B., Carbon-fiber electrode cell for square-wave voltammetric detection of biogenic-amines in high-performance liquid-chromatography. *Analytical Chemistry* **1989**, *61*, 1469-1472.
74. Trammell, S.A.; Melde, B.J.; Zabetakis, D.; Deschamps, J.R.; Dinderman, M.A.; Johnson, B.J.; Kusterbeck, A.W., Electrochemical detection of tnt with in-line pre-concentration using imprinted diethylbenzene-bridged periodic mesoporous organosilicas. *Sens. Actuators B* **2011**, *155*, 737-744.
75. Olsen, K.; Wang, J. *Detection and measurement of explosives in groundwater using in situ electrochemical sensors*; Strategic Environmental Research and Development Program (SERDP): 2002.
76. Higgins, B.; Simonson, D.; McGill, R.A.; Nguyen, V.; Stepnowski, J.; Pai, R.; Stepnowski, S.; Rake, M.; Ieee "Functionalized sorbent membranes for use with ion mobility spectrometry," IEEE Conference on Technologies for Homeland Security, Waltham, MA, 2008;
77. Martin, M.; Crain, M.; Walsh, K.; McGill, R.A.; Houser, E.; Stepnowski, J.; Stepnowski, S.; Wu, H.D.; Ross, S., Microfabricated vapor preconcentrator for portable ion mobility spectroscopy. *Sensors and Actuators B-Chemical* **2007**, *126*, 447-454.
78. Johnson, B.J.; Melde, B.J.; Thomas, C.; Malanoski, A.P.; Leska, I.A.; Charles, P.T.; Parrish, D.A.; Deschamps, J.R., Fluorescent silicate materials for the detection of paraoxon. *Sensors* **2010**, *10*, 2315-2331.

Appendix A: List of Technical Publications

Peer-reviewed journal articles

"Application of portable ion mobility spectrometer to detection of nitroenergetic contaminants in aqueous samples" B.J. Johnson, M. Nasir, P.T. Charles, I.A. Leska, N.F. Dyson, J.R. Taft, B.J. Melde, *manuscript in preparation* (2013)

"Enhancing electrochemical detection through preconcentration: Nitroenergetic contaminants" B.J. Johnson, R.L. Siefert, M. Nasir, I.A. Leska, P.T. Charles, B.J. Melde, J.R. Taft, *IEEE Sensors, manuscript in review* (2013)

"Extraction of perchlorate using porous organosilicate materials" B.J. Johnson, I.A. Leska, B.J. Melde, M.H. Moore, A.P. Malanoski, R.S. Siefert, J.R. Taft, J.R. Deschamps, *Materials*, 6, 1403-19 (2013). (Invited contribution to the special issue, "Advances in Mesoporous Materials")

"Toward *in situ* monitoring of water contamination by nitroenergetic compounds" B.J. Johnson, I.A. Leska, A. Medina, N.F. Dyson, M. Nasir, B.J. Melde, J.R. Taft, P.T. Charles, *Sensors* 12, 14953-67 (2012).

"Solid-phase extraction using hierarchical organosilicates for enhanced detection of nitroenergetic targets" B.J. Johnson, B.J. Melde, I.A. Leska, P.T. Charles, A.D. Hewitt, *Journal of Environmental Monitoring*, 31, 1404-9 (2011).

"Electrochemical detection of TNT with in-line pre-concentration using imprinted diethylbenzene-bridged periodic mesoporous organosilicas" S.A. Trammell, B.J. Melde, D. Zabetakis, J.R. Deschamps, M.A. Dinderman, B.J. Johnson, A.W. Kusterbeck, *Sensors & Actuators B – Chemical*, 155, 737-744 (2011).

"Mesoporous Materials in Sensing: Morphology and Functionality at the Meso-Interface" B.J. Melde, B.J. Johnson. *Analytical and Bioanalytical Chemistry*, 398, 1565-73 (2010). (Invited contribution Focus on Sensor Interfaces)

"Macroporous Silica for Concentration of Nitroenergetic Targets" B.J. Johnson, B.J. Melde, P.T. Charles, M.A. Dinderman, A.P. Malanoski, I.A. Leska, S. Qadri. *Talanta*, 80, 1454-60 (2010). *This article received 2010 NRL Research Publication Award.*

"Macroporous Periodic Mesoporous Organosilicas with Diethylbenzene Bridging Groups" B.J. Melde, B.J. Johnson, M.A. Dinderman, J.R. Deschamps. *Microporous and Mesoporous Materials*, 130, 180-8 (2010).

"Mesoporous Silicate Materials in Sensing" B.J. Melde, B.J. Johnson, P.T. Charles. *Sensors*, 8, 5202-28 (2008). (Invited contribution Special Issue on Molecular Recognition and Sensors)

"Imprinted Nanoporous Organosilicas for Selective Adsorption of Nitroenergetic Targets" B.J. Johnson, B.J. Melde, P.T. Charles, D.C. Cardona, M.A. Dinderman, A.P. Malanoski, S. Qadri. *Langmuir*, 224, 9024-9 (2008).

Published reports

"Preconcentration for improved long term monitoring of contaminants in groundwater: Sorbent development" B.J. White, B.J. Melde, P.T. Charles. 2013 NRL Formal Report #NRL/FR/6910--12-10,235.

"Contaminant Monitoring in Ground and Surface Water" B.J. White, B.J. Melde, P.T. Charles, A.P. Malanoski, M.A. Dinderman. *2010 Naval Research Laboratory Review*. John D. Bultman, Senior Science Editor, NRL Washington, DC, 151-153. (Selected as one of the NRL Top 20 Accomplishments of 2009)

"Periodic Mesoporous Organosilicas (PMOs) as Pre-concentration Elements for Improved Longterm Monitoring of Key Contaminants in Groundwater" B.J. White, P.T. Charles. 2009 Technical Report in the *Strategic Environmental Research & Development Program's (SERDP) On-Line Library*. (http://www.serdp.org/content/download/10211/127780/file/ER-1604-FR-Phase%20I.pdf)

Proceedings papers

"Functional and functionalized silicate materials" B.J. Johnson, B.J. Melde, B. Lin, P.T. Charles, A.P. Malanoski, M. Nasir. *Proceedings 2010 MRS Fall Meeting Symposium BB*, MRS Online Proceedings Library, 1306-BB02-07 (November 2010).

Presentations (oral)

Functional nanoporous organosilicates for air purification and remediation applications," B.J. Melde and B.J. Johnson. *244th ACS National Meeting and Exposition*, Philadelphia, PA, August 19-23, 2012.

"Mesoporous silica," B.J. White. *NRL-WINPAC Workshop on Nanomaterials*, Washington, DC, June 11-12, 2012. – Invited Talk

"Application of nanoporous organosilicates to detection of nitroenergetic compounds and volatile hydrocarbon solvents," B.J. Melde, B.J. Johnson, S.A. Trammell. *242nd ACS National Meeting*, Denver, CO, August 28, 2011.

"Functional and Functionalized Silicate Materials," B.J. Johnson. *Inorganic Seminar Series*, Department of Chemistry, Emory University, Atlanta, GA, February 1, 2011. - Invited Talk

"Functional and Functionalized Silicate Materials," B.J. White, B.J. Melde, B. Lin, P.T. Charles, A.P. Malanoski. 2010 Materials Research Society Fall Meeting, Boston, MA, USA, November 29 – December 3, 2010. - Invited Talk

"Porous Organosilicas for Concentration of Nitroenergetic and Organophosphate Compounds," B.J. Melde, B.J. Johnson, P.T. Charles, I.A. Leska, M.A. Dinderman, J.R. Deschamps. *ACS Fall 2010 National Meeting, Division of Colloid & Surface Chemistry*, Boston, MA, August 22-26, 2010.

"Multifunctional Periodic Mesoporous Organosilicas for Environmental Applications" B.J. Melde, B.J. Johnson, M.A. Dinderman, J.R. Deschamps. *238th ACS National Meeting, Division of Colloid & Surface Chemistry*, Washington, DC, August 16-20, 2009

"Porphyrin-embedded organosilicas for detection and decontamination," B.J. Johnson, B.J. Melde, P.T. Charles, A.P. Malanoski, M.A. Dinderman. *SPIE Defense, Security, and Sensing: Optics and Photonics in Global Homeland Security V*, Orlando, FL, USA, April 13 – 17, 2009. – Invited Talk

Presentations (poster)

"Preconcentration for improved monitoring of contaminants," B.J. White, B.J. Melde, I.A. Leska, J.R. Taft, M. Nasir, A. Medina, N. Dyson Jr., R.L Siefert, P.T. Charles. *The Partners in Environmental Technology Technical Symposium and Workshop*, Washington, DC, USA, November 29 - December 1, 2011.

"Pre-concentration for improved monitoring of contaminants in groundwater," B.J. White, B.J. Melde, M. Nasir, P.T. Charles, I.A. Leska, R.L. Siefert, M.A. Dinderman, N.Dyson, Jr. *The Partners in Environmental Technology Technical Symposium and Workshop*, Washington, DC, USA, November 30 - December 2, 2010.

"Porous Organosilicate Materials," B.J. White, B.J. Melde, B. Lin, P.T. Charles. *Tri-Service Biotechnology Technical Planning Meeting*, Potomac, MD, February 23 – 24, 2010.

"Imprinted Nanoporous Organosilicas for Selective Adsorption of Nitroenergetic Targets," B.J. Johnson, P.T. Charles, B.J. Melde, M. Nasir. *The Partners in Environmental Technology Technical Symposium and Workshop*, Washington, DC, USA, December 3 – 5, 2009.

"Hierarchical Organosilicas for Preconcentration of Nitroaromatic Targets," B.J. Johnson, B.J. Melde, P.T. Charles. *The Partners in Environmental Technology Technical Symposium and Workshop*, Washington, DC, USA, December 2 – 4, 2008.

Appendix B: Additional Information

Cost Analysis

The following data provides cost information for small scale production of MM1 as described in the Results and Accomplishments section at the time of this report. Large scale production would be expected to significantly reduce costs.

Chemicals	Unit Size	Cost	Supplier
1,2-bis(trimethoxysilyl)ethane	25 mL	$85.10	Sigma-Aldrich
bis(trimethoxysilylethyl)benzene	50 g	$132.00	Gelest, Inc.
Mesitylene	500 mL	$59.30	Sigma-Aldrich
Pluronic P123	1 L	$62.40	Sigma-Aldrich
nitric acid, 70%	500 mL	$39.20	Sigma-Aldrich
dichloromethane, ≥98%	1 L	$44.70	Sigma-Aldrich
Ethanol	1 pint	$2.00	Warner-Graham Company
3,5-dinitrobenzoyl chloride	25 g	$30.10	Sigma-Aldrich
magnesium turnings	250 g	$134.50	Sigma-Aldrich
sodium bicarbonate	500 g	$32.70	Sigma-Aldrich

Synthesis of Pluronic P123 imprint template; esterification of Pluronic P123 with 3,5-dinitrobenzoyl chloride.

Chemicals	Amount	Cost
Pluronic P123	8 g	$0.50
3,5-dinitrobenzoyl chloride	1.27 g	$1.53
dichloromethane	60 mL	$2.68
sodium bicarbonate	1.2 g	$0.08
magnesium turnings	0.2 g	$0.11
	Total	$4.90

Synthesis of the imprinted hierarchical BTE:DEB sorbent; batch size is approximately 2 g.

Chemicals	Amount	Cost
1,2-bis(trimethoxysilyl)ethane	0.988 mL	$3.36
bis(trimethoxysilylethyl)benzene	1.468 g	$3.88
mesitylene	0.64 mL	$0.08
Pluronic P123	1.66 mL	$0.10
imprint surfactant	0.24 g	$0.15
nitric acid	7.5 g 0.1 M	<$0.01
ethanol	1250 mL	$5.29
	Total	$12.86

SubChem Phase I Report on Prototype Development

The following document is incorporated as received (in pdf form) by email from Alfred Hanson, President, SubChem Systems, Inc on November 03, 2011.

Naval Research Laboratory
Portable Electrochemical TNT Sensor

Report Phase 1- Prototype Design

Contract No. N00173-11-P-3165
Requisition No. 69-0952-11

Scott Veitch
SubChem Systems, Inc.
65 Pier Rd.
Narragansett, RI 02882
Phone: (401) 783-4744 x109
Email: veitchsp@subchem.com
October 20, 2011

Revised: 11/3/2011

Executive Summary

This report contains the design recommendations of SubChem Systems for the fabrication of a portable electrochemical sensor system utilizing the Naval Research Laboratory's macroporous silica/liquid-liquid pre-concentration column and electrochemical flow cell while leveraging the available PalmSens device. This phase one design report represents the first part of three phase project outlined in the statement of work (see appendix). To arrive at the recommended design for phase 2, design criteria of the system were discussed with researchers at NRL and a summary of system requirements were documented. The flow characteristics of a sample pre-concentration column and the PalmSens flow cell were determined and tabulated. A brief study of OEM pump and valve technology was performed to assess the feasibility of the components within the application of the portable sensor. The capabilities of the OEM components were compared to the requirements of the flow characteristics pertaining to the flow cell and pre-concentration column. This then dictated which components were viable options.

After thorough review of commercially available OEM pump and valve technology, SubChem Systems is recommending using the Micropump GA series pump head, and driver with two Lee Company inert LFYA valves. At this stage in the project, the GA series pump head and driver will handle back pressure up to 75 psi. This will allow researchers to further the ongoing development of the pre-concentration column without being hindered by a flow system back pressure limitation. An alternate design using a Lee Company inert LPL pump is recommended if the pre-concentration column maintains a back pressure less than 10 psi. The Lee Company LPL series of pumps are solenoid operated and have a very high accuracy when dispensing volume.

The field case selected for this prototype was a Pelican Case #1550 with foam. The selected valves will be mounted to a micro-fluidic manifold accessible through an egress in an instrumentation panel. The foam would be altered to house several 250ml plastic containers for water sample, eluent, and waste. An instrumented panel with all the fluidic system components mounted underneath would be placed within the case. Power conditioning for use from a standard 120VAC outlet will be incorporated into the panel. A battery option is available for this design pending a field requirement for stand-alone power. Lastly, the PalmSens electrochemical detection system, presently used by NRL, will be located within the case adjacent to the fluidic system. All connections, fluidic and electrical, to the sensor will be made with the case open. Should there be a requirement to keep the case lid closed during a field deployment, accommodations can be easily made.

The fluidic system will be operated via SubChem Systems ChemVIEW software installed on a laptop. This software will leverage an existing application being developed for SubChem Systems commercially available sensors. The graphical interface will depict the fluid schematic provided for this instrument for an intuitive interface to the system. The sensor controller will have a logging capability to allow operators to record pump timing and volumes.

Phase 1 Objectives

The objective of phase 1 is to collaboratively prepare designs for a single channel portable prototype of an electrochemical sensor system utilizing the Naval Research Laboratory's, macroporous silica/liquid-liquid, pre-concentration column technology for detection of trinitrotoluene (TNT) and other targets of interest. The portable technology must be able to sense the desired constituents in ground water access points including rivers, wells, and lakes.

This deliverable will include a summary of the design criteria, a brief assessment of select OEM components, as well as design recommendations. The brief assessment of OEM components includes the testing of several commercially available pumps and valves that were deemed applicable to the design. It will also include an OEM set of engineering drawings (mechanical, electronic, and fluidic).

Phase 1 Design Criteria

The macroporous silica/liquid-liquid pre-concentration system proposed by the NRL researchers requires appropriate volumetric control and analysis of sample intake and eluent (methanol) intake to pre-concentrate a silica/liquid-liquid column. The concentrated product of eluent and target analyte is then moved to the in-line flow cell for an electro-chemical analysis. One or several valves will be used to select between the intake of sample or intake of eluent. A single pump will be used to bring the eluent or sample into the system and move the product through the pre-concentration column then to the flow cell. A second valve or set of valves can be used to select how to expel the system products (for example, if the eluent is to be collected where sample need not be).

The selection of the micro-fluidic components requires consideration of the chemical compatibility between the target constituent and eluent versus the wetted materials of the system. Incorporating valves into the fluidic system, dead volume should be limited to avoid potential adjacent path contamination. The system pump must be capable of accurate fixed volume dispensing to be able to provide the desired 100~120 ml intake of sample and the 1~2 ml of eluent. The flow rate of the system pump is less critical but a specification of 2~5 ml/min was recommended. The fluidic system must have the capability to operate against the back pressure of the pre-concentration column and in-line flow cell, see table 1 and table 2.

Flow rate (ml/min)	Back Pressure (psi)
1	7.07
2	18.01
>3	50

Table 1: Test results from the OMNIFIT macroporous silica column provided to SubChem Systems.

Flow rate (ml/min)	Back Pressure (psi)
1	0.55
2	0.81
3	1.06
4	1.51
5	1.87
6	2.12
7	2.39
8	2.71
9	2.98

Table 2: Test results from the PalmSens flow through sensor that was provided to SubChem Systems.

There is no need for this prototype to be submersible but at least a NEMA4X rating is recommended given the type of environment. The initial phase 2 prototype must incorporate the existing NRL PalmSens unit and flow cell whereas a phase 3 prototype can incorporate the OEM board level version of the PalmSens electronics. A waste and eluent container must also be incorporated to contain the eluent itself and the waste product of the eluent plus target constituent. The containers should be sized for approximately 100 samples. This would require two 200 ml containers minimum.

Leading into the phase 2 effort, all components must be in-stock or have minimal lead time to enable design, fabrication, and bench testing within the 2011 calendar year. A working fieldable prototype is expected to be delivered, tested and documented prior to the end of the calendar year.

Phase 1 Brief OEM Component Survey

SubChem Systems Inc. has many years of experience in the design, fabrication and fielding of a wide array of chemistry based sensing technology on multiple types of platforms. In such time, SubChem Systems engineers have amassed an "in-house" suite of pumping, valve, and microfluidic handling technology from commercial vendors. Such vendors include, but are not limited to, BioChem-Valve, The Lee Company, Micropump, HNP Mikrosysteme, Burkertt, Cole-Parmer, Instech, ASCO, Upchurch, Vici, and ThinXXS.

For this effort, a few pumps and valves available in this timeframe were selected, deemed appropriate for further review. These components included:

Bio-Chem Valve	079SP-S1676	Manifold mount solenoid pump 8uL per pulse
HNP	MZR2521	Annular Gear micropump
The Lee Company	LPLX0501550AA	Inert solenoid pump 50uL per pulse
Instech	P625	Peristaltic pump
MicroPump	GA series	Spur Gear magnetic pump head with drive

Table 3: A list of pumps selected for review to match with design criteria.

The Lee Company	LFYA0536032H	Inert 3-way solenoid valve
Cole-Parmer	EW-01540-11	3-way solenoid valve

Table 4: A list of valves selected for review to match with design criteria.

Figure 1: Bio-Chem Valve 079SP-S1676.

Bio-Chem Valve is a leading supplier of solenoid based micro-fluidic pumps and valves. The 079SP pump is a manifold based solenoid pump that has a specified displacement of 8uL. The wetted parts include PEEK, EPDM and Teflon. It is operated by applying 12VDC across the solenoid leads and this will aspirate the pump diaphragm. When removing 12VDC, the pump will dispense 8uL. The manufacturer states that the pump has a 25% error in accuracy. Sub-Chem Systems has confirmed this. The pump is capable of up to 1.0 ml/min. Bigger versions are capable of up to 25 ml/min. Based on the large error in pumping accuracy across this line of products from Bio-Chem, these pumps are not recommended but could be used in the phase 2 prototype.

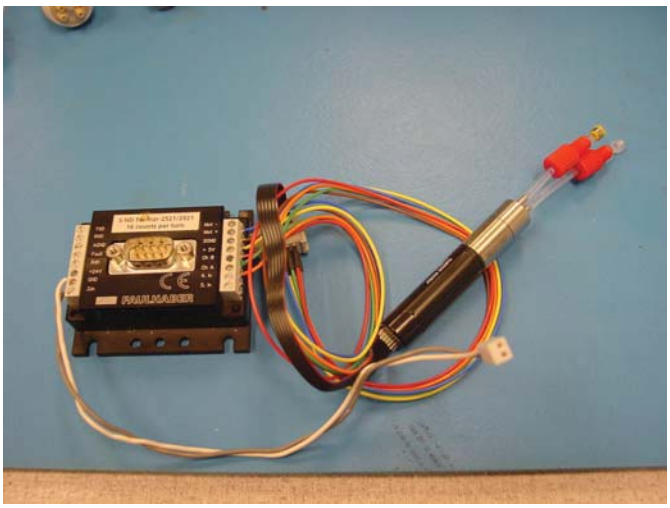

Figure 2: The MZR2521 annular gear pump and controller.

Micropump is a leading supplier of pump head and drive components. On their micro-fluidic product line is the MZR2521 pump. The MZR2521 consists of several components. The pump

head is manufactured in Germany, as is the motor controller. The motor used in the pump is manufactured in Switzerland. This combination of international suppliers drives the cost and availability of this pump higher than any other options being considered. However, this setup is the most accurate technology for either fixed dispensing or continuous flow with a flow rate capability of up to 9 ml/min. The wetted materials in this pump include Hastelloy, Stainless steel, ceramic, and EPDM. The pump does require slip fittings which would add volume to the fluidic path. A manifold version of this pump is available. What makes this setup unique is the motor used in the pump has a built in encoder. Using the encoder output, the motor controller can be programmed to dispense a very precise measurement of fluid at a time with an accuracy of 1.5uL. This pump setup is recommended for fluidic systems requiring a very high level of precision. For the Phase 2 prototype, use of this pump and motor controller will rely on whether the back pressure of the silica/liquid-liquid column can be lessened to under 20 psi at up to 5 ml/min.

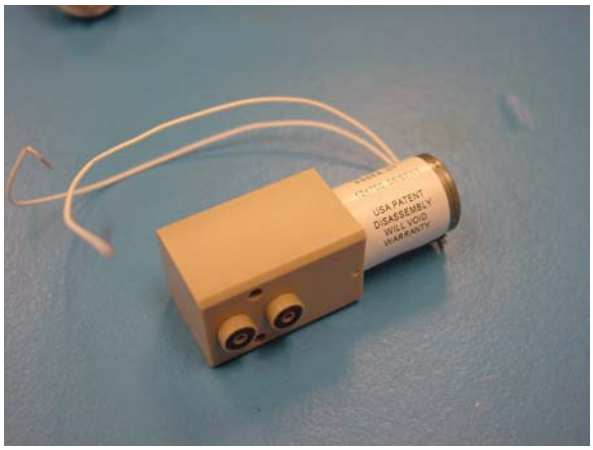

Figure 3: The Lee Company LPL fixed volume inert pump.

The Lee Company is a supplier of miniature hydraulic and micro-fluidic components including, pumps, valves, check valves, fittings, etc. The LPL pump is a manifold based solenoid pump that has a specified displacement of 50uL. The wetted parts include PEEK and Viton Fluoroelastomer (FCR). It is operated by applying 12VDC across the solenoid leads and this will aspirate the pump diaphragm. When removing 12VDC, the pump will dispense 50uL. The manufacturer states that the pump has a 5% error in accuracy, testing at SubChem Systems has verified this accuracy. The pump is capable of greater than 6 ml/min continuous flow. A flow rate of 6 ml/min was achieved. This pump is recommended for this effort pending the back pressure of the silica/liquid-liquid column can be lessened to under 10 psi at up to 5 ml/min.

Figure 4: The Instech P625 OEM peristaltic pump.

Instech is a supplier of medical and biological equipment to researchers and engineers. They have a product line of miniature OEM peristaltic pumps, the P625, with a wide range of configuration options covering flow rates from 0.34 uL/min to 19 ml/min. The flow rate is determined by RPM of the pump head and inner diameter of the flex tubing. Peristaltic pump tubes may not all be compatible with the eluent. Therefore, care must be taken to have the correct chemical compatibility. A test was performed with a P625.275 pump with 0.062 inch inner diameter tubing. The specified flow rate of 3.4 ml/min was achieved. Barbed fittings had to be placed on the tubing to be compatible with the ¼-28 fitting setup of the test fixture. The length of tubing required to run the pump suggests there would be a large volume needed in the flow path to use this pump as it is not a manifold mounted pump. It is not feasible to use this pump with the current OMNIFIT column. The column has a back pressure that is beyond the burst pressure of the peristaltic pump tubing. This pump could be used pending the back pressure can be lessened 20 psi at 5 ml/min.

Figure 5: The Micropump GA series pump head with DC magnetic driver.

Micropump is a manufacturer of external gear pumps with a product line flow rate capacity ranging from 0.1 ml/min to 42.9 L/min. SubChem Systems has extensive experience with the GA Series pump head and DC brushed motor driver. The pump head and drive are bought separately and mated using a magnetic coupling. What separates these pumps from the previously mentioned pumps is the ability of this product line to work flow against a differential pressure of up to 75 psi. The DC brushed motor driver can be supplied with up to 24VDC with a 12VDC option available. To generate the full range of flow rate capability, the voltage supply is adjusted by the control electronics. The full flow rate range of the GA Series pump head is 1 ml/min minimum to greater than 30 ml/min depending on the voltage range and the driver. Given the flow characteristics of the sample column that was sent for evaluation, this pump was selected as the best candidate for use with the current OMNIFIT silica/liquid-liquid column.

Figure 6: The Lee Company LFYA 3-way inert solenoid valve.

The Lee Company produces a line of solenoid valves as well as pumps. Of which there is an inert valve product line for aggressive fluids. The LFYA valve is an inert valve with wetted materials including Polyphenylene sulfide (PPS) and Viton Fluoroelastomer (FCR). The valve boasts zero dead volume and low internal volume. Preliminary testing at SubChem Systems has shown that this valve has very little back pressure (<0.11 PSI) with flow rates up to 9 ml/min. This version of the valve is manifold mounted. This is a viable option for the phase 2 prototype. The pressure rating of the valve is well within what is needed for the phase 2 prototype considering that the valve positions in the system are before the sample pump and after the column. Therefore, minimal pressure is experienced by the valves.

Figure 7: The Cole-Parmer 3-way solenoid valve.

Cole Parmer is a leading supplier of instrumentation to researchers and engineers alike. Among their multitude of products is a line of micro-fluidic solenoid valves. The EW-01540-11 is a 12VDC operated solenoid valve. All wetted parts are made of PTFE for use with aggressive chemicals. This is a non-manifold valve requiring the use of ¼"-28 flat bottom fittings. This will increase the dead volume in the prototype design. Also, SubChem Systems experience with these valves shows a track record of weak threads on the PTFE body. Tightening fittings on this valve can lead to stripping the threads on the ports. This valve is not recommended.

Prototype Fluidic System Concept Design

Based on the design criteria, in-house and readily available components, and fabrication experience, SubChem Systems is recommending a manifold based fluidic system which will effectively minimize fluidic paths more than tubing can. Given the prospect of multiple instruments in the future, manifold based designs provide better fabrication consistency across multiple devices. To remain cost effective, the proposed micro-fluidic system design incorporates a PVC manifold with two Lee Company LFYA 3-way solenoid valves. PVC was determined to have an appropriate chemical compatibility with the eluent and remain cost effective compared to other materials such as PEEK. The Micropump GA series pump will be used in the design as well as it can give the specified flow rate range through the OMNIFIT pre-concentration column. The GA Series pump is not offered in a manifold version so there will be minimal tubing between the manifold, column and pump head. Pending the column used, if the back pressure can be lessened to <10 psi at 6 ml/min, then the Lee Company LPL manifold mounted solenoid pump can be used. This switch between pumps can happen relatively easily with a simple manifold change. There will be minimal impact, if any, to the phase 2 and phase 3 design.

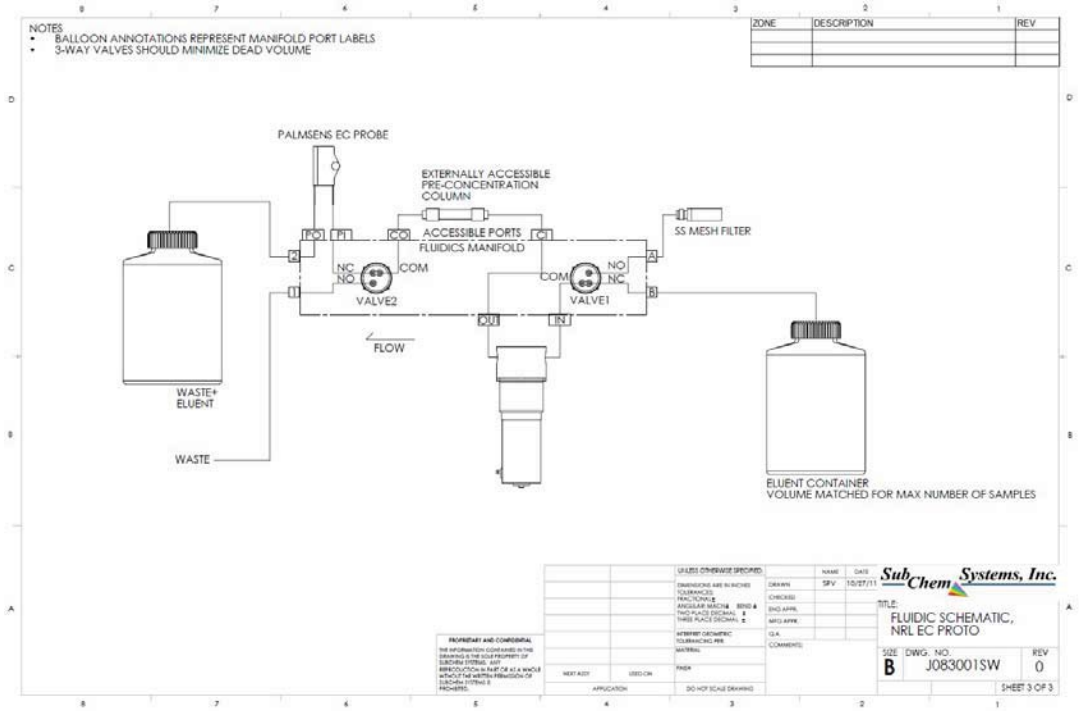

Figure 8: Proposed single pump, two 3-way valve fluidic system layout. An additional container can be used in place of the SS Mesh Filter.

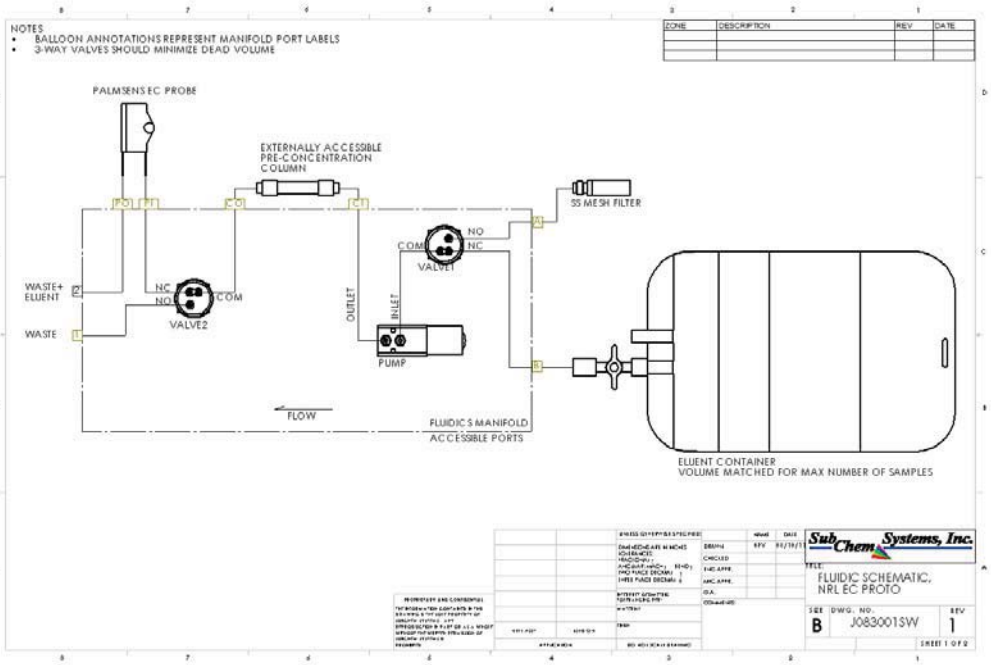

Figure 9: An alternative fluidic system incorporating two Lee Company LFYA valves with a LPL manifold mounted solenoid pump. Also shown is an optional standard IV bag for eluent storage. This would be a design alternative if the back pressure of the pre-concentration column can be brought below 10 psi.

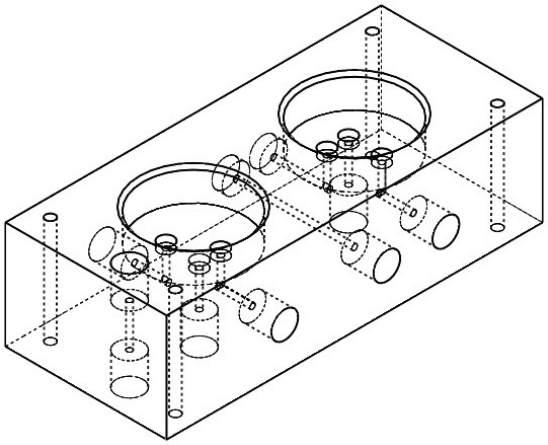

Figure 10: Proposed phase 2 micro-fluidic manifold utilizing the Lee Company LPL pump and LFYA valves.

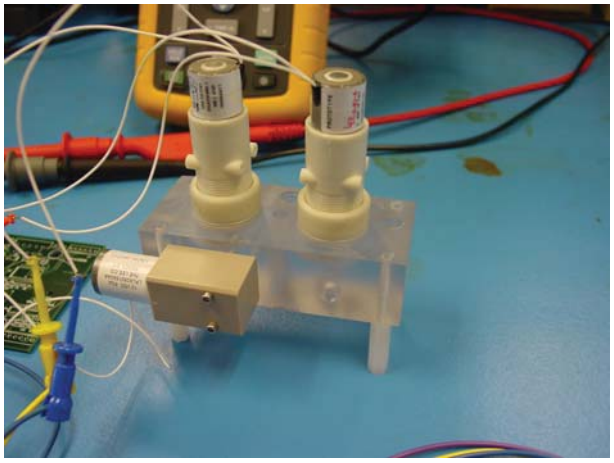

Figure 11: A test manifold fabricated for consideration to the phase 2 prototype.

Engineers at SubChem Systems designed and fabricated a concept phase 2 micro-fluidic manifold leveraging some transparent stock material available in-house. The manifold was designed to have minimum flow path lengths by optimizing the positions of the two LFYA valves and the LPL pump. All fluidic paths maintain a 0.052" inner diameter. Referencing figure 10, ports that will be routinely accessed, the column ports, the sample intake port and the two waste ports, will be accessed on the unpopulated side of the manifold. Therefore, the manifold can be mounted to a panel with the components underneath. This design accommodates a field-able instrument as well such that the ports can be external to the instrument housing with the components protected internally.

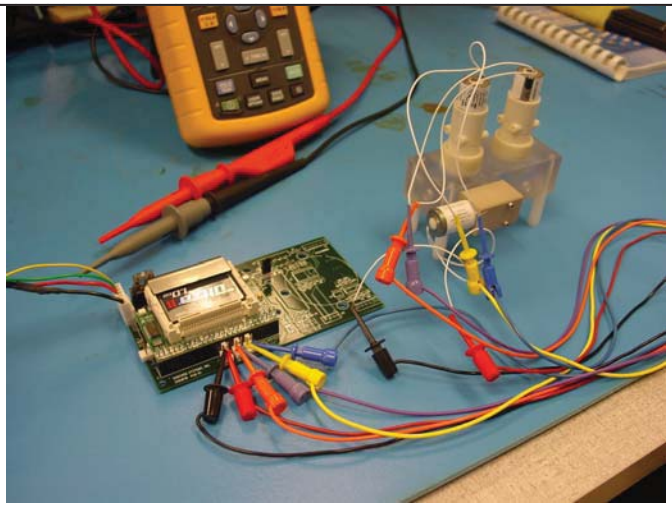

Figure 12: A leveraged controller for operation of the test manifold.

Leveraging a controller from a prior instrument design, engineers at SubChem Systems were able to operate all electro-mechanical aspects of the concept phase two fluidic system.

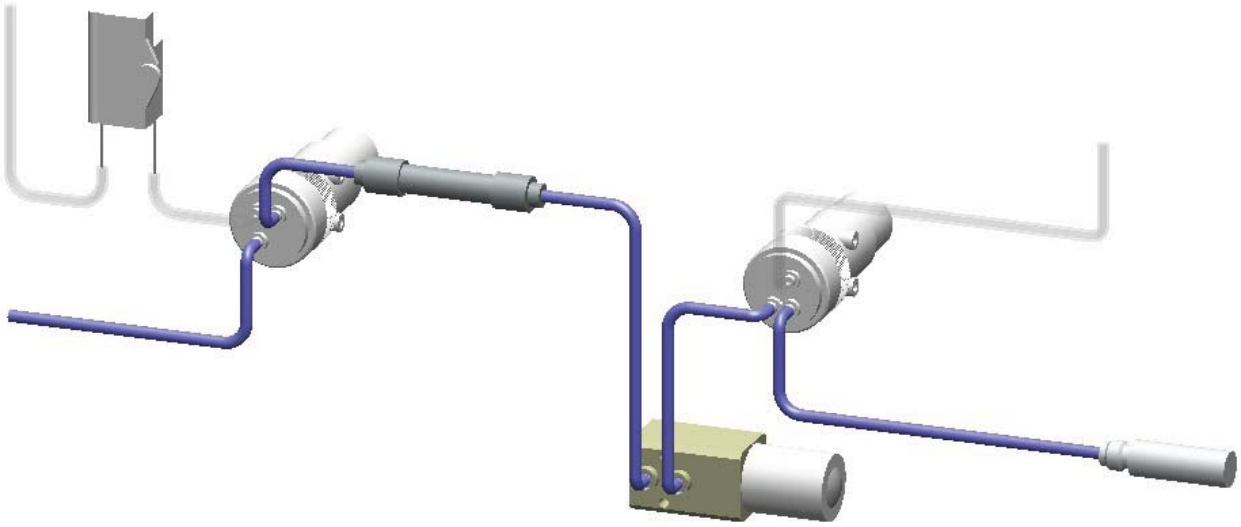

Figure 13: A diametric view of the fluidic system. Blue paths indicate the fluidic path that the sample intake travels along. Flow moves right to left.

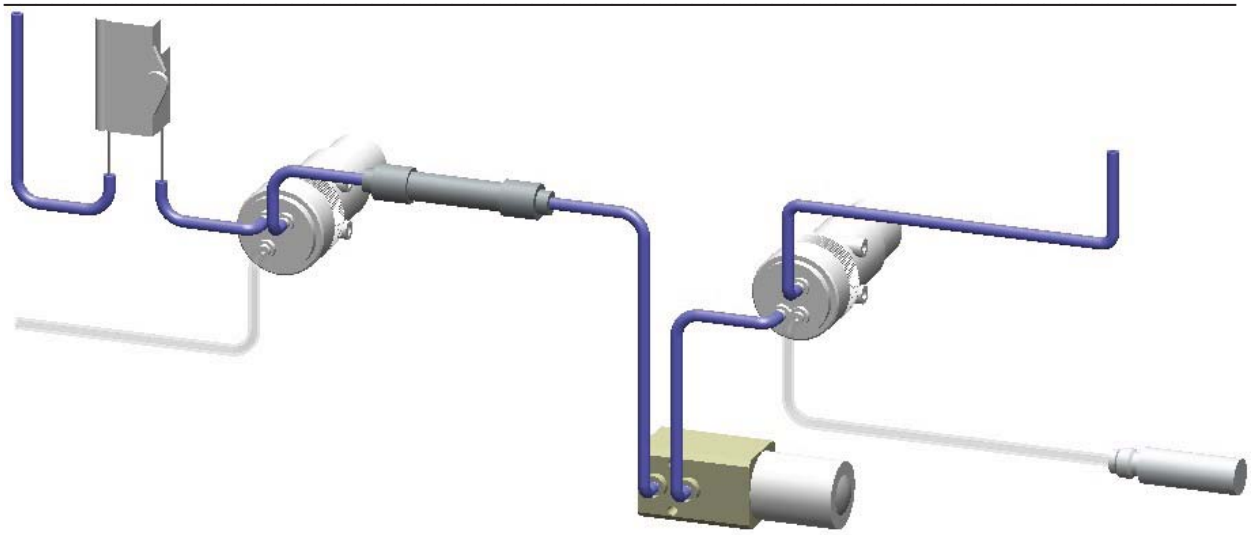

Figure 14: A diametric view of the alternate state of the fluidic system. Blue paths indicate the fluidic path the eluent travels along. Flow moves right to left.

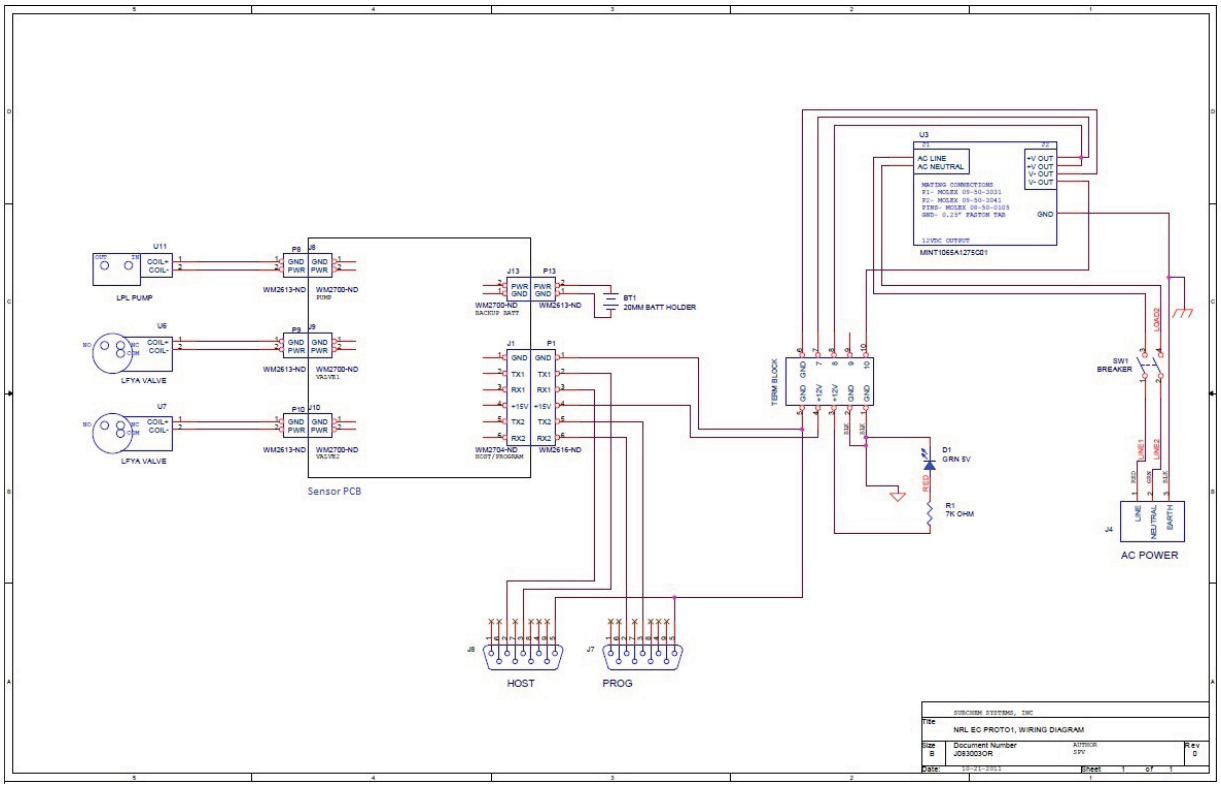

Figure 15: The NRL Electro-Chemical Prototype1 wiring diagram.

The phase 2 electronics will leverage SubChem Systems ongoing advancements in low power consumption micro-controller based instrument technology. The phase 2 prototype is ultimately going to be the coupling of the typical instrument deck box with the fluidic system. Therefore, the prototype will have an AC/DC power converter with breaker switch and fuse. There will be two communication ports available but only the PROG port will be mounted on the instrument panel. The PROG port will be used to program and operate the instrument. The AUX port is available for future sensor expansion. The sensor printed circuit board (PCB) will enable low power consumption when the prototype is at a suspended state (<20uA). When operating, the PCB will enable full control of the two solenoid valves and sample pump. The printed circuit board will be designed to occupy very minimal space such that a phase 3 prototype can be scaled down considerably when the PalmSens OEM board is available. A battery option will be available for the phase 2 and phase 3 prototypes should there be a need to leave the instrument unattended without available power.

The micro-controller based design of the instrument will leverage SubChem Systems ongoing firmware development. The company continues to develop a software package known as ChemVIEW. For prototypes, a baseline capability of ChemVIEW is taken and slight modifications are made to the graphical interface while maintaining basic functionality like the plotting tool and file transferring. The command and control structure of the instrument electronics remains standardized. This limits the need for software development across new prototypes. Every SubChem Systems instrument has a TEST mode feature which enables operator access to each individual component of the system. This mode is also used to program the instruments AUTO mode feature. AUTO mode is a feature on every instrument which allows the operator to adjust a suite of parameters to program the instrument to operate unattended. Sampling protocol is setup for AUTO mode and simple commands or automatic sampling is then enabled.

Prototype Software Graphical User Interface

Engineers at SubChem have laid out a user-friendly software application to control the operation of the Phase 2 prototype system. This application uses buttons, graphics, and a serial communication connection to the sensor to make operation simple and intuitive. The user can set the dispense volume and pump flow rate to inject a finite volume of sample or eluent into the system. When the **Pump Eluent** or **Pump Sample** button is pressed, a serial command is sent to the sensor controller which then adjusts the pump and valves. In addition, a graphic depicting the fluidic schematic is updated in the software, as shown in Figure 15 and Figure 16. Feedback from the controller provides data such as the remaining volume of eluent and volume of waste product of eluent and target. These values are used to update the corresponding ‘tanks’ shown in the software.

The software leverages serial communication and file transferring routines developed in SubChem’s ChemVIEW software. ChemVIEW is the graphical user interface software supplied with all of SubChem’s commercial chemical analyzers.

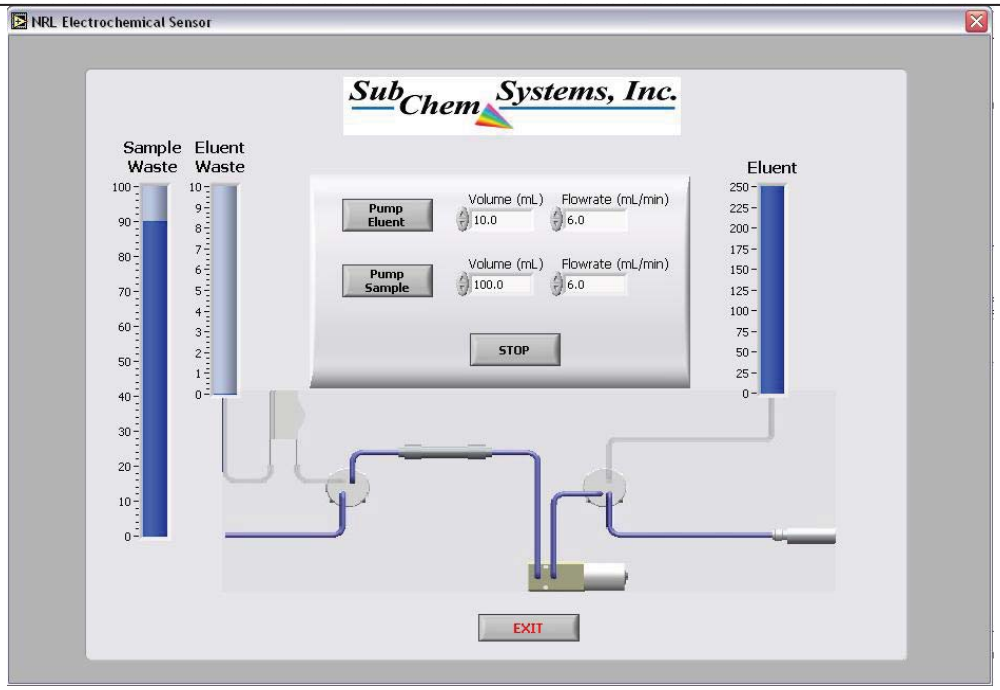

Figure 16: Screen shot of the NRL Sensor Prototype software pumping a sample. When pumping eluent, the graphic representing the fluidic schematic changes to reflect the actual valve positions.

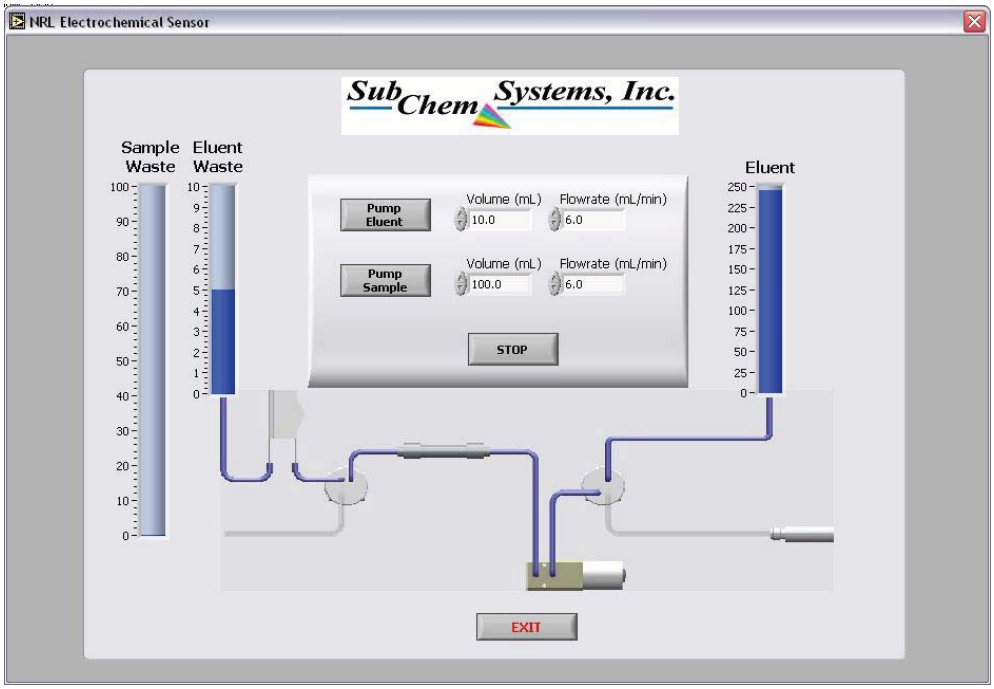

Figure 17: Screen shot of the NRL Sensor Prototype software pumping eluent. Notice how the fluidic schematic graphic changes and the Eluent tank decreases.

Phase 2 Mechanical Design

The phase 2 prototype design will essentially be the coupling of the SubChem Systems standard deck box and the electro-chemical fluidic system. For this initial design, a Pelican Case 1550 will be used to house the fluidic system, eluent and waste containers, and electronics. The approximate dimensions of this case are 20" by 17" by 8". The approximate weight will be 12~15lbs. The PalmSens held unit and flow through cell from NRL will be placed into the case as well for an entirely self contained setup. AC power (115VAC~230VAC) will be supplied to the panel inside the case. The switch, fuse, and communications ports will also be available from within the case. The fluidic system will be mounted on the panel such that the unpopulated side of the manifold is visible. Fluid can be seen moving through the manifold from this perspective. The pre-concentration column will be fixed to the operator's side of the panel such that the column can be removed and maintained without having to disassemble the instrument. The eluent and waste containers will also be placed within the case for convenience.

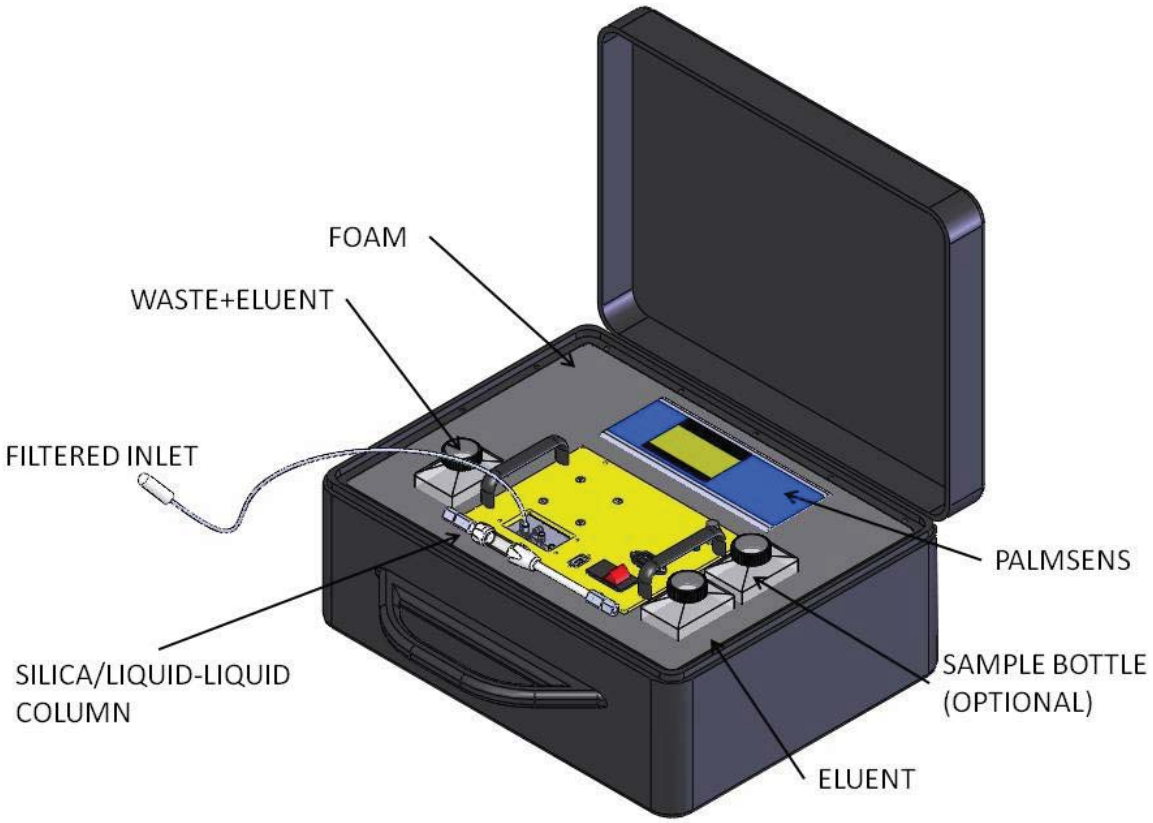

Figure 18: The phase 2 prototype design.

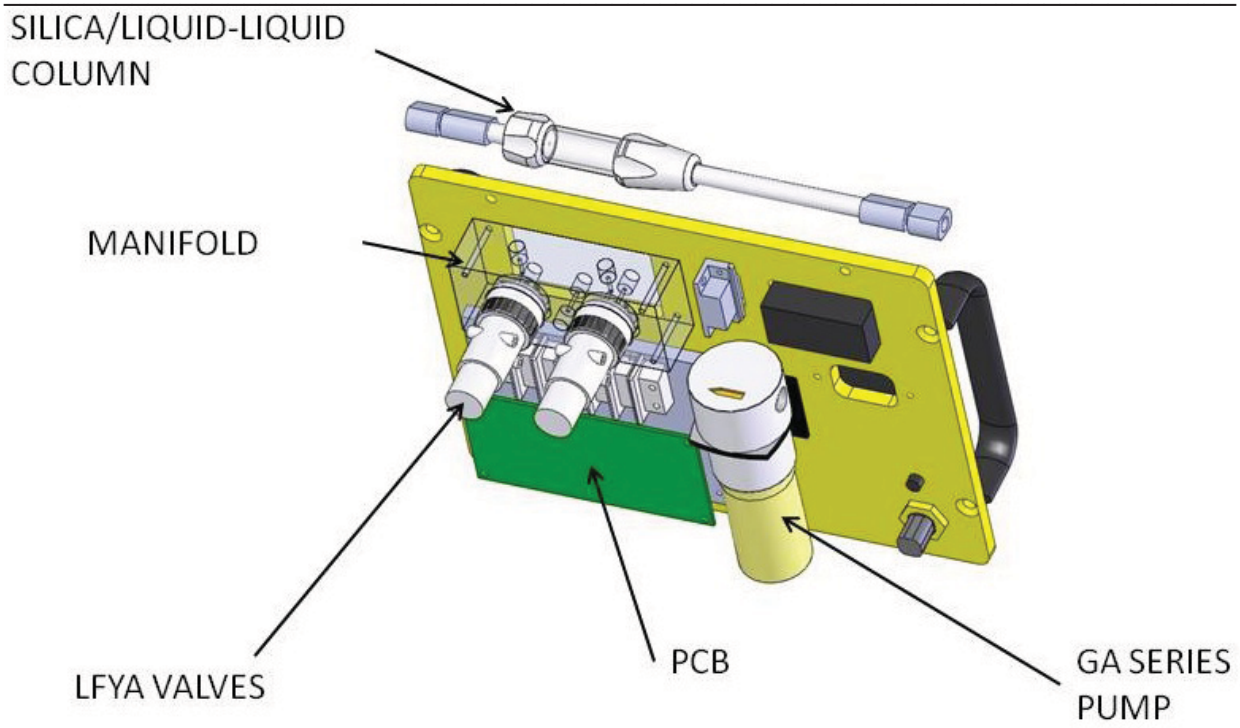

Figure 19: The bottom view of the fluidic system panel. This illustrates how the manifold is mounted with respect to the valves and electronics. A window is cut out of the panel to view the fluidics.

Summary

Presented in this document are the findings and design recommendations from SubChem Systems pertaining to the fabrication of a portable electro-chemical TNT sensor. The design incorporates all aspects requested including utilization of the same type of PalmSens electro-chemical sensor and flow cell, used by NRL. The design also accommodates several 250ml plastic containers for holding samples and eluent for analysis, as well as a waste container for the eluent. The sensor fluidic system is mounted entirely to a single aluminum panel. This will allow for greater accessibility to the fluidic system components. The valves will be mounted to a micro-fluidic manifold to lessen internal volume and to leverage the Lee Company LFYA series inert valves.

The phase 2 instrument design, derived from this phase 1 effort, is meant to allow for enough flexibility to test components such as the fluidic system and pre-concentration column. Findings from phase 2 will be incorporated into the phase 3 modifications along with placing an emphasis on a more compact field ready design.

Appendix – Statement of Work

Dr. Brandy J. Johnson
Center for Bio/Molecular Science & Engineering
US Naval Research Laboratory
4555 Overlook Ave.
Washington, DC 20375

August 1, 2011

Dear Brandy:

RE: The design and fabrication of a portable electrochemical sensor system, utilizing NRL's, macroporous silica/liquid-liquid preconcentration technology, for monitoring TNT and other UXO in ground and lake waters.

In discussing the project further with our engineers it seems appropriate to progressively develop the portable instrument in three phases. The estimated costs and delivery are shown for the first two phases and separate quotations are attached.

Phase 1: Prepare designs for a single-channel portable prototype of an electrochemical sensor system, utilizing NRL's, macroporous silica/liquid-liquid preconcentration technology. We envision that the prototype (Phase 1&2 concept preliminary drawing attached) would be contained in a weather-proof plastic case (Pelican Case) and designed to include the same miniature electro-fluidic components (i.e. pumps, valves and connections), and controller that we propose to use in the Phase 3 portable version. Provision would be made for reagent and waste reservoirs and a rechargeable battery. As part of this work, SubChem would test the applicability of various fluidic options and control components, with an NRL macroporous silica column. We envision that the Phase 1 portable prototype would utilize an electrochemical sensing system comprised of a PalmSens interface & type FC2 flow cell, identical to that presently being used by NRL researchers. The instrument will be controlled, and data collected, by a small notebook computer. The deliverable for Phase 1 will be a report and a complete set of engineering drawings (mechanical, electronic, fluidic and electrochemical). After design review and approval by NRL, we would proceed to Phase 2. Cost /delivery: $11,400 / 1 month after receipt of the purchase order.

Phase 2: Fabricate, test, deliver and evaluate a single-channel portable prototype. This would also include the development of the software for the embedded controller. After testing and satisfactory evaluation of the assembled prototype, by both SubChem and NRL, we could proceed to Phase 3. Cost/delivery: $21,600 / 1-2 months.

Phase 3: Design, fabricate, test and evaluate a second-generation, more-compact, portable instrument with a custom weather-proof housing and real-time data web-based reporting capability (Phase 3 concept drawing attached). This version will also include the incorporation of the Palm Instruments EmStat or EmStat2 OEM electrochemical interface board set. The first part of the deliverable would be a complete set of engineering drawings (mechanical, electronic, fluidic and optical) for the portable instrument. After design review and approval by NRL, we would proceed with fabrication. We would deliver the portable instrument to NRL for bench-top and field testing and evaluation. SubChem could participate in these field tests. Cost/delivery: to be determined.

Please contact me directly if I can provide additional information.

Sincerely yours,

Alfred K. Hanson

Alfred K. Hanson
President

PUBLICATION OR PRESENTATION RELEASE REQUEST

13-1231-3846

NRL/PST/5600.2

1. REFERENCES AND ENCLOSURES	2. TYPE OF PUBLICATION OR PRESENTATION	3. ADMINISTRATIVE INFORMATION
Ref: (a) NRL Instruction 5600.2 (b) NRL Instruction 5510.40D Encl: (1) Two copies of subject paper (or abstract)	( ) Abstract only, published ( ) Abstract only, not published ( ) Book ( ) Book Chapter ( ) Conference Proceedings (refereed) ( ) Conference Proceedings (not refereed) ( ) Invited speaker ( ) Multimedia report ( ) Journal article (refereed) ( ) Journal article (not refereed) ( ) Oral Presentation, published ( ) Oral Presentation, not published (x) Other, explain NRL report	STRN NRL/FR/6900--13-003 Route Sheet No. 6900-003FR Job Order No. 69-9629-03-5 Classification X U C Sponsor SERDP (b) (N1) approval obtained V yes ____ no

4. AUTHOR

Title of Paper or Presentation

Preconcentration for Improved Long-term Monitoring of Contaminants in Groundwater

Author(s) Name(s) *(First, Mi, Last)*, Code, Affiliation if not NRL

Brandy J. White (6920)and Brian J. Melde (6930)

It is intended to offer this paper to the _____
(Name of Conference)

_____
(Date, Place and Classification of Conference)

and/or for publication in NRL report _____ NRL _____
(Name and Classification of Publication) *(Name of Publisher)*

After presentation or publication, pertinent publication/presentation data will be entered in the publications data base, in accordance with reference (a).

It is the opinion of the author that the subject paper (is____) (is not X) classified, in accordance with reference (b).

This paper does not violate any disclosure of trade secrets or suggestions of outside individuals or concerns which have been communicated to the Laboratory in confidence. This paper (does____) (does not X) contain any militarily critical technology.

This subject paper (has____) (has never X) been incorporated in an official NRL Report.

Brandy White (6920) _____
Name and Code *(Principal Author)* (Signature)

5. ROUTING/APPROVAL

CODE	SIGNATURE	DATE	COMMENTS
Author(s) B White		11/20/13	
			This is a Final Security Review.
			Any changes made in the document, after approved by ~~Code 1231,~~ nullify the Security Review.
Section Head			
Branch Head AKusterbeck	acting	11/20/13	
Division Head B. Ratna		11/20/13	1. Release of this paper is approved. 2. To the best knowledge of this Division, the subject matter of this paper (has____) (has never X) been classified.
Security, Code 1221.1		11/25/13	1. Paper or abstract was released. 2. A copy is filed in this office.
Office of Counsel, Code 1008.2		12.2.13	Sponsor approved attached.
ADOR/Director NCST		06 DEC 2013	
Public Affairs *(Unclassified/ Unlimited Only)*, Code 1030		03 DEC 2013	
Division, Code			
Author, Code			

HQ-NRL 5511/6 (Rev. 12-98) (e)

THIS FORM CANCELS AND SUPERSEDES ALL PREVIOUS VERSIONS